

Spring 1-1-2017

Engineering Synthetic Antibiotics in Non-Traditional Pathways to Counter Antibiotic Resistance

Colleen Maxwell Courtney
University of Colorado at Boulder, colleen.courtney@colorado.edu

Follow this and additional works at: https://scholar.colorado.edu/chen_gradetds



Part of the [Chemical Engineering Commons](#), and the [Microbiology Commons](#)

Recommended Citation

Courtney, Colleen Maxwell, "Engineering Synthetic Antibiotics in Non-Traditional Pathways to Counter Antibiotic Resistance" (2017). *Chemical Engineering Graduate Theses & Dissertations*. 9.
https://scholar.colorado.edu/chen_gradetds/9

This Dissertation is brought to you for free and open access by Chemical Engineering at CU Scholar. It has been accepted for inclusion in Chemical Engineering Graduate Theses & Dissertations by an authorized administrator of CU Scholar. For more information, please contact cuscholaradmin@colorado.edu.

ENGINEERING SYNTHETIC ANTIBIOTICS IN NON-TRADITIONAL PATHWAYS TO
COUNTER ANTIBIOTIC RESISTANCE

by

Colleen Maxwell Courtney

B.S., University of Maryland, Baltimore County, 2012

M.S., University of Colorado, 2014

A thesis submitted to the

Faculty of the Graduate School of the

University of Colorado in partial fulfillment

of the requirement for the degree of

Doctor of Philosophy

Department of Chemical and Biological Engineering

2017

This thesis entitled:

Engineering Synthetic Antibiotics in Non-Traditional Pathways to Counter Antibiotic Resistance

written by Colleen Maxwell Courtney

has been approved for the Department of Chemical and Biological Engineering

Anushree Chatterjee, Committee Chair

Prashant Nagpal, Committee Member

Date _____

The final copy of this thesis has been examined by the signatories, and we
find that both the content and the form meet acceptable presentation standards
of scholarly work in the above mentioned discipline.

Abstract

Colleen Maxwell Courtney (Ph.D., Chemical and Biological Engineering)

Engineering synthetic antibiotics in non-traditional pathways to counter antibiotic resistance

Thesis directed by Professor Anushree Chatterjee

Antibiotic resistance is a growing threat to global healthcare that requires immediate action to avoid the post-antibiotic era. The inherent ability of bacteria to obtain resistance and the lack of new antibiotics has led to the current antibiotic crisis. Current antibiotics are typically found through soil compound screens and only target proteins within three cellular pathways: cellular replication, cell wall biosynthesis, and protein biosynthesis. In the last decade, strains have been isolated which have resistance to nearly all available antibiotics highlighting the urgent need for intervention. In this work we investigated the rational design of non-naturally derived antibiotics which target bacterial processes outside of the three traditional antibiotic target pathways.

Antisense therapeutics are nucleic acid oligomers that bind sequence-specifically via Watson-Crick base pairing with native nucleic acids and inhibit translation of the targeted gene. For this work, we use non-natural nucleic acid analog oligomers, peptide nucleic acids (PNA), for their demonstrated intracellular stability and high binding affinity for native nucleic acids. In our initial study, we show PNA oligomers targeted to TEM-1 β -lactamase re-sensitized drug-resistant *Escherichia coli* to a β -lactam antibiotic. We further adapted *E. coli* to low levels of PNA and β -lactam antibiotic and observed high variability in expression of stress response genes possibly suggesting a bet-hedging type adaptive resistance. In our next study, we designed PNA to target essential bacterial genes in non-traditional antibiotic target pathways. We designed the PNA

against the genome sequences of non-pathogenic, drug sensitive *E. coli*, *Klebsiella pneumoniae*, and *Salmonella enterica* and subsequently tested their antibacterial action in multidrug-resistant (MDR) clinical isolates of the same three species. We found that 54% of predicted targets were effective at inhibiting the MDR pathogens demonstrating the ability to design sequence-specific yet still broad-pathogen antisense therapeutics. We further demonstrated that combinations of these essential gene antisense PNA and small molecule antibiotics function synergistically to enhance bacterial inhibition despite the clinical strains high antibiotic resistance.

We next focused our efforts on designing an antimicrobial agent for perturbing bacterial redox homeostasis. Reactive oxygen species (ROS) have been studied for their effect on antibiotic efficacy and the emergence of drug resistance. In this work, we studied one ROS in particular, superoxide, for its role as an oxidative stress catalyst and its demonstrated disruption of metal homeostasis in bacteria. To controllably produce superoxide, we investigated the design of quantum dot nanoparticles. When quantum dots are excited over their nominal bandgap, excited electrons and holes are available for redox half reactions in the biological environment. In this work, we demonstrated the tuning of quantum dots for superoxide production from molecular oxygen and further showed the tuned nanoparticles inhibition of clinical isolates. Further, we established that *E. coli* could be eradicated from co-culture with mammalian cells; leaving the mammalian cells intact.

Given the role that ROS have been shown to have in bactericidal antibiotic efficacy, we hypothesized that our superoxide-producing nanoparticles would function synergistically with small molecule antibiotics. Indeed, our designed superoxide generating nanoparticles potentiated the activity of antibiotics in clinical MDR isolates in spite of their antibiotic resistance. In this study, superoxide potentiated the activity of bactericidal antibiotics as well as bacteriostatic

antibiotics, which had not been shown previously. To better understand the effect of superoxide generation on bacteria, we performed analysis of *E. coli*'s transcriptome during treatment. We removed material effects by comparing activated nanoparticle to both inactivated nanoparticle and a control benign nanoparticle treatment. Interestingly, we observed increased gene expression variability transcriptome-wide from superoxide generation. The most affected pathways both for differential expression and significantly changed expression variability were in classical and nitrogen metabolism, amino acid synthesis, and stress response to pH and heat. Overall this work demonstrates the ability to engineer antibiotics for non-traditional pathways and highlights their ability to inhibit MDR clinical isolates and function synergistically with small molecule antibiotics.

To the women who made me who I am today:

My grandmother Helen Roman

And

My mother Joanna Smith

Acknowledgments

I would like to first and foremost thank my adviser, Prof. Anushree Chatterjee. Throughout my thesis work, Anushree has given me the tools and freedom to explore my interests and develop my confidence as a scientist. She has gone above and beyond to not only advise in my research but also in my personal development for future endeavors. I appreciate her never ending passion to chase our shared scientific interests and her ability to keep me motivated and positive throughout my Ph.D. In the same vein, I would like to thank all members of the Chatterjee lab, old and new, for years of experimental troubleshooting, insightful discussion, and friendship. I have enjoyed sharing an office, happy hours, and Chatterjee lab camping trips with Keesha Erickson, Josep Casamada Ribot, Antoni Escalas Bordoy, and Peter Outopal. I would like to also thank a newer member of the group, Kristen Eller, for her support of some final experiments and anticipated continuation of the projects in this thesis.

I have collaborated extensively with the Nagpal lab for the quantum dot studies described in Chapters 5, 6, and 7 and would like to thank Prof. Prashant Nagpal for his continued help and support of my research endeavors. His passion and drive to answer scientific questions kept me motivated and focused. I would also like to thank members of his lab for their continued help, support, and research contributions: Samuel Goodman, Max Levy, Jessica McDaniel, and Yuchen Ding. They never failed to provide nanoparticle synthesis technical support and conduct meaningful characterization of nanomaterials used in this work.

I would also like to thank Prof. Corrella Detweiler for her support not only as a committee member but also a collaborator for the epithelial infection studies in Chapter 6. She did not hesitate in opening her lab to me for investigating intracellular infections and for that I am grateful. I would also like to thank her postdoctoral fellow, Toni Nagy. Toni made the intracellular infection

experiments possible and guided me in data analysis and representation of results. I appreciated her support, guidance, and friendship throughout the collaboration.

Throughout the course of this thesis, numerous friends and colleagues were helpful for discussions and collaborations. I would like to acknowledge T. Steele Reynolds in the Gill group for his collaboration on nanoparticle adaptation experiments mentioned in Chapter 7 and his patience in answering my never ending questions. I would like to acknowledge Weipeng Zhou at Georgia Institute of Technology who was a great friend during my undergraduate education and continued to support me in my graduate studies. He was helpful in determining methods and standard practices for my nematode studies used in Chapter 6.

Additionally, I would like to thank Prof. Stephanie Bryant and Prof. Robert Batey for their continued support on my thesis committee. Their advice and suggestions over the course of my thesis helped to define new avenues and strengthen the scientific support for the project. I thank Dr. Theresa Nahreini for use of and guidance in the BioFrontiers Cell culture facility and flow cytometry core and Jamie Prior and Jim Huntley for guidance in the BioFrontiers Next Generation Sequencing Facility. I would also like to thank Dr. Nancy Madinger and Marianne Dieterich at the University of Colorado Anschutz campus for supplying the multidrug-resistant clinical isolates used in our lab and answering our questions about their characterization. Additionally, I would like to acknowledge Dominique DeVangel for keeping me in line over the years with administrative details, even with the shortest notice.

This work would not have been possible without our funding sources. I would like to thank my funding from the National Science Foundation Graduate Research Fellowship program, the National Institutes of Health Pharmaceutical Biotechnology Training Grant program, and the University of Colorado, College of Engineering and Applied Science Dean's Outstanding Merit

Fellowship. I would also like to acknowledge funding sources to my advisor and our collaborators for their support of this work: University of Colorado start-up and William M. Keck Foundation funds to Anushree and Prashant, DARPA Young Faculty Award to Anushree, and NSF Career award to Prashant.

Over the course of my thesis, I worked with a number of undergraduate students who had a positive impact on my experience. I would like to especially thank Pallavi Bhusal who was my longest and most prolific undergraduate student. She was highly self-motivated and persisted through the pains of molecular cloning!

I could not have completed this work without the support of my friends throughout the years. I would like to thank my roommates at 2725 especially Matthew McBride, Ryan Mowbray, Samantha Summers, Marley, and Sherry D'Andrea. Additionally, I would like to thank Brian and Sarah Ehrhart, Katherine Morrissey, Lucas Sooy, Vince Dorzweiler, Stacey Skaalure, the Malbrough's, and friends at CrossFit MHz for their constant support and help in making these last few years a lot of fun! Sadella Santos, Amanda Knights, Madeline Reed, and Courtney Sibiga are the best girlfriends I could ask for and cannot measure the support they have given me throughout my scientific endeavors and life. My big brother Timothy Courtney and sister-in-law Ann Kashishian have also supported me throughout this process and he led the way in getting a Ph.D. in chemical engineering, though in a place way less beautiful than Colorado. I would like to thank my parents Joseph and Joanna Smith for their never-ending encouragement. My mom is my best-friend and biggest cheerleader, with or without the "Colleen's mom" attire. I would also like to thank my grandmother, Helen Roman, who always told me of my potential and poured over with pride of my accomplishments. I also appreciate the newest addition to my family, Otto, for his never ending puppy love and company as my writing buddy. And finally, I want to thank Kyle

Lieurance for all the support and encouragement along the way and for reminding me to chase my dreams and never settle for less than my best.

CONTENTS

I. Chapter 1 Introduction	1
1.1 Approaching the post-antibiotic era.....	1
1.2 Thesis scope and organization	2
1.3 References.....	4
II. Chapter 2 Background	6
2.1 Summary	6
2.2 Importance and complexity of antisense interactions in nature.....	7
2.1.1 Antisense Transcription: a widespread occurrence in genomes	7
2.1.2 Antisense RNAs and RNA interaction mechanisms in bacteria.....	9
2.1.3 Transcriptional Interference: mechanisms and switch response.....	12
2.1.4 Wreckage of RNAP collision: a source of antisense RNA?	16
2.1.5 Coupled effect of Transcriptional interference and Antisense RNA interaction..	18
2.1.6 Outlook: Antisense transcription a widespread mechanism of gene regulation ...	21
2.3 Antisense therapeutics: sequence-specific targeting.....	22
2.3.1 Problems with broad-spectrum antibiotics.....	23
2.3.2 Synthetic nucleic acids.....	24
2.3.3 Antisense antibiotic target selection	25
2.4 Reactive oxygen species for antimicrobial activity	26
2.4.1 ROS role in antibiotic resistance.....	26
2.4.2 Superoxide specific toxicity.....	27
2.4.3 Quantum dots for superoxide generation	28
2.5 Combination therapies	29
2.6 References.....	30
III. Chapter 3 Sequence-Specific Peptide Nucleic Acid-Based Antisense Inhibitors of TEM-1 β -lactamase and Mechanism of Adaptive Resistance	40
3.1 Abstract	40
3.2 Introduction.....	41
3.3 Results and Discussion	43
3.3.1 Reversing β -lactam resistance by targeting the ribosomal binding site and start codon	43
3.3.2 Translational inhibition mechanism of action of antisense inhibitors	48

3.3.3 Start codon targeting antisense inhibitor restores ampicillin sensitivity	49
3.3.4 The emergence of tolerance to antibiotics PNA-inhibitor combination	50
3.3.5 Adapted populations exhibit differential <i>sbmA</i> and heterogeneous stress response gene expression	54
3.4 Conclusions.....	58
3.5 Methods.....	59
3.5.1 Bacterial strains and cell culture conditions.	59
3.5.2 Colony forming unit analysis.....	59
3.5.3 Antisense Inhibitors	60
3.5.4 <i>bla</i> RNA collection	60
3.5.5 Mutant biological replicate collection	60
3.5.6 Ampicillin MIC of mutant isolates	60
3.5.7 RNA extraction and RT-qPCR	61
3.5.8 β -lactamase activity assay.....	61
3.5.9 Ampicillin sensitivity assay	62
3.5.10 Sequencing of <i>bla</i> gene on plasmid	62
3.5.11 Data analysis	62
3.5.12 Clustering analysis.....	63
3.6 Supplementary Information	63
3.6.1 Supplementary tables	63
3.6.2 Supplementary figures	65
3.7 References.....	71
IV. Chapter 4 Predictive Homology for Antisense RNA-Inhibitor Antibiotics in Non-Traditional Antibiotic Pathways.....	77
4.1 Abstract	77
4.2 Introduction.....	78
4.3 Results and Discussion	80
4.3.1 Antisense PNA RNA-inhibitor design and predictive homology.....	80
4.3.2 Clinical isolate characterization	82
4.3.3 Antisense PNA efficacy in MDR clinical isolates	82
4.3.4 Combination of antisense PNA with small molecule antibiotics.....	84
4.4 Conclusions.....	86
4.5 Materials and Methods.....	87

4.5.1 Peptide nucleic acid molecules	87
4.5.2 Cell culture.....	87
4.5.3 Antibiotic resistance screening	88
4.5.4 Peptide nucleic acid growth experiments	88
4.5.5 Combinatorial effect evaluation.....	88
4.5.6 Quantitative real-time polymerase chain reaction	89
4.5.7 Genome sequencing library prep and data analysis	89
4.5.8 Homology analysis for PNA in clinical isolates	90
4.5.9 Error and Significance Analysis	90
4.6 Supplementary Information	91
4.6.1 Supplementary figures	91
4.6.2 Supplementary tables	99
4.7 Author Contributions	103
4.8 References.....	103
V. Chapter 5 Photoexcited Quantum Dots for Killing Multidrug-Resistant Bacteria.....	106
5.1 Abstract	106
5.2 Introduction.....	106
5.3 Results and Discussion	109
5.3.1 Photo-excited quantum dot activity against multidrug-resistant bacteria.....	109
5.3.2 Quantum dot effect is dependent on tuned energy levels	112
5.3.3 Reactive oxygen species generation by quantum dots and selective bacterial inhibition	115
5.3.4 Design of quantum dot for improved bacterial growth.....	118
5.4 Conclusions.....	119
5.5 Materials and Methods.....	120
5.5.1 Synthesis chemicals	120
5.5.2 CdTe and CdSe quantum dot synthesis and sterilization.....	121
5.5.3 CuInS ₂ quantum dot synthesis and ligand exchange	122
5.5.4 Light source for cell studies	123
5.5.5 Quantum dot degradation analysis.....	123
5.5.6 Bacterial strains and cell culture conditions	125
5.5.7 Antibiotic susceptibility testing	125
5.5.8 Colony forming unit (CFU) analysis	126

5.5.9 Statistical analysis of data	126
5.5.10 Non-growth media experiment	126
5.5.11 Growth inhibition/enhancement analysis.....	127
5.5.12 Quantum yield (QY) determination	127
5.5.13 2',7'-Dichlorofluorescin diacetate microscopy and flow cytometry	128
5.5.14 Anaerobic cell culture	129
5.5.15 Uptake bioassay of CdTe-2.4.....	129
5.5.16 Mammalian cell culture	130
5.5.17 Co-culture experiment	131
5.5.18 Cyclic voltammetry measurements (C-V)	132
5.6 Supplementary Information	132
5.6.1 Supplementary discussion: role of ROS as the therapeutic mechanism of CdTe-2.4	132
5.6.2 Supplementary figures	134
5.7 Author Contributions	151
5.8 References.....	151
VI. Chapter 6 Potentiating Antibiotics in Drug-Resistant Clinical Isoaltes via Stimuli-Activated Superoxide Generation	155
6.1 Abstract	155
6.2 Introduction.....	156
6.3 Results and Discussion	158
6.3.1 Confirmation of intracellular superoxide production	158
6.3.2 Superoxide-producing CdTe-2.4 potentiates small molecule antibiotics in MDR clinical isolates	161
6.2.3 CdTe-2.4 and antibiotic inhibition of <i>Salmonella enterica</i> infected epithelial cells and nematodes	164
6.4 Conclusions.....	166
6.5 Materials and Methods.....	167
6.5.1 Quantum dot synthesis and characterization.....	167
6.5.2 Culture conditions	167
6.5.3 Bacterial strains.....	168
6.5.4 Cloning of sodB overexpression plasmid	168
6.5.5 GIC ₅₀ measurement.....	168
6.5.6 Combinatorial experiments	169

6.5.7 <i>Caenorhabditis elegans</i> infection experiments.....	169
6.5.8 Electron paramagnetic resonance spectroscopy.....	170
6.5.9 2, 7'-dichlorofluorescin diacetate imaging	171
6.5.10 Gentamicin protection assays	172
6.5.11 LDH cytotoxicity assay.....	172
6.5.12 Error and significance analysis	173
6.6 Supplementary Information	173
6.6.1 Supplementary discussion: EPR confirmation of superoxide.....	173
6.6.2 Supplementary figures	177
6.6.3 Supplementary Tables.....	194
6.7 Author Contributions	197
6.8 References.....	197
VII. Chapter 7 <i>Escherichia coli</i> Transcriptomic Response to Superoxide Generation from Cadmium Telluride Quantum Dots	200
7.1 Abstract	200
7.2 Introduction.....	201
7.3 Results and Discussion	202
7.3.1 Characterization of CdTe-2.4 and CdSe-2.4.....	202
7.3.2 Bioinformatic analysis workflow.....	204
7.3.3 Differential expression analysis	204
7.3.4 Differentially variable gene expression analysis	208
7.3.5 Small regulatory map of gene expression and variability changes in CdTe Light	211
7.4 Conclusions.....	213
7.5 Materials and Methods.....	216
7.5.1 Quantum dot synthesis.....	216
7.5.2 RNA extraction cell growth conditions	216
7.5.3 Electron paramagnetic resonance (EPR) spectroscopy.....	217
7.5.4 EPR to determine ROS concentration.....	218
7.5.5 RNA sample prep.....	218
7.5.6 RNA-seq data processing.....	218
7.6 Supplementary Information	219
7.6.1 Supplementary tables	219

7.7 Author Contributions	235
7.8 References.....	235
VIII. Chapter 8 Conclusions	239
8.1 Summary of key findings.....	239
8.2 Thesis Conclusions	240
8.4 Future Directions	241
8.5 Concluding Remarks.....	246
8.6 References.....	247
IX. Chapter 9 Bibliography.....	249

TABLES

Table 3.1 PNA sequences conjugated to O-linker and cell penetrating peptide (KFF) ₃ K. The PNA sequences are written from the N-terminus to the C-terminus.....	44
Table 3.2 Sequencing results of α -STC target site for mutant biological replicates and no treatment control populations. Target site is in bold.....	63
Table 3.3. Primers used for gene expression analysis qPCR.....	64
Table 4.1 CLSI sensitive/resistant breakpoints for 2016-2017 ¹³ used to determine antibiotic resistance of clinical isolates.....	99
Table 4.2 Antisense-PNA molecules ordered from PNA Bio Inc. Translation start site is bold and underlined, cell penetrating peptide (CPP) KFF ₃ K is shown in capital letters, and “-O-‘ represents the “O-linker” between CPP and PNA.....	99
Table 4.3 Predicted off-targets of antisense-PNA molecules. Gene targets are listed in table with “STC” indicating that the antisense-PNA is centered on the off-targets start site.....	100
Table 4.4 Unique antibiotic resistance genes identified in clinical isolates. Italicized label represents antibiotic class the gene confers resistance to where: <i>Bla</i> is for β -lactam resistance, <i>Flq</i> is for fluoroquinolone resistance, <i>AGly</i> is for aminoglycoside resistance, <i>Phe</i> is for phenicol resistance, <i>Tet</i> is for tetracycline resistance, <i>Sul</i> is for sulfonamide resistance, and <i>Tmt</i> if for trimethoprim resistance. Non-italicized portion is the unique gene identified by ARG-ANNOT.....	101
Table 4.5 Off-targets of antisense-PNA molecules in clinical isolates. Gene targets are listed in table with “STC” indicating that the antisense-PNA is centered on the off-targets start site.....	102
Table 4.6 RT-qPCR primers used for gene expression analysis. We tried to keep the length of product between 160 and 200 nt. Since <i>ftrS</i> is a small RNA, its product was outside of this range.....	103
Table 6.1 Details for clinical isolates used in the study. All strains were selected for the high resistance to multiple antibiotics and MDR <i>S. Enteritidis</i> was selected through a screen of strains for its lethality in the infection of <i>C. elegans</i> (Figure 6.S20). All strains were isolated from a <i>Homo sapiens</i> host by the University of Colorado Hospital and are part of the University of Colorado Hospital Clinical Microbiology Laboratory culture collection....	194
Table 6.2 Concentrations of antibiotics tested (μ g/mL) for each clinical isolate bacterial strain in combination therapy.....	195
Table 6.3 Non-clinically isolated <i>Escherichia coli</i> strains used in studies.....	196
Table 6.4 Sensitive/resistant breakpoints used for determining resistance of clinical strains. 2016-2017 CLSI breakpoints ³⁷ were used were when available.....	196
Table 7.1 Statistical overrepresentation in GO classification of differentially expressed genes between conditions by molecular function, biological process, and cellular component..	205

Table 7.2 Statistical overrepresentation in GO classification by molecular function, biological process, and cellular component of less or more variable genes in CdTe Light wrt condition.	210
Table 7.3 Barcodes used for multiplexing of samples.....	219
Table 7.4 Run statistics for HiSeq sequencing of RNA samples. The 3 lanes contained the same library of multiplexed samples.....	220
Table 7.5 Demultiplexing results.....	220
Table 7.6 Results of TRIMMOMATIC trimming for adapters, quality, and length.....	221
Table 7.7 Results of alignment using Bowtie2.....	222
Table 7.8 Calculated differentially expression genes and log2 fold change in expression, with 95% confidence interval.....	223
Table 7.9 Additional calculated differentially expressed genes and log2 fold change in expression, with 95% confidence interval.....	225
Table 7.10 Genes that were significantly more variable or less variable in the first listed condition compared to respective second condition in pair. Significance was determined if the difference in coefficient of variation between the two populations was more than 2 standard deviations outside the average CV for that comparison.	231

FIGURES

Figure 2.1 RNA regulatory mechanisms during antisense transcription.	9
Figure 2.2 Mechanisms of transcriptional interference.	12
Figure 2.3 Regulatory mechanisms during antisense transcription.	13
Figure 2.4 Coupled effect of antisense RNA interaction (AI) and transcriptional interference (TI) during antisense transcription.	20
Figure 2.5 Current antibiotics (left) and essential genes (right) in <i>E. coli</i> grouped by categories	26
Figure 2.6 Visualization of therapeutic combinatorial effects.....	29
Figure 3.1 Design of antisense inhibitors against TEM-1 β -lactamase.	44
Figure 3.2 Minimum inhibitory concentration and mechanism of antisense inhibitors.	47
Figure 3.3 Re-sensitization of drug-resistant bacteria using α -STC.	49
Figure 3.4 Mutants adapted to antisense inhibitors demonstrate heterogeneity in growth rate and MIC of ampicillin.	53
Figure 3.5 Mutants adapted to antisense inhibitors demonstrate gene expression heterogeneity	56
Figure 3.S6 Optimal and suboptimal RNA structures of <i>bla</i> target regions.	65

Figure 3.S7 Growth curves in the presence of α -STC, α -RBS, α -YUNR.	66
Figure 3.S8 Ampicillin sensitivity for the parent strain.....	67
Figure 3.S9 Growth curves of mutant populations 1 and 2 and regrowth of mutant under selection pressure.....	67
Figure 3.S10 Mutant Biological Replicates.....	68
Figure 3.S11 Minimum inhibitory concentrations (MICs) for individual no treatment, mutant population 1, and mutant population 2 colonies.....	69
Figure 3.S12 Expression of <i>bla</i> and stress response genes in mutant populations adapted to antisense inhibitors.	70
Figure 3.S13 Raw data from colony forming unit analysis. 71	
Figure 4.1 Antibiotic resistance characterization of clinical isolates and design of antisense-PNA.	81
Figure 4.2 Efficacy of antisense-PNA RNA-inhibitors, evaluation of homology and efficacy, and dose-response in <i>E. coli</i> MG1655 with RT-qPCR of targets.	83
Figure 4.3 Antisense-PNA as a potentiator and adjuvant with small-molecule traditional antibiotics.....	85
Figure 4.S4 Growth curves of clinical isolates with respective treatment.....	96
Figure 4.S5 Effect of 6 antisense-PNA RNA-inhibitors on the 6 clinical isolates.....	97
Figure 4.S6 Homology of antisense-PNA RNA-inhibitors in clinical isolates.	98
Figure 5.1 CdTe-2.4 quantum dots induce light-activated inhibition of growth in MDR bacterial strains.....	111
Figure 5.2 The effect of CdTe-2.4 is specific to the reduction and oxidation potentials.....	114
Figure 5.3 Formation of intracellular redox species which do not effect HEK 293T cells.	117
Figure 5.4 Photoproliferative response using CuInS ₂	119
Figure 5.S5 STM images	134
Figure 5.S6 Size distribution histograms of the respective quantum dots.	135
Figure 5.S7 Lamp emission spectrum (blue) and filter absorbance spectra (IR – black, UV – red) at 100% light intensity.....	136
Figure 5.S8 Absorbance spectra of the CdTe quantum dots over time light and dark incubated at 37°C.....	136
Figure 5.S9 CdSe stability.	137
Figure 5.S10 Growth inhibition and CFU/mL with CdTe-2.4 in <i>E. coli</i>	138
Figure 5.S11 Effect of CdTe-2.4 on cultures in PBS.....	139

Figure 5.S12 Optical density of respective MDR strains exposed to CdTe-2.4 as a function of time and concentration.....	140
Figure 5.S13 Photo-inhibition (Equation 5.4) as a function of concentration for respective quantum dots in <i>E. coli</i> DH5 α	141
Figure 5.S14 Quantum yield evaluation.	142
Figure 5.S15 Effect on CdSe-2.4 on bacterial growth.	143
Figure 5.S16 Photo-inhibition as a function of concentration for CdSe-2.6 quantum dots in <i>E. coli</i> DH5 α	144
Figure 5.S17 Flow cytometry data for <i>E. coli</i> MG1655 in M9 medium treated with DCFH-DA	145
Figure 5.S18 Growth curves of <i>E. coli</i> MG1655 in M9 medium grown under anaerobic conditions.	146
Figure 5.S19 Optical window evaluation.....	146
Figure 5.S20 Light flux effect on therapeutic intensity.	147
Figure 5.S21 <i>E. coli</i> MG1655 in M9 uptake bioassay with CdTe-2.4 showing significant photo-inhibition ($p<0.05$) from CdTe-2.4 even after removing the quantum dots from the media.	148
Figure 5.S22 HEK 293T monocultures.	148
Figure 5.S23 HEK 293T health.	149
Figure 5.S24 Optical density of <i>E. coli</i> DH5 α in presence of respective treatment.	149
Figure 5.S25 Optical density curves of <i>E. coli</i> MG1655 in M9 media with riboflavin.....	150
Figure 5.S26 Cyclin voltammograms confirming superoxide species from molecular oxygen.	151
Figure 6.1 Light-activated QDs engineered to produce superoxide in MDR isolates.	159
Figure 6.2 QDs potentiate antibiotic activity and lower antibiotic GIC ₅₀ values.	163
Figure 6.3 Increased inhibition of bacteria in infection models with addition of stimuli-activated ROS.	165
Figure 6.4 Quantum Dot Characterization and EPR analysis.....	177
Figure 6.5 Growth curves for sodB deletion and overexpression constructs.	178
Figure 6.6 Chloramphenicol GIC ₅₀	179
Figure 6.7 Streptomycin GIC ₅₀	180
Figure 6.8 Ciprofloxacin GIC ₅₀	181
Figure 6.9 Clindamycin GIC ₅₀	182
Figure 6.10 Ceftriaxone GIC ₅₀	183

Figure 6.S11 Growth curve of clinical strains subjected to treatment with different concentrations of streptomycin and CdTe-2.4.....	184
Figure 6.S12 Growth curve of clinical strains subjected to treatment with different concentrations of ciprofloxacin and CdTe-2.4.....	185
Figure 6.S13 Growth curve of clinical strains subjected to treatment with different concentrations of clindamycin and CdTe-2.4.....	186
Figure 6.S14 Growth curve of clinical strains subjected to treatment with different concentrations of chloramphenicol and CdTe-2.4.....	187
Figure 6.S15 Growth curve of clinical strains subjected to treatment with different concentrations of ceftriaxone and CdTe-2.4.....	188
Figure 6.S16 Effect of antibiotics in combination with CdTe-2.4.....	189
Figure 6.S17 S parameter heat maps for combinations of CdTe-2.4 and antibiotics.....	190
Figure 6.S18 LDH assay results for HeLa cells under CdTe-2.4 treatment.....	191
Figure 6.S19 Raw CFU/mL data for gentamicin protection assay.....	191
Figure 6.S20 Clinical strain screen for pathogen of <i>C. elegans</i>	192
Figure 6.S21 CdTe-2.4 superoxide production.....	193
Figure 7.1 Comparison of CdTe-2.4 and CdSe-2.4 in <i>E. coli</i> and EPR spectroscopy and RNA-seq workflow.....	203
Figure 7.2 Differentially expressed genes within and between conditions.....	207
Figure 7.3 Gene expression variability within conditions highlights genes and pathways of interest.....	209
Figure 7.4 Comparison of genes with significantly higher or lower variability in CdTe Light.	211
Figure 7.5 Network of genes with differential or significantly changed variability in expression with CdTe Light.....	212
Figure 8.1. Schematic of antibiotic resistance frequency trend in soil environment compared to clinical application of antibiotics. Figure from Chait et al. 2012 Nature Chemical Biology ¹⁹	246

Chapter 1

Introduction

1.1 Approaching the post-antibiotic era

Since the introduction of the first antibiotic, penicillin, antibiotic resistance has been observed in laboratory and clinical settings¹. Antibiotic resistance was initially combated by introducing a plethora of new antibiotics during the “Antibiotic Golden Age” of the 1940’s, 50’s, and 60’s. One-half of the antibiotics still commonly used today were discovered during this time period². As antibiotic use spread across the globe and industries, misuse and overuse coupled with a sharp decrease in the number of new antibiotics¹, has led to high prevalence and dissemination of antibiotic resistance mechanisms and resistance-conferring genes. This resistance has become uncontrollable and we are now approaching the post-antibiotic era where pathogens are resistant to all available antibiotics³. In the United States in 2013, there were over 2 million illnesses and 23,000 deaths that were directly attributed to antibiotic resistance¹. Repeatedly government agencies and worldwide committees of scientists and healthcare professionals have identified the development of new antibiotics as a pressing and urgent goal^{1,4,5}.

Many of the small molecule antibiotics used currently were discovered through compound screens, commonly from soil⁶. These compounds have often been chemically modified for the development of later generations of the drug class in attempts to retain activity against drug-resistant pathogens. It is reasonably extended that bacteria have been exposed to these classes of compounds in the soil for millennia as they are produced by bacteria’s competitors, often fungi. This is clearly demonstrated by bacterial penicillin resistance before its introduction as a human antibiotic¹. These current small molecule antibiotics target only three main pathways within

bacteria: cellular replication, protein biosynthesis, and cell wall biosynthesis⁷. While these targets have proven highly successful until the onset of resistance, the high degree of resistance mechanisms already present in these pathways makes them poor targets for future drug development. By focusing outside of these three main pathways we can potentially develop antibiotics that challenge the survival of bacteria in new ways and therefore bacteria may be more susceptible to treatment and less prone to develop resistance. We sought to follow a new approach and create rationally designed antibiotics.

1.2 Thesis scope and organization

This thesis investigates the rational design of antibiotics targeting non-traditional antibiotic pathways and demonstrates their inhibition of multidrug-resistant clinical bacterial isolates as monotherapies and as potentiators of current antibiotics. We show two approaches, the design of sequence-specific antisense RNA-inhibitors (Chapters 3 and 4) and the engineering of a light-activated, tunable nanoparticle for disrupting redox homeostasis in biological systems (Chapters 5, 6, and 7).

Our first investigation into sequence-specific antisense RNA-inhibitors was targeting TEM-1 β -lactamase, a β -lactam antibiotic resistance conferring gene (Chapter 3, Courtney et al. 2015)⁸. We targeted three sites along the gene: the ribosomal binding site, translation start codon, and a secondary structure stem loop with a YUNR (pyrimidine, uracil, any nucleotide, and purine) sequence motif. We demonstrate both the ribosomal binding site and the translation start codon as effective targets for re-sensitizing *Escherichia coli* to β -lactam antibiotics by reducing translation of TEM-1 β -lactamase. The translation start codon targeting molecule was the most effective and we next adapted *E. coli* at the minimum inhibitory concentration of the therapeutic to study the mechanism of resistance. We observed gene expression heterogeneity of stress response genes

from adaptation, implying a potential bet-hedging adaptive resistance mechanism to the antisense RNA-inhibitor antibiotic combination.

Using our findings in Chapter 3, we designed six antisense RNA-inhibitors against the translation start site of essential genes in *E. coli* (Chapter 4, Courtney et al. *In preparation*). We used predictive homology to design these molecules to target sequences conserved in *Salmonella enterica* and *Klebsiella pneumoniae*. Based on our findings in Chapter 3, we designed one RNA-inhibitor against *lexA*, a repressor in stress response which had high expression variability during adaptation of *E. coli* to our TEM-1 β-lactamase targeting RNA-inhibitor. We found that these new RNA-inhibitors targeted to essential genes inhibited multidrug-resistant clinical isolates and further acted as adjuvants or potentiators in combination with small molecule antibiotics, even overcoming the clinical isolates high level of antibiotic resistance.

In parallel, we investigated redox perturbing antibiotic design by engineering specific reactive oxygen species (ROS) production from nanoparticles (Chapter 5, Courtney et al. 2016)⁹. Superoxide generation is of interest as an antibiotic mechanism due to its disruption of iron homeostasis, redox balance, and metabolism in bacteria^{10,11}. We tuned a nanoparticle for light-activated production of superoxide and confirmed its antibacterial efficacy as resulting from our rational design of material energy states. We further demonstrated that the nanoparticle was specific to bacterial inhibition in co-culture with human embryonic kidney cells.

We next demonstrated that these engineered light-activated nanoparticles function synergistically in combination with a range of traditional small molecule antibiotics against MDR clinical isolates (Chapter 6, Courtney et al. *Submitted*). We confirmed the specific production of superoxide using electron paramagnetic spectroscopy and manipulations of intracellular superoxide dismutase. The combination of our tuned nanoparticle, with a variety of both

bactericidal and bacteriostatic small molecule antibiotics across different mechanisms, demonstrated synergy. The potentiation of small molecule antibiotics by the superoxide-generating nanoparticles increased the antibiotic susceptibility of the clinical isolates. We additionally show that our designed nanoparticle in combination with small molecular antibiotics inhibited intraepithelial *Salmonella enterica* serovar Typhimurium infection and decreased mortality of our nematode model from gut infection by *Salmonella enterica* serovar Enteritidis. This work provides new insight into superoxide's link to both bactericidal and bacteriostatic antibiotic efficacy and potentiation, which to our knowledge has not been previously reported.

To further understand nanoparticle generated superoxide's antibacterial action and potentially outline future design rules for nanoparticle antibiotics, we conducted transcriptome analysis of *E. coli*. We compared the nanoparticle effect, with and without activation, to decouple material effects on *E. coli* from activated effects (Chapter 7, Courtney et al. *In preparation*). In our analysis, we found that superoxide disrupting nanoparticle activation primarily showed signs of induced anaerobic metabolism, overexpression of amino acid synthesis, and induced cross-protection for high pH and heat shock. We further found that light activation increased gene expression heterogeneity similar to our observations of stressed cells in Chapter 3.

The body of work presented in this thesis provides evidence for several new modes of antibiotic design and target pathways for antibiotics. Furthermore, these new candidate treatment modes show effectiveness against some of the most serious drug-resistant microbes currently identified. The major findings of our work and future directions for development of new classes of antibiotics are discussed in our concluding remarks (Chapter 8).

1.3 References

1. United States Center for Disease Control. *Antibiotic Resistance Threats*. (2013).

2. Davies, J. Where have all the antibiotics gone? *Can. J. Infect. Dis. Med. Microbiol.* **17**, 287–290 (2006).
3. Falagas, M. E. & Bliziotis, I. a. Pandrug-resistant Gram-negative bacteria: the dawn of the post-antibiotic era? *Int. J. Antimicrob. Agents* **29**, 630–636 (2007).
4. Tacconelli, E. & Magrini, N. *Global priority list of antibiotic-resistant bacteria to guide research, discovery, and development of new antibiotics.* (2017).
5. Laxminarayan, R., Malani, A., Howard, D. & Smith, D. L. *Extending the cure: policy responses to the growing threat of antibiotic resistance.* (Resources for the Future, 2007).
6. Lewis, K. Platforms for antibiotic discovery. *Nat. Rev. Drug Discov.* **12**, 371–87 (2013).
7. Walsh, C. Molecular mechanisms that confer antibacterial drug resistance. *Nature* **406**, 775–781 (2000).
8. Courtney, C. M. & Chatterjee, A. Sequence-Specific Peptide Nucleic Acid-Based Antisense Inhibitors of TEM-1 β -Lactamase and Mechanism of Adaptive Resistance. *ACS Infect. Dis.* **1**, 253–263 (2015).
9. Courtney, C. M. *et al.* Photoexcited quantum dots for killing multidrug-resistant bacteria. *Nat. Mater.* **15**, 485–588 (2016).
10. Keyer, K., Strohmeier Gort, A. & Imlay, J. A. Superoxide and the Production of Oxidative DNA Damage. *J. Bacteriol.* **177**, 6782–6790 (1995).
11. Keyer, K. & Imlay, J. Superoxide accelerates DNA damage by elevating free-iron levels. *Proc. Natl. Acad. Sci. U. S. A.* **93**, 13635–13640 (1996).

Chapter 2

Background

This chapter is reproduced in part with copyright permissions from the *Journal of Gene Therapy* under the principles of Creative Commons Attribution License.

Courtney, C. & Chatterjee, A. cis-Antisense RNA and Transcriptional Interference: Coupled Layers of Gene Regulation. *J Gene Ther* **2**, 1–9 (2014).

2.1 Summary

Microorganisms have coexisted in soil and over time developed defenses against one another to outcompete and thrive in a more than a millennia-long survival of the fittest competition. The first antibiotic used commercially, penicillin, was reported in 1929¹ and was discovered by chance as fungus grew on a petri dish and prevented bacterial growth in its periphery. To this day, most classes of antibiotics have been found through random screens of compounds isolated from soil and many of these compounds are therefore attributed to other fungal or microbial producers. While these antibiotics have certainly aided world health and saved countless lives by curing infections during severe outbreaks, contaminated food-stock crises, traumatic wartimes with abundant injuries, and day-to-day ailments, overuse and misuse have led to the antibiotic crisis we now face. These current antibiotics target proteins within three main pathways: cell-wall biosynthesis, cellular replication, and protein biosynthesis². Within these pathways, the small molecule antibiotics interfere with enzymes and proteins. The overwhelming resistance to the current antibiotics led us to investigate a different approach to antibiotic discovery by rationally designing antibiotics against different cellular pathways and alternative target biomolecules within those pathways. In this chapter, we review background information for the two approaches used in this work: sequence-specific antisense RNA-inhibition and engineered reactive oxygen species production by tuned nanoparticles.

2.2 Importance and complexity of antisense interactions in nature

Antisense transcription is omnipresent occurring broadly in most living organisms. Growing evidence suggests the presence of non-coding *cis*-antisense RNA's that can silence gene expression. Recent studies also indicate the role of transcriptional interference in regulating expression of neighboring genes arranged in convergent orientation. A combination of transcriptional interference and *cis*-antisense RNA interaction has the potential to add multiple-levels of regulation which can allow such a system to have a tunable and complex higher-order system response to environmental stimuli. We find these complex natural systems motivating as evidence for RNA as a biomolecule of interest for therapeutic targeting. Here we review important insights into the functional role of antisense transcription.

2.1.1 Antisense Transcription: a widespread occurrence in genomes

Proteins which regulate gene expression have been studied in great detail, however, only recently RNA is coming to light as a key regulatory molecule that controls gene expression^{3,4}. The many pathways in which RNA can regulate gene expression include non-coding RNAs which can cause epigenetic modifications⁵, RNAs which interact with proteins to alter gene expression such as the CRISPR (clustered regularly interspaced short palindromic repeats)/Cas system^{6,7}, RNA interference in eukaryotes⁸, and direct interaction between complementary antisense RNAs^{9,10} that modify expression of genes participating in various cellular processes including physiological responses, housekeeping functions, metabolism, and pathogenic processes^{10–12}. In particular, with the recent advent of RNA-sequencing technologies and tiling arrays, a large number of sense-antisense RNA transcripts have been reported in both prokaryotic^{13–19} and eukaryotic genomes^{20–23}. Thousands of antisense gene pairs have been found in the human genome, many thought to be involved in life-threatening diseases including breast cancer²⁴, pancreatic cancer^{25,26} and HIV²⁷.

Until recently, the bulk of bacterial genomes were thought to consist of protein-coding regions, however, this picture is changing drastically with exponential increase in identification of *cis*-antisense RNA in a range of bacteria and archaea including *Escherichia coli*¹³, *Salmonella enterica*²⁸, *Mycoplasma pneumoniae*¹⁸, *Synechocystis* sp. PCC 6803²⁹, *Listeria* spp.¹⁷, *Bacillus subtilis*³⁰, *Vibrio cholere*a¹⁶, *Chlamydia trachomatis*³¹, *Pseudomonas aeruginosa*³², *Pseudomonas syringae*³³, *Staphylococcus aureus*³⁴, and *Sinorhizobium meliloti*³⁵. Increasing knowledge and information about the abundance of antisense genes has caused speculation that antisense transcription is an important hidden layer of regulation^{20,36–38}.

A pair of genes are said to be antisense to each other, when they are present on opposite strands of DNA (one on sense and other on the antisense strand), with corresponding promoters convergent to each other, such that there is a partial overlap between transcripts (Figure 2.1a-c). Such convergent transcription results in the production of complementary transcripts, also known as *cis*-encoded sense-antisense transcripts (asRNAs)³⁸. Two main mechanisms have been reported to operate among such sense and antisense transcripts, namely, transcriptional interference and antisense RNA interactions^{12,39,40}. Transcriptional interference is defined as the suppressive influence of one transcriptional process on an adjacent transcriptional process occurring in *cis* due to RNA polymerase (RNAP) traffic along the DNA³⁹ and has been reported in a number of studies in both prokaryotic^{36,41–43} and eukaryotic systems^{37,44,45}. Adding a layer of complexity, *cis*-encoded antisense RNAs generated from opposite strands of the DNA have the potential to form extensive base-pairing interactions with corresponding sense RNAs^{46,47} and target them for either transcriptional attenuation (Figure 2.1a), translational inhibition (Figure 2.1b), or RNA degradation (Figure 2.1c)^{40,48–50}.

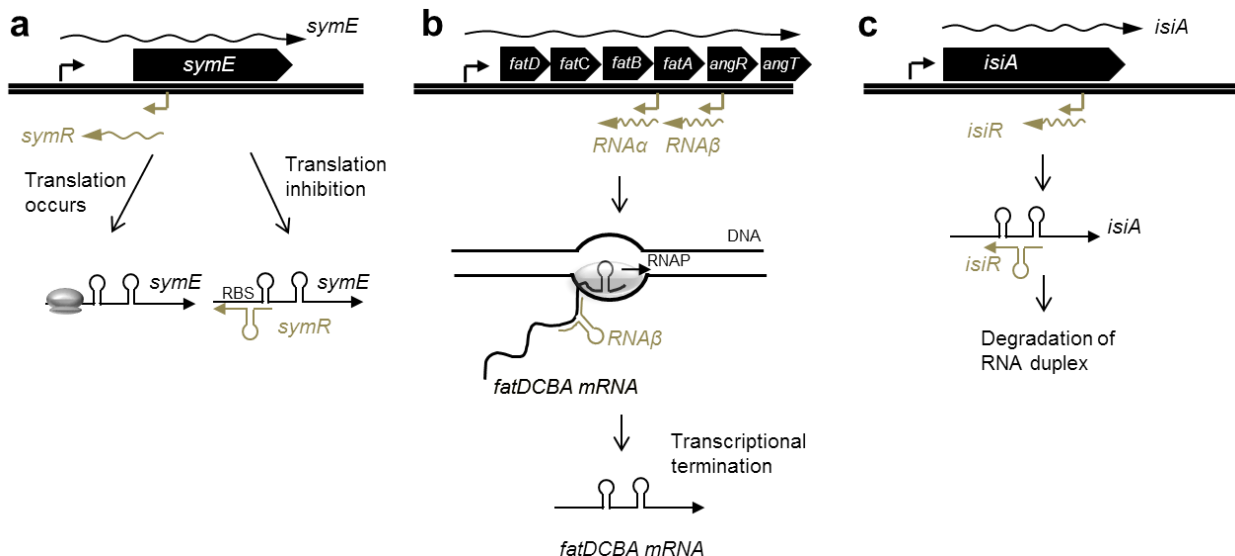


Figure 2.1 RNA regulatory mechanisms during antisense transcription. Sense and antisense RNA are indicated in black and grey respectively, the black block arrows represent protein coding regions/open reading frames (*orf*), 5' UTRs are the regions upstream of the *orf*. Three regulatory mechanisms are shown. (a) Translational inhibition: In *Escherichia coli*, binding of asRNA *symR* to *symE* blocks the RBS of *symE* mRNA, preventing production of toxin-like endonuclease SymE. (b) Transcriptional attenuation: In *Vibrio anguillarum* binding of *RNAβ* to a nascent *fatDCBA-angRT* transcript induces premature termination after *fatA* gene, resulting in high expression of *fatDCBA* mRNA and low expression of *angRT* mRNA. (c) RNA degradation or cleavage: In *Synechocystis* sp. PCC 6803, binding of asRNA *isiR* to *isiA* mRNA induces degradation of the duplex.

Much of the work on antisense transcription focuses either on the role of transcriptional interference alone or antisense interaction alone. Models have been created to individually characterize the effects of antisense interactions^{10,12,50} or transcriptional interference^{42,51,52} but little work has been reported on combined interference studies³⁶. We consider both these mechanisms, and the prospect of higher order system behavior when both of these mechanisms occur simultaneously.

2.1.2 Antisense RNAs and RNA interaction mechanisms in bacteria

cis-Antisense RNA are produced when transcription occurs from the DNA strand opposite to a transcriptional unit (Figure 2.1a-c). *cis*-Antisense RNA's tend to overlap either at the 5' end (head to head overlap), such as the *prgQ/prgX* gene pair of *E. faecalis*³⁶, *MgtC/AmgR* sense

antisense pair in *S. enterica*⁵³, *hok/sok* toxin-antitoxin system in *E. coli*⁵⁴; or at the 3' end (tail to tail overlap), such as in the case of *alr1690*, which overlaps the adjacent gene *all1691* gene encoding the ferric uptake regulator in *Cyanobacterium Anabaena* sp. PCC 7120⁵⁵ and *tpxA/ratA* sense-antisense pair in *B. subtilis*¹¹. *cis*-antisense RNAs can exist in various sizes in naturally occurring systems, ranging between short antisense RNAs, such as the 69 nt Sar RNA of bacteriophage 22⁵⁶, 77 nt *SymR* RNA of *E. coli*⁵⁷, 77 nt OOP RNA of bacteriophage λ ⁵⁸, and 104 nt Anti-Q RNA of *E. faecalis*³⁶, and long antisense RNA's, such as the 1200 nt *AmgR* asRNA of *S. enterica*, 2 kb Anti2095 RNA of *Listeria monocytogenes*¹⁷, and 7kb MED4 RNA of *Prochlorococcus spp.*⁵⁹.

Similar to proteins, RNA molecules require specific secondary and tertiary structures in order to be functional^{46,50,60,61}. Frequently, the interaction between two or more RNA molecules is catalyzed via single-stranded regions such as hairpins, stem loops, and bulges⁹. Typically, binding of sense/antisense RNA can cause three kinds of outcomes: (i) translational inhibition due to blocking of the ribosome binding site⁵⁷, (ii) RNA degradation due to action of RNases (RNases III, E, etc.)^{50,62}, and (iii) transcriptional attenuation due to structural changes which destabilize RNAP:RNA complex and consequently terminate transcription⁶³. Translational inhibition is exemplified by the regulation of *symE* mRNA, encoding the toxin-like endonuclease SymE in *E. coli*, by the asRNA *symR*⁵⁷. The *symE/symR* transcripts overlap at the 5' end, and include the ribosomal binding site (RBS) and start site of *symE* (Figure 2.1a). The *symE/symR* duplex results in blocking of the RBS of *symE*, thus preventing translation of *symE* transcript. Similarly, in *S. aureus* binding of asRNA *sprAIAS* to the Shine-Dalgarno sequence and AUG start site of *sprAI* mRNA prevents the translation of *sprAI* mRNA, thus inhibiting expression of the toxin SprAI⁶⁴ A

similar mechanism is shared by a number of Type I toxin-antitoxin systems, including *hok/sok* gene pair in *E. coli*, *tpxA/ratA* gene pair in *B. subtilis* and RNA I/RNA II systems in *E. faecalis*¹¹.

Transcriptional attenuation is exemplified by the interaction of *RNAβ* with the *fatDCBA* mRNA to induce transcriptional termination after the *fatA* gene in the *fatDCBA-angRT* operon in *Vibrio anguillarum*⁶⁵ (Figure 2.1b). This results in high levels of expression of *fatDCBA* mRNA, and consequently low levels of expression of *angRT* mRNA. In *E. faecalis*, the interaction between the 104 nt short asRNA Anti-Q produced from the *prgX* operon and the complementary *prgQ* mRNA prevents elongation of the nascent *prgQ* transcript past a putative terminator, causing premature termination of *prgQ* transcript via inhibition of anti-terminator formation⁶³.

Regulation of RNA stability due to antisense interaction is exemplified by the asRNA *gadY* which binds to polycistronic *gadXW* transcript to induce RNaseIII mediated cleavage and release of monocistronic *gadX* and *gadW* transcripts⁶⁶. Similarly, the 77nt *OOP* RNA of λ phage interacts with *CII* mRNA and targets it for degradation via RNaseIII-dependent cleavage, thus preventing production of the CII repressor⁵⁸. The *isiA/isiR* sense-antisense pairs in *Synechocystis sp PCC 6803* form a duplex, which causes degradation of the *isiR* mRNA, though via an unknown mechanism⁶⁷ (Figure 2.1c). On the other hand, binding of *MED4* asRNA to polycistronic complementary RNA, in fact, protects the latter from RNaseE mediated cleavage by protecting the RNaseE recognition sites, thereby affording stability to the polycistronic mRNA⁵⁹. Similarly, in *E. faecalis* the interaction between Qs RNA, produced from the *prgQ* operon, and the complementary *prgX* transcript causes RNaseIII-dependent cleavage of 5' UTR of the *prgX* mRNA which in turn enhances translation of the *prgX* mRNA⁶⁸.

2.1.3 Transcriptional Interference: mechanisms and switch response

Transcriptional interference occurs when one transcriptional process suppresses an adjacent transcriptional process due to RNAP traffic along the DNA³⁹ and has been reported in a number of studies in both prokaryotic^{41–43} and eukaryotic systems^{37,44,45,69}. Transcriptional interference utilizes RNAP traffic to control gene expression and serves as a short-cut to gene regulation as it can interfere with transcriptional initiation, elongation as well as termination³⁹. Transcriptional interference can occur via four mechanisms: (i) RNA polymerase collision, whereby elongating RNA polymerase fired from both the promoters collide with each other (Figure 2.2a), (ii) sitting Duck model, in which an elongating RNAP collides with a stationary RNAP (Figure 2.2b), (iii) road block model, where a DNA bound protein complex hinders RNAP movement along the DNA (Figure 2.2c), and (iv) occlusion model, where movement or binding

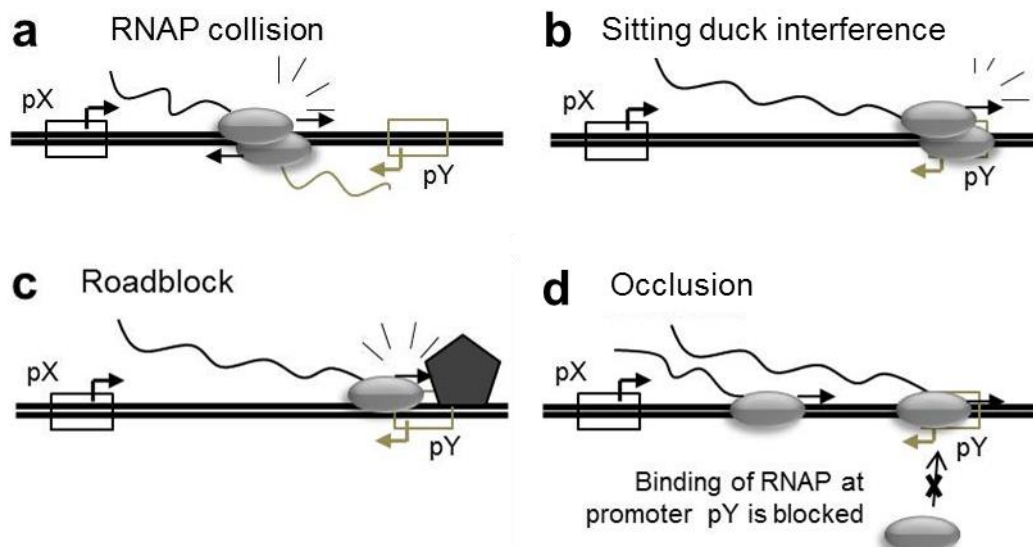


Figure 2.2 Mechanisms of transcriptional interference. Schematic of a general system of convergent promoters pX and pY is shown. As an example pX is shown to be the aggressive promoter. Four modes of transcriptional interference are shown. (a) RNAP collision, converging RNAPs collide within the overlapping DNA. (b) Sitting duck collision, an elongating RNAP from pX collides with a stationary RNAP at the weaker pY promoter. (c) Roadblock, DNA bound protein complex proximal to pY hinders an elongation complex from pX. (d) Promoter occlusion, binding of RNAP at the pY promoter is hindered by elongation complex from pX (or by binding of RNAP at pX when the distance between pX-pY is short, not shown here).

of RNAP at one of the promoters blocks RNAP from binding at the other promoter (Figure 2.2d), potentially also causing competition for activators³⁹.

During convergent transcription for successful transcription to occur RNAPs need to traverse the length of overlapping DNA to form a full-length transcript. Co-transcription from such a locus either results in successful transcription where RNAPs continue elongation in absence of converging RNAPs from the opposing promoter, or failed transcription when converging RNAPs collide, causing one or both RNAPs to fall-off the DNA (Figure 2.3). While a significant fraction of collided RNAPs fall off the DNA, a fraction of collided RNAPs backtrack and resume movement along the DNA after a temporary stall⁷⁰. For set of two general convergent promoters pX and pY (Figure 2.3), the frequency of RNAP collision due to co-transcription from both the promoters depends on multiple factors: (i) relative strengths of promoter pX and pY, (ii) length of

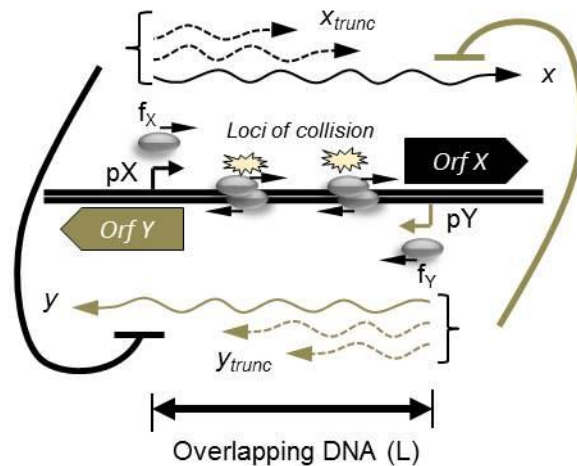


Figure 2.3 Regulatory mechanisms during antisense transcription. Schematic of a general system of convergent promoters pX and pY driving the expression of genes X and Y respectively, the black and grey block arrows represent protein coding regions/open reading frames (*orf*). The overlapping DNA between the pX-pY promoters is indicated by length L. RNAPs fire from pX and pY with frequency f_X and f_Y respectively. Successful transcription results in expression of full length transcripts x and y (bold arrows) from pX and pY respectively. During RNAP collision one or both of the elongating RNAP's fall off the DNA giving rise to different sizes of truncated RNA x_{trunc} and y_{trunc} (dashed arrows) from pX and pY respectively depending on the loci of RNAP collision. Full-length and truncated RNA share extensive base-pairing and potentially exert antisense interactions on each other.

overlapping DNA between the two promoters (the probability of RNAP collisions increases with distance), (iii) sequence context of overlapping DNA.

Under biologically relevant conditions the relative strengths of promoters pX-pY can vary between two states, one in which pX is more aggressive than pY promoter, i.e. rate of RNAP firing from pX promoter (f_X) is higher than that from pY (f_Y) and other in which pY promoter is more aggressive than pX (i.e. $f_X < f_Y$). In state 1, the RNAPs firing from the aggressive promoter pX are more likely to succeed in making a successful x transcript and RNAP collision would be more fatal for pY promoter with little or no production of successful y transcripts (Figure 2.3). When pX is the aggressive promoter, most of the collisions would occur proximal to the weaker promoter pY as has been seen for the convergent promoters pR-pL of coliphage 186⁴¹ and P_Q-P_X of pCF10 plasmid in *E. faecalis*^{36,71}. Similarly, the opposite holds true for state 2 when pY is the more aggressive promoter. RNAP collisions would exert greater suppression of x expression in state 2, compared to y expression. This is exemplified by studies on the *gal7* and *gal10* genes of *S. cerevisiae*, where arranging genes in convergent orientation suppresses transcription from this region due to increased RNAP collision⁴⁴.

Although it was first thought that only transcriptional interference from strong promoters could affect weak promoters, both mathematical modeling^{36,42,51,72} and experiments^{36,41,42} suggest that minor differences in strengths of convergent promoters can give rise to significant transcriptional interference. Stochastic simulations and experimental analysis of convergent transcription in the P_R-P_{RE} promoter pair of bacteriophage λ showed a 5.5 fold change in expression from the stronger P_R promoter due to interference from the weaker P_{RE} promoter⁴². This was attributed mainly to the presence of RNAP initiation complexes at the weaker promoter,

which acted as sitting ducks for collision with elongating RNAP originating from the stronger promoter, such as that seen in the pR-pL promoters of coliphage 186⁴¹.

The probability of RNAP collision depends on the residence time of converging RNAPs in the overlapping DNA. If the length of the overlapping DNA is short then occlusion effects are more likely⁷³. For longer overlapping DNA (>>RNAP footprint), occlusion effects can be neglected and RNAP collision is the more dominant mechanism of transcriptional interference. RNAP collision is also more pronounced when the overlapping distance is increased⁴¹ or when the velocity of RNAP decreases within the overlapping region due to the presence of pause sites as reported for P_R-P_{RE} promoter pair in bacteriophage λ⁴². Both these effects can increase the net residence time of RNAP in the overlapping region, thus increasing the probability of RNAP collision.

During antisense transcription, under biologically relevant conditions where the relative strengths of promoters pX-pY vary between two states, the net effect of transcriptional interference tends to amplify the gap between expression levels of full length transcripts *x* and *y*, compared to a case if the promoters were arranged in tandem. In cases where pX and pY drive expression of genes which give rise to opposing phenotypes, transcriptional interference can serve as an important gene regulatory mechanism that can give rise to switch-like behavior. This is exemplified by the role of transcriptional interference in conferring a bistable genetic-switch behavior to the *prgQ/prgX* operon controlling the conjugative transfer of drug-resistance plasmid pCF10 between donor and recipient cells in pathogen *E. faecalis*³⁶. It was shown that under a “conjugationally-incompetent” or “off” state, expression from a repressed P_Q promoter (driving *prgQ* expression) decreased 90 fold due to convergent transcription from an equally strong P_X promoter (driving *prgX* expression). On the other hand, in a “conjugationally-competent” or “on”

state, transcription from the Px promoter had only marginal effect on the transcription from a 10-fold stronger de-repressed P_Q promoter, causing expression of the 530 nt Q_L RNA capable of inducing conjugation-causing genes in the donor cell. Transcriptional interference has also been shown to facilitate two distinct bistable phenotypes in infectious pathogen *Bordetella bronchiseptica*⁷⁴. The interference causes two populations to exist in the lungs: Bvg⁺ responsible for the *in vivo* infectious state and Bvg⁻ responsible for survival *ex vivo*. The interference which causes these bistable phenotypes allows the infection to thrive in the lungs and survive to infect others.

2.1.4 Wreckage of RNAP collision: a source of antisense RNA?

During antisense transcription, collision between converging RNAPs results in premature termination of transcriptional progress of one or both elongation complexes, thus giving rise to a mixture of truncated and full length sense and antisense RNA sequences³⁶. Depending on the relative firing rates of RNAP and overlapping sequence, converging RNAPs may collide at various loci along the DNA, thus giving rise to a distribution of different sizes of truncated RNA both in the sense and antisense direction (denoted by X_{trunc} and Y_{trunc} in Figure 2.3). A less explored aspect of transcriptional interference relates to the potential regulatory role of such truncated RNA. It is plausible that truncated transcripts with a certain minimum size possess secondary structures that can cause interaction with antisense counter transcripts. Though the sequence of overlapping DNA would vary between different systems, the advantage of antisense transcription is that it allows for extensive base pairing between truncated RNA and the full-length antisense counter transcripts, hence enhancing the probability of RNA interaction. Both short antisense-RNAs^{54,56–58,75,76} and long antisense RNA^{17,53,77,78} have been shown to participate in antisense interaction in various bacterial systems. Therefore it is possible that the resulting sense, antisense RNA hybrid

complexes between truncated and full-length RNA may be subjected to similar mechanisms of RNA degradation, transcriptional attenuation or translational inhibition^{9,50}.

The presence and functional role of truncated RNA produced as a result of RNAP collision have been shown for the *prgQ/prgX* operon of pCF10 plasmid in *E. faecalis*³⁶. Under repressed conditions when effect of transcriptional interference is more pronounced in *prgQ/prgX* locus, truncated P_Q and P_X transcripts of sizes ranging between approximately 100-200 nt and 80-200 nt respectively are observed, all which lie within the overlapping region of 223 bp of *prgQ/prgX* genes. Under derepressed conditions when transcriptional interference effects were less pronounced, truncated RNA are less abundant. Northern analysis showed that overexpression of a 223 nt truncated P_Q RNA *in trans* repressed expression of *prgX* mRNA, whereas overexpression of a 104 nt truncated P_X RNA *in trans* repressed expression of *prgQ* mRNA, thus indicating that truncated RNA are capable of suppressing the expression of counter transcripts. Similarly in the *ubiG/mccBA* operon of *Clostridium acetobutylicum* truncated RNA of various sizes ranging between 200-700 nt lacking Rho-dependent terminator structures at 3' end were found⁷⁹. The expression of the truncated RNA was independent of RNase III and RNase J1/J2 cleavage, which could potentially hint at RNAP collision based termination mechanism. Northern analysis of sense-antisense transcripts in higher eukaryotes such as mouse and *A. thaliana* indicates the presence of shorter transcripts that lack poly-A tail and are nuclear localized³⁷. These truncated transcripts have been found to be richer at 5' ends compared to 3'ends (poly A rich), thus indicating that these could be an outcome of transcriptional interference or local sense, antisense effects.

With exception of few studies^{36,72,79,80}, the presence of truncated RNA has not yet been vigorously investigated in systems with antisense transcription. The plethora of *cis*-antisense non-coding RNAs found in bacteria could potentially be the wreckage of RNAP collision due to

transcription from conditionally activated hidden promoters, thus hinting that this could be rather a ubiquitous phenomenon.

2.1.5 Coupled effect of Transcriptional interference and Antisense RNA interaction

The combined effect of transcriptional interference and antisense interaction between truncated and full-length sense and antisense RNA can further sharpen the switch response compared to when only one of these mechanisms exist. Transcriptional interference can potentially give rise to two-fold regulation, (i) reduction of full-length transcript levels due to RNAP collision, (ii) generation of truncated RNA capable of exerting antisense interactions on counter transcripts. Four potential combinations of transcriptional interference and antisense regulation effects are shown in Figure 2.4a-d. The sharpest switching response is likely to when both these mechanisms occur simultaneously (Figure 2.4e-f). Depending on the relative strength of promoters pX-pY, the loci of collision will shift towards the weaker promoter. If we consider pX is the stronger promoter, collisions would occur near the pY promoter, thus the truncated RNA from pY would be very short and unlikely to interact with sense pX RNA. In this case, the majority of the truncated sense pX RNA will have nearly the length of overlapping region, and hence possess a higher potential to interact with a nascent pY transcripts. Therefore, even if a nascent pY transcript escapes RNAP collision, it would still be swamped by the relatively large pool of truncated sense pX RNA (Figure 2.4e). The relative stoichiometry of sense and antisense would influence the final extent of suppression. The situation would be reversed when pY becomes the stronger promoter (Figure 2.4f).

Antisense transcription can result in complex cellular behavior, especially in the context of a biological gene network. Since antisense transcription can amplify the gap between transcript expression between two physiologically different states, such a gene regulatory mechanism is

capable of showing reciprocal switch like behaviors such as bistable switch response in *prgQ/prgX* operon of *E. faecalis*^{36,8081} and *scbA/scbR* operon of *S. coelicolor*⁷². Antisense transcription from the *prgQ/prgX* locus of conjugative plasmid pCF10 of *E. faecalis*, allows controlling the expression of long *prgQ* mRNA, which induces expression of downstream conjugation-causing genes. Transcriptional interference from downstream Px promoter, as well as, antisense RNA interaction exerted by a 104 nt non-coding Anti-Q RNA expressed from the Px promoter, causes premature termination of a nascent *prgQ* transcript, thus preventing the conjugative transfer of pCF10 plasmid. Both experiments and mathematical modeling showed that for this system bistable switch behavior was only observed when both mechanisms of transcriptional interference and antisense interaction operate simultaneously. Using mathematical modeling it was shown that antisense transcription confers a bistable switch to the *scbA/scbR* gene pair of *S. coelicolor*, which allows regulation of expression of *scbA* mRNA, which encodes the key enzyme ScbA involved in synthesis of γ -butyrolactones that regulate antibiotic biosynthesis in the *S. coelicolor*⁷².

In *ubiG/mccBA* operon of *C. acetobutylicum*, both mechanisms of transcriptional interference and RNA interaction confer a genetic switch regulating the expression of *ubiG* operon, which contains genes required for conversion of methionine to cysteine⁷⁹. In presence of methionine, transcription from the stronger T-box promoter causes premature termination of the antisense S-box transcripts. As a result, the levels of S-box riboswitch antisense RNA decreases, which in turn increases the expression of full length *ubiG* mRNA, which encodes enzymes required for conversion of methionine to cysteine. On the other hand, under conditions of high levels of cysteine, transcription from the downstream S-box promoter tends to reduce the expression of *ubiG* mRNA. Similarly, antisense transcription from the *icsA/RnaG* locus of virulence plasmid

pINV of *Shigella flexneri*, allows controlling the expression of *icsA* mRNA, which encodes an invasion protein required for colonization of host by the bacterial pathogen⁸². This locus encodes a non-coding antisense *RnaG* RNA, which overlaps with *icsA* mRNA at the 5' end, and has been shown to cause premature termination of *icsA* mRNA following a transcriptional attenuation mechanism⁸². In addition to antisense RNA interaction mediated regulation, the stronger *RnaG* promoter exerts transcriptional interference on the weaker *icsA* promoter P_{*icsA*}, further reducing the activity of the latter.

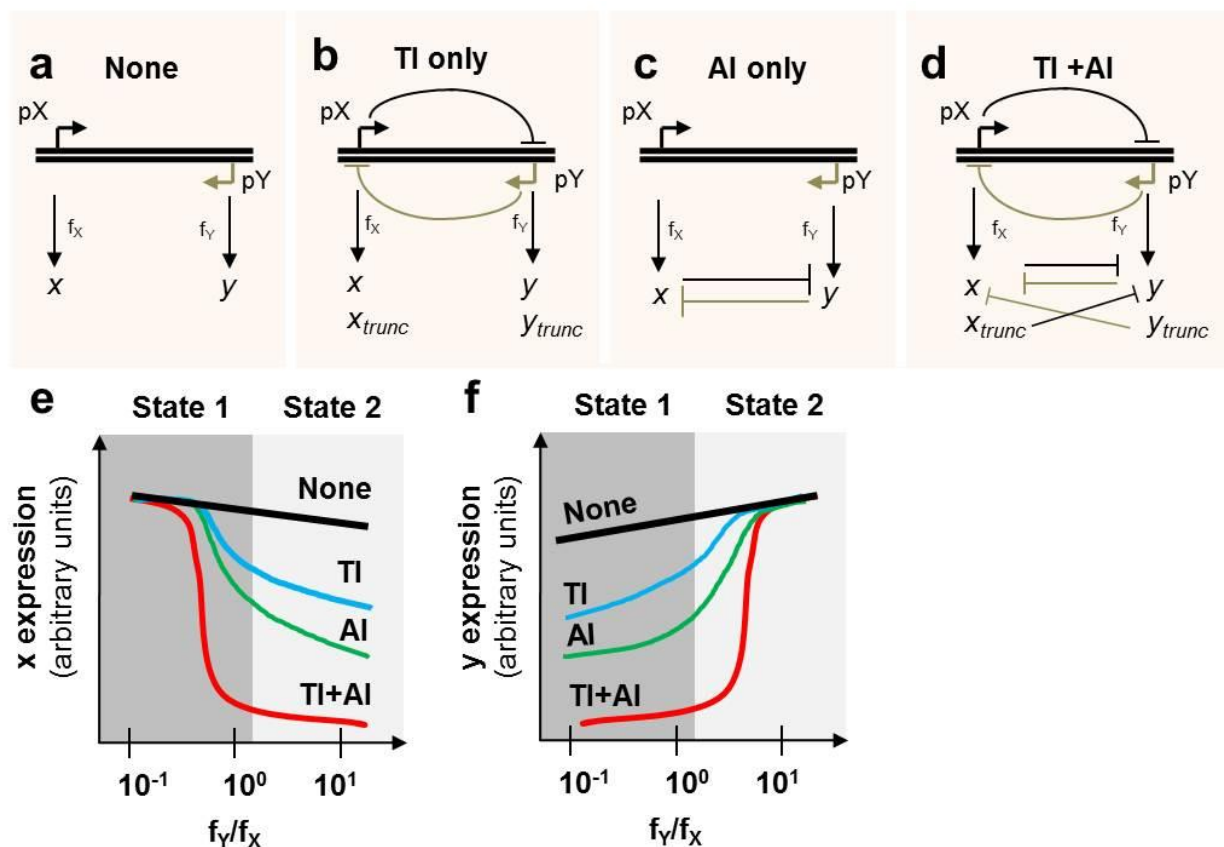


Figure 2.4 Coupled effect of antisense RNA interaction (AI) and transcriptional interference (TI) during antisense transcription. (a-d) Schematic showing four possible combinations of mechanisms of transcriptional interference (TI) and Antisense interaction (AI) regulating expression from pX and pY: None (a), TI only (b), AI only (c), both TI and AI (d). (e-f) Steady state levels of full-length RNA x (e) and y (f), expressed from promoters pX and pY respectively, for various ratios of f_y/f_x for the four cases considered in a-d. For a system transitioning from one value of f_y/f_x to other, maximum switching response occurs when both TI and AI effects are present.

2.1.6 Outlook: Antisense transcription a widespread mechanism of gene regulation

Antisense transcription is omnipresent in bacteria, archaea, and eukaryotic genomes. One could argue that shorter prokaryotic genomes use antisense transcription for conserving space, however presence of thousands of such *cis*-antisense gene pairs in relatively larger eukaryotic genomes^{20–23} clearly refutes such an argument and points towards potential role of antisense transcription as a mechanism of gene regulation conserved over evolution⁸³. A large fraction of mechanistic studies on antisense transcription have been performed in prokaryotic systems which are characterized by shorter intergenic distances^{36,41–43,50}. There are many systems yet to be characterized that hypothetically will exhibit both antisense interactions and transcriptional interference. The large number of *cis*-oriented promoters found in bacteria, yeast, flies, HIV, and mouse⁵² may lead one to speculate why these systems are so prevalent in nature and what is their role in gene regulation and phenotype determination.

Antisense transcription may have a more pronounced effect in systems with a longer overlapping region, found commonly in mammalian genomes²⁰. It is interesting to note that in a large fraction of convergent promoter based gene pairs in mammalian genomes, often one out of the two genes tends to express non-coding RNA⁸⁴, potentially opposing the coding RNA. In many cases, such convergent transcription gives rise to reciprocally regulated switch^{37,84}. Bioinformatics techniques are being used to identify *cis*-antisense pairs in order to characterize more of these systems in diverse species. Using bioinformatics, the prevalence of *cis*-oriented genes has been reported to be: 26.3% in humans^{21,85,86}, 21.9% in mice^{20,87–89}, 16.8% in drosophila^{90,91}, 2.8% in *C. elegans*, 15.8% in sea squirt, 6.6% in chickens, 4.5% in rats, 4.3% in frogs, 2.2% in zebrafish, 3.8% in cows⁸⁹, and 8.9% in Arabidopsis^{91–93}. While bioinformatics has been useful to identify *cis*-antisense loci, the extent of the activity of these non-coding RNAs and the exact function of

most sense, antisense pairs remains to be determined^{38,94}. Moreover, a concerted effort is required to examine these systems for antisense interactions and transcriptional interference to determine their combined role in regulating gene expression levels and phenotype determination.

We highlight the regulatory advantage that cells can achieve via coupled role of transcriptional interference and *cis*-asRNA based regulation during antisense transcription. Importantly, antisense transcription and RNA regulation offer a number of control advantages over regulatory proteins. In general, regulatory proteins take a longer time to act since both steps of transcription and translation are required for the proteins to be functional, compared to asRNA which only require transcription. For *trans*-asRNA based regulation the relative stoichiometry of sense and antisense RNA influences the final extent of suppression allowing tight control over therapeutic effect. Given the plethora of sense, antisense pairs in both prokaryotic and eukaryotic genomes, the next obvious question to ask is whether sense, antisense pairs are being regulated by both transcriptional interference and antisense regulation at a genome scale. From a synthetic biology point of view, antisense transcription could be exploited to tweak naturally existing networks or create novel networks for obtaining desired characteristics through antisense RNA-targeting. These complex, RNA regulated systems that defined cellular outcomes including conjugation and pathogenicity highlight our interest in targeting RNA for antimicrobials.

2.3 Antisense therapeutics: sequence-specific targeting

Antisense therapy for use as antimicrobials unveils the ability to quickly design antibiotics in non-traditional antibiotic pathways for any gene of interest by simply knowing the organism of interest's genome sequence. Further, these antisense antimicrobials are sequence-specific allowing for greater control over which cell types are targeted. The sequence specificity can allow for a reduction in broad-range effects from current antibiotics and possibly prevent or reduce eradication

of the patient gut microbiome during antibiotic courses. Below we review our approach to the design of antisense antimicrobials and their advantages as antimicrobial agents.

2.3.1 Problems with broad-spectrum antibiotics

Many small molecule antibiotics are broad-spectrum, meaning they non-specifically kill both Gram-negative and positive bacteria. While broad range activity is sometimes essential, it has also led to problems by providing an avenue for opportunistic pathogens, like *Clostridium difficile*, as well as increasing the antibiotic resistance of the post-antibiotic course patient microbiome⁹⁵. This increase in microbiome antibiotic resistance is due both to the enrichment of those bacteria who survive the antibiotic course and the lateral transfer of resistance genes. The residence time of these antibiotic resistance genes after antibiotic-course can be over one year and it has been proposed that this could increase the likelihood of dissemination of resistance characteristics to future human pathogens⁹⁶.

While these long-term changes to the resistome of the microbiome can be detrimental, the immediate changes to the microbiome can also allow for resistant, opportunistic pathogens to thrive in absence of microbiome pressure against colonization⁹⁷. *C. difficile* is perhaps the most known for causing infection after antibiotic treatment since it cannot thrive in the presence of an undisrupted microbiome. While *C. difficile* used to be considered somewhat of an antibiotic treatment side-effect, it is now being observed outside of hospitals in individuals who have not recently undergone antibiotic treatment⁹⁸. This spread of opportunistic pathogens and the possibility for dissemination of resistance genes to the environment from broad-spectrum antibiotic treatment highlights the need for pathogen-specific antibiotics. It was shown by Mondhe et al. that gene specific, antisense therapeutics could be useful in targeted sequences conserved in pathogens and absent in the microbiome⁹⁹. This approach could allow for pathogen-specific

antibiotic development and lower disruption of the microbiome and its resistome, further motivating the rational design of antibiotics using antisense targeting.

2.3.2 Synthetic nucleic acids

While antisense interactions in nature occur between RNA molecules with reverse complementary regions, RNA's poor pharmacokinetic properties, including low stability and poor transport, make it less than ideal for therapeutic applications¹⁰⁰. While conjugation or encapsulation of RNA has been an area of focus for increased transport and improved stability^{101,102}, there have also been efforts to create synthetic nucleic acids and remove the use of native RNA as a therapeutic agent entirely. Synthetic nucleic acids have modified backbones for altered stability and/or transport and nucleic acid functional groups. There are currently six synthetic nucleic acids: 1,5-anhydrohexitol, cyclohexene, threose, glycol, locked, and peptide nucleic acids¹⁰³. All of these synthetic nucleic acids utilize the same four nucleobases and all except peptide nucleic acids (PNA) have a triphosphate-based backbone. PNA are synthetic nucleic acids which have a backbone of N-(2-aminoethyl)-glycine units that are linked by peptide bonds and maintain DNA and RNA-like spacing of the nucleic acid functional groups it displays¹⁰⁴. This structure allows for the maintenance of sequence-specific antisense binding via Watson and Crick base pairing. Another benefit of PNA is that it binds more strongly to native nucleic acids than DNA or RNA because of reduced electrostatic repulsions due to its neutral backbone. This neutral backbone, however, leads to problems in transport across cellular membranes which have largely been mitigated by conjugation to charged peptides. Studies have shown that the choice of conjugated peptides can be specific for transport across the target organisms cell membranes further increasing control over non-specific effects¹⁰⁵.

Once a PNA of interest has been designed for its sequence-specific target, the antisense interaction is found to occur with greater affinity for RNA than DNA leading to reduced translation by blocking ribosomal binding or migration¹⁰⁶. This gene knockdown effect can hypothetically be applied to any gene of interest in any organism, given the proper transport peptide is conjugated and the proper region of the target gene is selected to have a high effect. It has been shown that target regions primarily at the translation start codon, ribosomal binding site, or 5' untranslated region are effective at reducing gene expression¹⁰⁷. While PNA has been explored largely for protein coding mRNA¹⁰⁸ it has also been shown to effectively target and change the activity of non-coding RNA targets. Targeting of non-coding RNA could allow disruption of complex cellular antisense systems and RNA regulation mechanisms such as those required for conjugation and pathogenicity described above. Further, peptide-PNA conjugates have been shown to have high residence times and accumulate in bacteria allowing for a constant and prolonged antibiotic pressure which could help in mitigating the development of drug resistance¹⁰⁹. These aspects combined, make PNA an interesting candidate for engineering synthetic antisense interactions.

2.3.3 Antisense antibiotic target selection

With the ability to target any sequence of interest, the question becomes what to target for antibacterial purposes. We find two main goals motivating: inhibiting bacteria by knocking down genes essential for viability and/or targeting antibiotic resistance and pathogenicity conferring genes. The model bacterium, *Escherichia coli*, has a well-characterized set of essential genes¹¹⁰ which compared to the current targets of small molecule antibiotics highlights the potential use of antisense therapy for designing antibiotics in non-traditional antibiotic pathways (Figure 2.5). With over 1,600 unique resistance genes identified in the NCBI GenBank database¹¹¹, there is an overabundance of potential antisense targets for PNA against antibiotic resistance-conferring

genes. For the scope of this thesis, we explore both a small set of essential genes, coding and non-coding, as well as an antibiotic resistance-conferring gene.

2.4 Reactive oxygen species for antimicrobial activity

Bacterial cells that grow in aerobic environments regularly experience physiological levels of reactive oxygen species (ROS) which play a key role in cellular processes such as metabolism, pathogenicity, and signal transduction. Hydrogen peroxide and superoxide are the primary reduced oxygen species that exist in bacteria as byproducts of aerobic respiration and metabolism¹¹². Though superoxide occurs naturally, elevated levels create a multitude of deleterious effects^{113–116} and it has been implicated in antibiotic efficacy and the emergence of drug resistance. We review below our approach to designing a superoxide-based antibiotic.

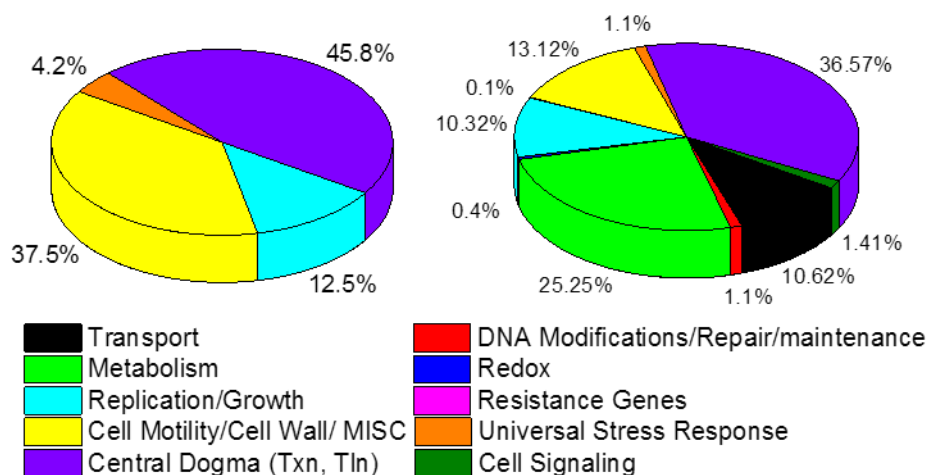


Figure 2.5 Current antibiotics (left) and essential genes (right) in *E. coli* grouped by categories demonstrating the disparity between current antibiotics and available essential genes for targeting with antisense therapies.

2.4.1 ROS role in antibiotic resistance

Elevation of intracellular ROS during bactericidal antibiotic treatment has been studied as a result of treatment or possibly as a mechanism of action for the antibiotics^{117–120}. Antibiotic-induced ROS has further been shown to play a role in bacteria obtaining drug resistance¹²¹.

Kohanski et al. 2010 showed that sub-lethal levels of antibiotics produce ROS which causes antibiotic resistance through mutagenesis. Sub-lethal levels of antibiotic are often postulated as a large competent of the misuse of antibiotics that has led to the current antibiotic resistance crisis. If ROS are indeed part of the mechanism of action of bactericidal antibiotics, keeping the intracellular ROS elevated for deleterious effects and cell death rather than low for mutagenesis could be key in preventing the development of antibiotic resistance.

Elevated ROS has also been shown effective in reducing the prevalence of *Mycobacterium tuberculosis* persisters.¹²² Persisters are bacterial cells which enter a dormant state under stress and typically makeup only a small fraction of a bacterial population in culture. When the stress is removed or depleted, the dormant cells are again able to grow. The persister phenotype is not a resistant or tolerant state but rather a switch. If regrown, the persister cells remain sensitive to the stress and the stress will again reduce the bacterial population to the same fraction of persister cells¹²³. Persister cells are implicated in chronic infection and the eventual development of drug resistance so the ability to potentially kill this population with further elevated ROS could improve antibiotic efficacy.

2.4.2 Superoxide specific toxicity

In this work, we focus on one primary ROS, superoxide. We find superoxide interesting as a ROS of interest because of its longer lifetime compared to hydroxyl radical, allowing it to diffuse within the cytosol to different targets and the suggestion that it potentiates oxidative damage in cells by the following mechanism. Superoxide disrupts enzyme iron-sulfur clusters and alters iron homeostasis in bacteria by reducing ferric to ferrous iron (Equation 2.1) creating an increased free iron pool¹¹⁶. Superoxide dismutes to hydrogen peroxide or water spontaneously when superoxide concentration is elevated or facilitated by native superoxide dismutase enzymes. Free ferrous iron

is especially deleterious because it localizes to DNA and then facilitates Fenton chemistry, with hydrogen peroxide from dismuted superoxide, to form hydroxyl (Equation 2.2) proximal to DNA causing DNA mutations and lesions¹²⁴. Hydroxyl radicals react at diffusion limiting rates making localization of hydroxyl generation key for cellular damage. Free iron also associates with lipids and proteins suggesting that superoxide may also increase damage to those species through hydroxyl localization. Due to these toxicity mechanisms, superoxide has been suggested as a potentiator or catalyst for oxidative damage making it of interest for antibiotic design.



2.4.3 Quantum dots for superoxide generation

Nanomaterials are widely studied and developed for their use as therapeutics, delivery agents, and diagnostics¹²⁵. For diagnostics, they have been applied as standalone imaging agents or as bio-conjugate imaging agents as binding indicators. The small, controllable size of nanoparticles has made them useful in drug delivery using encapsulation or surface stabilizing methods. Nanotechnology has also proven useful in formulating nanocrystals of drugs for controlled release and predictable particle size. Nanomaterials as the therapeutic agent itself have been studied ranging from cancer biology to antimicrobials. Of interest for our purposes is a class of nanoparticles called quantum dots which are nanoparticles made of semi-conducting materials. Due to quantum confinement, quantum dots have tunable energetic properties. When quantum dots are excited across their nominal bandgap, an excited electron and hole are available for redox half reactions at the tuned energy levels. Excitation of the material is controlled by the bandgap and can be designed for a desired wavelength of energy and gives spatiotemporal control over the therapeutic action. The tunable energetic properties, the reduction and oxidation potential and

bandgap, facilitate control over the redox reactions that can occur allowing for the rational design of an antimicrobial nanoparticle for superoxide generation.

2.5 Combination therapies

Combination therapy has been used in a number of disease states from cancer therapy to bacterial infections. Antibiotic combination therapies can be made of components that are directly related in efficacy, such as β -lactam/ β -lactamase inhibitor combinations, or unrelated compounds such as common Neosporin, a combination of neomycin and polymyxin B. Combinations can elicit different effects: antagonistic, additive or no interaction, and synergistic (Figure 2.6). In some cases, both components of the combination have antibiotic efficacy alone and in others, a component may be an adjuvant that has no antimicrobial efficacy alone yet works to increase the antibiotic efficacy of the combination.

Different combination effects have varied biological relevance and implications. No interaction or additive generally indicates that the two targeted pathways are unrelated. Using a multiplicative model, additive combination are defined as the inhibition of the combination being approximately equal to inhibition of drug A plus the inhibition of drug B on the remaining bacterial fitness after drug A inhibition (Figure 2.6). Antagonistic and synergistic interactions imply a relationship between the drug targets and mean less or more bacterial inhibition with combination

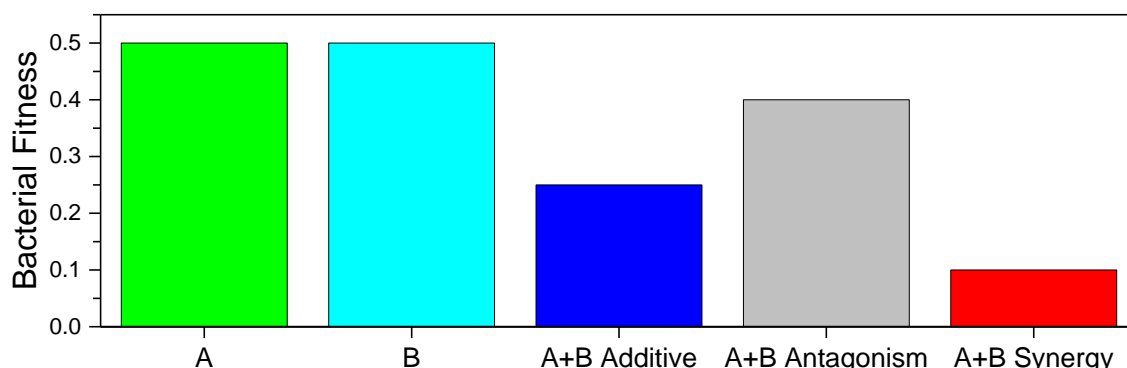


Figure 2.6 Visualization of therapeutic combinatorial effects. Y-axis is arbitrary bacterial fitness. A and B are different therapeutic agents and A+B indicates combination therapy.

compared to additive, respectively. It has been shown that synergy and antagonism result directly from the targeted pathways topology. Synergy is thought to arise from pathways that are parallel or serial whereas antagonism generally occurs from targeted pathways linked by positive feedback¹²⁶. Antagonistic interactions imply less than additive bacterial inhibition upon combination which may not be advantageous however it has been suggested that antagonistic combination therapy can select against antibiotic resistance¹²⁷. This antagonistic benefit is because resistance to one antibiotic induces a less fit state to the other antibiotic in combination meaning the resistant bacteria is not selected for as the most fit. Synergistic interactions imply a combination that is better than additive and can also include adjuvant activity. Both of these deviations from additive are of interest to study in designing antibiotic combination therapy. While a lot of work has focused on classifying and studying the antibiotic interactions between the current small molecule antibiotics^{127–130} or using mathematical modeling to predict and study deviation from additive^{126,131–133}, rationally designing antibiotics for pathways of interest can allow us to uniquely probe and better understand the combinatorial antibiotic space.

2.6 References

1. Fleming, A. On the antibacterial action of cultures of a penicillium, with special reference to their use in the isolation of *B. influenzae*. *Br. J. Exp. Pathol.* **10**, 226–236 (1929).
2. Walsh, C. Molecular mechanisms that confer antibacterial drug resistance. *Nature* **406**, 775–781 (2000).
3. Sesto, N., Wurtzel, O., Archambaud, C., Sorek, R. & Cossart, P. The excludon: a new concept in bacterial antisense RNA-mediated gene regulation. *Nat. Rev. Microbiol.* **11**, 75–82 (2013).
4. Bordoy, A. E., Varanasi, U. S., Courtney, C. M. & Chatterjee, A. Transcriptional Interference in Convergent Promoters as a Means for Tunable Gene Expression. *ACS Synth. Biol.* **5**, 1331–1341 (2016).
5. Magistri, M., Faghihi, M. A., St Laurent, G. & Wahlestedt, C. Regulation of chromatin structure by long noncoding RNAs: focus on natural antisense transcripts. *Trends Genet.*

28, 389–96 (2012).

6. Sorek, R., Kunin, V. & Hugenholtz, P. CRISPR-a widespread system that provides acquired resistance against phages in bacteria and archaea. *Nat. Rev. Microbiol.* **6**, 181–6 (2008).
7. Garneau, J. E., Dupuis, M.-È., Villion, M., *et al.* The CRISPR/Cas bacterial immune system cleaves bacteriophage and plasmid DNA. *Nature* **468**, 67–71 (2010).
8. Wilson, R. C. & Doudna, J. a. Molecular mechanisms of RNA interference. *Annu. Rev. Biophys.* **42**, 217–39 (2013).
9. Brantl, S. Antisense-RNA regulation and RNA interference. *Biochim. Biophys. Acta* **1575**, 15–25 (2002).
10. Waters, L. S. & Storz, G. Regulatory RNAs in bacteria. *Cell* **136**, 615–28 (2009).
11. Gerdes, K. & Wagner, E. G. H. RNA antitoxins. *Curr. Opin. Microbiol.* **10**, 117–24 (2007).
12. Sesto, N., Wurtzel, O., Archambaud, C., Sorek, R. & Cossart, P. The excludon: a new concept in bacterial antisense RNA-mediated gene regulation. *Nat. Rev. Microbiol.* **11**, 75–82 (2013).
13. Dornenburg, J. E., Devita, A. M., Palumbo, M. J. & Wade, J. T. Widespread antisense transcription in Escherichia coli. *MBio* **1**, e00024–10 (2010).
14. Sharma, C. M., Hoffmann, S., Darfeuille, F., *et al.* The primary transcriptome of the major human pathogen Helicobacter pylori. *Nature* **464**, 250–5 (2010).
15. Han, Y., Lin, Y. B., An, W., *et al.* Orientation-dependent regulation of integrated HIV-1 expression by host gene transcriptional readthrough. *Cell Host Microbe* **4**, 134–46 (2008).
16. Liu, J. M., Livny, J., Lawrence, M. S., *et al.* Experimental discovery of sRNAs in Vibrio cholerae by direct cloning, 5S/tRNA depletion and parallel sequencing. *Nucleic Acids Res.* **37**, e46 (2009).
17. Toledo-Arana, A., Dussurget, O., Nikitas, G., *et al.* The Listeria transcriptional landscape from saprophytism to virulence. *Nature* **459**, 950–956 (2009).
18. Güell, M., van Noort, V., Yus, E., *et al.* Transcriptome Complexity in a Genome-Reduced Bacterium. *Science* **326**, 1268–1271 (2009).
19. Georg, J., Voss, B., Scholz, I., *et al.* Evidence for a major role of antisense RNAs in cyanobacterial gene regulation. *Mol. Syst. Biol.* **5**, 305 (2009).
20. Katayama, S., Tomaru, Y., Kasukawa, T., *et al.* Antisense transcription in the mammalian transcriptome. *Science* **309**, 1564–6 (2005).
21. Yelin, R., Dahary, D., Sorek, R., *et al.* Widespread occurrence of antisense transcription in the human genome. *Nat. Biotechnol.* **21**, 379–86 (2003).

22. Misra, S. & Crosby, M. Annotation of the *Drosophila melanogaster* euchromatic genome: a systematic review. *Genome Biol.* **3**, 1–22 (2002).
23. Yamada, K., Lim, J., Dale, J. M., *et al.* Empirical analysis of transcriptional activity in the *Arabidopsis* genome. *Science* **302**, 842–6 (2003).
24. Berteaux, N., Aptel, N., Cathala, G., *et al.* A novel H19 antisense RNA overexpressed in breast cancer contributes to paternal IGF2 expression. *Mol. Cell. Biol.* **28**, 6731–45 (2008).
25. Monti, L., Cinquetti, R., Guffanti, A., *et al.* In silico prediction and experimental validation of natural antisense transcripts in two cancer-associated regions of human chromosome 6. *Int. J. Oncol.* **34**, 1099–108 (2009).
26. Marshall, L. & White, R. J. Non-coding RNA production by RNA polymerase III is implicated in cancer. *Nat. Rev. Cancer* **8**, 911–4 (2008).
27. Coiras, M., López-Huertas, M. R., Pérez-Olmeda, M. & Alcamí, J. Understanding HIV-1 latency provides clues for the eradication of long-term reservoirs. *Nat. Rev. Microbiol.* **7**, 798–812 (2009).
28. Kroger, C., Dillon, S. C., Cameron, A. D., *et al.* The transcriptional landscape and small RNAs of *Salmonella enterica* serovar Typhimurium. *Proc. Natl. Acad. Sci. U. S. A.* **109**, E1277–86 (2012).
29. Mitschke, J., Georg, J., Scholz, I., *et al.* An experimentally anchored map of transcriptional start sites in the model cyanobacterium *Synechocystis* sp. PCC6803. *Proc. Natl. Acad. Sci. U. S. A.* **108**, 2124–9 (2011).
30. Nicolas, P., Mader, U., Dervyn, E., *et al.* Condition-Dependent Transcriptome Reveals High-Level Regulatory Architecture in *Bacillus subtilis*. *Science* **335**, 1103–1106 (2012).
31. Albrecht, M., Sharma, C. M., Reinhardt, R., Vogel, J. & Rudel, T. Deep sequencing-based discovery of the *Chlamydia trachomatis* transcriptome. *Nucleic Acids Res.* **38**, 868–77 (2010).
32. Wurtzel, O., Yoder-Himes, D. R., Han, K., *et al.* The single-nucleotide resolution transcriptome of *Pseudomonas aeruginosa* grown in body temperature. *PLoS Pathog.* **8**, e1002945 (2012).
33. Filiatrault, M. J., Stodghill, P. V., Bronstein, P. A., *et al.* Transcriptome analysis of *Pseudomonas syringae* identifies new genes, noncoding RNAs, and antisense activity. *J. Bacteriol.* **192**, 2359–72 (2010).
34. Beaume, M., Hernandez, D., Farinelli, L., *et al.* Cartography of methicillin-resistant *S. aureus* transcripts: detection, orientation and temporal expression during growth phase and stress conditions. *PLoS One* **5**, e10725 (2010).
35. Schlüter, J.-P., Reinkensmeier, J., Daschkey, S., *et al.* A genome-wide survey of sRNAs in

the symbiotic nitrogen-fixing alpha-proteobacterium *Sinorhizobium meliloti*. *BMC Genomics* **11**, 245 (2010).

36. Chatterjee, A., Johnson, C. M., Shu, C.-C., *et al.* Convergent transcription confers a bistable switch in *Enterococcus faecalis* conjugation. *Proc. Natl. Acad. Sci. U. S. A.* **108**, 9721–6 (2011).
37. Hongay, C. F., Grisafi, P. L., Galitski, T. & Fink, G. R. Antisense transcription controls cell fate in *Saccharomyces cerevisiae*. *Cell* **127**, 735–45 (2006).
38. Georg, J. & Hess, W. R. *cis*-antisense RNA, another level of gene regulation in bacteria. *Microbiol. Mol. Biol. Rev.* **75**, 286–300 (2011).
39. Shearwin, K. E., Callen, B. P. & Egan, J. B. Transcriptional interference-a crash course. *Trends Genet.* **21**, 339–45 (2005).
40. Thomason, M. K. & Storz, G. Bacterial antisense RNAs: how many are there, and what are they doing? *Annu. Rev. Genet.* **44**, 167–88 (2010).
41. Callen, B. P., Shearwin, K. E. & Egan, J. B. Transcriptional Interference between Convergent Promoters Caused by Elongation over the Promoter. *Mol. Cell* **14**, 647–656 (2004).
42. Palmer, A. C., Ahlgren-Berg, A., Egan, J. B., Dodd, I. B. & Shearwin, K. E. Potent transcriptional interference by pausing of RNA polymerases over a downstream promoter. *Mol. Cell* **34**, 545–55 (2009).
43. Ward, D. F. & Murray, N. E. Convergent Transcription in Bacteriophage lambda: Interference with Gene Expression. *J. Mol.* **133**, 249–266 (1979).
44. Greger, I. H., Aranda, A. & Proudfoot, N. Balancing transcriptional interference and initiation on the GAL7 promoter of *Saccharomyces cerevisiae*. *Proc. Natl. Acad. Sci. U. S. A.* **97**, 8415–8420 (2000).
45. Gullerova, M. & Proudfoot, N. J. Cohesin complex promotes transcriptional termination between convergent genes in *S. pombe*. *Cell* **132**, 983–95 (2008).
46. Franch, T., Petersen, M., Wagner, E. G., Jacobsen, J. P. & Gerdes, K. Antisense RNA regulation in prokaryotes: rapid RNA/RNA interaction facilitated by a general U-turn loop structure. *J. Mol. Biol.* **294**, 1115–25 (1999).
47. Bennett, C. F. & Swayze, E. E. RNA targeting therapeutics: molecular mechanisms of antisense oligonucleotides as a therapeutic platform. *Annu. Rev. Pharmacol. Toxicol.* **50**, 259–93 (2010).
48. Johnson, E. & Srivastava, R. Volatility in mRNA secondary structure as a design principle for antisense. *Nucleic Acids Res.* **41**, 1–10 (2012).

49. Yamaguchi, Y., Park, J.-H. & Inouye, M. Toxin-antitoxin systems in bacteria and archaea. *Annu. Rev. Genet.* **45**, 61–79 (2011).
50. Brantl, S. Regulatory mechanisms employed by cis-encoded antisense RNAs. *Curr. Opin. Microbiol.* **10**, 102–9 (2007).
51. Sneppen, K., Dodd, I. B., Shearwin, K. E., *et al.* A mathematical model for transcriptional interference by RNA polymerase traffic in *Escherichia coli*. *J. Mol. Biol.* **346**, 399–409 (2005).
52. Palmer, A. C., Egan, J. B. & Shearwin, K. E. Transcriptional interference by RNA polymerase pausing and dislodgement of transcription factors. *Transcription* **2**, 9–14 (2011).
53. Lee, E.-J. & Groisman, E. a. An antisense RNA that governs the expression kinetics of a multifunctional virulence gene. *Mol. Microbiol.* **76**, 1020–33 (2010).
54. Thisted, T. & Gerdes, K. Mechanism of Post-segregational Killing of Plasmid R1 by the hok / sok System Sok Antisense RNA Regulates hok Gene Expression Indirectly Through the Overlapping mok Gene. *J. Mol. Biol.* **41**–54 (1997).
55. Hernández, J. A., Muro-Pastor, A. M., Flores, E., *et al.* Identification of a furA cis antisense RNA in the cyanobacterium *Anabaena* sp. PCC 7120. *J. Mol. Biol.* **355**, 325–34 (2006).
56. Liao, S. M., Wu, T. H., Chiang, C. H., Susskind, M. M. & McClure, W. R. Control of gene expression in bacteriophage P22 by a small antisense RNA. I. Characterization in vitro of the Psar promoter and the sar RNA transcript. *Genes Dev.* **1**, 197–203 (1987).
57. Kawano, M., Aravind, L. & Storz, G. An antisense RNA controls synthesis of an SOS-induced toxin evolved from an antitoxin. *Mol. Microbiol.* **64**, 738–54 (2007).
58. Krinke, L. & Wulff, D. L. OOP RNA, produced from multicopy plasmids, inhibits lambda cII gene expression through an RNase III-dependent mechanism. *Genes Dev.* **1**, 1005–1013 (1987).
59. Stazic, D., Lindell, D. & Steglich, C. Antisense RNA protects mRNA from RNase E degradation by RNA-RNA duplex formation during phage infection. *Nucleic Acids Res.* **39**, 4890–9 (2011).
60. Montange, R. K. & Batey, R. T. Riboswitches: emerging themes in RNA structure and function. *Annu. Rev. Biophys.* **37**, 117–33 (2008).
61. Wan, Y., Kertesz, M., Spitale, R. C., Segal, E. & Chang, H. Y. Understanding the transcriptome through RNA structure. *Nat. Rev. Genet.* **12**, 641–55 (2011).
62. Arraiano, C. M., Andrade, J. M., Domingues, S., *et al.* The critical role of RNA processing and degradation in the control of gene expression. *FEMS Microbiol. Rev.* **34**, 883–923 (2010).

63. Johnson, C. M., Manias, D. A., Haemig, H. A. H., *et al.* Direct evidence for control of the pheromone-inducible prgQ operon of *Enterococcus faecalis* plasmid pCF10 by a countertranscript-driven attenuation mechanism. *J. Bacteriol.* **192**, 1634–42 (2010).
64. Sayed, N., Jousselin, A. & Felden, B. A cis-antisense RNA acts in trans in *Staphylococcus aureus* to control translation of a human cytolytic peptide. *Nat. Struct. Mol. Biol.* **19**, 105–12 (2012).
65. Stork, M., Di Lorenzo, M., Welch, T. J. & Crosa, J. H. Transcription termination within the iron transport-biosynthesis operon of *Vibrio anguillarum* requires an antisense RNA. *J. Bacteriol.* **189**, 3479–88 (2007).
66. Opdyke, J. A., Fozo, E. M., Hemm, M. R. & Storz, G. RNase III participates in GadY-dependent cleavage of the gadX-gadW mRNA. *J. Mol. Biol.* **406**, 29–43 (2011).
67. Dühring, U., Axmann, I. M., Hess, W. R. & Wilde, A. An internal antisense RNA regulates expression of the photosynthesis gene isiA. *Proc. Natl. Acad. Sci. U. S. A.* **103**, 7054–8 (2006).
68. Johnson, C. M., Haemig, H. H. A., Chatterjee, A., *et al.* RNA-Mediated Reciprocal Regulation between Two Bacterial Operons Is RNase III Dependent. *MBio* **2**, (2011).
69. Prescott, E. M. & Proudfoot, N. J. Transcriptional collision between convergent genes in budding yeast. *Proc. Natl. Acad. Sci. U. S. A.* **99**, 8796–8801 (2002).
70. Crampton, N., Bonass, W. a, Kirkham, J., Rivetti, C. & Thomson, N. H. Collision events between RNA polymerases in convergent transcription studied by atomic force microscopy. *Nucleic Acids Res.* **34**, 5416–25 (2006).
71. Shu, C.-C., Chatterjee, A., Dunny, G., Hu, W.-S. & Ramkrishna, D. Bistability versus Bimodal Distributions in Gene Regulatory Processes from Population Balance. *Plos Comput. Biol.* **7**, (2011).
72. Chatterjee, A., Drews, L., Mehra, S., *et al.* Convergent transcription in the butyrolactone regulon in *Streptomyces coelicolor* confers a bistable genetic switch for antibiotic biosynthesis. *PLoS One* **6**, e21974 (2011).
73. Bendtsen, K. M., Erdosy, J., Csiszovszki, Z., *et al.* Direct and indirect effects in the regulation of overlapping promoters. *Nucleic Acids Res.* **39**, 6879–85 (2011).
74. Mason, E., Henderson, M. W., Scheller, E. V., Byrd, M. S. & Cotter, P. a. Evidence for phenotypic bistability resulting from transcriptional interference of bvgAS in *Bordetella bronchiseptica*. *Mol. Microbiol.* **90**, 716–733 (2013).
75. Stougaard, P., Molin, S. & Nordstrom, K. RNAs involved in copy-number control and incompatibility of. *Proc. Natl. Acad. Sci. U. S. A.* **78**, 6008–6012 (1981).
76. Tomizawa, J.-I. & Itoh, T. Plasmid ColE1 incompatibility determined by interactionn of

- RNA I with primer transcript. *Proc. Natl. Acad. Sci. United States Am.* **78**, 6096–6100 (1981).
77. Hernández, J. a., Muro-Pastor, A. M., Flores, E., *et al.* Identification of a furA cis antisense RNA in the cyanobacterium Anabaena sp. PCC 7120. *J. Mol. Biol.* **355**, 325–34 (2006).
 78. Stazic, D., Lindell, D. & Steglich, C. Antisense RNA protects mRNA from RNase E degradation by RNA-RNA duplex formation during phage infection. *Nucleic Acids Res.* **39**, 4890–9 (2011).
 79. André, G., Even, S., Putzer, H., *et al.* S-box and T-box riboswitches and antisense RNA control a sulfur metabolic operon of Clostridium acetobutylicum. *Nucleic Acids Res.* **36**, 5955–69 (2008).
 80. Chatterjee, A., Cook, L. C. C., Shu, C.-C., *et al.* Antagonistic self-sensing and mate-sensing signaling controls antibiotic-resistance transfer. *Proc. Natl. Acad. Sci. U. S. A.* **110**, 7086–90 (2013).
 81. Cook, L., Chatterjee, A., Barnes, A., *et al.* Biofilm growth alters regulation of conjugation by a bacterial pheromone. *Mol. Microbiol.* **81**, 1499–1510 (2011).
 82. Giangrossi, M., Prosseda, G., Tran, C. N., *et al.* A novel antisense RNA regulates at transcriptional level the virulence gene icsA of Shigella flexneri. *Nucleic Acids Res.* **38**, 3362–75 (2010).
 83. Chen, J., Sun, M., Hurst, L. D., Carmichael, G. G. & Rowley, J. D. Genome-wide analysis of coordinate expression and evolution of human cis-encoded sense-antisense transcripts. *Trends Genet.* **21**, 322–6 (2005).
 84. Kiyosawa, H., Mise, N., Iwase, S., Hayashizaki, Y. & Abe, K. Disclosing hidden transcripts: mouse natural sense-antisense transcripts tend to be poly(A) negative and nuclear localized. *Genome Res.* **15**, 463–74 (2005).
 85. Zhang, Y., Liu, X. S., Liu, Q.-R. & Wei, L. Genome-wide in silico identification and analysis of cis natural antisense transcripts (cis-NATs) in ten species. *Nucleic Acids Res.* **34**, 3465–75 (2006).
 86. Chen, J., Sun, M., Kent, W. J., *et al.* Over 20% of human transcripts might form sense-antisense pairs. *Nucleic Acids Res.* **32**, 4812–20 (2004).
 87. Kiyosawa, H., Yamanaka, I., Osato, N., Kondo, S. & Hayashizaki, Y. Antisense transcripts with FANTOM2 clone set and their implications for gene regulation. *Genome Res.* **13**, 1324–34 (2003).
 88. Okazaki, Y., Furuno, M., Kasukawa, T. & Adachi, J. Analysis of the mouse transcriptome based on functional annotation of 60,770 full-length cDNAs. *Nature* **420**, 563–573 (2002).
 89. Zhang, Y., Liu, X. S., Liu, Q.-R. & Wei, L. Genome-wide in silico identification and

- analysis of cis natural antisense transcripts (cis-NATs) in ten species. *Nucleic Acids Res.* **34**, 3465–75 (2006).
90. Misra, S. & Crosby, M. Annotation of the *Drosophila melanogaster* euchromatic genome: a systematic review. *Genome Biol.* **3**, 1–22 (2002).
 91. Jin, H., Vacic, V., Girke, T., Lonardi, S. & Zhu, J.-K. Small RNAs and the regulation of cis-natural antisense transcripts in *Arabidopsis*. *BMC Mol. Biol.* **9**, 6 (2008).
 92. Jen, C.-H., Michalopoulos, I., Westhead, D. R. & Meyer, P. Natural antisense transcripts with coding capacity in *Arabidopsis* may have a regulatory role that is not linked to double-stranded RNA degradation. *Genome Biol.* **6**, R51 (2005).
 93. Wang, X.-J., Gaasterland, T. & Chua, N.-H. Genome-wide prediction and identification of cis-natural antisense transcripts in *Arabidopsis thaliana*. *Genome Biol.* **6**, R30 (2005).
 94. Sorek, R. & Cossart, P. Prokaryotic transcriptomics: a new view on regulation, physiology and pathogenicity. *Nat. Rev. Genet.* **11**, 9–16 (2010).
 95. Sommer, M. O. a & Dantas, G. Antibiotics and the resistant microbiome. *Curr. Opin. Microbiol.* **14**, 556–563 (2011).
 96. Sommer, M. O., Dantas, G. & Church, G. M. Functional characterization of the antibiotic resistance reservoir in the human microflora. *Science* **325**, 1128–1131 (2009).
 97. Buffie, C. G. & Pamer, E. G. Microbiota-mediated colonization resistance against intestinal pathogens. *Nat Rev Immunol* **13**, 790–801 (2013).
 98. Rupnik, M., Wilcox, M. H. & Gerding, D. N. *Clostridium difficile* infection: new developments in epidemiology and pathogenesis. *Nat. Rev. Microbiol.* **7**, 526–36 (2009).
 99. Mondhe, M., Chessher, A., Goh, S., Good, L. & Stach, J. E. M. Species-selective killing of bacteria by antimicrobial peptide-PNAs. *PLoS One* **9**, e89082 (2014).
 100. Bennett, C. F. & Swayze, E. E. RNA targeting therapeutics: molecular mechanisms of antisense oligonucleotides as a therapeutic platform. *Annu. Rev. Pharmacol. Toxicol.* **50**, 259–293 (2010).
 101. Burnett, J. C. & Rossi, J. J. RNA-based therapeutics: current progress and future prospects. *Chem. Biol.* **19**, 60–71 (2012).
 102. Wang, J., Lu, Z., Wientjes, M. G. & Au, J. L.-S. Delivery of siRNA therapeutics: barriers and carriers. *AAPS J.* **12**, 492–503 (2010).
 103. Schmidt, M. Xenobiology: A new form of life as the ultimate biosafety tool. *BioEssays* **32**, 322–331 (2010).
 104. Hyrup, B. & Nielsen, P. E. Peptide Nucleic Acids (PNA): Synthesis, Properties and

Potential Applications. *Bioorg. Med. Chem.* **4**, 5–23 (1996).

105. Milletti, F. Cell-penetrating peptides: Classes, origin, and current landscape. *Drug Discov. Today* **17**, 850–860 (2012).
106. Nielsen, P. E. Peptide nucleic acids as antibacterial agents via the antisense principle. *Expert Opin. Investig. Drugs* **10**, 331–341 (2001).
107. Dryselius, R., Aswasti, S. K., Rajarao, G. K., Nielsen, P. E. & Good, L. The translation start codon region is sensitive to antisense PNA inhibition in Escherichia coli. *Oligonucleotides* **13**, 427–33 (2003).
108. Good, L. & Nielsen, P. E. Antisense inhibition of gene expression in bacteria by PNA targeted to mRNA. *Nat. Biotechnol.* **16**, 355–358 (1998).
109. Nikravesh, A., Dryselius, R., Faridani, O. R., *et al.* Antisense PNA accumulates in Escherichia coli and mediates a long post-antibiotic effect. *Mol. Ther.* **15**, 1537–42 (2007).
110. Baba, T., Ara, T., Hasegawa, M., *et al.* Construction of Escherichia coli K-12 in-frame, single-gene knockout mutants: the Keio collection. *Mol. Syst. Biol.* **2**, 1–11 (2006).
111. Gupta, S. K., Padmanabhan, B. R., Diene, S. M., *et al.* ARG-annot, a new bioinformatic tool to discover antibiotic resistance genes in bacterial genomes. *Antimicrob. Agents Chemother.* **58**, 212–220 (2014).
112. Imlay, J. A. Cellular defenses against superoxide and hydrogen peroxide. *Annu. Rev. Biochem.* **77**, 755–776 (2011).
113. Avery, S. V. Molecular targets of oxidative stress. *Biochem. J.* **434**, 201–10 (2011).
114. Imlay, J. A. The molecular mechanisms and physiological consequences of oxidative stress: lessons from a model bacterium. *Nat. Rev. Microbiol.* **11**, 443–54 (2013).
115. Imlay, J. a. Pathways of oxidative damage. *Annu. Rev. Microbiol.* **57**, 395–418 (2003).
116. Keyer, K. & Imlay, J. Superoxide accelerates DNA damage by elevating free-iron levels. *Proc. Natl. Acad. Sci. U. S. A.* **93**, 13635–13640 (1996).
117. Kohanski, M. a., Dwyer, D. J., Hayete, B., Lawrence, C. a. & Collins, J. J. A Common Mechanism of Cellular Death Induced by Bactericidal Antibiotics. *Cell* **130**, 797–810 (2007).
118. Kottur, J. & Nair, D. T. Reactive Oxygen Species Play an Important Role in the Bactericidal Activity of Quinolone Antibiotics. *Angew. Chemie* **55**, 2397–2400 (2016).
119. Dwyer, D. J., Belenky, P. a, Yang, J. H., *et al.* Antibiotics induce redox-related physiological alterations as part of their lethality. *Proc. Natl. Acad. Sci. U. S. A.* **111**, E2100–9 (2014).

120. Liu, X., Marrakchi, M., Jahne, M., Rogers, S. & Andreescu, S. Real-time investigation of antibiotics-induced oxidative stress and superoxide release in bacteria using an electrochemical biosensor. *Free Radic. Biol. Med.* **91**, 25–33 (2016).
121. Kohanski, M. A., DePristo, M. A. & Collins, J. J. Sublethal Antibiotic Treatment Leads to Multidrug Resistance via Radical-Induced Mutagenesis. *Mol. Cell* **37**, 311–320 (2010).
122. Grant, S. S., Kaufmann, B. B., Chand, N. S., Haseley, N. & Hung, D. T. Eradication of bacterial persisters with antibiotic-generated hydroxyl radicals. *Proc. Natl. Acad. Sci. U. S. A.* **109**, 12147–12152 (2012).
123. Lewis, K. Persister cells, dormancy and infectious disease. *Nat. Rev. Microbiol.* **5**, 48–56 (2007).
124. Keyer, K., Strohmeier Gort, A. & Imlay, J. A. Superoxide and the Production of Oxidative DNA Damage. *J. Bacteriol.* **177**, 6782–6790 (1995).
125. Moghimi, S. M., Hunter, A. C. & Murray, J. C. Nanomedicine: current status and future prospects. *FASEB J.* **19**, 311–30 (2005).
126. Yin, N., Ma, W., Pei, J., *et al.* Synergistic and antagonistic drug combinations depend on network topology. *PLoS One* **9**, (2014).
127. Chait, R., Craney, A. & Kishony, R. Antibiotic interactions that select against resistance. *Nature* **446**, 668–671 (2007).
128. Yeh, P., Tschumi, A. I. & Kishony, R. Functional classification of drugs by properties of their pairwise interactions. *Nat. Genet.* **38**, 489–494 (2006).
129. Chait, R., Shrestha, S., Shah, A. K., Michel, J. B. & Kishony, R. A differential drug screen for compounds that select against antibiotic resistance. *PLoS One* **5**, 1–8 (2010).
130. Tängdén, T., Hickman, R. a., Forsberg, P., *et al.* Evaluation of double- and triple-antibiotic combinations for VIM- and NDM-producing klebsiella pneumoniae by in vitro time-kill experiments. *Antimicrob. Agents Chemother.* **58**, 1757–1762 (2014).
131. Zou, J., Ji, P., Zhao, Y.-L., *et al.* Neighbor communities in drug combination networks characterize synergistic effect. *Mol. Biosyst.* **8**, 3185 (2012).
132. Jansen, G., Lee, A. Y., Epp, E., *et al.* Chemogenomic profiling predicts antifungal synergies. *Mol. Syst. Biol.* **5**, 338 (2009).
133. Koizumi, Y. & Iwami, S. Mathematical modeling of multi-drugs therapy: a challenge for determining the optimal combinations of antiviral drugs. *Theor. Biol. Med. Model.* **11**, 41 (2014).

Chapter 3

Sequence-Specific Peptide Nucleic Acid-Based Antisense Inhibitors of TEM-1 β-Lactamase and Mechanism of Adaptive Resistance

Reprinted with permission from Courtney, C. M., and Chatterjee, A. (2015) Sequence-Specific Peptide Nucleic Acid-Based Antisense Inhibitors of TEM-1 β-Lactamase and Mechanism of Adaptive Resistance. *ACS Infect. Dis.* 1, 253–263 DOI: 10.1021/acsinfecdis.5b00042. Copyright 2015 American Chemical Society.

3.1 Abstract

The recent surge of drug-resistant superbugs and shrinking antibiotic pipeline are serious challenges to global health. In particular, the emergence of β-lactamases has caused extensive resistance against the most frequently prescribed class of antibiotics, β-lactams. Here, we develop novel synthetic peptide nucleic acid based antisense inhibitors that target the start codon and ribosomal binding site of the TEM-1 β-lactamase transcript and act via translation inhibition mechanism. We show that these antisense inhibitors are capable of re-sensitizing drug-resistant *Escherichia coli* to β-lactam antibiotics exhibiting 10 fold reduction in the minimum inhibitory concentration (MIC). To study the mechanism of resistance, we adapted *E. coli* at MIC levels of the β-lactam/antisense inhibitor combination and observed a bet-hedging based adaptive antibiotic resistance response as evidenced by phenotypic heterogeneity as well as heterogeneous expression of key stress response genes. Our data shows that both the development of new antimicrobials and understanding the cellular response during development of tolerance could aid in mitigating the impending antibiotic crisis.

3.2 Introduction

Antibiotic resistance is one of the world's most pressing health problems¹ with a number of antibiotic resistant pathogens reported including multidrug-resistant New Delhi metallo-β-lactamase-1 producing *Klebsiella pneumoniae*,² carbapenem resistant *Escherichia coli*,³ and multi-drug resistant *Salmonella enterica*⁴. While bacteria are rapidly developing resistance to current therapeutics, fewer therapeutics are being developed^{5,6}. β-lactam antibiotics, including cephalosporins, penicillins, carbapenems, and monobactams, are some of the most frequently prescribed antibiotics for the treatment of bacterial infections; however, emergence of β-lactamases has caused extensive resistance against β-lactams^{7,8}. Due to the onset of resistance from β-lactamases, β-lactam antibiotics are often combined with β-lactamase inhibitors, such as clavulanic acid, sulbactam, and tazobactam,^{8–11} in therapeutic applications. Recently, resistance has also developed to the β-lactam/β-lactamase inhibitor combinations due to extended spectrum β-lactamases and carbapenemases,³ including New Delhi metallo-β-lactamase 1,² providing another avenue for widespread antibiotic resistance.

With an ever shrinking arsenal of efficacious antibiotics, there is a need for developing novel antimicrobials. Sequence-specific antisense therapeutics have the ability to be pathogen-specific and offer a powerful antimicrobial strategy without nonspecific broad-spectrum activity¹². Antisense therapeutics are nucleotide sequence based therapeutics which target specific RNA or DNA sequences and interact via complementary Watson-Crick base pairing between the target and antisense sequence^{13,14}, thereby causing decrease in gene expression by blocking transcription, ribosomal binding, preventing ribosomal migration, or inducing cleavage by RNases^{15,16}. Antisense therapies are not limited to natural nucleic acids,^{17,18} but can also utilize synthetic nucleic acids such as locked nucleic acids (LNA), bicyclic nucleic acids (BNA), and peptide

nucleic acids (PNA), among others¹³. These synthetic nucleic acids have been used to target a multitude of genes including, LNA targeted against *ftsZ* in methicillin-resistant *Staphylococcus aureus*¹⁹ and PNA targeted to *dnaK* in *E. coli* and *S. enterica*²⁰. PNA, conjugated to cell penetrating peptides (CPPs) for increased transport into cells, has been used to target ribosomal RNA to disrupt protein synthesis, and *acp*, to disrupt cell wall formation, in *E. coli*.²¹ Although there are challenges associated with the delivery of antisense therapeutics¹³, the recent FDA approval of two antisense therapeutics, Fomivirsen for retinitis and Mipomersen for cholesterol reduction, highlights their potential use in practical applications¹⁷.

Despite success of these methods, the ability of bacteria to adapt to antisense therapeutics has not been investigated in depth. Given that bacterial pathogens possess the intrinsic ability to acquire resistance via horizontal gene transfer^{22,23} as well as develop adaptive antibiotic resistance^{6,24–26}, there is a need to understand the mechanism of resistance to antisense therapeutics. Adaptive antibiotic resistance is the induction of resistance due to the presence of a specific signal or stressor and can be genetic^{25,27} or non-genetic²⁸. Non-genetic adaptive antibiotic resistance can be transient and is often observed as changes in gene expression.²⁸ Adaptive antibiotic resistance has been observed in the form of elevated efflux pump expression in *Acinetobacter baumannii*, in the presence of minocycline, ciprofloxacin, meropenem, tetracycline, and tigecycline,²⁹ and *S. enterica*, in the presence of kanamycin³⁰. It has also been observed as the up regulation of genes in the anaerobic respiratory pathway in *Pseudomonas aeruginosa* in response to aminoglycoside exposure.²⁸

Here we designed PNA based antisense therapeutics to target the TEM-1 β-lactamase (*bla*) mRNA, in order to re-sensitize drug-resistant *E. coli* (encoding TEM-1 β-lactamase) to β-lactam antibiotics, and studied the mechanism of resistance to this antisense therapeutic strategy. We

demonstrate that antisense inhibitors can serve as novel antibiotics and an alternative to conventional β -lactamase inhibitors which have been developed to interfere with bacterial enzymes including transpeptidase, carboxypeptidase, and endopeptidase³¹. We performed a focused study to investigate the mechanism of resistance to the β -lactam/PNA based antisense inhibitor combination. Through sequencing analysis of the antisense inhibitor target site, we find that mutants which develop tolerance to the β -lactam/antisense inhibitor combination do not have genetic mutations in the *bla* antisense inhibitor target site. Further we demonstrate that the mutants exhibit phenotypic heterogeneity as well as variable expression of representative stress response genes in the multiple antibiotic resistance regulon (Mar), general stress response, and SOS response pathways, implying a role of bet-hedging based mechanism in the development of adaptive antibiotic resistance. This resistance mechanism has not been previously reported for nucleic acid targeting antisense therapeutics.

3.3 Results and Discussion

3.3.1 Reversing β -lactam resistance by targeting the ribosomal binding site and start codon

We designed three novel antisense molecules, α -RBS, α -STC, and α -YUNR against the ribosomal binding (RBS) site, translation start codon (STC) site, and a YUNR motif, respectively, proximal to the 5' UTR of TEM-1 *bla* mRNA (Figure 3.1, Figure 3.S6, Table 3.1) in order to prevent the production of truncated, but potentially active β -lactamase enzyme.³² *Trans*-antisense interactions have been shown to be effective at the RBS in preventing translation of CmeABC multidrug efflux pumps³³ and at the STC in targeting a plasmid encoded Tn3 β -lactamase in *E. coli*.³² Additionally, it has been shown that longer antisense sequences can reduce target translation by binding to both the RBS and STC such as the natural toxin/antitoxin system of *symE/symR*.³⁴ The antisense molecules studied here are predicted to sterically hinder the ribosome from binding

and/or migrating on the *bla* transcript and consequently prevent its translation to β -lactamase protein.

Table 3.1 PNA sequences conjugated to O-linker and cell penetrating peptide (KFF)₃K. The PNA sequences are written from the N-terminus to the C-terminus.

Antisense Molecule	Conjugated components and PNA sequence
α -RBS	KFFKFFKFFK-O-ccttttcaata
α -STC	KFFKFFKFFK-O-tactcatactct
α -YUNR	KFFKFFKFFK-O-gaataaggcgaa

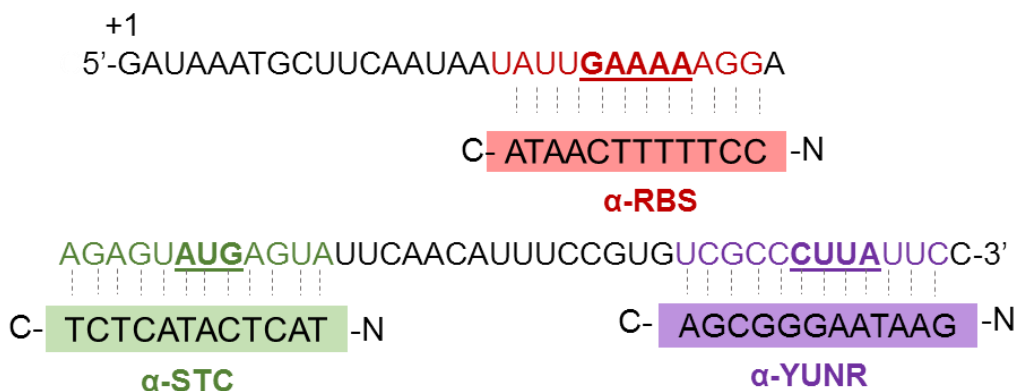
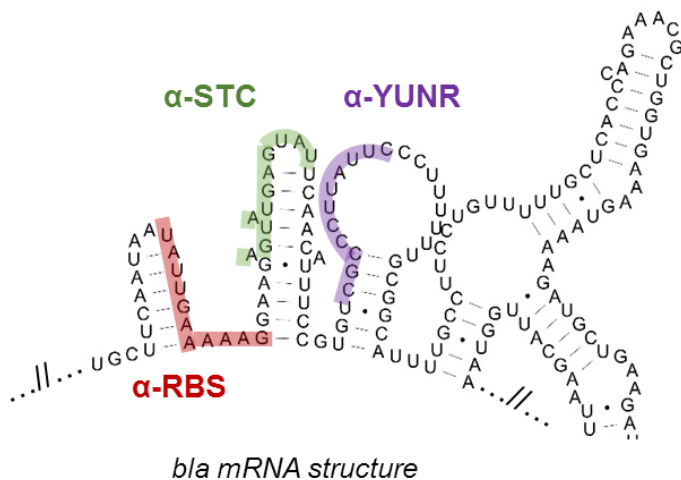


Figure 3.1 Design of antisense inhibitors against TEM-1 β -lactamase. Target sites of PNA based antisense inhibitors are shown on the secondary structure of *bla* RNA encoding the TEM-1 β -lactamase enzyme. PNA molecules are 12-mers where the C-terminus is conjugated to (KFF)₃K cell penetrating peptide via an O-linker (Table 3.1). The ribosomal binding site (RBS), translational start site (STC), and the YUNR motif are underlined in the *bla* sequence (bottom panel). Antisense agents α -RBS, α -STC, and α -YUNR targeting ribosomal binding site, translational start site, and YUNR motif respectively are shown.

To prevent degradation of antisense oligomers by endonucleases expressed by the host cell, we used non-natural antisense PNA oligomers. PNA's have a modified peptide backbone with nucleic acid functional groups and exhibit no known enzymatic cleavage, leading to increased stability in cells³⁵. PNA molecules are known to have higher binding affinity and form more stable interactions with RNA and DNA than natural nucleic acids due to a neutral backbone¹⁴. TEM-1 β -lactamase has been targeted before with PNA molecules but the molecules we present here are novel and have not been characterized previously³⁶.

Based on previous stepwise target analysis with antisense PNA, the antisense oligomers were designed with the target sequence in the middle of the oligomer, with 3-5 nucleotides flanking the target region.³² To prevent translation of β -lactamase, two 12-mer antisense oligomers, α -RBS (C-ATAAACTTTTCC-N; RBS underlined) and α -STC (C-TCTCATACTCAT-N; start codon underlined) were designed against the RBS and STC, respectively (Figure 3.1, Figure 3.S6). While α -RBS was designed to prevent the ribosomal binding, α -STC was designed to prevent ribosomal migration, both causing inhibition of translation of *bla* transcript. The third antisense inhibitor, α -YUNR (C-AGCGGGAATAAG-N; YUNR underlined), was designed to target the YUNR sequence motif on the stem loop between nucleotides 61-78 of the β -lactamase transcript (Figure 3.1, Figure 3.S6). The YUNR motif (pyrimidine, uracil, any ribose nucleic acid, and a purine) has been shown to have high antisense binding affinity, due to formation of intraloop hydrogen bonds facilitating a U-turn structure, and is known to initiate rate limiting interactions in a number of naturally occurring systems.^{37,38} The targeted YUNR motif was in a single stranded region of a stem loop proximal to the 5' UTR in 14/19 free energy secondary structures of the *bla* RNA modeled using RNAstructure³⁹ (Figure 3.S6). α -YUNR was also designed to prevent ribosomal migration, thus inhibiting translation of *bla* to β -lactamase enzyme.

The α -RBS, α -STC, and α -YUNR PNA molecules were designed as 12-mers for optimal affinity to the target site⁴⁰. The 12-mers were conjugated, via an O-linker, to (KFF)₃K CPP for increased transport across the membrane into gram-negative bacterial cells⁴⁰ (Table 3.1). The O-linker was added to reduce steric interference between the PNA and cell penetrating peptide during target binding⁴⁰. The 12-mer antisense sequences were searched against the *E. coli* K-12 genome (U00096.2) using NCBI BLAST to evaluate target selectivity and to avoid off-target interactions. α -RBS, α -STC, and α -YUNR searches returned no matches to the *E. coli* K-12 genome.⁴¹

We next evaluated the therapeutic potential of α -RBS, α -STC, and α -YUNR by identifying a minimum inhibitory concentration (MIC) where the antisense inhibitors re-sensitized drug-resistant *E. coli* to 300 μ g/mL ampicillin. The drug-resistant *E. coli* used for this study was Zymo Dh5a transformed with *bla* producing pAKgfp1 plasmid (Addgene plasmid # 14076). α -RBS, α -STC, and α -YUNR were tested to identify a MIC between 1-25 μ M based on concentrations reported in previous studies conducted in *E. coli* using CPP conjugated PNA^{32,35,36,40}. *E. coli* cultures treated overnight with respective antisense inhibitors, in the absence of ampicillin, grew similar to untreated cells demonstrating the non-toxic effect of the antisense inhibitors (Figure 3.2a, Figure 3.S7a-c).

Strikingly, in the presence of 300 μ g/mL ampicillin and 2.5 μ M α -STC, the growth rate of ampicillin-resistant *E. coli* was significantly reduced ($p<0.05$) (Figure 3.2a, Figure 3.S7d). Similar inhibition of growth of drug-resistant *E. coli* was observed with the α -RBS antisense inhibitor at an elevated MIC of 25 μ M α -RBS and 300 μ g/mL ampicillin ($p<0.05$) (Figure 3.2a, Figure 3.S7e). In contrast, α -YUNR did not show growth inhibition up to 25 μ M with 300 μ g/mL ampicillin ($p>0.05$) (Figure 3.2a, Figure 3.S7f). Both α -STC and α -RBS re-sensitized drug-resistant *E. coli*

to ampicillin and hindered cell growth, only in the presence of ampicillin, indicating gene specific targeting of the *bla* gene.

The difference in MICs of α -STC and α -RBS could be attributed to the different binding affinities of α -STC and α -RBS to the respective target sites; leading to different extents of blocking ribosomal binding or migration³². Similarly, lower binding affinity could also explain lack of *bla* translational inhibition by α -YUNR. The YUNR motif has not been studied previously as a target

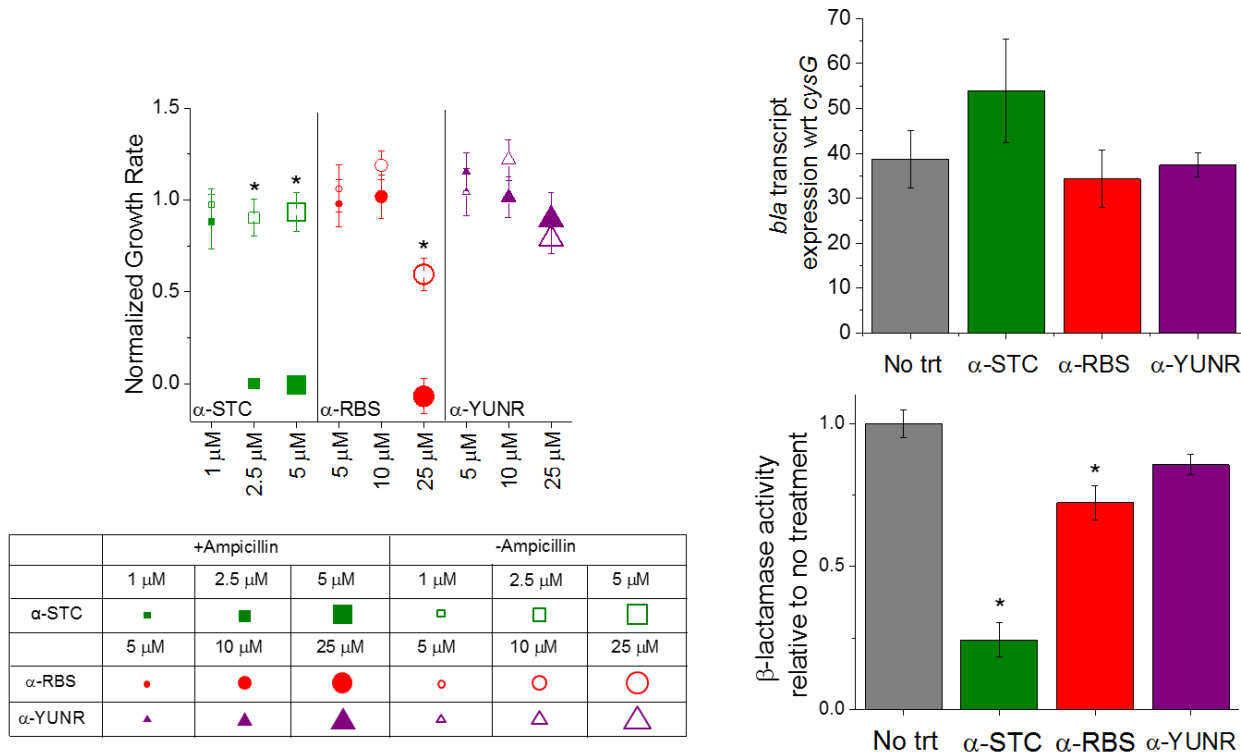


Figure 3.2 Minimum inhibitory concentration and mechanism of antisense inhibitors. a. Normalized growth rate of overnight cultures after treatment with different concentrations of antisense inhibitors is shown. Specific growth rate of cells under treatment with antisense inhibitors (y-axis) is normalized to specific growth rate in absence of treatment. The cultures are treated with respective concentrations of antisense inhibitors either in absence (empty data points) or presence of ampicillin (filled data points) (300 μ g/mL). The MIC of α -STC, α -RBS and α -YUNR are shown at 2.5 μ M, 25 μ M, and greater than 25 μ M respectively. b. *bla* mRNA expression in *E. coli* treated with respective antisense molecule in the absence of ampicillin. α -STC is at 5 μ M, α -RBS is at 25 μ M, and α -YUNR is at 25 μ M for both (b-c). No significant change in *bla* mRNA expression is observed. c. β -lactamase activity assay with respective antisense molecule in the absence of ampicillin. Significant change is observed for α -STC and α -RBS. Data shown are an average of three independent experiments (error bars are standard deviation from average values). Significance ($p < 0.05$) is represented with an asterisk.

for PNA molecules and could be potentially ineffective due to the presence of tertiary structures that may sterically hinder the target site¹³. In addition, since YUNR stem loop motifs are important in natural rate limiting antisense interactions, it is possible that the U-turn structure formed by the motif only aids in binding to other RNA stem loops and not the structure void PNA molecules.

3.3.2 Translational inhibition mechanism of action of antisense inhibitors

We next investigated the mechanism of action for α -STC, α -RBS, and α -YUNR antisense inhibitors. Using quantitative real-time polymerase chain reaction (qPCR), we measured expression levels of the *bla* gene in presence of the antisense inhibitors with respect to uroporphyrin III C-methyltransferase, *cysG*, a moderately expressed housekeeping gene⁴². Studies were carried out at 5 μ M α -STC, 25 μ M α -RBS, or 25 μ M α -YUNR in the absence of ampicillin. RNA expression analysis of *bla* transcript showed similar levels of *bla* RNA both in absence and presence of treatment with the antisense inhibitors ($p>0.05$) (Figure 3.2b), indicating that the antisense inhibitors did not inhibit the expression of *bla* transcript and were not causing significant degradation of transcripts. To evaluate the impact of the antisense inhibitors on translation of the *bla* gene, we used a β -lactamase activity assay to measure β -lactamase protein activity.⁴³ Indeed we observed that α -STC and α -RBS significantly reduced β -lactamase activity ($p<0.05$) (Figure 3.2c). On the other hand, α -YUNR had no impact on protein activity ($p>0.05$). These results demonstrate that α -STC and α -RBS reduced β -lactamase activity, but did not affect *bla* transcript levels, thus indicating that α -STC and α -RBS act via translational inhibition mechanism. These results are consistent with the growth behavior shown in Figure 3.2a and Figure 3.S7, where α -STC and α -RBS impact growth of drug-resistant *E. coli* in presence of ampicillin and α -YUNR had no impact on cell growth.

3.3.3 Start codon targeting antisense inhibitor restores ampicillin sensitivity

To evaluate the therapeutic potential of antisense inhibitors, we investigated the best-performing antisense inhibitor, α -STC, in the following studies. Overnight cultures of ampicillin-resistant *E. coli* were pre-treated with different concentrations of α -STC; followed by treatment with ampicillin. Since α -STC inhibits β -lactamase production, we expected that α -STC would restore the bactericidal effect of ampicillin. Indeed, α -STC decreased cell viability, at the MIC of 2.5 μ M and higher, by at least 1000 fold within the first three hours of treatment with ampicillin (Figure 3.3a). Below the MIC of α -STC (no treatment case and 1 μ M α -STC), colony forming units increased with time.

We next evaluated the degree of re-sensitization exerted by α -STC in the presence of varying concentrations of ampicillin, above and below the MIC determined for α -STC. Two

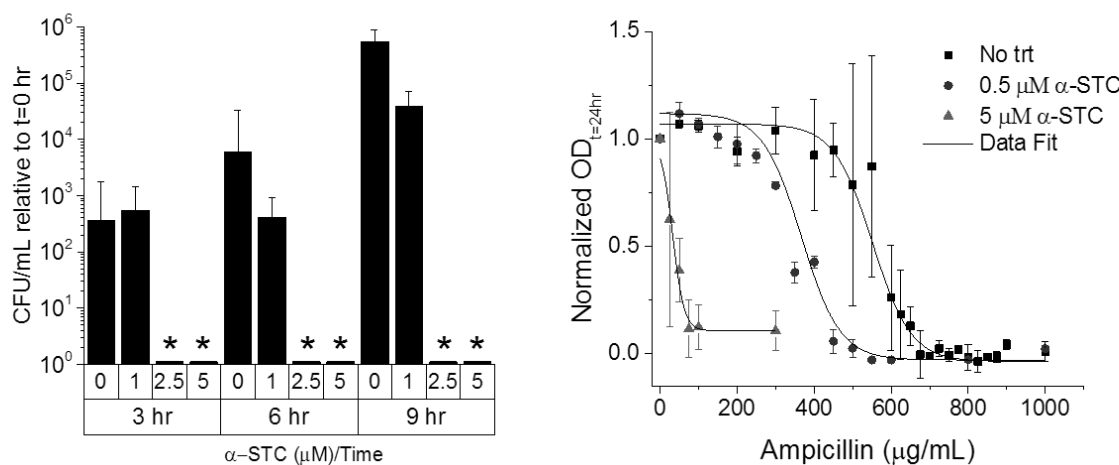


Figure 3.3 Re-sensitization of drug-resistant bacteria using α -STC. a. Colony forming units per milliliter (CFU/mL) for cultures treated with different concentrations of α -STC and 300 μ g/mL ampicillin. Cultures with significant decrease in growth ($p < 0.05$) are represented with an asterisk. b. Ampicillin sensitivity analysis for cultures treated with 0 μ M, 0.5 μ M (below MIC) and 5 μ M (above MIC) of α -STC and a range of ampicillin concentrations. Optical density of cultures treated with a range of α -STC and ampicillin concentrations for 24 hr is shown. The data is normalized to the OD at 24 hr with 0 μ g/mL ampicillin. The three conditions demonstrate different degrees of sensitivity as shown using a Boltzman data fit. Data shown are an average of three independent experiments (error bars are standard deviation from average values).

concentrations of α -STC were tested and compared to no treatment: 0.5 μM α -STC (5-fold below MIC), and 5 μM α -STC (2-fold above MIC) (See Methods) (Figure 3.3b). In the absence of treatment, ampicillin-resistant *E. coli* was able to grow up to 300 $\mu\text{g}/\text{mL}$ ampicillin without inhibition, and showed a gradual decrease in growth until 700 $\mu\text{g}/\text{mL}$ ampicillin, where no growth was observed. At below MIC level of 0.5 μM α -STC ampicillin-resistant *E. coli* grew unhindered up to a reduced ampicillin concentration of 250 $\mu\text{g}/\text{mL}$ and showed no growth at 550 $\mu\text{g}/\text{mL}$ when compared to the no treatment case. Strikingly, at 5 μM α -STC (above MIC), ampicillin-resistant *E. coli* only grew unhindered without ampicillin and showed a decrease in growth as low as 25 $\mu\text{g}/\text{mL}$ and no growth at 75 $\mu\text{g}/\text{mL}$ ampicillin, elucidating in a drastic 10 fold decrease in the MIC of ampicillin compared to the no treatment cultures, exhibiting behavior closer to antibiotic sensitive parent *E. coli* strain (Figure 3.S8). Data fitting (see 3.5.9 Ampicillin sensitivity assay) of the drug-sensitivity curves showed that the slope of the transition state, from resistant to sensitive, is altered drastically and depends on both the concentration of the α -STC antisense inhibitor and ampicillin (Figure 3.3b). Greater than a two fold increase in negative slope for above MIC (-0.010 OD/ $\mu\text{g}/\text{mL}$) compared to below MIC (-0.0038 OD $\text{mL}\mu\text{g}^{-1}$) and no treatment (-0.0051 OD $\text{mL}\mu\text{g}^{-1}$) indicates that while the α -STC is re-sensitizing the *E. coli* to ampicillin, it is changing the sensitivity landscape with respect to the resistant strain.

3.3.4 The emergence of tolerance to antibiotics PNA-inhibitor combination

Since resistance has been reported for enzyme based β -lactamase inhibitors,⁹ we investigated the potential emergence of tolerance to the α -STC/ampicillin combination both above and at the MIC. Ampicillin-resistant cultures were pretreated overnight with either 5 μM (above MIC) or 2.5 μM (at MIC) α -STC and then subjected to selection pressure of 300 $\mu\text{g}/\text{mL}$ of ampicillin and 5 μM or 2.5 μM α -STC respectively for 24 hours. Interestingly, we did not observe

the emergence of tolerance when ampicillin-resistant cultures were treated with 5 μ M α -STC and 300 μ g/mL of ampicillin. However, when we subjected the ampicillin-resistant cultures to MIC concentrations of α -STC (2.5 μ M), 2 out of 35 cultures broke the trend and showed emergence of tolerance. The two cultures which developed tolerance to ampicillin/ α -STC combination over 24 hours were collected, hereby referred to as mutant populations 1 and 2 (Figure 3.4a, Figure 3.S9a). Mutant populations 1 and 2 were diluted and re-grown under selection pressure for another 24 hours. Notably, the mutants grew (Figure 3.4b, Figure 3.S9b) confirming they were stable mutants that had developed tolerance to α -STC and their growth was not an artifact of ampicillin or α -STC degradation.

The *bla* gene in the mutant populations was sequenced to determine whether the cause of tolerance was a mutation in α -STC's target site. Three biological replicates each from mutant population 1, mutant population 2, and a no treatment population were grown overnight after which the plasmid containing the *bla* gene was extracted and the *bla* gene was sequenced. Interestingly, no genetic mutations were found in the α -STC target site (Figure 3.4a, Table 3.2). In contrast to our findings, piperacillin/tazobactam, a traditional β -lactam/ β -lactamase inhibitor drug combination has been shown to lose clinical efficacy in part due to the development of mutations at the target site of tazobactam in the β -lactamase gene.¹¹

Interestingly, the biological mutant replicates showed high variability in growth rate compared to the no treatment biological replicates (Figure 3.4b, Figure 3.S10). The heterogeneity in growth rate led us to investigate the MIC of ampicillin as a second indicator of heterogeneity. We analyzed the MIC of ampicillin, ranging between 0-2000 μ g/mL, for 40 individual colonies from each population to investigate heterogeneity in ampicillin sensitivity. For the colonies sampled, 20 out of the 40 from the no treatment population, 29 out of the 40 from mutant

population 1, and 38 out of the 40 from mutant population 2 had a MIC between 0-2000 µg/mL. For the following analysis, only colonies with a MIC in the range sampled were considered. Averages of the MIC of ampicillin for the populations were 1555 µg/mL for the no treatment population, 1269 µg/mL for mutant population 1, and 1376 µg/mL for mutant population 2 (Figure 3.4c, Figure 3.S11). The analysis of population averages elucidated that the average MIC in the no treatment population was significantly different than that of mutant population 1 ($p=0.002$) and 2 ($p=0.007$). Furthermore, we observed a wider range of MIC of ampicillin for mutant population 1 (700-1900) µg/mL and mutant population 2 (900-1900 µg/mL) compared to the no treatment population (1200-1900 µg/mL) (Figure 3.4c), indicating greater heterogeneity in the mutant populations. This is also evident from box plots which show larger inner (25%) and upper (75%) quartiles of the MIC's in mutant population 1 and 2 while the no treatment population MICs are centered on the mean, with tight inner and upper quartile ranges. This difference in the spread of the data shows that the MIC of ampicillin for biological replicates from the mutant populations is more heterogeneous than the no treatment population.

Similar phenotypic heterogeneity has also been observed in *Salmonella enterica* for adaptive resistance to bile salt sodium deoxycholate and has been described as an indicator of a bet-hedging phenomenon⁴⁴. Bet-hedging is an evolutionary principle in which cells in a population vary gene expression to find an adaptive state by stochastic chance⁴⁵. The nature of bet-hedging and stochastic variation generates heterogeneity within a population. Recently, it was shown that resistance of *S. enterica* to kanamycin is facilitated by bet-hedging observed as heterogeneous expression of *ompC* efflux porin which generates two populations; one which is resistant to kanamycin with low *ompC* and one which is not resistant to kanamycin with high *ompC*.³⁰ It was also shown that virulence in *S. enterica* is facilitated by the development of two populations, a

virulent and an avirulent population, through a bet-hedging based phenomenon.⁴⁶ Interestingly, we identified two populations within mutant population 1 based on the MIC of ampicillin, one which is centered at 1000 µg/mL ampicillin and one centered at 1700 µg/mL ampicillin. The observed heterogeneity in growth rate and development of two populations in MIC of ampicillin in mutant

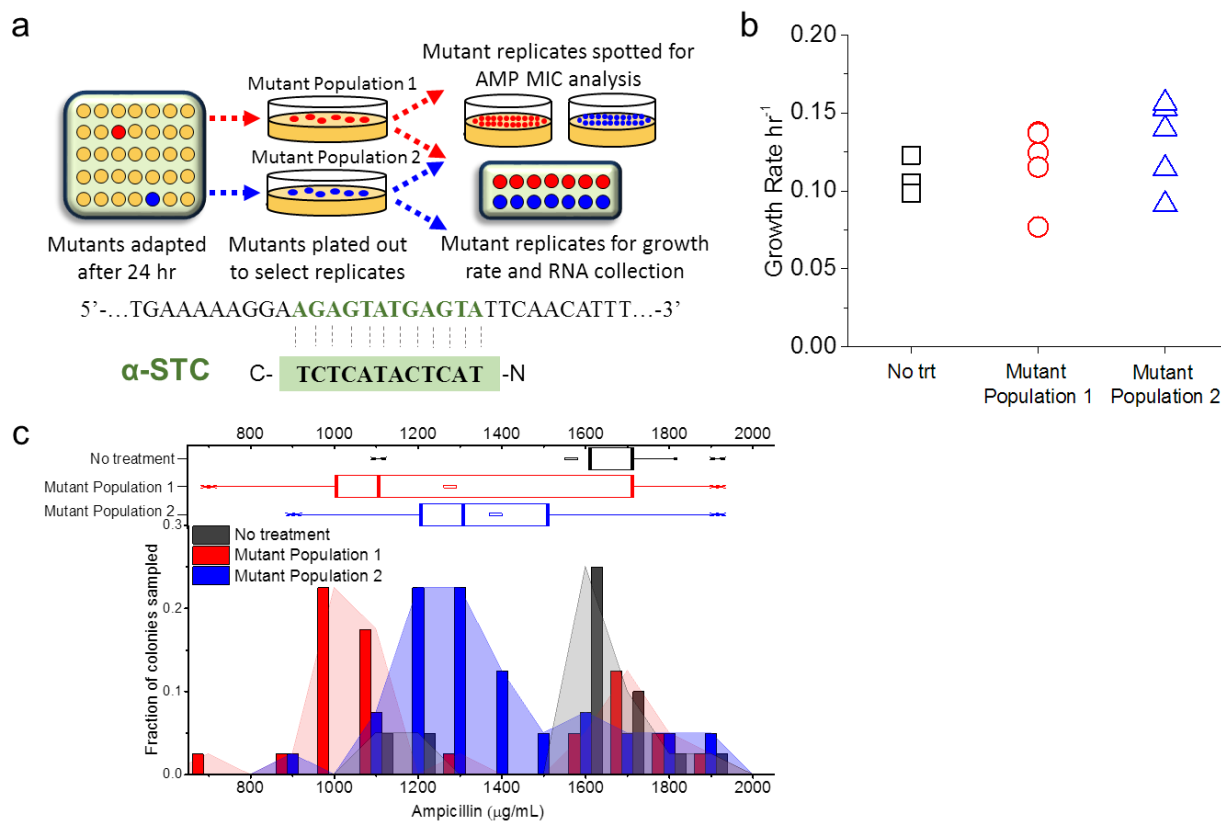


Figure 3.4 Mutants adapted to antisense inhibitors demonstrate heterogeneity in growth rate and MIC of ampicillin. a. Schematic showing the process of selecting adapted mutants. 35 independent cultures were grown at the MIC level of 2.5 µM α -STC and 300 µg/mL of ampicillin to investigate the emergence of resistance. The two mutant populations were plated onto solid media and individual colonies were sampled from each population. Sequencing of the *bla* gene in individual colonies confirmed that the target site of α -STC was not mutated in the no treatment population (n=3), mutant 1 population (n=3), and mutant 2 population (n=3). b. Growth rate for individual replicates in no treatment population (n=6 biological replicates), mutant population 1 (n=6), and mutant population 2 (n=5). c. MIC of ampicillin for individual replicates from no treatment population (n=40), mutation 1 population (n=40), and mutant 2 population (n=40) was measured ranging from 0-2000 µg/mL of ampicillin (lower panel). The box plot of the data (upper panel) analyzes only those replicates whose MIC was within the ampicillin range sampled (0-2000 µg/mL). The box plot shows the range of the data in asterisks, the vertical line in the box represents the median, the small box represents the mean, and the horizontal capped lines represent the lower (25%) and upper (75%) quartiles.

population 1 led us to perform gene expression studies to further investigate whether bet-hedging and heterogeneity would be observed in *bla* resistance and stress response gene expression as an adaptive antibiotic resistance mechanism.

3.3.5 Adapted populations exhibit differential *sbmA* and heterogeneous stress response gene expression

We next measured the change in expression in a previously reported PNA efflux protein, *sbmA*, and a set of key stress response genes to elucidate a tolerance mechanism. The *sbmA* gene is a peptide transporter which was previously shown to be an importer of PNA⁴⁷. We measured the expression level of *sbmA* in the no treatment population as well as in mutant populations 1 and 2. Mutant population 2 had significant decrease in expression of *sbmA* relative to both the no treatment population and mutant population 1 ($p<0.05$) (Figure 3.5a). Mutant population 1 did not exhibit differential expression of *sbmA* relative to the no treatment population ($p>0.05$). This finding confirms that mutant population 1 and 2 are distinct mutants which adapted by unique mechanisms to the α -STC/ampicillin combination and further supports our hypothesis of bet-hedging as a mechanism of resistance. The decreased expression of *sbmA* in mutant population 2 agrees with previously reported resistance to PNA observed as a mutation in the upstream region of the *sbmA* gene which reduced its expression⁴⁷.

To further probe the tolerance mechanism, expression of thirteen representative stress response genes were measured using qPCR (Figure 3.5b-d). Stress response genes were chosen based on a survey of common drug resistance, global stress response, and mutagenesis genes. We examined *marA*, a transcriptional activator of broad range efflux pumps,⁴⁸ and two coupled efflux genes which *marA* activates, *acrA* and *tolC*⁴⁹. *acrA* and *tolC* are outer membrane proteins implicated in multidrug efflux^{48,50}. The expression level of *rpoS*, a sigma factor for global stress

response and stationary phase, was examined because it is shown to regulate 10% of the *E. coli* genome during stress and is associated with DNA damage repair^{51,52}. Expression of cytochrome oxidase subunit, *cyoA*,⁵³ and *hfq*, a regulator of sRNA interactions,⁵⁴ were examined for their role in stress response upstream of *rpoS*⁵⁵. Expression of two error prone DNA polymerases associated with stress response were measured, *dinB* for DNA polymerase IV that does not exhibit proofreading⁵⁶ and *polB* encoding DNA polymerase II which exhibits proofreading²⁵. Expression of *mutS*, a gene encoding a mismatch repair enzyme was examined because it was shown to reduce mutagenesis in *E. coli* during antibiotic stress⁵⁷. The expression of three transcriptional regulators of stress response, *lexA*, a transcriptional repressor of SOS stress response,⁵⁸ *rob*, which codes for a transcriptional activator of stress response genes,⁴⁸ and *soxS*, which regulates the expression of over 100 genes during stress response,⁵⁹ were measured. In addition, *recA* expression was measured for its role in homologous recombination and in initiating the SOS response by acting as a protease which cleaves the *lexA* stress response repressor^{60,61}.

Strikingly, the fold change in expression level for the set of stress response genes relative to no treatment case ($\Delta\Delta C_q$) exhibited a large range of fold changes across biological replicates (Figure 3.5b-d, Figure 3.S12a). Some noteworthy genes with large relative fold change range included *hfq* which varied from 0.03-1.7 (Figure 3.5c), *acrA* varied from 0.18-2.5 (Figure 3.5c), and *lexA* varied from 0.5-7 (Figure 3.5b). Interestingly, *bla* mRNA was expressed tightly across all biological replicates, with a fold change ranging between 0.8-1.7 for the mutant populations with respect to no treatment case (Figure 3.S12b). The observation of large deviations in fold change for individual mutant biological replicates and the observed phenotypic heterogeneity in growth rate and MIC of ampicillin within mutant populations led us to analyze the variance within the mutant population's gene expression.

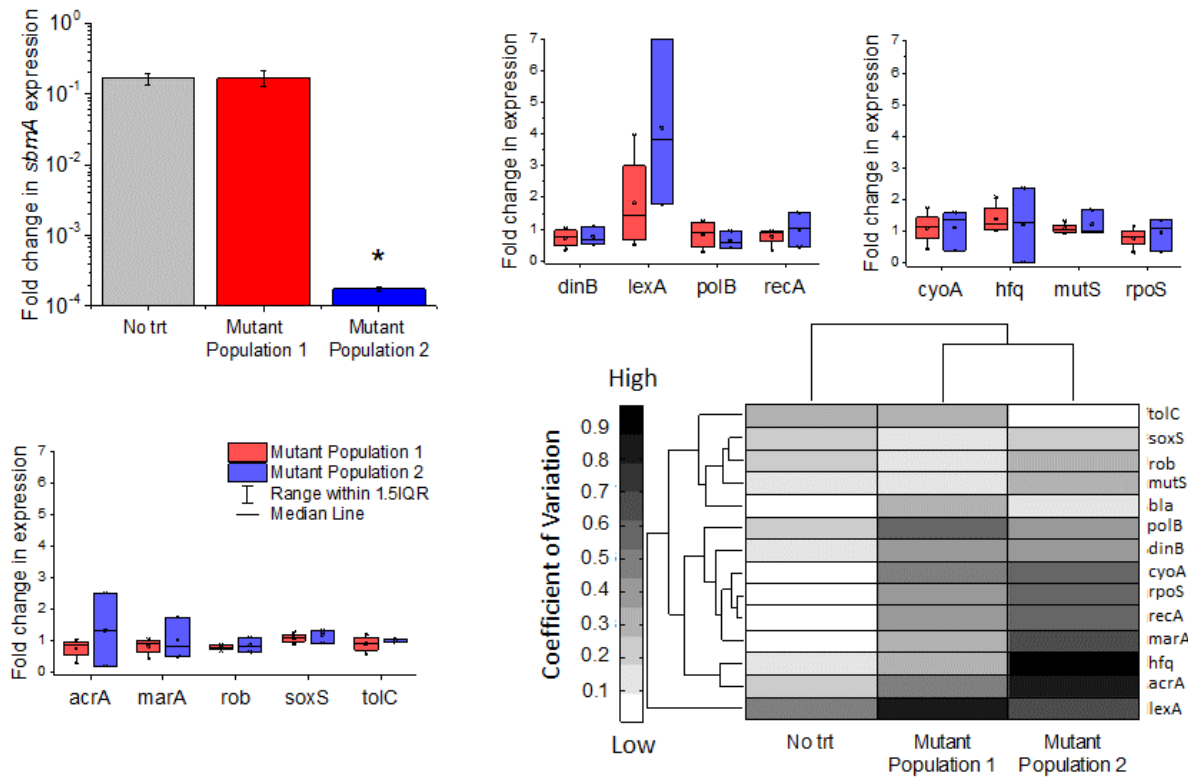


Figure 3.5 Mutants adapted to antisense inhibitors demonstrate gene expression heterogeneity. a. Expression of *sbmA* with respect to moderately expressed housekeeping gene *cysG*. Significance ($p < 0.05$) is represented with an asterisk. b-d. Expression of genes in the SOS response pathway (b), general stress response pathway (c), and Mar regulon (d) with respect to *cysG* in no treatment population ($n=3$), and mutant populations 1 ($n=4$) and 2 ($n=3$). e. Hierarchical clustering analysis showing significant difference in the coefficient of variation between no treatment case and mutant populations 1 and 2. Heatmap values indicate coefficient of variation of $-\Delta C_q, \text{avg}$ between biological replicates of no treatment population ($n=3$), mutant population 1 ($n=4$) and mutant population 2 ($n=3$). Clustering is based on Euclidean distance. Data shown are an average of ' n ' biological replicates (error bars are standard deviation from average values).

Notably, we observed significant gene expression heterogeneity across the 7 biological replicates from mutant populations 1 and 2 (Figure 3.5b-d). The three populations, no treatment, mutant population 1, and mutant population 2, were clustered to examine the relationships between the coefficients of variation (COV) of cycle numbers (C_q) of the stress response genes measured using qPCR (Figure 3.5e) with respect to housekeeping gene *cysG* (ΔC_q) (Figure 3.S12c). Hierarchical clustering analysis showed that the mutant populations were clustered separately from the no treatment case based on the high degree of variability. Higher COV was observed in 10 out

of 13 stress response genes within mutant population 1, and 12 out of 13 stress response genes in mutant population 2 (Figure 3.5e). The existence of a few tightly expressed genes indicated that the variation seen in specific stress response genes is unique to the adapted state.

Surprisingly, mutant population 1 and 2 both showed at least a 30 fold increase in the COV for *marA* expression compared to no treatment case, suggesting that varied levels of transcriptional activation of broad range efflux pumps may be important in obtaining tolerance to α -STC. MarA has been identified as an activator of efflux pumps which gives resistance to unrelated antibiotics, classifying it as an activator of a non-specific efflux system⁶². Surprisingly, variance in two efflux pump genes regulated by *marA*, *acrA* and *tolC*, did not follow the same trend where *acrA* had greater COV in mutant population 1 and 2 and *tolC* expression had similar or reduced COV in the mutant populations. Interestingly, the MtrCDE efflux system in *Neisseria gonorrhoeae* has been shown to confer resistance to a diverse range of antimicrobial peptides and other hydrophobic agents^{63,64} and is stated to be similar to the *acrA* locus in *E. coli* which had increased variance in the mutant populations.

Both mutant populations displayed high COV for *rpoS* expression; which has been implicated in facilitating cross-protection⁵⁴ and shown to be key in obtaining antibiotic resistance to biapenem and imipenem in *Pseudomonas aeruginosa*⁶⁵. Accordingly, *cyoA* and *hfq*, upstream regulators of *rpoS*, showed increased COV in mutant populations. Interestingly, expression level of *recA* and *lexA* was varied in mutant populations. When RecA cleaves the LexA repressor, a number of SOS related genes are de-repressed, thus initiating a global stress response as reflected in the increased variance of two SOS related genes, *dinB* and *polB*. Within the mutant populations, *mutS*, which has previously been shown to reduce lethality of β -lactam antibiotics,⁵⁷ had increased variance but it is unclear whether this is in response to α -STC and/or the β -lactam in the therapeutic

combination. Stress response gene expression signatures of resistance to traditional β -lactamase inhibitors have not been reported previously, so we could not ascertain whether there is similarity in resistance signatures to the designed synthetic β -lactamase antisense inhibitor.

3.4 Conclusions

The heterogeneity observed in growth rate and MIC of ampicillin, difference in *sbmA* expression between mutant population 1 and 2, and expression heterogeneity of stress response genes indicate role of evolutionary bet-hedging in development of adaptive antibiotic resistance to the ampicillin/ α -STC combination⁶⁶. Preventing bet-hedging is not currently understood, but limiting the bet-hedging of stress response genes could potentially reduce the ability of bacteria to adapt to antibiotics. Antisense therapeutics have the potential to target any gene in the genome. This can allow for a limiting of bet-hedging using a combination antisense therapy of molecules targeted not only to the essential or antibiotic resistance conferring gene, but also to stress response genes such as *marA* or *lexA* which had a high variability of expression in the mutant populations. Studying the genes which enable and take part in bet-hedging will allow for a better understanding of how to produce efficacious antibiotics.

While α -STC and α -RBS were successful at re-sensitizing resistant bacteria, they also demonstrate a clear opportunity for future antisense-based antimicrobials. Antisense molecules could be designed to target other resistance mechanisms such as NDM-1 β -lactamase, carbapenemase, extended spectrum β -lactamase, aminoglycoside acetyltransferase, and dihydropteroate synthase^{67,68}. Antisense-based therapeutics are inherently specific due to their sequence based targeting. This makes them advantageous as antibiotics because it removes side effects associated with broad range antibiotics including preventing extreme changes in the resistome and populations of the patients microbiome⁶⁹. We show that antisense inhibitors may

provide an opportunity for mitigating the first sign of emergence of antibiotic resistance with quick development of antisense-based inhibitors; which require only the sequence of an identified target site and synthesis of the cognate antisense molecule. In the development of new antibiotics and resistance-inhibitors it is important to study the emergence of resistance, both *in vitro* and *in vivo*, to begin mitigating the antibiotic resistance crisis. Targeting resistance head-on rather than waiting for it to develop could be useful in designing antibiotics that prevent resistance and remain efficacious for years to come.

3.5 Methods

3.5.1 Bacterial strains and cell culture conditions.

pAKgfp1 plasmid was a gift from Attila Karsi (Addgene plasmid # 14076) encoding TEM-1 β -lactamase gene, *bla*⁷⁰. The plasmid was cloned into chemically competent Zymo DH5a *E. coli* (Expressys). Liquid cultures were grown in 2% lysogeny broth (LB), incubated at 37°C and shaken at 225 rpm. Solid cultures were grown on 2% LB broth, 1.5% agar at 37°C. Ampicillin sodium salt (Sigma Aldrich) was used for selection. Optical density measurements were taken using a Tecan GENios at 562 nm with a bandwidth of 35 nm. Growth rates were calculated from the exponential growth phase of the growth curves (Figure 3.S7). MICs were determined by observing the lowest concentration at which the antisense inhibitor and/or ampicillin prevented a measurable increase in optical density or observable colonies on solid media over 24 hr. All bacterial freezer stocks were stored in 40% glycerol at -80°C.

3.5.2 Colony forming unit analysis

Cultures were sampled at respective time points and serial dilutions were performed ranging from 10²-10¹⁰. Dilutions were plated on solid media and 300 μ g/mL ampicillin sodium

salt and grown at 37°C for 24 h followed by cell counting. CFU/mL was normalized to t=0 for each respective condition. Raw data seen in Figure 3.S13.

3.5.3 Antisense Inhibitors

PNAs were purchased from PNA Bio, Inc (Thousand Oaks, CA). PNA was re-suspended in 5% DMSO in water at 100 µM. Working stocks were stored at 4°C and long term stocks at -20°C to limit freeze thaw cycles.

3.5.4 *bla* RNA collection

Cultures were pretreated overnight in respective PNA in liquid media in the absence of ampicillin and collected for RNA at 16 hr. Three biological replicates were used for *bla* mRNA expression analysis.

3.5.5 Mutant biological replicate collection

Biological replicates from each mutant population were used for sequencing and gene expression analysis. Mutant populations 1 and 2 were re-grown from respective freezer stocks in liquid media with 2.5 µM α-STC and 300 µg/mL ampicillin at 37°C with shaking. At 16 hr, 1:100 dilutions were plated onto solid media with 300 µg/mL ampicillin and grown at 37°C for 16 hr. Individual colonies were selected and regrown in liquid media, 2.5 µM α-STC, and 300 µg/mL ampicillin. For samples used in gene expression analysis, samples were collected when they reached mid-log phase (OD 0.4-0.5). This method was used to sample individual biological replicates in the mutant populations.

3.5.6 Ampicillin MIC of mutant isolates

Freezer stocks of a no treatment population and mutant population 1 and 2 were plated onto solid media with a selection pressure of 300 µg/mL of ampicillin. Individual colonies were selected

from the no treatment (n=40), mutant 1 population (n=40), and mutant population 2 (n=40) and suspended in 100 μ L of liquid media. 5 μ L of each colony suspension was spotted onto solid media with ampicillin concentrations ranging between 0-2000 μ g/mL. After 24 hr of growth at 37°C, colonies were examined to determine their MIC. The MIC was reported as the concentration at which no cell growth occurred. Analysis of populations and box plot statistics was performed using OriginPro 9.1. Raw data for isolates shown in Figure 3.S11a.

3.5.7 RNA extraction and RT-qPCR

50 μ L of the respective culture was added to Bacteria RNAProtect (Qiagen) and pelleted for storage following manufacturer's instructions. Samples were flash frozen in an ethanol dry ice bath and stored at -80°C. Precautions were taken to protect RNA from RNases using RNaseZap (Life Technologies). RNA was extracted from frozen cell pellets using GeneJET RNA purification kit (Thermo Scientific) followed by treatment with Turbo DNA-free (Ambion). 50 ng cDNA was synthesized using Maxima Universal First Stand cDNA synthesis kit (Thermo Scientific). Primers for qPCR were purchased from Integrated DNA Technologies and are listed in Table 3.3. 1.5 ng of cDNA was used for qPCR with Maxima SYBR Green qPCR master mix with ROX normalization (Thermo Scientific) using Illumina Eco qPCR system. Transcript levels were analyzed using the ΔC_q method with respect to moderately expressed housekeeping gene *cysG*⁴². Transcript levels were further analyzed for the mutant populations using the $\Delta\Delta C_q$ method with respect to the no treatment populations.

3.5.8 β -lactamase activity assay

Fluorocillin™ Green 495/525 β -lactamase substrate soluble product (Life Technologies) was used at a concentration of 2.2 μ M as a β -lactamase substrate and measured using a Tecan GENios microplate reader in black flat bottom 96 well plate at 485/535 nm with a bandwidth of

35 nm. Three biological replicates were grown from colonies for 12 hours in liquid media in the presence of the respective antisense inhibitors, diluted 1:10 into liquid media with Fluorocillin green and monitored in the Tecan GENios for 5 hr at 37°C measuring every 2 min. The slope of the exponential, linear region of fluorescence measured was used as a measure of β -lactamase activity as described in Kong et al. 2010.⁷¹

3.5.9 Ampicillin sensitivity assay

Three biological replicates were selected from colonies and pretreated for 16 hr with respective α -STC concentration in liquid media, followed by 1:100,000 dilution into liquid media with respective concentration of ampicillin and α -STC and allowed to grow with shaking at 37°C for 24 hr. The final OD at 562 nm at 24 hr was used for data analysis. Data fitting of sensitivity curves was performed in OriginPro 6.1. Data was fit to sigmoidal/decay Boltzmann function.

3.5.10 Sequencing of *bla* gene on plasmid

Mutant cultures were regrown from freezer stocks with three biological replicates being sampled from each mutant population 1 and mutant population 2 as well as no treatment control. The mutant cultures were regrown in 300 μ g/mL ampicillin for 16 hr and the plasmid was extracted using a GeneJET Plasmid Miniprep Kit (Thermo Scientific). The samples were sequenced using Sanger sequencing and primer 5'-GAATTCGAATTCT**CAGAAGTAAGTTGGCCGCA**-3'. Sequence homologous to the *bla* gene is in bold. Sanger sequencing was performed by GeneWiz.

3.5.11 Data analysis

Data are represented as mean \pm standard deviation. Single factor ANOVA was performed with confidence of $p < 0.05$. Replicates shown are biological replicates.

3.5.12 Clustering analysis

The coefficient of variation (COV) is defined as the standard deviation divided by the mean of the samples. The COV was calculated for the no treatment population (n=3), mutant population 1 (n=4), and mutant population 2 (n=3) using data from the ΔC_q method with respect to *cysG*. The clustergram function in the MATLAB Bioinformatics Toolbox (The Mathworks, Inc., Natick, MA) was used to perform hierarchical clustering of the COV's for gene expression analysis and to generate the heat map and dendrogram. Standard setting of optimal leaf ordering, Euclidean pairwise distance calculation, and unweighted average distance linkage function were used.

3.6 Supplementary Information

3.6.1 Supplementary tables

Table 3.2 Sequencing results of α -STC target site for mutant biological replicates and no treatment control populations. Target site is in bold.

Population	Sequence (5' → 3')
No treatment	TGAAAAAAGGAAGAGTAT GAGTATTCAACATT T
No treatment	TGAAAAAAGGAAGAGTAT GAGTATTCAACATT T
No treatment	TGAAAAAAGGAAGAGTAT GAGTATTCAACATT T
Mutant Population 1	TGAAAAAAGGAAGAGTAT GAGTATTCAACATT T
Mutant Population 1	TGAAAAAAGGAAGAGTAT GAGTATTCAACATT T
Mutant Population 1	TGAAAAAAGGAAGAGTAT GAGTATTCAACATT T
Mutant Population 2	TGAAAAAAGGAAGAGTAT GAGTATTCAACATT T
Mutant Population 2	TGAAAAAAGGAAGAGTAT GAGTATTCAACATT T
Mutant Population 2	TGAAAAAAGGAAGAGTAT GAGTATTCAACATT T

Table 3.3. Primers used for gene expression analysis qPCR.

Gene target	Forward Primer (5'→3')	Reverse Primer (5'→3')	Product Length (nt)
acrA	AAGCCCTTCTTCCAGACGTG	AACGGCAAAGCCAAAGTGTC	189
ampR	GCCTTCCTGTTTGCTCAC	ATAATACCGCGGCCACATAGC	186
cyoA	TGGTAATGGGCTTCTCGTCG	TGGTTCGCCTGGAAGTACC	197
dinB	GGCCAGTTGTGATTACGCC	CTACGCTCCCACAAAATGCG	200
hfq	ATCCGTTCTGAACGCACTG	ACTGTGATGAGAAACCGGGC	191
lexA	GTTAACGGCCAGGCAACAAG	TCAATAACGCCCTTGCCTGC	162
marA	AATCGCGCAAAAGCTGAAGG	GCGATTGCCCTGCATATTG	155
mutS	ATGGAACGTGAGCAGGACAG	CAGCCAGCGTTCAGCATAC	156
polB	GATCCAGCGTTGACCAAGTG	CGCCAGATACCATTGATGCG	179
recA	AGGGCGTCACAGATTCCAG	GTAAAACCACGCTGACGCTG	184
rob	ATCAGCGCGTATCTTCCAG	ACCGCTTCGACTCTAACAG	178
rpoS	AACGGGGCAATTTCAG	AACTGTTATCGCAGGGAGCC	195
sbmA	TATCTTCTGGCAAGCCGGTG	CAGTATTGCCAACGATGCGG	186
soxS	TCTGCTGCGAGACATAACCC	ACTTGCAACGAATGTTCCGC	150
tolC	ACGCACTACCACCAAGTAACG	TTTGTCTCCGGGACCAGTG	189
cysG	ATTCCGTTCTCGGTGGTTCC	CCAGCGTCTGTTTCTGCC	172

3.6.2 Supplementary figures

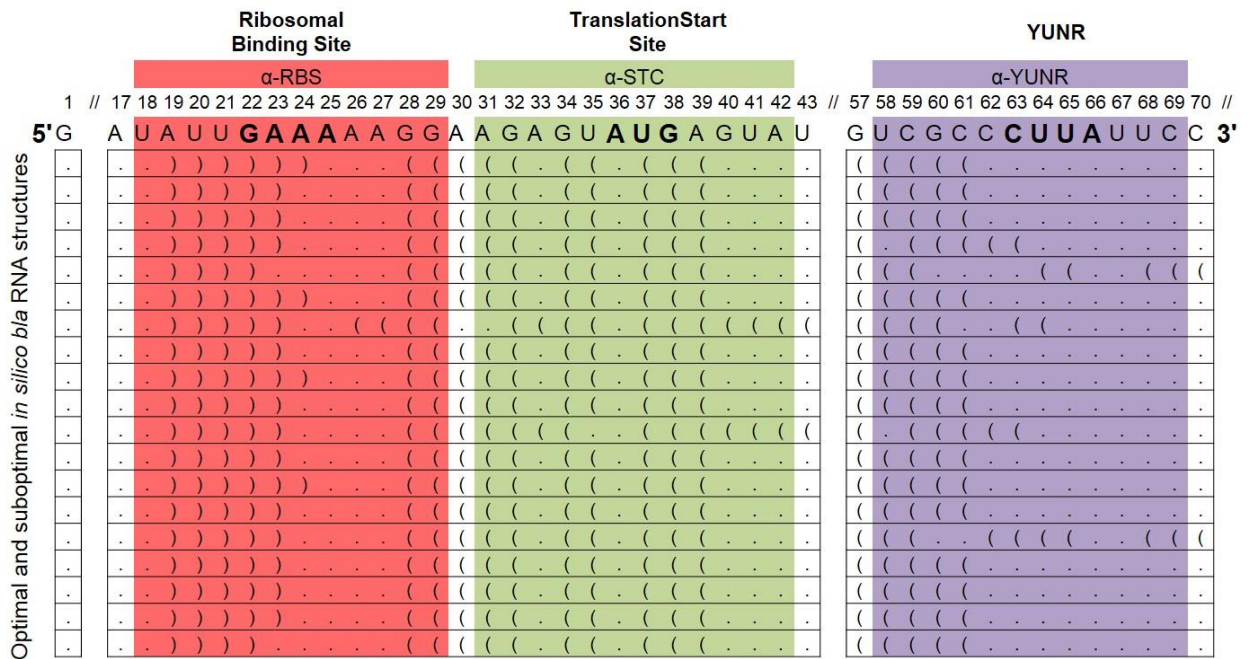


Figure 3.S6 Optimal and suboptimal RNA structures of *bla* target regions. RNA structures were modeled in RNAstructure software.³⁹ α-RBS (red), α-STC (green), and α-YUNR (purple) are shown on the sequence with their structure. The “(“ and “)” symbols represent nucleotides which are double stranded and “.” symbols represent single stranded nucleotides. The ribosomal binding site (RBS), translation start codon (STC), and YUNR motif for the designed antisense molecules are indicated.

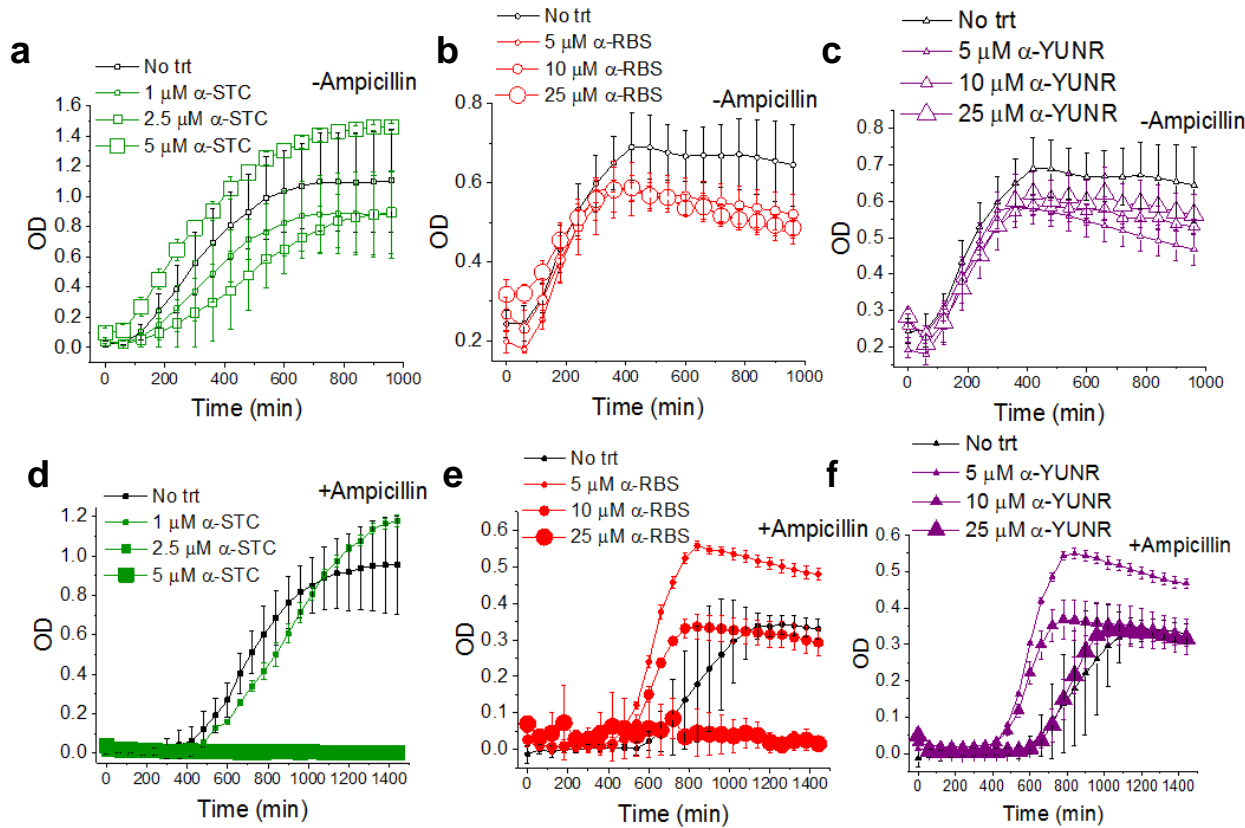


Figure 3.S7 Growth curves in the presence of α -STC, α -RBS, α -YUNR. a-c. Optical density (562 nm) vs. time for three biological replicates in the presence of respective concentrations of α -STC (a) or α -RBS (b) or α -YUNR (c) without ampicillin. d-f. Optical density (562 nm) vs. time for three biological replicates pretreated overnight in respective concentrations of α -STC (d) or α -RBS (e) or α -YUNR (f) in absence of ampicillin, and diluted into medium containing 300 μ g/mL of ampicillin and same concentration of α -STC (d) or α -RBS (e) or α -YUNR (f) respectively. Data shown are an average of three independent experiments (error bars are standard deviation from average values).

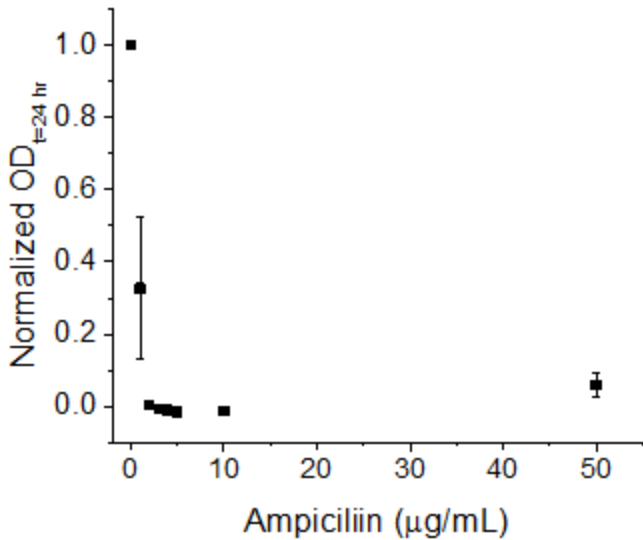


Figure 3.S8 Ampicillin sensitivity for the parent strain. Ampicillin sensitivity for the parent Zymo Dh5a strain before transformation with pAKgfp1 plasmid. The data is normalized to the OD at 24 hr with 0 $\mu\text{g}/\text{mL}$ ampicillin.

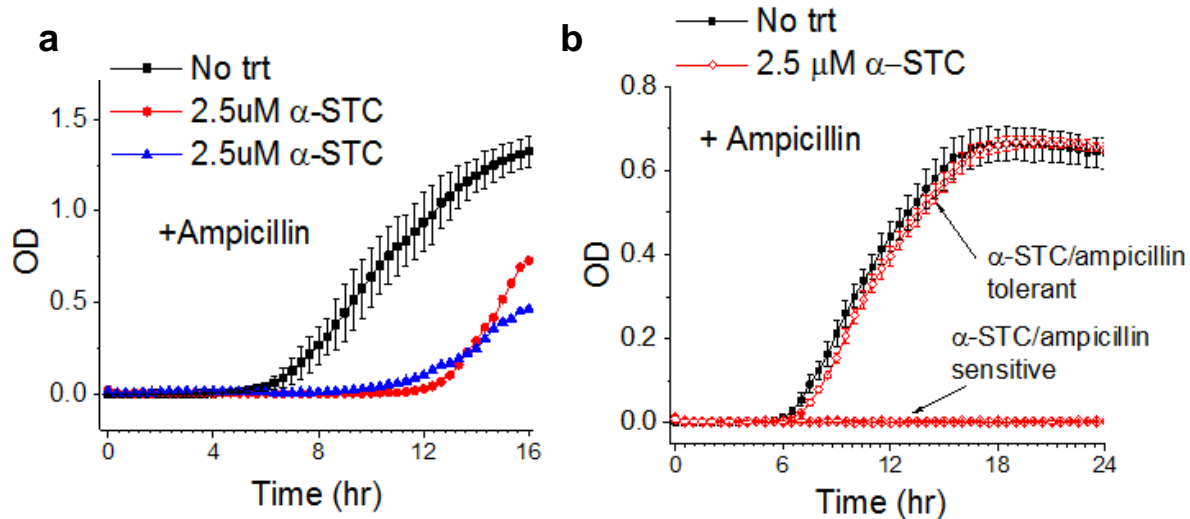


Figure 3.S9 Growth curves of mutant populations 1 and 2 and regrowth of mutant under selection pressure. a. Optical density (562 nm) vs. time of mutant populations 1 and 2 (red and blue curves) grown in the presence of 2.5 μM α -STC and 300 $\mu\text{g}/\text{mL}$ of ampicillin during their adaptation. No treatment population grown in the absence of α -STC and presence of 300 $\mu\text{g}/\text{mL}$ of ampicillin is shown in black. b. Optical density (562 nm) vs. time of α -STC/ampicillin tolerant mutant cultures, α -STC/ampicillin sensitive cultures, and no treatment culture in the presence of ampicillin.

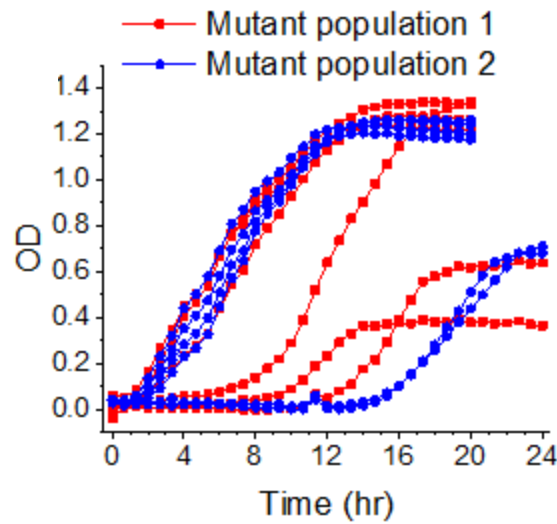


Figure 3.S10 Mutant Biological Replicates. Biological replicates grown from mutant 1 and 2 freezer stocks in 2.5 μM α -STC and 300 $\mu\text{g/mL}$ ampicillin. The mutant samples grew with different growth characteristics including varied lag phase and varied growth rate. The lag phase ranged between 2-12 hr for colonies from mutant population 1 and 7-14 hr for colonies from mutant population 2. The growth rates varied between 0.08-0.14 hr^{-1} for mutant population 1 and 0.09-0.16 hr^{-1} for mutant population 2.

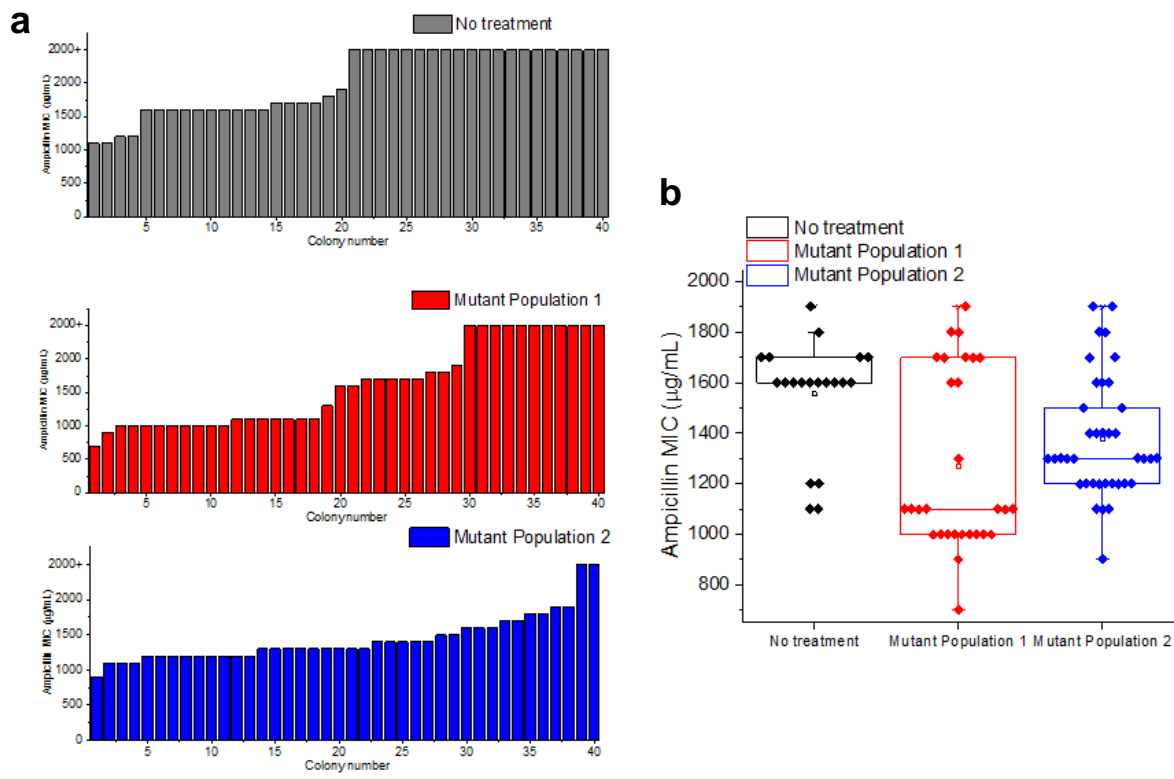


Figure 3.S11 Minimum inhibitory concentrations (MICs) for individual no treatment, mutant population 1, and mutant population 2 colonies a. MIC of ampicillin for individual replicates from no treatment population ($n=40$), mutation population 1 ($n=40$), and mutant population 2 ($n=40$). 2000+ represents any culture which grew up to 2000 $\mu\text{g}/\text{mL}$. b. Box plots of MIC of ampicillin for no treatment and mutant populations 1 and 2 corresponding to the colonies which had a MIC at or below 2000 $\mu\text{g}/\text{mL}$. The asterisk in the box plot represents the range of the data, the vertical line in the box represents the median, the small box represents the mean, and the horizontal capped lines represent the lower (25%) and upper (75%) quartiles. Data points indicate MIC of individual biological replicates.

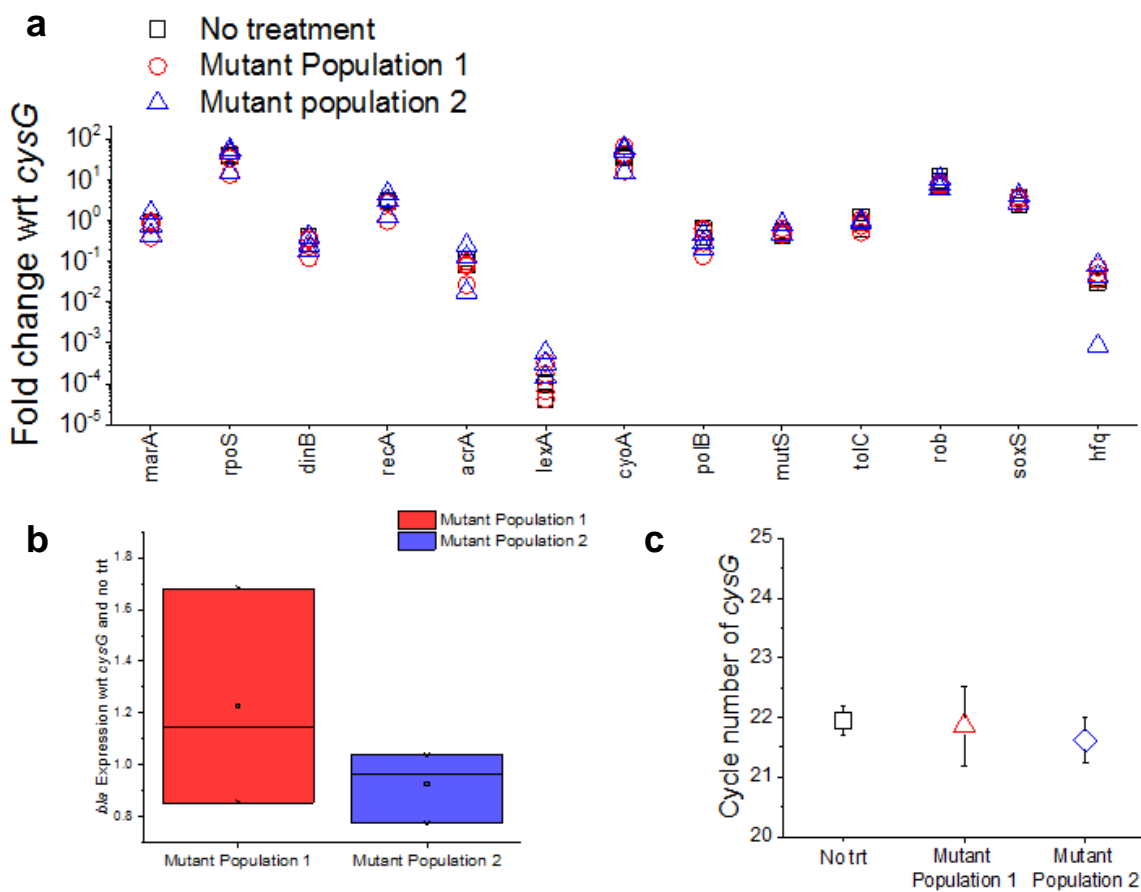


Figure 3.S12 Expression of *bla* and stress response genes in mutant populations adapted to antisense inhibitors. a. Fold change in expression of stress response genes with respect to housekeeping gene *cysG* for individual biological replicates of the no treatment population, mutant population 1, and mutant population 2. b. *bla* RNA expression for mutant population 1 ($n=4$) and 2 ($n=3$) with respect to no treatment population and moderately expressed housekeeping gene *cysG*. The asterisk in the box plot represents the range of the data, the vertical line in the box represents the median, and the small box represents the mean. The *bla* RNA expression level in mutant populations 1 and 2 was not statistically different compared to the no treatment population ($p>0.05$). c. Cycle number for the housekeeping gene *cysG* is consistent across the no treatment population ($n=3$ biological replicates), mutant population 1 ($n=4$), and mutant population 2 ($n=3$). Data shown are an average of ‘n’ biological replicates (error bars are standard deviation from average values).

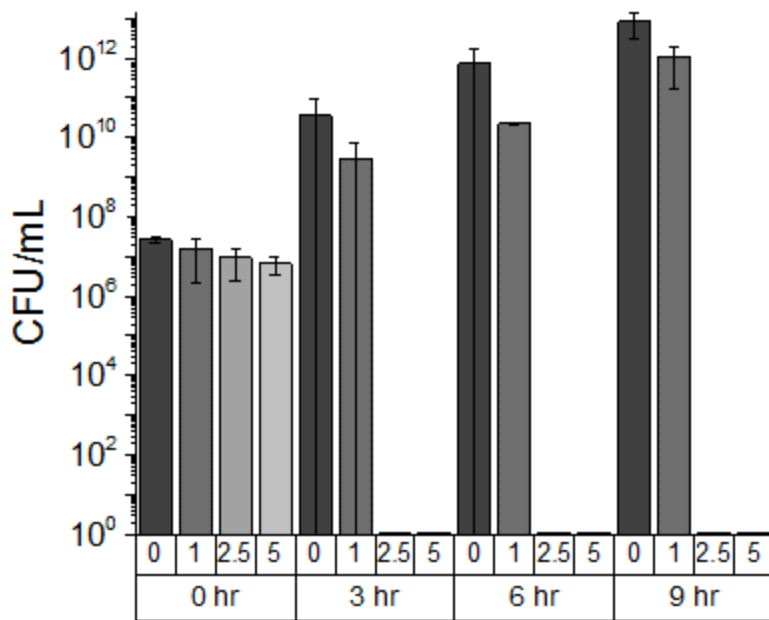


Figure 3.S13 Raw data from colony forming unit analysis. Colony forming units/mL (CFU/mL) for cultures treated with different concentrations of α -STC and 300 μ g/mL ampicillin. Overnight cultures were pretreated with respective concentrations of α -STC, followed by 1:100,000 dilution into fresh media in presence of respective of α -STC concentrations and 300 μ g/mL ampicillin.

3.7 References

1. United States Center for Disease Control. *Antibiotic Resistance Threats*. (2013).
2. Brink, A. J., Coetzee, J., Clay, C. G., *et al.* Emergence of New Delhi metallo- β -lactamase (NDM-1) and Klebsiella pneumoniae carbapenemase (KPC-2) in South Africa. *J. Clin. Microbiol.* **50**, 525–527 (2012).
3. Queenan, A. M. & Bush, K. Carbapenemases: the versatile β -lactamases. *Clin. Microbiol. Rev.* **20**, 440–458 (2007).
4. Hendriksen, R. S., Joensen, K. G., Lukwesa-Musyani, C., *et al.* Extremely drug-resistant *Salmonella enterica* Serovar Senftenberg infections in patients in Zambia. *J. Clin. Microbiol.* **51**, 284–286 (2013).
5. World Health Organization. *Global Tuberculosis Report*. (2012).
6. Davies, J. & Davies, D. Origins and evolution of antibiotic resistance. *Microbiol. Mol. Biol. Rev.* **74**, 417–433 (2010).

7. Bush, K. & Jacoby, G. a. Updated functional classification of β -lactamases. *Antimicrob. Agents Chemother.* **54**, 969–76 (2010).
8. Bush, K. Proliferation and significance of clinically relevant β -lactamases. *Ann. N. Y. Acad. Sci.* **1277**, 84–90 (2013).
9. Drawz, S. M., Papp-Wallace, K. M. & Bonomo, R. A. New β -lactamase inhibitors: a therapeutic renaissance in an MDR world. *Antimicrob. Agents Chemother.* **58**, 1835–1846 (2014).
10. Livermore, D. M. β -lactamase-mediated resistance and opportunities for its control. *J. Antimicrob. Chemother.* **41**, 25–41 (1998).
11. Shlaes, D. M. New β -lactam- β -lactamase inhibitor combinations in clinical development. *Ann. N. Y. Acad. Sci.* **1277**, 105–114 (2013).
12. Mondhe, M., Chessher, A., Goh, S., Good, L. & Stach, J. E. M. Species-selective killing of bacteria by antimicrobial peptide-PNAs. *PLoS One* **9**, e89082 (2014).
13. Bennett, C. F. & Swayze, E. E. RNA targeting therapeutics: molecular mechanisms of antisense oligonucleotides as a therapeutic platform. *Annu. Rev. Pharmacol. Toxicol.* **50**, 259–293 (2010).
14. Egholm, M., Buchardt, O., Christensen, L., *et al.* PNA hybridizes to complementary oligonucleotides obeying the Watson-Crick hydrogen-bonding rules. *Nature* **365**, 566–568 (1993).
15. Johnson, E. & Srivastava, R. Volatility in mRNA secondary structure as a design principle for antisense. *Nucleic Acids Res.* **41**, e43 (2013).
16. Massé, E., Escorcía, F. E. & Gottesman, S. Coupled degradation of a small regulatory RNA and its mRNA targets in *Escherichia coli*. *Genes Dev.* **17**, 2374–2383 (2003).
17. Kole, R., Krainer, A. R. & Altman, S. RNA therapeutics: beyond RNA interference and antisense oligonucleotides. *Nat. Rev. Drug Discov.* **11**, 125–140 (2012).
18. Courtney, C. & Chatterjee, A. cis-Antisense RNA and Transcriptional Interference: Coupled Layers of Gene Regulation. *J. Gene Ther.* **2**, 1–9 (2014).
19. Meng, J., Da, F., Ma, X., *et al.* Antisense Growth Inhibition of Methicillin-Resistant *Staphylococcus aureus* by Locked Nucleic Acid Conjugated with Cell-Penetrating Peptide as a Novel FtsZ Inhibitor. *Bios* **59**, 914–922 (2015).
20. Kiran, D. & Sriranganathan, N. The antimicrobial effect of anti- dnaK peptide nucleic acids on multidrug resistant strains of *Escherichia coli* and *Salmonella enterica* serovar Typhimurium. *Bios* **85**, 48–56 (2014).
21. Marin, V. L., Roy, S. & Armitage, B. a. Recent advances in the development of peptide

- nucleic acid as a gene-targeted drug. *Expert Opin. Biol. Ther.* **4**, 337–348 (2004).
- 22. Chatterjee, A., Cook, L. C. C., Shu, C.-C., *et al.* Antagonistic self-sensing and mate-sensing signaling controls antibiotic-resistance transfer. *Proc. Natl. Acad. Sci. U. S. A.* **110**, 7086–90 (2013).
 - 23. Chatterjee, A., Johnson, C. M., Shu, C.-C., *et al.* Convergent transcription confers a bistable switch in *Enterococcus faecalis* conjugation. *Proc. Natl. Acad. Sci. U. S. A.* **108**, 9721–6 (2011).
 - 24. Mwangi, M. M., Wu, S. W., Zhou, Y., *et al.* Tracking the *in vivo* evolution of multidrug resistance in *Staphylococcus aureus* by whole-genome sequencing. *Proc. Natl. Acad. Sci. U. S. A.* **104**, 9451–6 (2007).
 - 25. Bjedov, I., Tenaillon, O., Gérard, B., *et al.* Stress-induced mutagenesis in bacteria. *Science* **300**, 1404–1409 (2003).
 - 26. Neidig, A., Yeung, A. T. Y., Rosay, T., *et al.* TypA is involved in virulence, antimicrobial resistance and biofilm formation in *Pseudomonas aeruginosa*. *BMC Microbiol.* **13**, 77 (2013).
 - 27. Napolitano, R., Janel-Bintz, R., Wagner, J. & Fuchs, R. P. All three SOS-inducible DNA polymerases (Pol II, Pol IV and Pol V) are involved in induced mutagenesis. *EMBO J.* **19**, 6259–6265 (2000).
 - 28. Fernández, L., Breidenstein, E. B. M. & Hancock, R. E. W. Creeping baselines and adaptive resistance to antibiotics. *Drug Resist. Updat.* **14**, 1–21 (2011).
 - 29. Blanchard, C., Barnett, P., Perlmutter, J. & Dunman, P. M. Identification of *Acinetobacter baumannii* Serum-Associated Antibiotic Efflux Pump Inhibitors. *Antimicrob. Agents Chemother.* **58**, 6360–6370 (2014).
 - 30. Sánchez-Romero, M. A. & Casadesús, J. Contribution of phenotypic heterogeneity to adaptive antibiotic resistance. *Proc. Natl. Acad. Sci. U. S. A.* **111**, 355–60 (2014).
 - 31. Blumberg, P. M. & Strominger, J. L. Interaction of penicillin with the bacterial cell: penicillin-binding proteins and penicillin-sensitive enzymes. *Bacteriol. Rev.* **38**, 291–335 (1974).
 - 32. Dryselius, R., Aswasti, S. K., Rajarao, G. K., Nielsen, P. E. & Good, L. The translation start codon region is sensitive to antisense PNA inhibition in *Escherichia coli*. *Oligonucleotides* **13**, 427–33 (2003).
 - 33. Oh, E., Zhang, Q. & Jeon, B. Target optimization for peptide nucleic acid (PNA)-mediated antisense inhibition of the CmeABC multidrug efflux pump in *Campylobacter jejuni*. *J. Antimicrob. Chemother.* **69**, 375–80 (2014).
 - 34. Fozo, E. M., Hemm, M. R. & Storz, G. Small toxic proteins and the antisense RNAs that

repress them. *Microbiol. Mol. Biol. Rev.* **72**, 579–89 (2008).

35. Hatamoto, M., Ohashi, A. & Imachi, H. Peptide nucleic acids (PNAs) antisense effect to bacterial growth and their application potentiality in biotechnology. *Appl. Microbiol. Biotechnol.* **86**, 397–402 (2010).
36. Good, L. & Nielsen, P. E. Antisense inhibition of gene expression in bacteria by PNA targeted to mRNA. *Nat. Biotechnol.* **16**, 355–358 (1998).
37. Franch, T., Petersen, M., Wagner, E. G., Jacobsen, J. P. & Gerdes, K. Antisense RNA regulation in prokaryotes: rapid RNA/RNA interaction facilitated by a general U-turn loop structure. *J. Mol. Biol.* **294**, 1115–1125 (1999).
38. Brunel, C., Marquet, R., Romby, P. & Ehresmann, C. RNA loop-loop interactions as dynamic functional motifs. *Biochimie* **84**, 925–944 (2002).
39. Reuter, J. S. & Mathews, D. H. RNAstructure: software for RNA secondary structure prediction and analysis. *BMC Bioinformatics* **11**, 129 (2010).
40. Good, L., Awasthi, S. K., Dryselius, R., Larsson, O. & Nielsen, P. E. Bactericidal antisense effects of peptide-PNA conjugates. *Nat. Biotechnol.* **19**, 360–364 (2001).
41. Wang, J., Nielsen, P. E., Jiang, M., *et al.* Mismatch-sensitive hybridization detection by peptide nucleic acids immobilized on a quartz crystal microbalance. *Anal. Chem.* **69**, 5200–5202 (1997).
42. Zhou, K., Zhou, L., Lim, Q. 'En, *et al.* Novel reference genes for quantifying transcriptional responses of Escherichia coli to protein overexpression by quantitative PCR. *BMC Mol. Biol.* **12**, 18–26 (2011).
43. Rukavishnikov, A., Gee, K. R., Johnson, I. & Corry, S. Fluorogenic cephalosporin substrates for β -lactamase TEM-1. *Anal. Biochem.* **419**, 9–16 (2011).
44. Hernández, S. B., Cota, I., Ducret, A., Aussel, L. & Casadesús, J. Adaptation and preadaptation of *Salmonella enterica* to bile. *PLoS Genet.* **8**, (2012).
45. Beaumont, H. J. E., Gallie, J., Kost, C., Ferguson, G. C. & Rainey, P. B. Experimental evolution of bet hedging. *Nature* **462**, 90–93 (2009).
46. Arnoldini, M., Vizcarra, I. A., Peña-Miller, R., *et al.* Bistable Expression of Virulence Genes in *Salmonella* Leads to the Formation of an Antibiotic-Tolerant Subpopulation. *PLoS Biol.* **12**, e1001928 (2014).
47. Ghosal, A., Vitali, A., Stach, J. E. M. & Nielsen, P. E. Role of SbmA in the Uptake of Peptide Nucleic Acid (PNA)-Peptide Conjugates in *E. coli*. *ACS Chem. Biol.* **8**, 360–367 (2013).
48. Rosner, J. L. & Martin, R. G. Reduction of cellular stress by TolC-dependent efflux pumps

- in *Escherichia coli* indicated by BaeSR and CpxARP activation of spy in efflux mutants. *J. Bacteriol.* **195**, 1042–1050 (2013).
49. Barbosa, T. M. & Levy, S. B. Differential expression of over 60 chromosomal genes in *Escherichia coli* by constitutive expression of MarA. *J. Bacteriol.* **182**, 3467–3474 (2000).
 50. Hobbs, E. C., Yin, X., Paul, B. J., Astarita, J. L. & Storz, G. Conserved small protein associates with the multidrug efflux pump AcrB and differentially affects antibiotic resistance. *Proc. Natl. Acad. Sci. U. S. A.* **109**, 16696–16701 (2012).
 51. Weber, H., Polen, T., Heuveling, J., *et al.* Genome-Wide Analysis of the General Stress Response Network in *Escherichia coli* : S -Dependent Genes, Promoters, and Sigma Factor Selectivity. *J. Bacteriol.* **187**, 1591–1603 (2005).
 52. Merrikh, H., Ferrazzoli, A. E., Bougdour, A., Olivier-Mason, A. & Lovett, S. T. A DNA damage response in *Escherichia coli* involving the alternative sigma factor, RpoS. *Proc. Natl. Acad. Sci. U. S. A.* **106**, 611–6 (2009).
 53. Cotter, P. A., Chepuri, V., Gennis, R. B. & Gunsalus, R. P. Cytochrome o (cyoABCDE) and d (cydAB) Oxidase Gene Expression in *Escherichia coli* Is Regulated by Oxygen, pH, and the fnr Gene Product. *J. Bacteriol.* **172**, 6333–6338 (1990).
 54. Battesti, A., Majdalani, N. & Gottesman, S. The RpoS-mediated general stress response in *Escherichia coli*. *Annu. Rev. Microbiol.* **65**, 189–213 (2011).
 55. Al Mamun, A. A. M., Lombardo, M.-J., Shee, C., *et al.* Identity and function of a large gene network underlying mutagenic repair of DNA breaks. *Science* **338**, 1344–1348 (2012).
 56. Wagner, J., Gruz, P., Kim, S. R., *et al.* The dinB gene encodes a novel *E. coli* DNA polymerase, DNA pol IV, involved in mutagenesis. *Mol. Cell* **4**, 281–286 (1999).
 57. Dwyer, D. J., Belenky, P. a, Yang, J. H., *et al.* Antibiotics induce redox-related physiological alterations as part of their lethality. *Proc. Natl. Acad. Sci. U. S. A.* **111**, E2100–9 (2014).
 58. Kawano, M., Aravind, L. & Storz, G. An antisense RNA controls synthesis of an SOS-induced toxin evolved from an antitoxin. *Mol. Microbiol.* **64**, 738–754 (2007).
 59. Chiang, S. M. & Schellhorn, H. E. Regulators of oxidative stress response genes in *Escherichia coli* and their functional conservation in bacteria. *Arch. Biochem. Biophys.* **525**, 161–169 (2012).
 60. Gonzalez, R., Tao, H., Purvis, J. E., *et al.* Gene array-based identification of changes that contribute to ethanol tolerance in ethanologenic *Escherichia coli*: comparison of KO11 (parent) to LY01 (resistant mutant). *Biotechnol. Prog.* **19**, 612–623 (2003).
 61. Little, J. W. & Mount, D. W. The SOS Regulatory System of *Escherichia coli*. *Cell* **29**, 11–22 (1982).

62. Okusu, H. & Nikaido, H. AcrAB efflux pump plays a major role in the antibiotic resistance phenotype of *Escherichia coli* multiple-antibiotic-resistance (Mar) mutants. *J. Bacteriol.* **178**, 306–308 (1996).
63. Yeaman, M. R. & Yount, N. Y. Mechanisms of Antimicrobial Peptide Action and Resistance. *Pharmacol. Rev.* **55**, 27–55 (2003).
64. Rouquette, C., Harmon, J. B. & Shafer, W. M. Induction of the mtrCDE-encoded efflux pump system of *Neisseria gonorrhoeae* requires MtrA, an AraC-like protein. *Mol. Microbiol.* **33**, 651–658 (1999).
65. Murakami, K., Ono, T., Viducic, D., *et al.* Role for rpoS gene of *Pseudomonas aeruginosa* in antibiotic tolerance. *FEMS Microbiol. Lett.* **242**, 161–167 (2005).
66. Erickson, K. E., Otoupal, P. B. & Chatterjee, A. Gene Expression Variability Underlies Adaptive Resistance in Phenotypically Heterogeneous Bacterial Populations. *ACS Infect. Dis.* **1**, 555–567 (2016).
67. Magnet, S., Smith, T., Zheng, R., Nordmann, P. & Blanchard, J. S. Aminoglycoside Resistance Resulting from Tight Drug Binding to an Altered Aminoglycoside Acetyltransferase. *Antimicrob. Agents Chemother.* **47**, 1577–1583 (2003).
68. Triglia, T., Menting, J. G., Wilson, C. & Cowman, A. F. Mutations in dihydropteroate synthase are responsible for sulfone and sulfonamide resistance in *Plasmodium falciparum*. *Proc. Natl. Acad. Sci. U. S. A.* **94**, 13944–13949 (1997).
69. Sommer, M. O. a & Dantas, G. Antibiotics and the resistant microbiome. *Curr. Opin. Microbiol.* **14**, 556–563 (2011).
70. Karsi, A. & Lawrence, M. L. Broad host range fluorescence and bioluminescence expression vectors for Gram-negative bacteria. *Plasmid* **57**, 286–95 (2007).
71. Kong, Y., Yao, H., Ren, H., *et al.* Imaging tuberculosis with endogenous β -lactamase reporter enzyme fluorescence in live mice. *Proc. Natl. Acad. Sci. U. S. A.* **107**, 12239–44 (2010).

Chapter 4

Predictive homology for antisense RNA-inhibitor antibiotics in non-traditional antibiotic pathways

Courtney, C.M., Erickson, K.E., Madinger, N.E., Chatterjee, A. *In Preparation.*

4.1 Abstract

Multidrug-resistant (MDR) infections are a pressing concern to global health which is made worse by the lack of new antibiotics being introduced. Developing sequence-specific antimicrobials enables us to target non-traditional antibiotic pathways to utilize new antibiotic targets and investigate potential combination therapies. Using *Escherichia coli* as a model organism we created peptide nucleic acid antisense molecules which target essential genes in non-traditional antibiotic pathways including metabolism, cell signaling, and stress response and have predicted homology in varied species of Enterobacteriaceae. Although the antisense molecules were designed against essential genes in non-pathogenic, drug-sensitive *E. coli*, these molecules demonstrate therapeutic potential against pathogenic, MDR clinical isolates of *E. coli*, *Klebsiella pneumoniae*, and *Salmonella enterica*, thus highlighting the potential to create broad-pathogen yet gene-specific antibiotics using predictive homology. The clinical isolates used in this study are highly resistant to most classes of antibiotics, yet when the antisense molecules are used in combination with traditional antibiotics we observe a strong synergistic effect that significantly inhibits cell growth greater than either mono-therapy. Our findings highlight the potential utility of applying antisense technology to novel targets in non-traditional antibiotic pathways.

4.2 Introduction

Antibiotic-resistant bacteria are threatening our ability to treat common infections causing an estimated 20 billion dollars in direct healthcare costs. This health crisis is due to the intersection of rapidly evolving antibiotic-resistant bacteria and the lack of new antibiotics being developed¹. Current antibiotics are limited to small molecules targeting proteins within three main pathways in bacteria: cellular replication, protein biosynthesis, and cell wall biosynthesis. There is a clear disparity between the current antibiotic targets and the potential essential bacterial genes that could be targeted for antimicrobial purposes using antisense technology. There are approximately 303 essential genes in *E. coli* with 139 of those existing in non-traditional antibiotic pathways such as metabolism, cell motility and secretion, and even those of unknown function². Antisense therapeutics enable sequence-specific targeting of RNA, allowing for design of molecules which target essential genes in non-traditional antibiotic target pathways.

Antisense therapies are nucleic acids, natural or synthetic, which are the reverse complement of the target sequence enabling antisense interactions via Watson-Crick base pairing which can inhibit transcription and/or translation^{3,4}. Using antisense molecules to capitalize on novel antimicrobial pathways is practical, even on a small scale, due to the ease of design against any gene sequence in an organism of interest. For our study, we have chosen to use peptide nucleic acid (PNA) 12-mers targeted to the translation start codon⁴ of the gene of interest. PNA is a synthetic nucleic acid which has a modified protein backbone and nucleic acid functional groups leading to increased stability in the cells due to no known enzymatic degradation. Additionally, the neutral backbone of PNA has reduced electrostatic repulsion resulting in increased nucleic acid binding affinity compared to natural nucleic acids⁵. While the neutral backbone of PNA is advantageous for binding to native nucleic acids it presents a transport issue which we mitigated

by using PNA conjugated to (KFF)₃K cell penetrating peptides for increased transport into *E. coli*⁶, *K. pneumoniae*⁷, and *S. enterica*⁸. Single-stranded PNA forms sequence-specific duplexes with RNA at higher stability compared to duplexes with DNA⁹ leading to lower translation of the targeted RNA as opposed to transcriptional inhibition^{10,11}. PNA antisense molecules have been shown as effective antimicrobial agents against a multitude of traditional antibiotic targets including β-lactamase drug resistance genes¹⁰, 23S and 16S ribosomal RNA¹¹, and cell division proteins such as *ftsZ*¹².

Antisense antimicrobials have previously been designed for pathogen-specific applications¹² however we find broad-range activity within a class of pathogens advantageous to investigate considering the possibility of using antisense therapy against an unknown or multi-pathogen infection. For our study, we investigated the utility of predictive homology in designing gene-specific antisense-PNA RNA-inhibitors against clinical patient isolates of Enterobacteriaceae. Antisense antibiotics targeting non-traditional antibiotic targets could be impactful against clinical isolates which already have developed resistance to traditional antibiotics.

Using *E. coli* MG1655 as the reference genome, we designed PNA antisense molecules which target essential genes in non-traditional antibiotic pathways including metabolism, signaling, and stress response. We chose to design with *E. coli* as our organism of interest because the set of essential genes for growth is well characterized². We analyzed and tuned the target sequences for homology in two other Enterobacteriaceae: *K. pneumoniae* MGH 78578 and *Salmonella enterica* serovar Typhimurium SL1344. Here we show that predictive homology is useful in designing broad pathogen, gene specific RNA-inhibitors which have efficacy as monotherapy and function synergistically in combination with small molecule antibiotics.

4.3 Results and Discussion

4.3.1 Antisense PNA RNA-inhibitor design and predictive homology

For the study we chose two clinical isolates each of *E. coli* (*E. coli*-1 and 2), *K. pneumoniae* (KPN-1 and 2) and *S. enterica*, one of which was known to be serovar Typhimurium (STm) and one of unknown serovar (SE). To first characterize the clinical isolates, we performed antibiotic screening to determine “sensitive” (S), “intermediate” (I), and “resistant” (R) phenotypes using the 2016-2017 Clinical & Laboratory Standards Institute sensitive/resistant breakpoint values¹³ (Table 4.1). We screened nine antibiotics of varied mechanism: ampicillin (AMP), ceftriaxone (FRX), meropenem (MER), gentamicin (GEN), kanamycin (KAN), tetracycline (TET), ciprofloxacin (CIP), nalidixic acid (NXA), and chloramphenicol (CHL) (Figure 4.1a). These antibiotics have varied mechanisms of action and belong to the following antibiotic classes: penicillins, cephems, carbapenems, aminoglycosides, tetracyclines, fluoroquinolones, quinolones, and phenicols. We found all isolates to have resistance to two or more antibiotics. In the extreme case, *E. coli*-1 showed resistance to all nine antibiotics tested. All strains were resistant to ampicillin and ceftriaxone.

We designed PNA molecules targeting four essential genes in non-traditional antibiotic pathways (Table 4.2): H2-folate synthetase (*folC*) in folate biosynthesis¹⁴, the signal recognition particle protein gene (*ffh*) which is essential for protein translocation¹⁵, the gene for SOS response repressor protein¹⁶ (*lexA*), and a small non-coding Hfq regulated RNA (*fnrS*) which plays a role in the transition from aerobic to anaerobic metabolism¹⁷ (Figure 4.1b). We chose these genes for their varied roles in cellular pathways. We also designed two RNA-inhibitors against traditional antibiotic targets: gyrase subunit B (*gyrB*) and 30S ribosomal protein S4 (*rpsD*) which have similar targets compared to fluoroquinolones and tetracyclines/aminoglycosides, respectively. The

antisense molecules are 12 nucleotides long centered on the translation start codon of the gene of interest (Figure 4.1b). The antisense molecules targeting *folC* (α -*folC*) and *fnrS* (α -*fnrS*) were only homologous to *E. coli*. The remaining four antisense molecules, targeting *rpsD* (α -*rpsD*), *ffh* (α -*ffh*), *lexA* (α -*lexA*), and *gyrB* (α -*gyrB*), were designed for homology against *E. coli*, *K. pneumoniae*, and *S. enterica*. Interestingly, α -*rpsD* had homology in *S. enterica* centered on the start site of *rtcA* which codes for RNA 3'-terminal phosphate cyclase and plays a role in end healing within a RNA repair pathway¹⁸. There were other instances of the 12-nt sequences in off-

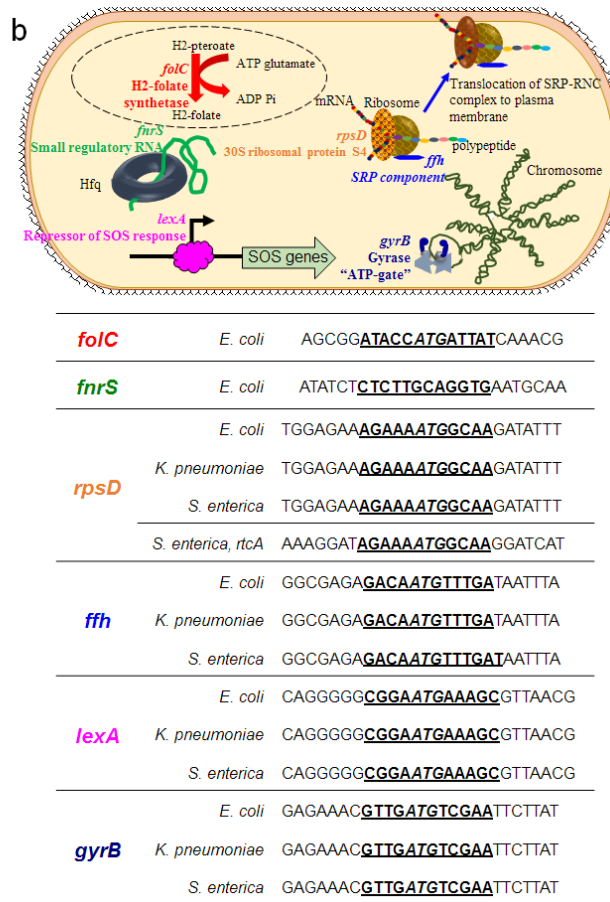
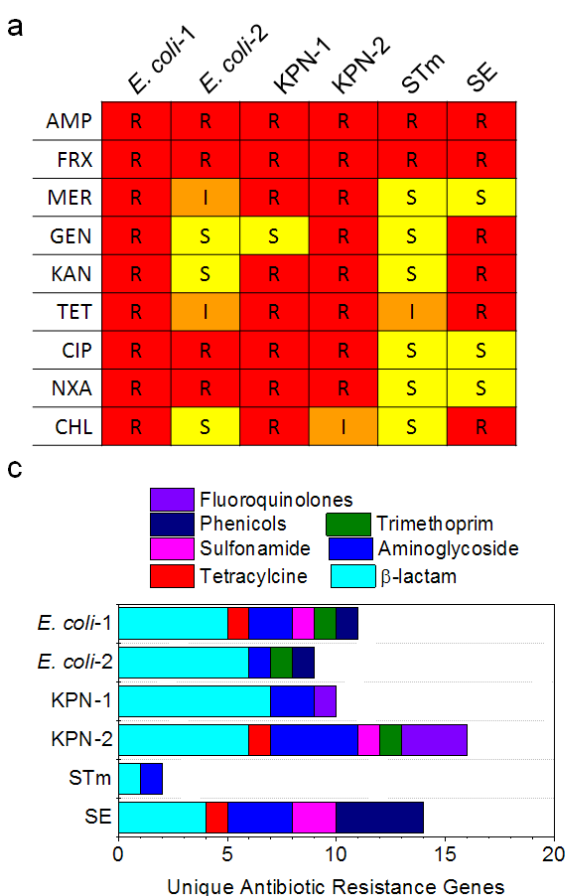


Figure 4.1 Antibiotic resistance characterization of clinical isolates and design of antisense-PNA. a. Antibiotic resistance, based on 2016-2017 CLSI sensitive/resistant breakpoints, of clinical strains used in study. b. Design of antisense-PNA against six targets in *E. coli* and homology in *K. pneumoniae* and *S. enterica*. Antisense-PNA target is bold and underlined with translation start site italicized. Cell schematic shows function of genes targeted with antisense-PNA. c. Unique antibiotic resistance genes in clinical isolates identified by genome sequencing and ARG-ANNOT evaluation.

target genes not centered on start site (Table 4.3). We did not consider non-start site off-target gene effects on cellular inhibition since PNA has been shown to have the highest efficacy when the antisense molecule is centered around the start codon^{4,10}. We, however, did consider potential sequestration of antisense-PNA by the off-targets in later discussion of molecule efficacy.

4.3.2 Clinical isolate characterization

After designing our antisense RNA-inhibitors, we sequenced the six clinical isolates using Illumina MiSeq. After *de novo* assembly, we characterized their unique antibiotic resistance genes using the ARG-ANNOT tool (Antibiotic Resistance Gene-ANNOTation) (Table 4.4). We found that all of the clinical strains had at least two unique antibiotic resistance genes and at the extreme, KPN-2 has sixteen unique antibiotic resistance genes. All clinical isolates in the study have at least one β -lactamase gene, which confers resistance to varied β -lactam antibiotics, and across the set of six isolates are genes for eight unique β -lactamases: NDM-1, TEM, CTX, SHV, AmpC, KPC, OXA, and CMY highlighting the need to develop therapeutics in alternative pathways (Figure 4.1c).

4.3.3 Antisense PNA efficacy in MDR clinical isolates

We next tested the six antisense-PNA molecules at 10 μ M in the clinical strains. A control PNA molecule, α -nonsense, was also run at 10 μ M and showed no deviation from no treatment indicating the observed inhibition from target molecules is not due to PNA or CPP chemical toxicity. α -folC significantly reduced growth in *E. coli*-2 (Figure 4.2a, Figure 4.S4, and Figure 4.S5). Interestingly, α -fnrS significantly reduced growth in KPN-1, STm, and SE. α -rpsD was the most effective molecule and significantly reduced growth of *E. coli*-1 and 2, KPN-1 and 2, and STm. α -gyrB, α -ffh, and α -lexA significantly inhibited *E. coli*-1 and 2 and STm. Given that these antisense molecules were designed against non-pathogenic, drug-sensitive genomes and based on

only *E. coli*'s set of essential genes, the number of significantly inhibited strains is a remarkable 54% of predicted targets (Figure 4.2b). This highlights the benefit of rationally designed therapeutics compared to random screens in which successful compounds often comprise <0.0001% of compounds tested¹⁹.

We performed sequence analysis of the six antisense targets in the clinical isolate genomes and found that all strains contained their predicted targets centered on the translation start codon in the gene of interest (Figure 4.S6). We also looked for possible off targets in the clinical isolates (Table 4.5) and again identified the only translation start site 12-mer off-target match was *rtcA* in

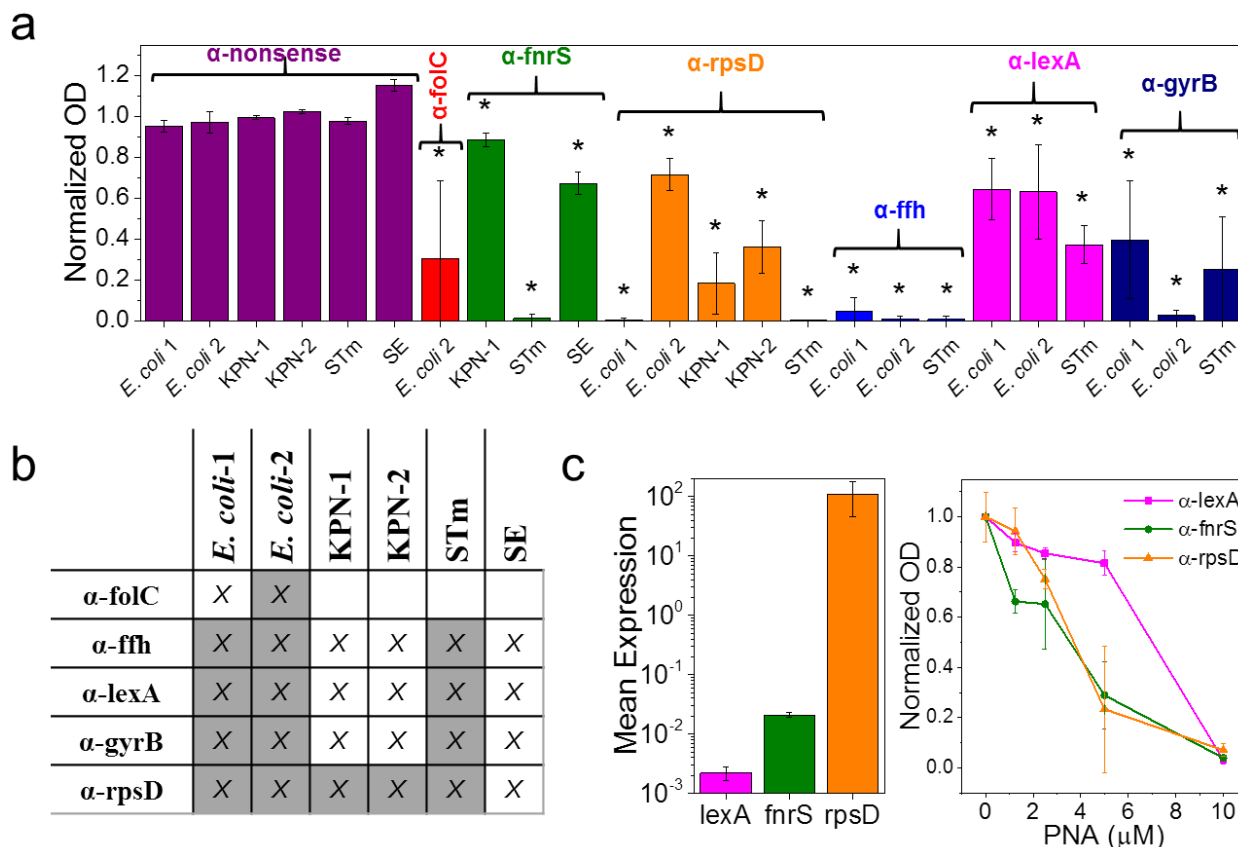


Figure 4.2 Efficacy of antisense-PNA RNA-inhibitors, evaluation of homology and efficacy, and dose-response in *E. coli* MG1655 with RT-qPCR of targets. a. Normalized optical density of respective clinical strain with 10 μ M of respective PNA. Significance (represented by asterisk) was determined relative to α -nonsense with a 95% confidence interval. b. Evaluation of predicted homology (X) and significant growth inhibition (gray shading) demonstrating 54% success in designing effective inhibitors with predictive homology. c. Expression of gene targets and dose-response of *E. coli* MG1655 with respective antisense-PNA demonstrating no direct correlation between RNA expression and antisense-PNA efficacy.

STm and SE. α -fnrS had unexplained activity in KPN-1, STm, and SE considering it did not have a 12-mer match anywhere in the genome.

As an investigation into possible effects from target transcript level, we performed growth analysis of *E. coli* MG1655 in presence of 1.5-10 μ M PNA and quantitative real-time polymerase chain reaction of the gene targets in absence of PNA. We hypothesized that a higher expressed gene may have reduced effect simply due to stoichiometry between the target RNA and the antisense-PNA. We observed no direct correlation between expression level of *rpsD*, *lexA*, and *fnrS* and dose response as evidenced by varied expression of the target genes and similar dose-response of *E. coli* to the antisense-PNA (Figure 4.2c). We reject our hypothesis and do not believe the difference in efficacy between clinical isolates is solely due to differences in RNA target expression levels. We did observe signs of sequestration of antisense-PNA by non-translation start codon off-targets (Table 4.5) in comparing the efficacy of α -folC and α -gyrB in *E. coli*-1 and 2. α -folC and α -gyrB targets were present in the gene of interest in both strains but α -folC and α -gyrB have two off-targets in *E. coli*-1 and no off-targets in *E. coli*-2. In both instances, the antisense-PNA had greater efficacy against *E. coli*-2 compared to *E. coli*-1 indicating potential reduction in efficacy from off-target sequestration.

4.3.4 Combination of antisense PNA with small molecule antibiotics

Given that the clinical isolates display multidrug-resistance against multiple classes of antibiotics, we wanted to test our antisense-PNA RNA-inhibitors ability to work in combination with small-molecule therapeutics as possible potentiators or adjuvants. We held the antisense-PNA concentration constant at 10 μ M and used an antibiotic concentration which was below the minimum inhibitory concentration of antibiotic for the isolate. We focused on bacterial isolate, antibiotic pairs where the isolate was “intermediate” or “resistant” to the small-molecule antibiotic.

We used the Bliss-Independence model²⁰ to evaluate the effect of combination (see 4.5 Materials and Methods, (Equation 4.1)). We first focused on KPN-1 and the three antisense-PNA with homology but no significant growth inhibition at 10 μM : α -ffh, α -lexA, and α -gyrB. While at 10 μM the antisense-PNA did not significantly inhibit growth, we hypothesized that the inhibition of gene expression could work in combination with an antibiotic. Given KPN-1's resistance profile, we used 32 $\mu\text{g/mL}$ tetracycline which is the “intermediate” sensitive/resistant CLSI breakpoint. We observed strong adjuvant activity of the antisense-PNA molecules with tetracycline whereby alone, they had no inhibition, but in combination they significantly increased inhibition (Figure 4.3a, b). All combinations had a positive S-value indicating the synergistic effect of the antisense-

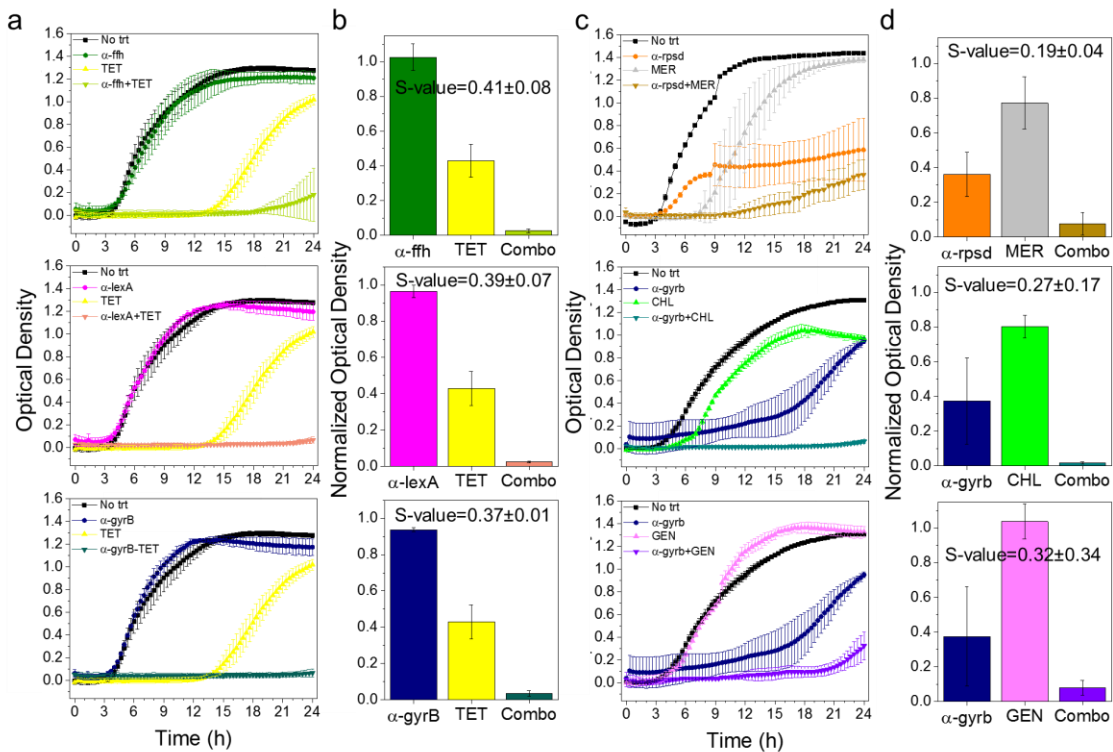


Figure 4.3 Antisense-PNA as a potentiator and adjuvant with small-molecule traditional antibiotics. a. Growth curves of KPN-1 tetracycline combinations with respective low effectiveness antisense-PNA at 10 μM . b. Normalized optical density of KPN-1 with respective mono- or combinatorial treatment and respective S-value from the Bliss Independence model demonstrating strong adjuvant and synergistic activity. c. Growth curves of KPN-2 (top) and *E. coli*-1 (middle and bottom) with varied combinations of low effectiveness antibiotics and 10 μM antisense-PNA. d. Normalized optical density of KPN-2 (top) and *E. coli*-1 (middle and bottom) with labeled mono- or combinatorial treatment. S-values show synergistic nature of combinations.

PNA molecules when added to tetracycline treatment. We then investigated cases where the antisense-PNA exhibited significant monotherapy effect and the antibiotic was highly ineffective. We focused on KPN-2 with meropenem and *E. coli*-1 with chloramphenicol and gentamicin. KPN-2 and meropenem combination is an interesting case because KPN-2 produces NDM-1 β -lactamase (Table 4.4) which is an especially broad-range β -lactamase. We significantly increased inhibition of KPN-2 with addition of 10 μ M α -rpsD to 8 μ g/mL meropenem (Figure 4.3c, d top). We next tested the ability of α -gyrB in combination with 8 μ g/mL chloramphenicol or 4 μ g/mL gentamicin (Figure 4.3c, d middle and bottom). We observed significantly increased inhibition of *E. coli*-1 with addition of α -gyrB to previously ineffective antibiotic treatment and calculated S-values which indicate α -gyrB's synergy with both antibiotics.

4.4 Conclusions

In conclusion, we have demonstrated the utility of predictive homology for designing broad-pathogen, gene-specific antisense RNA-inhibitors against clinical isolates of Enterobacteriaceae. We show that designed antisense-PNA molecules in non-traditional antibiotic pathways were effective at inhibiting cell growth at 10 μ M even in MDR clinical isolates. While not all RNA-inhibitors were effective at 10 μ M in monotherapy, their inhibitory effect made them useful adjuvants or potentiators in combination with traditional antibiotics. Remarkably, we potentiated the activity of meropenem against NDM-1 β -lactamase producing *K. pneumoniae*. The rational design of antisense antibiotics allows for new targets or combinations to be pinpointed with a high success rate and ease compared to compound screening. The design of broad-pathogen, gene-specific antibiotics in non-traditional antibiotic pathways could be instrumental in designing new antibiotics for already pervasive MDR pathogens.

4.5 Materials and Methods

4.5.1 Peptide nucleic acid molecules

Peptide nucleic acid (PNA) molecules were ordered from PNA Bio Inc. (Newbury Park, CA) conjugated to cell penetrating peptide KFFKFFFKKFFK. PNA were re-suspended in H₂O with 5% DMSO at 100 μM. Stocks were stored at -20C for long-term and at 4C for working stocks to minimize freeze/thaw cycles.

4.5.2 Cell culture

The clinical isolates were obtained from the lab of Nancy Madinger at the University of Colorado Anschutz campus. Clinical isolates were grown in Cation Adjusted Mueller Hinton broth (CAMHB) (Becton, Dickinson and Company 212322) at 37°C with 225 rpm shaking or on solid CAMHB with 1.5% agar at 37°C. Clinical isolates were maintained as freezer stocks in 90% CAMHB, 10% glycerol at -80°C. Freezer stocks were streaked out onto solid CAMHB and incubated for 16 h to produce single colonies prior to experiments. For each biological replicate, a single colony was picked from solid media and grown for 16 h in liquid CAMHB prior to experiments. *E. coli* MG1655 (ATCC700926) was cultured in liquid 2% lysogeny broth (LB) or on 2% LB with 1.5% agar for solid plates and was stored in 60% LB broth, 40% glycerol at -80°C. Freezer stocks were streaked out onto solid LB and incubated for 16 h to produce single colonies prior to experiments. For biological replicates, single colonies were started in liquid LB and grown for 16 hours prior to experiments. *E. coli* MG1655 PNA growth experiments were carried out in M9 media (1x M9 minimal media salts solution (MP Biomedicals), 2.0 mM MgSO₄, and 0.1 mM CaCl₂ in sterile water) with 0.4% glucose.

4.5.3 Antibiotic resistance screening

Sensitive/resistant breakpoints were taken from the 2016-2017 Clinical & Laboratory Standards Institute report¹³ (Table 4.1). Liquid cultures of the clinical strains were diluted to a 0.5 McFarland standard and added to respective antibiotic test condition. The antibiotic minimum inhibitory concentration (MIC) for each clinical isolate was determined as the lowest antibiotic concentration which prevented visible cell growth for 24 h. Strains were: “sensitive” if the MIC was equal to or below the sensitive-breakpoint concentration, “resistant” if the MIC was greater than or equal to the resistant-breakpoint concentration, and “intermediate” if the MIC was in-between.

4.5.4 Peptide nucleic acid growth experiments

Biological replicates were diluted 1:10,000 into treatment condition in 384-well plates and measured for 24 h in a Tecan GENios at 562 nm with a bandwidth of 35 nm. Media absorbance blanks were subtracted from data prior to analysis. Normalized optical density (OD) data is shown normalized to the time point where the “no treatment” growth curves reached saturation phase which varied across biological replicates.

4.5.5 Combinatorial effect evaluation

Combinatorial effects were evaluated using the Bliss Independence model²⁰ where the S parameter defines deviation from no interaction as is defined as:

$$S = \left(\frac{OD_{AB}}{OD_0} \right) \left(\frac{OD_{PNA}}{OD_0} \right) - \left(\frac{OD_{AB,PNA}}{OD_0} \right) \quad (\text{Equation 4.1})$$

where OD_{AB} is the OD at saturation time in only antibiotic, OD_0 is the OD at saturation in no treatment, OD_{PNA} is the OD at saturation in only antisense-PNA at 10 μM , and $OD_{AB,PNA}$ is the OD at saturation in combination of antibiotic and antisense-PNA. Saturation time was determined

as the time when the no treatment control reached its saturation growth phase. S>0 is a deviation towards synergy and S<0 is a deviation towards antagonism.

4.5.6 Quantitative real-time polymerase chain reaction

Individual colonies of *E. coli* MG1655 were grown 16 h in liquid and subsequently diluted 1:10,000 into liquid media. Cells were collected when they reached exponential phase; determined as OD 0.4-0.5. 200 µL of culture was added to Bacteria RNAProtect (Qiagen) and pelleted following the manufacturer's instructions. Samples were flash frozen in an ethanol dry ice bath and stored at -80°C. RNaseZap (Life Technologies) was used to protect extracted RNA from RNases. GeneJET RNA purification kit (Thermo Scientific) was used to extract RNA from frozen cell pellets followed by treatment with Turbo DNA-free kit (Ambion). 100 ng of cDNA was synthesized using Maxima Universal First Stand cDNA synthesis kit (Thermo Scientific). Primers for qPCR, listed in Table 4.6, were purchased from Integrated DNA Technologies. 1.5 ng of cDNA was used for 10 µL qPCR reaction with Maxima SYBR Green qPCR master mix with ROX normalization (Thermo Scientific) using QuantStudio 6 flex system (Thermo Scientific). Transcript levels were analyzed following the ΔCq method with respect to moderately expressed housekeeping gene cysG²¹.

4.5.7 Genome sequencing library prep and data analysis

Liquid cultures were inoculated from individual colonies off solid CAMHB for each clinical isolate. Cultures were grown for 16 h as described above and then 1 mL of culture was used to isolate DNA using the Wizard DNA Purification Kit (Promega). A Nanodrop 2000 (Thermo Scientific) was used to measure DNA concentration and purity. For library preparation, >2 µg of DNA was submitted in 50-100 µL samples. The libraries were prepared for sequencing

using Nextera XT DNA Library Preparation Kit (Illumina) and the sequencing was run with a 2x250 bp MiSeq run (Illumina).

Sequencing reads were first trimmed using TRIMOMATIC v0.32²² for length and quality with a sliding window. For further analysis, the trimmed files, of only paired sequences, were transferred to Illumina BaseSpace (<http://basespace.illumina.com>). We assessed the sequencing quality using FASTQC v1.0.0 and performed de novo genome assembly with SPAdes Genome Assembler v3.6.0^{23,24}. The assembly was further corrected and improved using Rescaf v 1.0.1 and then we performed annotation using PROKKA v1.0.0²⁵. Antibiotic resistance genes were identified and characterized using SEAR and ARG-ANNOT pipelines^{26,27}. Integrated Genomics Viewer²⁸ was used for data visualization.

4.5.8 Homology analysis for PNA in clinical isolates

Genome assemblies with annotation were loaded as contigs into UGENE v1.26.0. 12-mer sequences were searched for in UGENE and resultant nucleotide sequences were used to determine homology. Further analysis was done using NCBI's nucleotide BLAST²⁹.

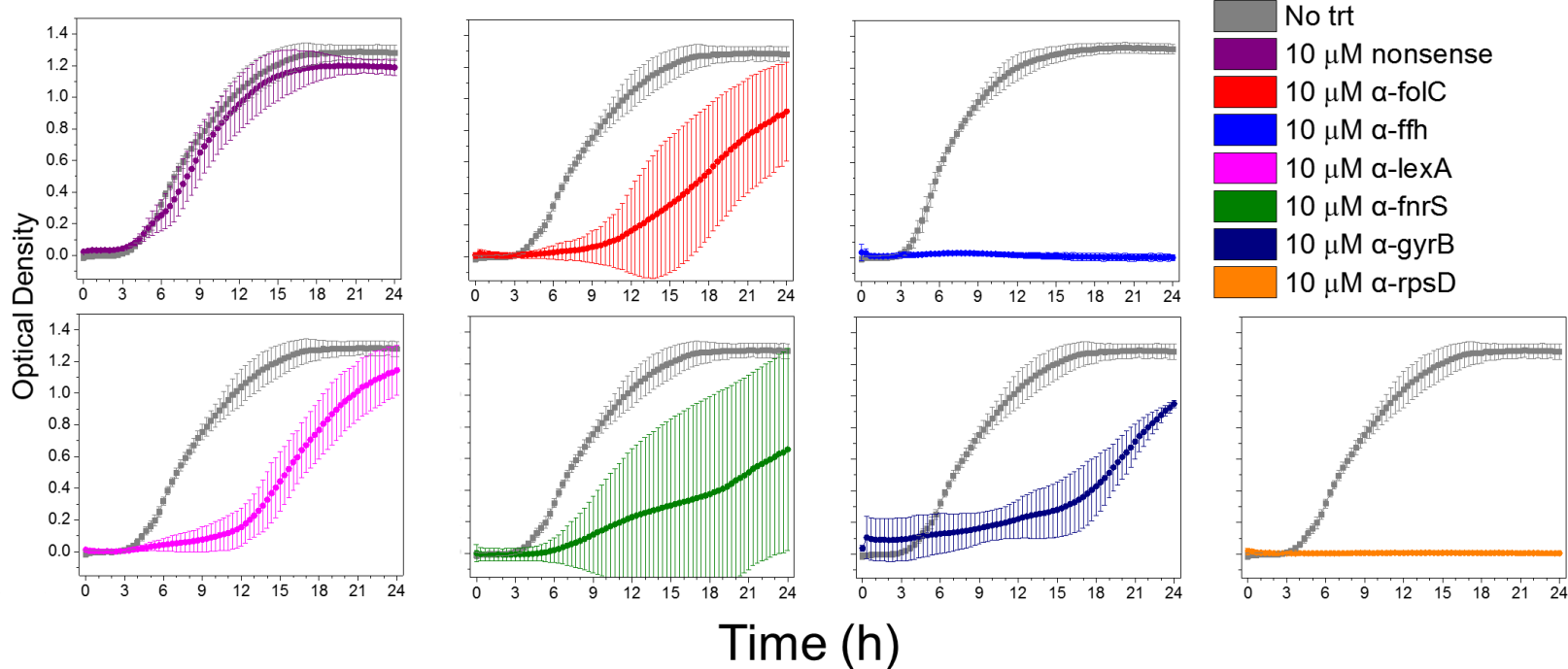
4.5.9 Error and Significance Analysis

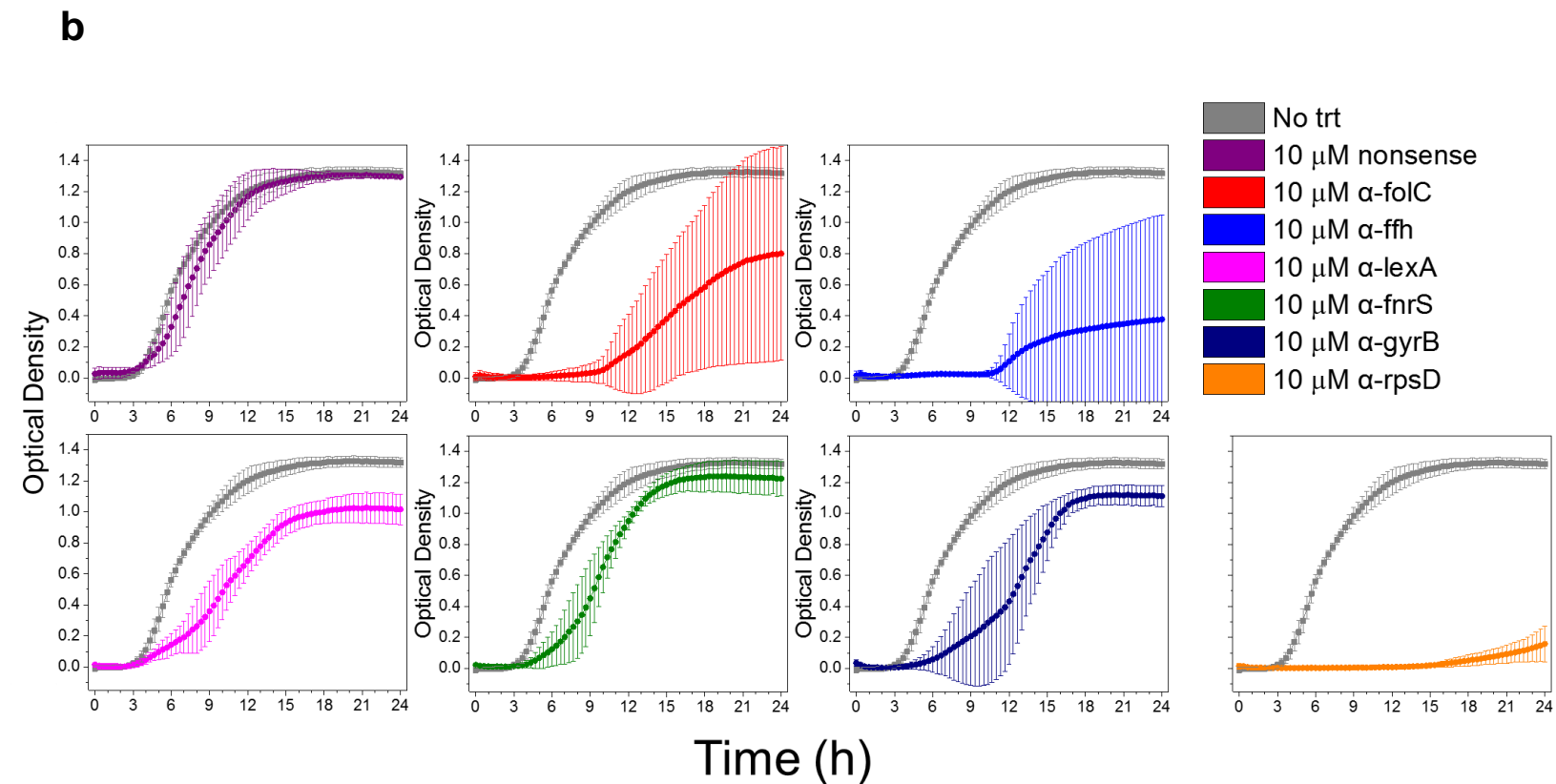
Error bars represent one standard deviation from the mean of biological replicates. In all cases, significance designated with an asterisk (*) is defined as $p < 0.05$.

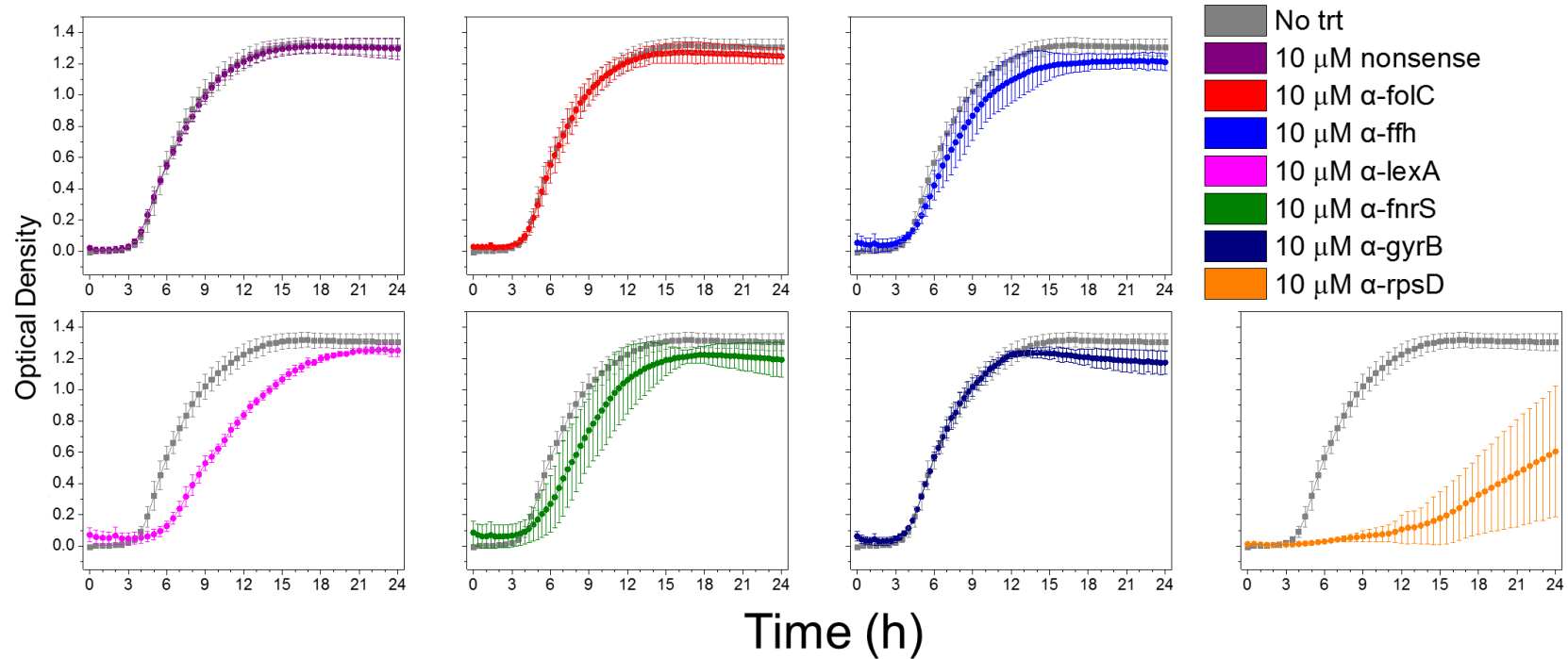
4.6 Supplementary Information

4.6.1 Supplementary figures

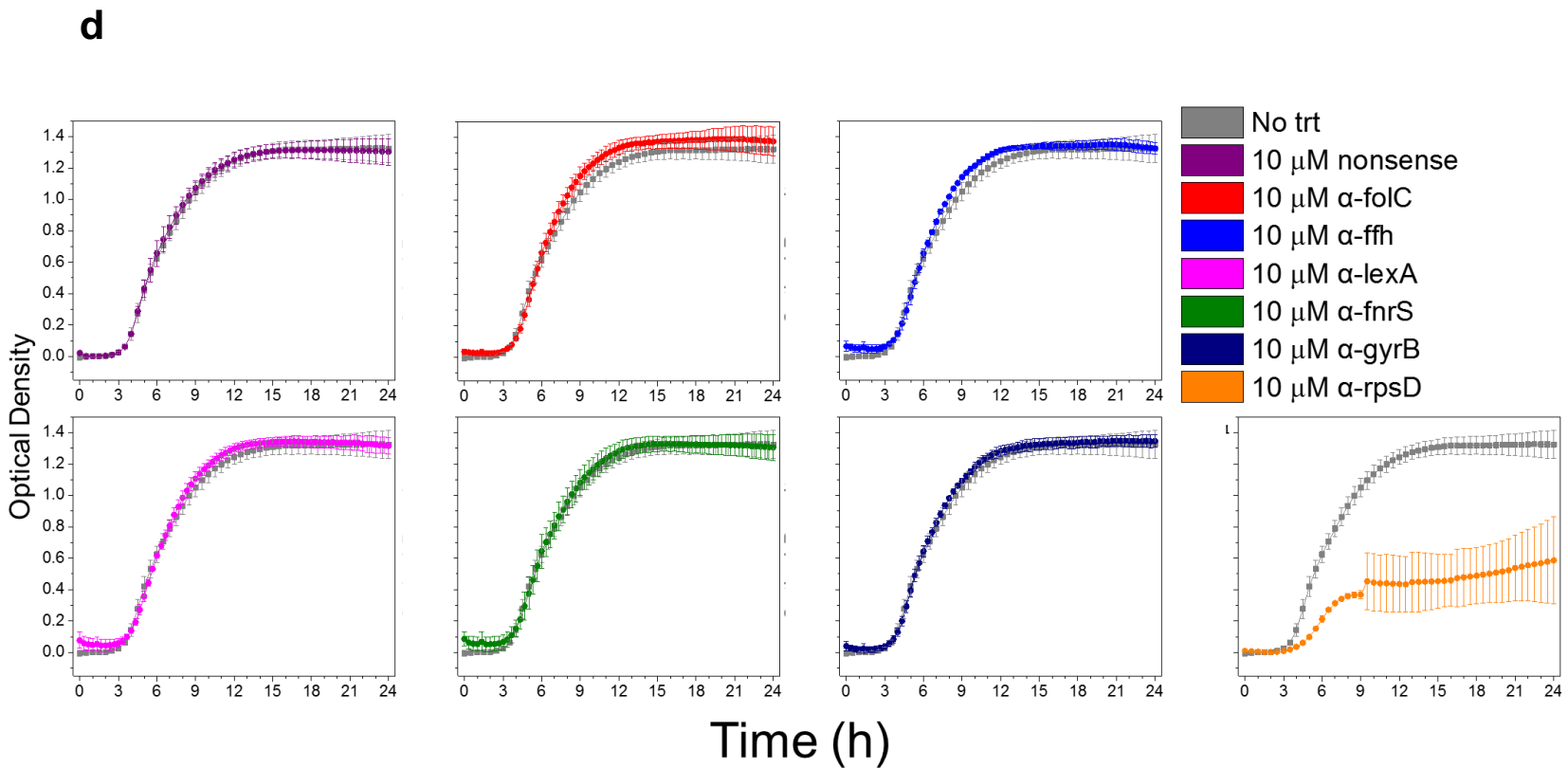
a





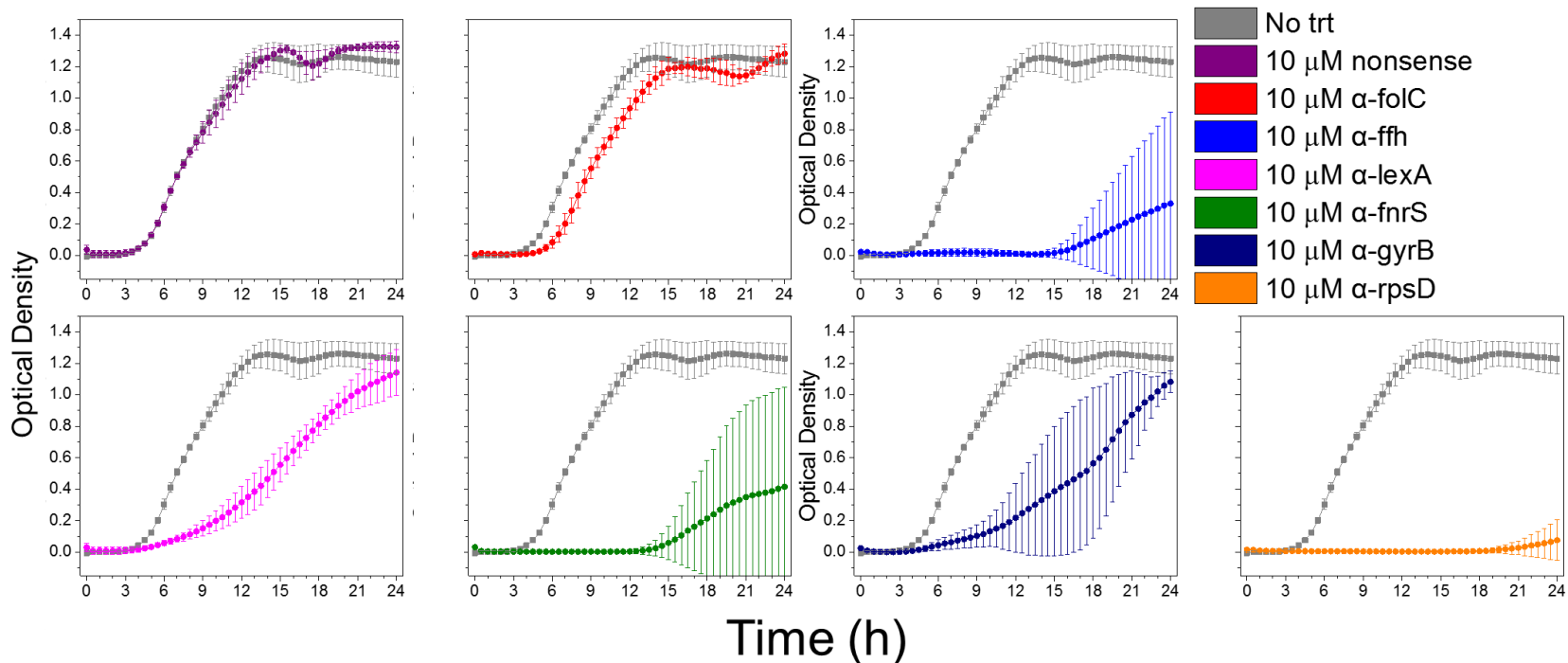
C

#6



S6

e



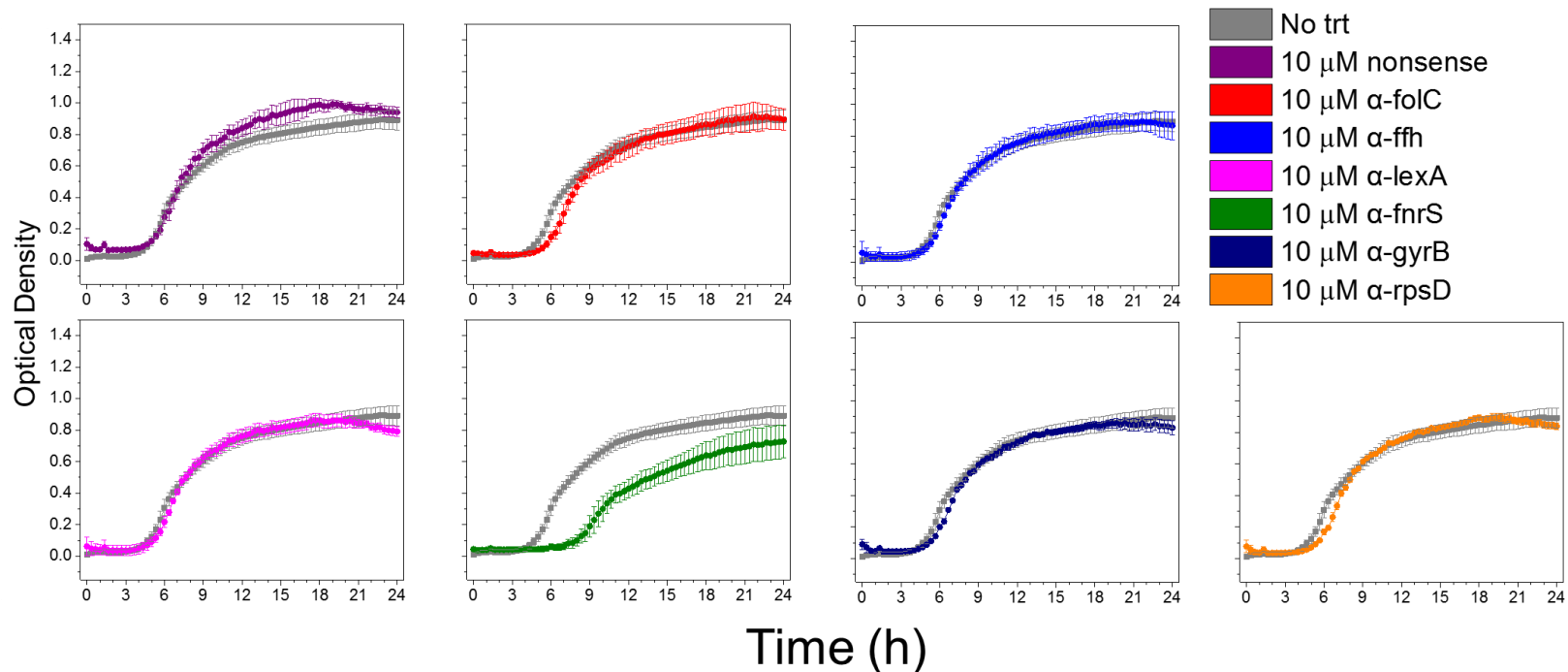
f

Figure 4.S4 Growth curves of clinical isolates with respective treatment. Growth curves are shown for a. *E. coli*-1, b. *E. coli*-2, c. KPN-1, d. KPN-2, e. STm, and f. SE. Curves shown are the average of three biological replicates with error bars representing standard deviation and were used for data shown in Figure 4.2a and Figure 4.3 of the main text.

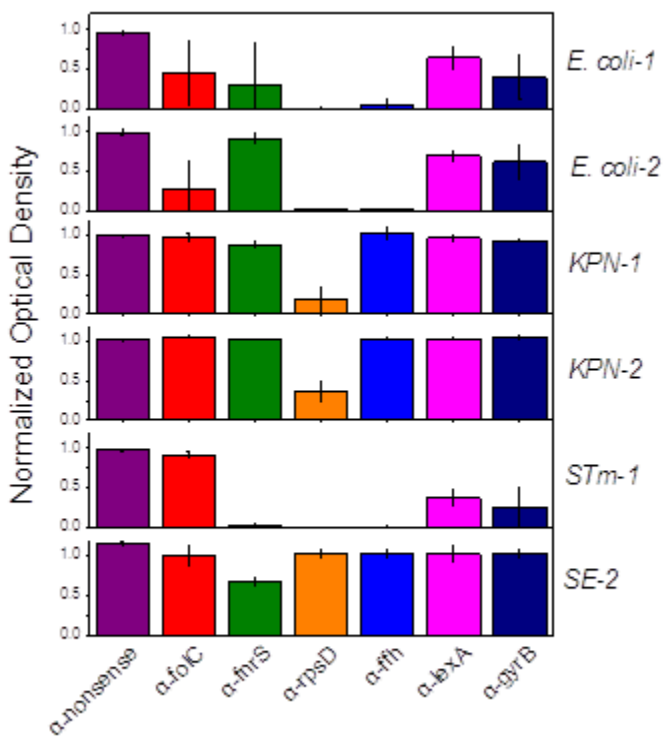


Figure 4.S5 Effect of 6 antisense-PNA RNA-inhibitors on the 6 clinical isolates. Normalized optical density with 10 μ M of respective treatment in respective strain. Data shown are the average of 3 biological replicates with standard deviation shown as error bars. Data is normalized to no treatment at the time point where no treatment reached stationary phase.

α -folC

E. coli-1 **ATACCATGATT** TCAAACGCACTCCTCAAGCCGCGTCG
E. coli-2 **ATACCATGATT** TCAAACGCACTCCTCAAGCCGCGTCG

α -fnrS

E. coli-1 **CTCTTGCAGGT** AATGCAACGTCAAGCGATGGCGTTG
E. coli-2 **CTCTTGCAGGT** AATGCAACGTCAAGCGATGGCGTTG

α -rpsD

E. coli-1 **AGAAAATGGCAA** GATATTGGGTCTTAAGCTCAAGCTG
E. coli-2 **AGAAAATGGCAA** GATATTGGGTCTTAAGCTCAAGCTG
 KPN-1 **AGAAAATGGCAA** GATATTGGGTCTTAAGCTCAAGCTG
 KPN-2 **AGAAAATGGCAA** GATATTGGGTCTTAAGCTCAAGCTG
 STm **AGAAAATGGCAA** GATATTGGGTCTTAAGCTCAAGCTG
 SE **AGAAAATGGCAA** GATATTGGGTCTTAAGCTCAAGCTG

α -ffh

E. coli-1 **GACAATGTTGATA** ATTAAACCGATCGTTGTCGCGTAC
E. coli-2 **GACAATGTTGATA** ATTAAACCGATCGTTGTCGCGCAC
 KPN-1 **GACAATGTTGATA** ATTAAACCGATCGTTGTCGCGTAC
 KPN-2 **GACAATGTTGATA** ATTAAACCGATCGTTGTCGCGTAC
 STm **GACAATGTTGATA** ATTAAACCGATCGTTGTCGCGCAC
 SE **GACAATGTTGATA** ATTAAACCGATCGTTGTCGCGCAC

α -lexA

E. coli-1 **CGGAATGAAAGCGTTA** ACGGCCAGGCAACAAGAGGTG
E. coli-2 **CGGAATGAAAGCGTTA** ACGGCCAGGCAACAAGAGGTG
 KPN-1 **CGGAATGAAAGCGTTA** ACGACCAGGCAGCAAGAGGTG
 KPN-2 **CGGAATGAAAGCGTTA** ACGACCAGGCAGCAAGAGGTG
 STm **CGGAATGAAAGCGTTA** ACGGCCAGGCAACAAGAGGTG
 SE **CGGAATGAAAGCGTTA** ACGGCCAGGCAACAAGAGGTG

α -gyrB

E. coli-1 **GTTGATGTCGA** ATTCTTATGACTCCTCCAGTATCAAAGT
E. coli-2 **GTTGATGTCGA** ATTCTTATGACTCCTCCAGTATCAAAGT
 KPN-1 **GTTGATGTCGA** ATTCTTATGACTCCTCCAGTATCAAAGT
 KPN-2 **GTTGATGTCGA** ATTCTTATGACTCCTCCAGTATCAAAGT
 STm **GTTGATGTCGA** ATTCTTATGACTCCTCCAGTATCAAAGT
 SE **GTTGATGTCGA** ATTCTTATGACTCCTCCAGTATCAAAGT

Figure 4.S6 Homology of antisense-PNA RNA-inhibitors in clinical isolates. After sequencing UGENE was used to search for the 12 nucleotide antisense-PNA targets in the gene of interest. The targets predicted in the non-pathogenic, drug-sensitive strains were present in all cases. Sequences are listed 5' → 3' with the antisense-PNA target bold and underlined with the translation start codon italicized.

4.6.2 Supplementary tables

Table 4.1 CLSI sensitive/resistant breakpoints for 2016-2017¹³ used to determine antibiotic resistance of clinical isolates.

Antibiotic	Sensitive	Intermediate	Resistant
Ampicillin (AMP)	8	16	32
Ceftriaxone (FRX)	1	2	4
Meropenem (MER)	1	2	4
Gentamicin (GEN)	4	8	16
Kanamycin (KAN)	16	32	64
Tetracycline (TET)	4	8	16
Ciprofloxacin (CIP) (<i>E. coli</i> and <i>K. pneumoniae</i>)	1	2	4
Ciprofloxacin (<i>Salmonella enterica</i>)	0.06	0.125	1
Nalidixic Acid (NXA)	6	N/A	32
Chloramphenicol (CHL)	8	16	32

Table 4.2 Antisense-PNA molecules ordered from PNA Bio Inc. Translation start site is bold and underlined, cell penetrating peptide (CPP) KFF₃K is shown in capital letters, and “-O-‘ represents the “O-linker” between CPP and PNA.

Gene target	Antisense PNA ordered
α -folC	KFFKFFKFFK-O-taatcatggtat
α -ffh	KFFKFFKFFK-O-tcaaacattgtc
α -lexA	KFFKFFKFFK-O-gtttcattccg
α -fnrS	KFFKFFKFFK-O-cacctgcaagag
α -gyrB	KFFKFFKFFK-O-ttcgacatcaac
α -rpsD	KFFKFFKFFK-O-ttgccattttct

Table 4.3 Predicted off-targets of antisense-PNA molecules. Gene targets are listed in table with “STC” indicating that the antisense-PNA is centered on the off-targets start site.

	<i>E. coli</i> MG1655	<i>K. pneumoniae</i> MGH 78578	<i>Salmonella enterica</i> serovar Typhimurium SL1344
α -folC	None	KPN_04193 (putative 6-phosphofructokinase) <i>uxaC</i>	None
α -fnrS	Non-protein coding region	None	None
α -rpsD	<i>cueO</i> <i>narI</i>	Non-protein coding region	<i>wcaM</i> <i>rtcA</i> (STC)
α -ffh	None	None	None
α -lexA	None	None	None
α -gyrB	Last 5 nt of <i>psiE</i>	None	None

Table 4.4 Unique antibiotic resistance genes identified in clinical isolates. Italicized label represents antibiotic class the gene confers resistance to where: *Bla* is for β-lactam resistance, *Flq* is for fluoroquinolone resistance, *AGly* is for aminoglycoside resistance, *Phe* is for phenicol resistance, *Tet* is for tetracycline resistance, *Sul* is for sulfonamide resistance, and *Tmt* if for trimethoprim resistance. Non-italicized portion is the unique gene identified by ARG-ANNOT.

<i>E. coli</i> -1	<i>E. coli</i> -2	KPN-1	KPN-2	STm	SE
<i>Bla</i> AmpC1	<i>Bla</i> AmpC2	<i>Bla</i> SHV-11	<i>Bla</i> TEM-217	<i>AGly</i> Aac6-Iaa	<i>Bla</i> CMY-44
<i>Bla</i> AmpH	<i>Bla</i> PBP	<i>Bla</i> AmpH	<i>Bla</i> NDM-1	<i>Bla</i> PBP	<i>Bla</i> Oxa-235
<i>Bla</i> AmpC2	<i>Bla</i> AmpH	<i>Bla</i> Oxa-9	<i>Bla</i> STX-M		<i>Bla</i> PBP
<i>Bla</i> CMY-94	<i>Bla</i> TEM-219	<i>Bla</i> TEM-171	<i>Bla</i> SHV-73		<i>Bla</i> Tem-217
<i>Bla</i> BPB	<i>Bla</i> TEM-10	<i>Bla</i> TEM-220	<i>Bla</i> PBP		<i>AGly</i> StrB
<i>AGly</i> AadB	<i>Bla</i> CTX-M	<i>Bla</i> KPB-3	<i>Bla</i> AmpH		<i>AGly</i> Aac6-Iy
<i>AGly</i> StrA/B	<i>AGly</i> Sat-2A	<i>Bla</i> PBP	<i>Bla</i> PBP		<i>AGly</i> AadB
<i>Phe</i> PheCml45	<i>Tmt</i> DfrA1	<i>Flq</i> OqxBgb	<i>Flq</i> QnrB1		<i>Phe</i> CatA1
<i>Tet</i> TetB	<i>Phe</i> CatA1	<i>AGly</i> AadA1-pm	<i>Flq</i> Qnr-S1		<i>Phe</i> CmlA1
<i>Sul</i> SulI		<i>AGly</i> Aac5-Ib	<i>Flq</i> OqxBgb		<i>Phe</i> FloR
<i>Tmt</i> Dfe24			<i>AGly</i> StrB		<i>Phe</i> PheCmlA5
			<i>AGly</i> RmtF		<i>Tet</i> TetA/R
			<i>AGly</i> Ant3		<i>Sul</i> SulI
			<i>Tet</i> TetA/R		<i>Sul</i> SulII
			<i>Sul</i> SulII		
			<i>Tmt</i> DfrA1		

Table 4.5 Off-targets of antisense-PNA molecules in clinical isolates. Gene targets are listed in table with “STC” indicating that the antisense-PNA is centered on the off-targets start site.

	<i>E. coli</i> -1	<i>E. coli</i> -2	KPN-1	KPN-2	STm	SE
α -folC	Prokka 00542 Prokka 03005	None	<i>pfkA1</i>	<i>pfkA1</i>	None	None
α -fnrS	21-9 bp upstream of <i>hslO</i> (STC)	15-4 bp upstream of <i>hslR</i> (STC)	None	None	None	None
α -rpsD	<i>cueO</i>	<i>cueO</i>	<i>frlD</i> Non-protein coding region	Non-protein coding region	Prokka03791 Prokka 03488 <i>rtcA</i> (STC)	Prokka00937 <i>rtcA</i> (STC)
α -ffh	<i>uhpC</i>	<i>uhpC</i>	<i>yhes1</i>	<i>yheS2</i>	None	None
α -lexA	None	None	None	None	None	None
α -gyrB	Non-protein coding region Last 5 bp of <i>yhbX</i>	None	Non-protein coding region	None	None	None

Table 4.6 RT-qPCR primers used for gene expression analysis. We tried to keep the length of product between 160 and 200 nt. Since *fnrS* is a small RNA, its product was outside of this range.

Gene	Forward Primer (5' → 3')	Reverse Primer (5' → 3')	Product Length
<i>fnrS</i>	GCAGGTGAATGCAACGTCAA	CGACTCATCAAAGTCGGCGT	112
<i>gyrB</i>	CGGGTCCATAGTGGTTCCC	GTGAGAAACTGCGTGGCTTG	191
<i>folC</i>	GCTCAAGCAGTTGTTCTGCC	TCTCACCGGGCGTATGAAAG	176
<i>ffh</i>	TTCCATACGCACCAGCACTT	CGCGCAGGCAGAGAAATTAG	193
<i>rpsD</i>	CAGCCAGGTTGGCTTTCAC	AGAACGCACGTCAGCTGGTTA	178
<i>lexA</i>	TTAACGGCCAGGCAACAAG	TCAATAACGCCTTGCCTGC	162

4.7 Author Contributions

C.M.C. and A.C. conceived of the idea. N.E.M. provided the clinical isolates and K.E.E. conducted clinical isolate genome sequencing. C.M.C. performed all other experiments and analysis.

4.8 References

1. United States Center for Disease Control. *Antibiotic Resistance Threats*. (2013).
2. Baba, T., Ara, T., Hasegawa, M., et al. Construction of Escherichia coli K-12 in-frame, single-gene knockout mutants: the Keio collection. *Mol. Syst. Biol.* **2**, 1–11 (2006).
3. Courtney, C. & Chatterjee, A. cis-Antisense RNA and Transcriptional Interference: Coupled Layers of Gene Regulation. *J. Gene Ther.* **2**, 1–9 (2014).
4. Dryselius, R., Aswasti, S. K., Rajarao, G. K., Nielsen, P. E. & Good, L. The translation start codon region is sensitive to antisense PNA inhibition in Escherichia coli. *Oligonucleotides* **13**, 427–33 (2003).
5. Nielsen, P. E., Egholm, M., Berg, R. H. & Buchardt, O. Sequence-selective recognition of DNA by strand displacement with a thymine-substituted polyamide. *Science* **254**, 1497–500 (1991).
6. Hatamoto, M., Ohashi, A. & Imachi, H. Peptide nucleic acids (PNAs) antisense effect to bacterial growth and their application potentiality in biotechnology. *Appl. Microbiol. Biotechnol.* **86**, 397–402 (2010).

7. Kurupati, P., Tan, K. S. W., Kumarasinghe, G. & Poh, C. L. Inhibition of gene expression and growth by antisense peptide nucleic acids in a multiresistant β -lactamase-producing *Klebsiella pneumoniae* strain. *Antimicrob. Agents Chemother.* **51**, 805–811 (2007).
8. Soofi, M. A. & Seleem, M. N. Targeting essential genes in *Salmonella enterica* serovar typhimurium with antisense peptide nucleic acid. *Antimicrob. Agents Chemother.* **56**, 6407–6409 (2012).
9. Hyrup, B. & Nielsen, P. E. Peptide Nucleic Acids (PNA): Synthesis, Properties and Potential Applications. *Bioorg. Med. Chem.* **4**, 5–23 (1996).
10. Courtney, C. M. & Chatterjee, A. Sequence-Specific Peptide Nucleic Acid-Based Antisense Inhibitors of TEM-1 β -Lactamase and Mechanism of Adaptive Resistance. *ACS Infect. Dis.* **1**, 253–263 (2015).
11. Good, L. & Nielsen, P. E. Inhibition of translation and bacterial growth by peptide nucleic acid targeted to ribosomal RNA. *Proc. Natl. Acad. Sci. U. S. A.* **95**, 2073–2076 (1998).
12. Mondhe, M., Chessher, A., Goh, S., Good, L. & Stach, J. E. M. Species-selective killing of bacteria by antimicrobial peptide-PNAs. *PLoS One* **9**, e89082 (2014).
13. CLSI M100 S27:2017-Performance Standards to Antimicrobial Susceptibility Testing; 27th Edition. 62–71 (2017). Available at: <http://em100.edaptivedocs.info/dashboard.aspx>.
14. Bognar, A. L., Osborne, C., Shane, B., Singer, S. C. & Ferone, R. Folylpoly- γ -glutamate synthetase-dihydrofolate synthetase. *J. Biol. Chem.* **260**, 5625–5630 (1985).
15. Phillips, G. J. & Silhavy, T. J. The *E. coli* *ffh* gene is necessary for viability and efficient protein export. *Nature* **359**, 744–746 (1992).
16. Little, J. W. & Mount, D. W. The SOS Regulatory System of *Escherichia coli*. *Cell* **29**, 11–22 (1982).
17. Durand, S. & Storz, G. Reprogramming of Anaerobic Metabolism by the FnRS Small RNA. *Mol. Microbiol.* **75**, 1215–123122 (2010).
18. Das, U. & Shuman, S. 2'-Phosphate cyclase activity of RtcA: a potential rationale for the operon organization of RtcA with an RNA repair ligase RtcB in *Escherichia coli* and other bacterial taxa. *Rna* **19**, 1355–1362 (2013).
19. Bérdy, J. Thoughts and facts about antibiotics: Where we are now and where we are heading. *J. Antibiot. (Tokyo)* **65**, 441–441 (2012).
20. Hegeness, M., Shoresh, N., Damian, D., Hartl, D. & Kishony, R. Accelerated evolution of resistance in multidrug environments. *Proc. Natl. Acad. Sci. U. S. A.* **105**, 13977–81 (2008).
21. Zhou, K., Zhou, L., Lim, Q. 'En, *et al.* Novel reference genes for quantifying transcriptional responses of *Escherichia coli* to protein overexpression by quantitative PCR. *BMC Mol.*

Biol. **12**, 18–26 (2011).

22. Bolger, A. M., Lohse, M., Usadel, B., *et al.* Trimmomatic: A flexible trimmer for Illumina sequence data. *Bioinformatics* **30**, 2114–2120 (2014).
23. Zerbino, D. R. & Birney, E. Velvet: algorithms for de novo short read assembly using de Bruijn graphs. *Genome Res.* **18**, 821–829 (2008).
24. Bankevich, A., Nurk, S., Antipov, D., *et al.* SPAdes: a new genome assembly algorithm and its applications to single-cell sequencing. *J. Comput. Biol.* **19**, 455–477 (2012).
25. Seemann, T. Prokka: rapid prokaryotic genome annotation. *Bioinformatics* **30**, 2068–2069 (2014).
26. Rowe, W., Baker, K. S., Verner-jeffreys, D., *et al.* Search Engine for Antimicrobial Resistance: A Cloud Compatible Pipeline and Web Interface for Rapidly Detecting Antimicrobial Resistance Genes Directly from Sequence Data. *PLoS One* **10**, e0133492 (2015).
27. Gupta, S. K., Padmanabhan, B. R., Diene, S. M., *et al.* ARG-annot, a new bioinformatic tool to discover antibiotic resistance genes in bacterial genomes. *Antimicrob. Agents Chemother.* **58**, 212–220 (2014).
28. Thorvaldsdóttir, H., Robinson, J. T. & Mesirov, J. P. Integrative Genomics Viewer (IGV): high-performance genomics data visualization and exploration. *Brief. Bioinform.* **14**, 178–92 (2013).
29. Johnson, M., Zaretskaya, I., Raytselis, Y., *et al.* NCBI BLAST: a better web interface. *Nucleic Acids Res.* **36**, 5–9 (2008).

Chapter 5

Photoexcited Quantum Dots for Killing Multidrug-Resistant Bacteria

This chapter includes copyright permissions from *Nature Materials*: Courtney, C. M.#, Goodman, S.M.#, McDaniel, J.A., Madinger, N.E., Chatterjee, A.*, Nagpal, P.* Photoexcited quantum dots for killing multidrug-resistant bacteria. *Nat. Mater.* 15, 485–588 (2016).

5.1 Abstract

Multidrug-resistant bacterial infections are an ever-growing threat because of the shrinking arsenal of efficacious antibiotics. Metal nanoparticles can induce cell death, yet the toxicity effect is typically non-specific. Here, we show that photoexcited quantum dots (QDs) can kill a broad range of multidrug-resistant bacterial clinical isolates, including methicillin-resistant *Staphylococcus aureus*, carbapenem-resistant *Escherichia coli*, and extended-spectrum β -lactamase-producing *Klebsiella pneumoniae* and *Salmonella typhimurium*. The killing effect is material-independent and controlled by the redox potentials of the photogenerated charge carriers, which selectively alter the cellular redox state. We also show that the QDs can be tailored to kill 92% of bacterial cells in a mono-culture and in a co-culture of *E. coli* and HEK 293T cells, while leaving the mammalian cells intact, or to increase bacterial proliferation. Photoexcited QDs could be used in the study of the effect of redox states on living systems and lead to clinical phototherapy for the treatment of infections.

5.2 Introduction

Multi-drug resistant (MDR) bacteria are a serious international health problem with devastating consequences to patient health care. The ability of bacteria to rapidly develop antibiotic resistance^{1–3} and the lack of new antibiotics⁴ has caused an arms race between the evolution of resistance in bacteria and therapeutic development. According to the 2013 Centers for

Disease Control report, infection from antibiotic resistant “superbugs” affects nearly two million people, while killing at least 23,000 people annually in the US due to the absence of effective antibiotics⁵. The frequency of antibiotic resistance in numerous bacterial pathogens is continuing to increase around the world at an alarming rate, with new outbreaks of carbapenem-resistant Enterobacteriaceae (CRE), drug-resistant *Clostridium difficile*⁶, and drug-resistant *Neisseria gonorrhoeae* being reported frequently^{7,8}. We are approaching a post-antibiotic era in which antibiotic treatments are no longer functional due to pandrug-resistant bacteria⁹. With the rising danger of antibiotic resistance, there is a need to develop new antibiotics which will be efficacious against MDR bacteria.

Here we present a light-activated nano-therapeutic which inhibits MDR bacteria through targeted interactions with the cellular redox environment. Cells growing in aerobic environments possess mechanisms to mitigate or use oxidative species through processes¹⁰, including metabolism and signal transduction¹¹. The generation of the specific oxidative species can perturb cell’s redox homeostasis, and has been shown to be linked to cell death in *Escherichia coli*¹², cancer, cardiovascular disease, and aging in humans¹³, and irreversible tissue damage in plants¹⁴. Current antibiotics, such as ampicillin, gentamicin, and ciprofloxacin, have been reported to induce a global, non-specific redox lethality^{15,16}. The tunability of the electronic properties of semiconductor nanomaterials allows for an avenue to induce specific perturbations in redox environments, by simply altering the size, shape, or composition dependent “molecule-like” electronic states of semiconductor nanoparticles, or quantum dots (QDs), and illuminating these QDs with light (above their nominal bandgap) to generate redox-active species. Using the tailored redox potentials of QDs, we can induce light-activated redox species (LARS) for therapeutics and prevent potential side-effects of therapy by spatial and temporal localization using light sources,

or examine the effect of redox states in living systems. For topical infections, the LARS can be used for localized application and therapy, whereas systemic infections can be treated by uniformly dispersed nanoparticles generating LARS during phototherapy. Investigation of these effects using visible and near-infrared radiation can also allow for avenues of using the biological window of optical transparency¹⁷.

Several investigations for development of nano-therapeutics have focused on gold, silver, and other metal nanoparticles^{18–21} which act as infrared absorbers and induce global, non-specific cell death by heating the surrounding medium via surface plasmon resonance. Some investigations on phototherapies using ultraviolet (UV) semiconductor QDs ($E_g > 3.1$ eV) have shown toxicity in cells, but this toxic effect has been attributed to the damage from generation of non-specific free radicals and reactive species^{22,23}. Such stimulation is inherently non-specific due to the susceptibility of all cells to this form of stress, while the treatment itself is toxic due to the application of DNA-damaging UV radiation²⁴. Other studies on generation of reactive oxidative species due to QDs also suffer from non-specific cell interactions²⁵.

Here, we show QDs, tuned via size-dependent quantum confinement, which generate specific LARS through their bandedge redox states. It has been demonstrated that nanoparticles due to their small diameter (2-4 nm) diffuse across membranes and accumulate in the intracellular environment or associate with outer cellular membranes^{25,26}. Additionally, QDs can energetically stimulate biochemical agents, indicating their potential utility if properly tuned for the target of interest²⁷. Illustrated in Figure 5.1a, populations of bacteria are exposed to QDs with and without light stimulation. In this scheme, the redox species generated when the QDs absorb light can interfere with the redox homeostasis of the target cells by coupling to susceptible chemical species present inside the cells (see 5.6.1 Supplementary discussion: role of ROS as the therapeutic

mechanism of CdTe-2.4). We present work on the tunability of visible/near-infrared light absorbing QDs and their effects in cellular environments through the formation of controllable LARS. We show the use of toxic LARS generated from tuned QDs to target MDR pathogenic bacteria and confirm that this cellular phenotype tuning is not a material property but is dependent on the selected electronic properties of the QDs. We also show the opposite effect whereby proliferative LARS increase the growth of *E. coli* cells upon the application of light.

5.3 Results and Discussion

5.3.1 Photo-excited quantum dot activity against multidrug-resistant bacteria

MDR clinical isolates and lab strains (MG1655 and DH5 α) of *Escherichia coli* were exposed to cadmium telluride QDs, with a bandgap of 2.4 eV (517 nm, CdTe-2.4), in the presence and absence of illumination to investigate the cellular response to photoexcited QDs (Figure 5.1a-b, Figure 5.S5, Figure 5.S6). These green emitting nanoparticles have a lower bandgap than metal oxide materials and desired oxidation and reduction potentials. The redox active species from these QDs are generated only when illuminated with light, which produces photoexcited electrons and holes available for the generation of specifically tuned LARS depending upon their reduction and oxidation potential. As a control sample, we used a QD treated cell population in a dark environment to observe material specific effects, which has been largely ignored in previous studies, thus contributing to the wide range of reported dark/inherent toxicities for CdTe QDs (Figure 5.1c)²⁸. To further eliminate possible confounding factors of ultraviolet toxicity and thermal stress from infrared absorption, we limited the range of incident light from 400-700 nm (Figure 5.S8). In addition, we confirmed that under these conditions the QDs do not release divalent cadmium that can have toxic effects²⁹ (Figure 5.S7, Figure 5.S8).

In the absence of illumination, we observed insignificant deviation of growth from non-treated *E. coli* DH5 α up to 50 nM CdTe-2.4 and *E. coli* MG1655 up to 35 nM CdTe-2.4, indicating this concentration is below the inherent toxicity of the nanomaterial (Figure 5.1c, Figure 5.S10). Strikingly, when illuminated with light, *E. coli* treated with 35 nM CdTe-2.4 exhibited a significant decrease in growth, possibly due to cell death (Figure 5.1c). Subsequent colony forming unit (CFU) analysis confirmed that after 6 h of treatment with CdTe-2.4 and illumination, the number of viable cells decreased from time t=0 and was significantly lower than no treatment and CdTe-2.4 in dark indicating the light specific killing effect of the QDs (Figure 5.1c, Figure 5.S10). Further evidence of the therapeutic effect of CdTe-2.4 was obtained by a cell viability assay in non-growing phosphate buffered saline solution, clearly showing strong light-induced toxicity for bacteria from the CdTe-2.4 treatment (Figure 5.S11). To observe the effect of light intensity on cell death we treated *E. coli* MG1655 with 35 nM CdTe-2.4 and performed a colony forming unit analysis to elucidate the kinetics of killing at difference light fluxes. After 6 h with the nominal light intensity, a maximum of 80% of cells were killed (Figure 5.1c, empty stars) and after 8 h with triple the nominal intensity a maximum of 92% of cells were killed (Figure 5.1c, filled stars).

Following our studies in lab strain *E. coli*, we sought to test the light-activated, phototoxic effect of CdTe-2.4 on clinical patient isolates of MDR bacterial strains (Figure 5.1d, Figure 5.S12). To confirm the high degree of resistance of these MDR strains, we exposed them to a panel of 9 antibiotics at concentrations corresponding to CLSI breakpoints, where applicable³⁰. Most of the clinical MDR strains demonstrated resistance to all antibiotics tested, which further underscores the prevalence of the problem of antibiotic drug- resistance. To evaluate the light-activated phototoxic effect of CdTe-2.4 on these strains, we compared their growth in light to the growth in

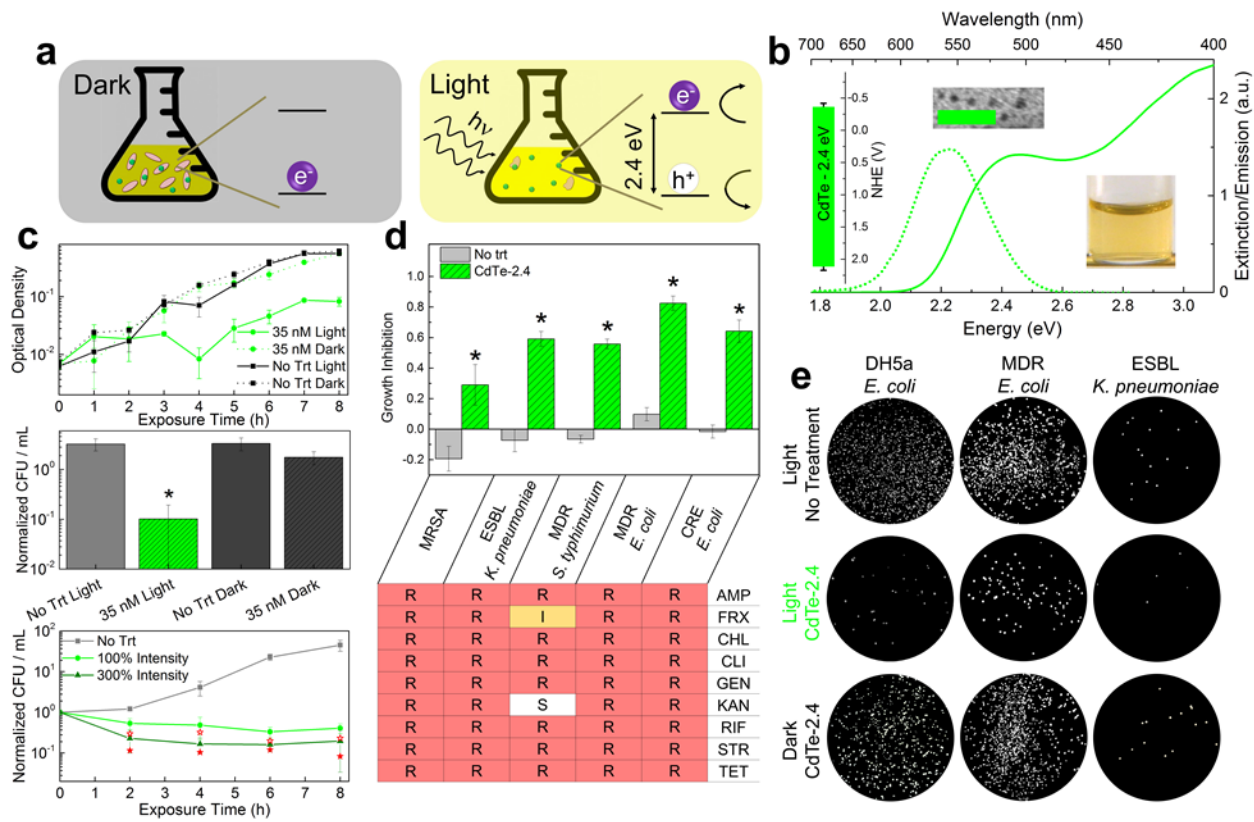


Figure 5.1 CdTe-2.4 quantum dots induce light-activated inhibition of growth in MDR bacterial strains. a. Schematic illustrating effect of light-activated nanomaterial. In dark, nanoparticles have no effect on the bacterial growth. In light, the nanomaterial is activated and significantly alters bacterial growth. The light activates the quantum dot by exciting an electron to the conduction band leaving a hole in the valence band. This excited state is responsible for the light-activated effect. b. Optical properties of 2.4 eV CdTe quantum dots, absorbance: solid line, emission: dotted line. Insets show the redox potentials of the QDs relative to the normal hydrogen electrode (NHE) for the photogenerated electrons and holes (left), transmission electron micrograph of the particles (upper inset, 25 nm scale bar), and a photograph of the nanoparticles suspended in aqueous media (lower inset). c. Optical density (OD) of *E. coli* MG1655 cultures treated with 35 nM CdTe-2.4 in dark and light (top), normalized CFU/mL (middle, with respect to t=0) after 6 h of treatment with and without QDs (semi-log scale), and normalized CFU/mL (bottom, with respect to t=0) as a function of time with respective treatment and either nominal (100%) or 300% light intensity. The stars represent the biological replicate with the highest killing in respective treatment (empty star is highest killing at 100% intensity and filled star is for 300%, semi-log scale). d. Growth inhibition (using optical density at 8 h) of CdTe-2.4 for MDR clinical isolates (top). Data shown is for treatment at 100 nM. A value above 0 indicates therapeutic effect with illumination. Significance was determined by comparison to growth inhibition of light vs. dark no treatment. Antibiotic resistance for the clinical isolates is in the table (bottom). Tested concentrations followed CLSI 2015 breakpoints where applicable and are listed in methods. “R” is drug-resistant, “S” is sensitive, and “I” is intermediately resistance. e. Bacterial cultures were treated with 50 nM CdTe-2.4 for 7 h, in light and dark, and then plated on solid media to visualize viable cells. Data shown in c and d are an average of three independent experiments. Significance, $p < 0.05$, is represented with an asterisk.

light with treatment (here defined as the growth inhibition, $1 - \frac{OD_{L,trt}}{OD_{L,notrt}}$ where $OD_{L,trt}$ is the optical density in light with CdTe-2.4 and $OD_{L,notrt}$ is the optical density in light, at the same late time point ($t=8$ h). In the presence of 100 nM CdTe-2.4 and light, the growth of five clinical, MDR patient isolates were significantly reduced (Figure 5.1d). The growth of a patient isolate of methicillin-resistant *Staphylococcus aureus* (MRSA) was significantly reduced by 29% ($p=0.015$); this strain of MRSA was resistant to 9 out of 9 antibiotics tested. 100 nM CdTe-2.4 under illumination inhibited the growth of a patient isolate of *Klebsiella pneumoniae*, which expressed extended spectrum β -lactamases (ESBLs), by 59% ($p=0.017$). This strain not only expressed ESBLs but was also resistant to 9 of the 9 tested antibiotics. A clinical isolate of MDR *Salmonella enterica* serovar Typhimurium showed 56% growth inhibition at 100 nM CdTe-2.4 with illumination ($p=0.003$). This strain of *S. Typhimurium* was resistant to 7 out of 9 antibiotics tested. Two MDR *E. coli* isolates, one which was resistant to 9 out of 9 antibiotics tested and one which is classified as a carbapenem-resistance Enterobacteriaceae (CRE) and was resistant to all antibiotics tested, were effectively treated with 100 nM CdTe-2.4 and had 83% and 64% growth inhibition, respectively ($p=0.005$ and $p=0.0002$, respectively). To visualize the difference in cell density, cells were plated out after 7 hours of treatment with CdTe-2.4 and light illumination (Figure 5.1e). It is clear that for DH5 α , MDR *E. coli*, and ESBL *K. pneumoniae* there are fewer cells with CdTe-2.4 in light after 7 hours of treatment.

5.3.2 Quantum dot effect is dependent on tuned energy levels

To further support that the observed light-activated effect is not simply a material dependent property or simply generation of electron-hole pairs in QDs, but is strongly dependent on the specific reduction and oxidation potentials of the nanomaterial, we examined the effect of

altering the bandedge redox potentials via changing the nanomaterial size. Two additional batches of CdTe were synthesized, one with a 2.3 eV bandgap (CdTe-2.3) and the other with a 2.2 eV bandgap (CdTe-2.2, Figure 5.2a-b, Figure 5.S5, Figure 5.S6), which are both only slightly larger in diameter than CdTe-2.4 (3.2 ± 0.4 nm for CdTe-2.2 compared to 3 ± 0.5 nm for CdTe-2.4, Figure 5.2a, Figure 5.S6). Along with the decreased bandgaps of these particles (increased absorption) their redox potentials are also shifted relative to CdTe-2.4, especially the conduction band (reduction state, Figure 5.2b). We observed a corresponding attenuation of photo-inhibition with decreasing bandgap, such that CdTe-2.2 exhibits a negligible effect (Figure 5.2c, Figure 5.S13, (Equation 5.2)). If the observed phototoxic response is due in part to change in the cellular environment, particle degradation, or simple heating, it would be expected that larger particles, with their increased surface areas, more absorbed light, and greater amount of releasable material, would be increasingly toxic at the same nominal concentrations. What we observe instead supports the role of the specific redox properties governing the photoeffect of the nanoparticles, from which even a small deviation in redox potential (100-200 mV) leads to a loss of the light-activated effect. To further eliminate the possibility of any minor variations in surfaces and hence efficiency of generating electron-hole pairs on light illumination, we measured the quantum yield (QY) of all three CdTe sizes (Figure 5.2d, Figure 5.S14). All three sizes of CdTe (-2.4, -2.3, -2.2) exhibited similar radiative QYs within the range of 4-5%, which further shows that since a similar number of excited charge carriers for generating LARS species should be available for each size; thus the phototoxicity decrease from CdTe-2.4 to CdTe-2.2 is likely due to the change in redox potential. These results highlight the role of specific redox potentials in LARS generation and the light-activated therapeutic effect of CdTe-2.4.

Next, we decoupled the influence of redox potentials and bandgap on phototoxicity by comparing the photoresponse of CdTe-2.4 to CdSe particles with a 2.4 eV bandgap (CdSe-2.4, Figure 5.2a,b). This comparison allows the effect of bandgap to be decoupled from the redox potentials because while both absorb the same amount and energy of light, the redox potentials of CdSe are shifted relative to CdTe by ~250 mV (Figure 5.2b). If the light-induced killing is an effect of non-specific oxidative species, as opposed to our predicted tuned redox response, we

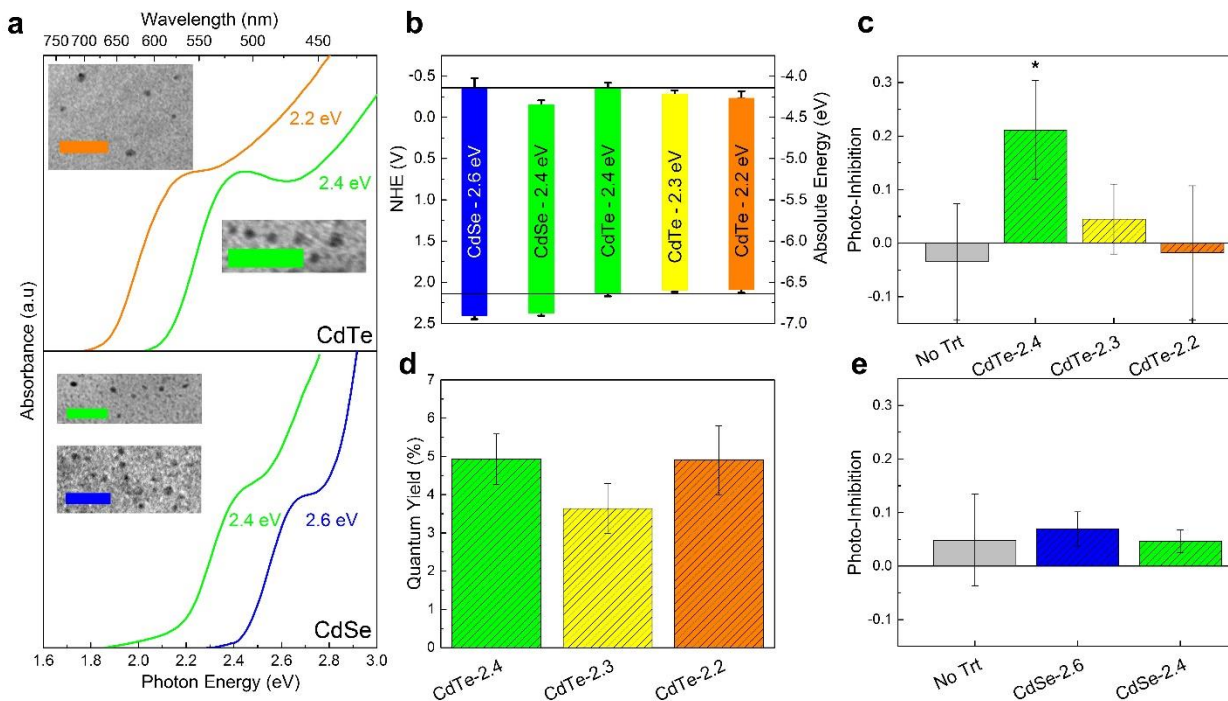


Figure 5.2 The effect of CdTe-2.4 is specific to the reduction and oxidation potentials. a. Absorbance spectra for CdTe and CdSe particles of several sizes. Insets show TEM images with color-coded scale bars (50 nm except for CdTe-2.4 which is 25 nm). b. Scanning tunneling spectroscopy (STS) measurements of CdSe and CdTe particles on the NHE (left axis) and absolute (vacuum) scales (right axis). c. Photo-inhibition (using optical density at 8 h) of different sized CdTe at 25 nM concentration on *E. coli* DH5α. d. Fluorescence quantum yield of the three CdTe sizes calculated using a FITC standard for comparison. e. Photo-inhibition (using optical density at 8 h) of CdSe-2.4 and CdSe-2.6 on *E. coli* DH5α. Data shown in c, d, and e are an average of three independent experiments (error bars are standard deviation from average values). Significance, $p < 0.05$, is represented with an asterisk and is relative to no treatment. Photo-inhibition is defined as $1 - \frac{OD_{L,trt}}{OD_{D,trt}}$ where $OD_{L,trt}$ is the optical density in light with QDs and $OD_{D,trt}$ is the optical density in dark with the same treatment, at the same late time point (8 h) (Equation 5.4).

would expect to see higher photo-inhibition with illumination of CdSe-2.4 particles due to their higher oxidation potential. Strikingly, in the presence of CdSe-2.4 and illumination, we observe no significant cell death in *E. coli*, even up to 250 nM (Figure 5.2e, Figure 5.S15). This is confirmed after plating the cells, where no reduced cell density is observed, and holds for the MDR strains as well (Figure 5.S15). We also tested CdSe particles with a 2.6 eV bandgap (CdSe-2.6) to evaluate the effect of the reduction potential, which was aligned to the reduction potential of the phototoxic CdTe-2.4 (Figure 5.2b). We observed no effect on growth of *E. coli* DH5 α with CdSe-2.6 and illumination which confirms that both the oxidation and reduction potentials are important for inducing the therapeutic effect of CdTe-2.4 (Figure 5.S16). Thus, the source of the light-induced therapeutic is the specifically tuned redox potentials of the QDs and not solely the 2.4 eV bandgap or reduction potential of the CdTe-2.4 particles.

5.3.3 Reactive oxygen species generation by quantum dots and selective bacterial inhibition

The redox mechanism of therapeutic effect from CdTe-2.4 LARS species was probed using several techniques. We introduced 2',7'-dichlorofluorescin diacetate (DCFH-DA) to cultures of *E. coli* MG1655 grown with and without CdTe-2.4 in light and dark. When exposed to oxidizing species such as ONO_2^- and $\cdot\text{OH}$, DCFH-DA is oxidized to fluorescent 2',7'-dichlorofluorescin (DCFH) resulting in the green color observed in Figure 5.3a. From these images we see negligible fluorescence from the cells treated in dark compared to very clear responses from the light treated cultures, indicating a possible role of reactive oxidative species in the light-activated therapeutic^{10,11,13,14}. This observation was further quantified using flow cytometry (Figure 5.3b, Figure 5.S17) which shows that only those cells exposed to light and CdTe-2.4 show significant increases in reactive oxidative species. The reduction potential of the CdTe-2.4 bandedge state aligns with the reduction of oxygen, resulting in the superoxide radical when a quantum dot

donates its photoexcited electron (Equation 5.1). The products of these reactions can further lead to side reactions likely generating peroxide, other oxygen radicals, and reactive oxidative species in aqueous solution (5.6.1 Supplementary discussion: role of ROS as the therapeutic mechanism of CdTe-2.4)^{13,31}.



To further test the likely role of generation of these oxidative species, we performed an anaerobic experiment (removing oxygen to prevent these reactions), and the photoeffect was strongly attenuated due to the removal of dissolved oxygen (Figure 5.S18). Since tissues and complex media can decrease the generation of these LARS species due to absorption and scattering (Figure 5.S19), we evaluated the effect of lower light intensities on phototherapy. While a two or four-fold reduction in light intensity can be expected between the visible and near-infrared optical windows, the growth curves indicate that with even 25 nM CdTe-2.4, a therapeutic effect can be observed down to 25% of nominal light power (Figure 5.S20). This light intensity dependence of the growth and saturation of the oxidative stress further supports light-activated redox generation as a plausible mechanism for therapeutic action. We also tested whether these LARS species are generated inside the cells for phototoxicity. The cells were allowed to incubate with CdTe-2.4 in dark for 1 h, before being washed twice with PBS, to remove any particles not internalized or associated with the cells. We tested the growth of these washed cells in light and dark (Figure 5.S21) and found a significant therapeutic effect. A combination of the uptake bioassay, along with the single cell microscopy with DCFH dye indicates that the photoeffect is maintained following this treatment and the quantum dots are therapeutically active within the cells.

Given the increasing threat of antibiotic resistance, a clear application of the phototoxic response observed with CdTe-2.4 is as a therapeutic agent for combating localized bacterial

infections. Such treatments would be dependent on the QDs being selective for inhibiting bacteria while leaving the surrounding host cells healthy and intact, requiring the QDs to be tuned to the specific cellular redox environment of the target organism. To this end, we performed co-culture experiments with *E. coli* and HEK 293T cells. HEK 293T were grown for 24 h to obtain 80% confluence, and then inoculated with *E. coli* and subjected to respective nanoparticle treatment conditions for 24 h. To evaluate cell health, the HEK 293T cells were stained with nuclear stain

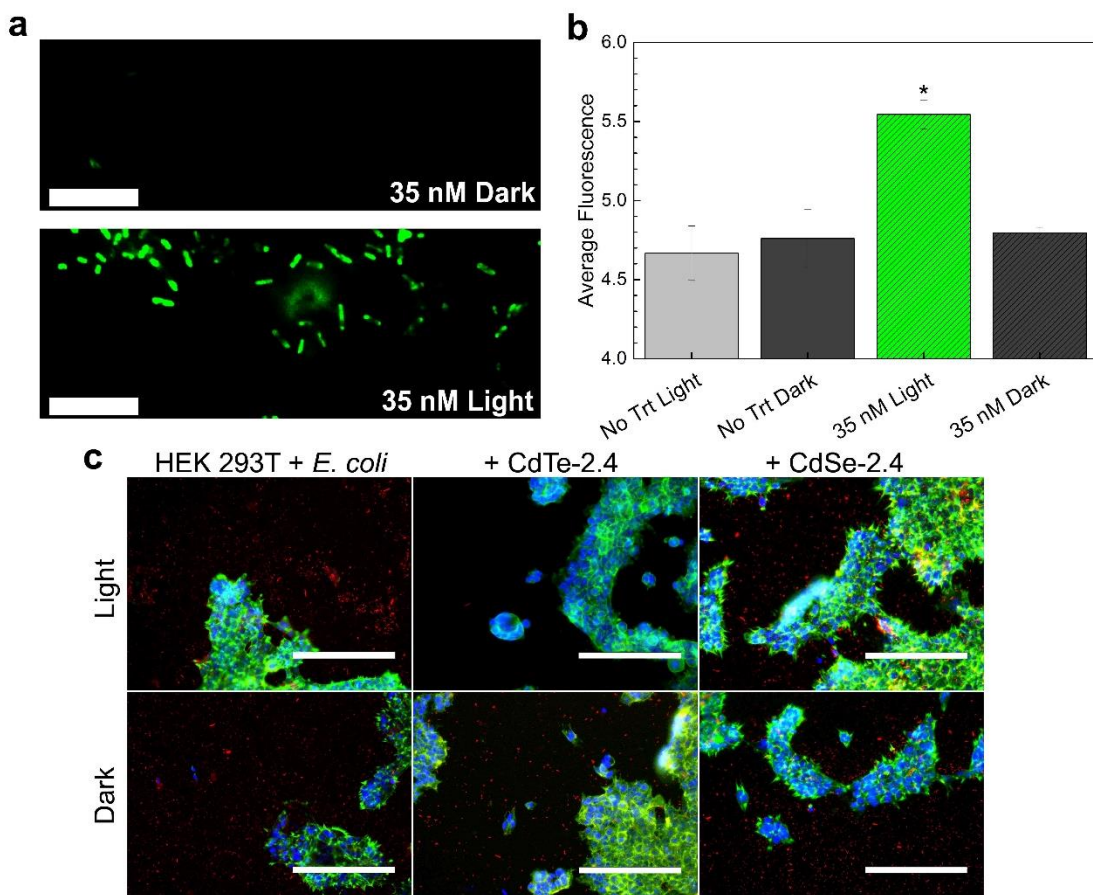


Figure 5.3 Formation of intracellular redox species which do not effect HEK 293T cells. a. Images of *E. coli* MG1655 treated with the redox activated reagent 2',7'-dichlorofluorescin diacetate showing the likely generation of oxidative species when the *E. coli* are exposed to light, but not in dark. b. Fluorescence levels of *E. coli* MG1655 populations exposed to 2',7'-dichlorofluorescin diacetate as measured by flow cytometry. c. Composite fluorescence images of HEK 293T cells (blue: DAPI, nuclear, green: Phalloidin, actin) and *E. coli* (red: mCherry fluorescent protein) exposed to CdSe-2.4 (100 nM) and CdTe-2.4 (35 nM) and no treatment controls. Scale bars are 200 μ m. Significance, $p < 0.05$, is represented with an asterisk and is relative to no treatment.

DAPI (blue) and actin stain Phalloidin Cruzfluor 488 conjugate (green) to observe cell morphology. Prior to the co-culture *E. coli* DH5 α was transformed to maintain a plasmid constitutively expressing the mCherry fluorescent protein (red). HEK 293T cells, in absence of bacteria, did not exhibit a morphological or viability observable photoeffect or inherent material toxicity in the presence of CdTe-2.4 or CdSe-2.4 (Figure 5.S22, Figure 5.S23). When co-cultured without QDs, there was comparable growth of *E. coli* and consistent cell morphology of HEK 293T in light as well as dark (Figure 5.3c). *E. coli* and HEK 293T co-cultures did not display a phototoxic effect in the presence of CdSe-2.4, corresponding with observations in the monocultures (Figure 5.2e, Figure 5.3c, Figure 5.S22, Figure 5.S23). In contrast, CdTe-2.4 in light prevented growth of the *E. coli* culture while the HEK 293T cells were healthy (using morphology and viability, Figure 5.3c, Figure 5.S22, Figure 5.S23), thus providing a proof of concept for using these particles in therapeutic applications and for cell specific phototoxicity.

5.3.4 Design of quantum dot for improved bacterial growth

The complexity of the intracellular redox environment implies that it could be possible to stimulate other cellular responses besides cell toxicity. To test this hypothesis we chose to evaluate 1.9 eV bandgap CuInS₂ particles (CIS-1.9, Figure 5.4a, b), which have a similar reduction potential as CdSe-2.4 and a lower oxidation potential than CdSe-2.4 or CdTe-2.4 along with a smaller bandgap in the near-infrared. Surprisingly, 50 nM CIS-1.9 upon illumination causes a photo-proliferative effect whereby bacteria demonstrate 35% *growth enhancement* (Figure 5.4c, Figure 5.S24, $p=0.007$). Our tuned CIS-1.9 treatment is the first demonstration of a nanoscaled material to have this effect. The high selectivity of each redox potential is exemplified by larger CuInS₂, with a smaller bandgap of 1.6eV (CIS-1.6, Figure 5.4), which does not exhibit the photo-proliferation effect. As the bandgap was not the source of the difference in photoeffect between

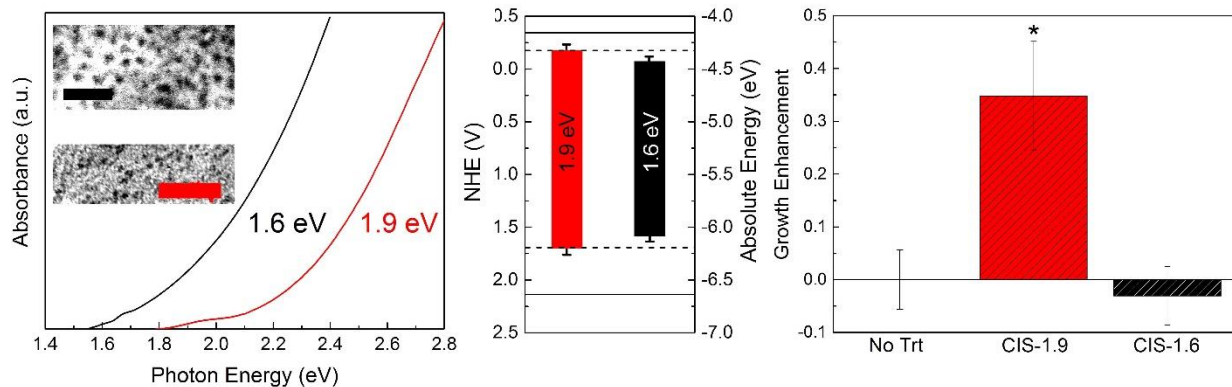


Figure 5.4 Photoproliferative response using CuInS₂. a. Absorption spectra of CuInS₂ particles: CIS-1.9 and CIS-1.6. Insets show TEM images with color-coded scale bars (50 nm). b. Positions of the reduction and oxidation states for the two CuInS₂ sizes. Solid horizontal lines indicate the phototoxic redox states from CdTe-2.4. f. Comparison of the growth enhancement (using optical density at 8 h) of 50 nM CIS-1.9 and CIS-1.6 in *E. coli* DH5α. Significance, $p < 0.05$, is represented with an asterisk and is relative to no treatment. Growth Enhancement is defined as $\frac{OD_{L,trt}}{OD_{L,no,trt}} - 1$

where $OD_{L,trt}$ is the optical density in light with QDs and $OD_{L,no,trt}$ is the optical density in light with no treatment, at the same late time point (8 h) (Equation 5.4).

CdTe-2.4 and CdSe-2.4, we can reasonably conclude that the CIS-1.9 photo-proliferation compared to CdSe-2.4 is due to the 0.5 V shift in oxidation potential between the two materials.

5.4 Conclusions

In this study, we have shown the utility of a tunable light-activated response in bacteria using quantum dots for inducing both therapeutic effects by killing MDR clinical isolates as well as increased cell growth in *E. coli*. We confirmed the dependence of the cellular effect on the quantum dot oxidation and reduction potentials, decoupling the effect from the material and the bandgap. We have also shown a plausible mechanism for the formation of reactive oxidative species for light-activated therapy from CdTe-2.4, and provide the likely identification of specific oxygen species through DCFH dye microscopy, flow cytometry, anaerobic growth, light intensity variation, and the lack of dependence of phototoxicity on QY of the dots. We were able to use these redox properties to hinder the growth of highly pathogenic and MDR bacterial strains, which

is extended to a proof of concept study where we demonstrate the ability to selectively hinder the growth a bacterial culture in co-culture with a healthy mammalian culture. We have shown a unique photo-proliferative effect with CIS-1.9 particles where cell growth is enhanced by light stimulation and the resulting LARS. These findings show that with further studies and additional QDs fine-tuned to cellular redox states, this technology can be applied for the selective phenotypic manipulation of a host of cell types. These results can lead to development of semiconductor nanoparticles for treatment of both topical and systemic infections using phototherapy in clinical settings, and disinfecting surfaces and devices using LARS. Furthermore, this technology can also be applied to improving cell growth in bioreactors using LARS, and to study the effect of redox states in living systems.

5.5 Materials and Methods

5.5.1 Synthesis chemicals

3-Mercaptopropionic acid ($\geq 99\%$) was purchased from Acros Organics. Cadmium(II) chloride (technical grade), 10 mM phosphate-buffered saline, oleic acid (90%), copper(II) acetylacetonate ($\geq 99.99\%$), indium(III) acetate (99.99%), sulfur (99.5%), and oleylamine (technical grade) were purchased from Sigma Aldrich. Tellurium -325 mesh powder (99.99% metal basis), and selenium -325 mesh powder (99.5%) were purchased from Alfa Aesar. Sodium borohydride (98%), and sodium hydroxide ($\geq 97.0\%$), were purchased from Fisher Scientific. Compressed nitrogen (pre-purified), and oxygen (ultra-high purity) were purchased from Airgas. Ethanol (200 proof) was purchased from Decon Laboratories INC. All purchased materials were used as provided without further purification.

5.5.2 CdTe and CdSe quantum dot synthesis and sterilization

Deionized water was initially degassed using bubbling nitrogen for 30 min. 1 mL degassed water was used to dissolve NaBH₄ (35 mg, 0.93 mmol), and the resulting solution was transferred to a septum-capped 2 mL vial (Thermo Scientific) containing tellurium (Te) powder (40 mg, 0.31 mmol). -325 mesh was used for the reaction as coarser Te does not react well. A needle was inserted into the septum for outgassing during the reaction, which was allowed to proceed until the Te precursor solution became optically clear and light pink, and ceased bubbling (40-60 min). A cadmium precursor solution was created by dissolving CdCl₂ (3.7 mg, 0.020 mmol) and 3-mercaptopropionic acid (MPA, 1.8 μL, 2.2 mg, 0.021 mmol) in 10 mL of degassed water. The reaction solution was made by mixing 250 μL of the cadmium (Cd) precursor solution, 250 μL degassed water, 1 μL of the Te precursor solution, and 10 μL of 0.5 M NaOH (total volume 511 μL). Reactions were scaled up to a maximum of 1.5 mL total volume. 100 μL aliquots of the reaction solutions were divided into PCR tubes (Thermo Scientific) and placed in a thermocycler (Bio-Rad T100). The tubes were held at 98°C for the reaction duration (approximately 1.5 h for CdTe-2.4, 2.5-3 h for CdTe-2.3, >5 h for CdTe-2.2). CdSe was prepared using the same procedure using Se (25 mg, 0.32 mmol) and NaBH₄ (25 mg, 0.66 mmol), the reaction between the two occurring at a much higher rate (<30 min). General procedure was adapted from Tikhomirov et al³². The resulting dots are sterile.

Prior to integration with cells, the CdX quantum dots were washed in the following manner. The stock was initially bulk centrifuged at 10 krpm for 5 min to precipitate unreacted materials and poorly stabilized QDs. An Omega 4K Nanosep filter was initially sterilized with 100 μL 100% ethanol and centrifuged at 10,000 rpm for 6 min. 200 μL of the stock QD solution was then filtered to dryness (about 6-7 min). The dots were then washed twice with 100 μL of sterile pH 11 water

(4 min centrifugation). The cleaned dots are then re-dispersed in pH 11 water. The concentrations of these purified solutions were determined optically using published extinction coefficients³³. Size distributions for the various sized dots used in this study are shown in Figure 5.S6.

5.5.3 CuInS₂ quantum dot synthesis and ligand exchange

A 100 mL three-necked flask was charged with copper(II) acetylacetonate (260 mg, 1.0 mmol), indium(III) acetate (290 mg, 1.0 mmol), oleylamine (1.0 mL, 1.2 g, 4.5 mmol), and o-dichlorobenzene (7 mL). The flask was then connected to a Schlenk line and purged with alternating vacuum and nitrogen refilling. After three cycles the temperature was increased to 110°C using a J KEM Scientific Model 210 temperature controller. The sulfur precursor solution was made by dissolving sulfur (64 mg, 2 mmol) in o-dichlorobenzene (3 mL) via gently heating. Once dissolved, the sulfur was rapidly injected into the reaction flask and the temperature was increased to 180°C for the duration of CIS growth. Once the desired reaction time had elapsed the flask was quenched in a water bath, and the contents transferred to a centrifuge tube. Excess ethanol was added and the mixture was centrifuged at 5,000 rpm for 5 min. The precipitated particles were then re-dispersed in hexane, and centrifuged again to remove poorly passivated dots. Dots were stored in hexane for further use along with excess oleylamine to promote stability. Size distributions for the various dots are shown in Figure 5.S6. Procedure was adapted from Panthani et al³⁴.

The long-chain amine ligands were exchanged with MPA in the following way. The hexane stock solution (100 μL), 0.5 M NaOH (200 μL), ethanol (500 μL), and MPA (400 μL) were mixed in a 1.5 mL Eppendorf tube which were left in the dark for 3 h. The tubes were then centrifuged at 10,000 rpm for 15 min. The liquid phase was then removed completely, and the precipitated dots were concentrated in a small volume (<50 μL) of ethanol. This was transferred to a new sterile

tube and was vacuum dried to yield a powder. Sterile Phosphate buffer saline (PBS) was then used to re-disperse the dots for use with cells. Concentrations were determined optically using published correlations³⁵. This procedure was scaled by adding more exchange tubes.

5.5.4 Light source for cell studies

Cells were illuminated using a tungsten lamp (GE 35200-EKE) placed externally of the incubator via a fiber optic cable. The lamp was equipped with filters to remove UV (Thorlabs FEL0400) and IR light, creating a bandpass filter from 400-700 nm (Figure 5.S7). The lamp spectrum was quantified using a Princeton Instruments Action SP2150 monochromator with filters to remove 2nd order diffraction (Thor Labs 315-710 nm Band Pass filter) with absolute intensities recorded with a NIST calibrated Newport Power Meter Model 1918-R (full lamp intensity entered the monochromator and the detector was placed 6 cm from the exit aperture). Lamp output was kept consistent for all measurements except those examining the effect of light intensity, which are defined relative to the nominal value.

5.5.5 Quantum dot degradation analysis

One hypothesis for the source of CdX toxicity is the release of free cadmium into the intracellular medium. Though this has been called into question by previous studies which show little association between QD toxicity and intracellular Cd²⁺concentration, we performed control measurements to track the changes in the QDs for the duration of the cell exposure. The changes in the quantum dots as a result of continued light illumination were examined by absorption and photoluminescence measurements. Absorbance measurements of CdSe particles indicate that the smallest particles are relatively stable in dark and under illuminated reaction conditions, experiencing an attenuation of the excitonic peak slowly over 24 h of illumination, which is consistent with previous results³⁶ (Figure 5.S9a). The largest CdSe particles are, however, less

stable than their smaller counterparts, and experience significant absorbance changes within 5-6 h of illumination.

While these results indicate that changes to the particles are taking place, the exact nature of those changes are not readily apparent from these absorbance measurements. Because CdTe is photoluminescent in aqueous media, we tracked changes in the PL peak position over time under the same conditions. What we observe is an initial red shift of the emitted light, which is indicative of defect states forming on the quantum dot surfaces, likely oxygen replacing tellurium (Figure 5.S8). Such red-shifts have been previously reported for quantum dots of this type²⁵. Later, the shift reverses, such that the emitted light decreases in wavelength. This is consistent with the continuing oxidation of the quantum dot leading to a smaller CdTe core which emits lower wavelength light. This blue shift occurs more rapidly in the larger particles likely due to the lower relative passivation of tellurium rich facets. As CdO has very low solubility in buffered solution, the source of the quantum dot toxicity in light is due to the formation of LARS, and not the release of free Cd²⁺ ions. There is a difference between light and dark exposed quantum dots insofar as the intensity of light emission decreases much more rapidly when exposed to light, indicating that the LARS are contributing to the formation of less ordered particles which facilitates non-radiative recombination. This decrease in intensity over time is consistent with other studies examining PL from QDs in cells^{37,38}.

There were less overall changes in the CuInS₂ over time compared to the cadmium based dots (Figure 5.S9b), likely due to the greater oxygen stability of sulfur as an anion compared to the other chalcogens.

5.5.6 Bacterial strains and cell culture conditions

Liquid cultures of DH5 α (Zymo) were grown overnight in 2% lysogeny broth (LB) (Sigma Aldrich) (incubated at 37°C), diluted 1:10 into LB with respective quantum dots, and rocked. Liquid cultures of *E. coli* MG1655 (ATCC700926) were grown overnight in M9 medium (consisting of 5X M9 minimal media salts solution from MP Biomedicals, 2.0 mM MgSO₄, and 0.1 mM CaCl₂ in sterile water) with 0.4% glucose (incubated at 37°C), diluted 1:100 into M9 with respective quantum dots, and rocked. Solid cultures were grown on 2% LB broth, 1.5% agar (Becton Dickson) at 37°C. All multi-drug resistant (MDR) clinical strains were obtained from Dr. Nancy Madinger at the University of Colorado Anschutz Medical Campus. MDR strains were cultured in cation adjusted Mueller Hinton broth (CAMHB) (DIFCO) liquid or CAMHB and 1.5% agar solid for all studies. Replicates were started from individual colonies off solid media and grown overnight in 1 mL respective media. Cultures were diluted 1:100 from the overnight for MDR photoeffect experiments. Photoeffect experiments were carried out in 50 or 100 μ L cultures in 384 well transparent flat bottom plates. Optical density measurements were taken using a Tecan GENios at 562 nm with a bandwidth of 35 nm. *E. coli* DH5 α and MG1655 freezer stocks were stored in 40% glycerol at -80°C. All MDR bacterial freezer stocks were stored in 10% glycerol at -80°C.

5.5.7 Antibiotic susceptibility testing

MDR strains were grown overnight in CAMHB and diluted to a 0.5 McFarland standard into corresponding antibiotic concentration. Concentration followed CLSI breakpoints for 2015 where applicable³⁰. Some antibiotics were tested at two concentrations based on an intermediate resistance level reported in the CLSI breakpoints. Tested concentrations were as follows: ampicillin (AMP) 8 μ g/mL, ciprofloxacin (FRX) 1 and 2 μ g/mL, chloramphenicol (CHL) 8

$\mu\text{g/mL}$, clindamycin (CLI) 0.25 and 0.5 $\mu\text{g/mL}$, gentamicin (GEN) 1 and 4 $\mu\text{g/mL}$, kanamycin (KAN) 10, rifampicin (RIF) 0.06 and 0.5 $\mu\text{g/mL}$, streptomycin (STR) 10 $\mu\text{g/mL}$, tetracycline (TET) 1 and 2 $\mu\text{g/mL}$. All antibiotics were purchased from Sigma Aldrich. The cultures were grown for 24 h at 37°C with shaking at 225 rpm. Resazurin sodium salt (Sigma Aldrich) solution was added at 24 h and allowed to react for 4 h, after which a color change to pink was used as an indicator of cell growth, and therefore, resistance.

5.5.8 Colony forming unit (CFU) analysis

Cultures were sampled at respective time points during a bacterial toxicity study and serial dilutions were performed ranging from 10^1 - 10^9 . Dilutions were plated on 2% LB and 1.5% agar for *E. coli* MG1655, or CAMHB and 1.5% agar for MDR strains, and grown at 37°C for 24 h and counted (Figure 5.1c, Figure 5.S10c, d). Images of cells on petri dishes shown in Figure 5.1e, Figure 5.S15b are treated for 7 h and diluted 10^3 fold before plating 10 μL on solid media. CFU was normalized to the respective biological replicates at t=0 CFU/mL. Raw CFU data can be seen in Figure 5.S10c, d. The t=0 CFU/mL shown in raw CFU data represents the starting cell dilution which is a 1:100 dilution from overnight.

5.5.9 Statistical analysis of data

All biological replicate data was analyzed using single factor ANOVA with a significance of $p<0.05$ represented with an asterisk (*). Significance was analyzed in comparison to the no treatment populations. Error bars are standard deviation from average values.

5.5.10 Non-growth media experiment

E. coli MG1655 cells were diluted 1:100 into M9 media and allowed to grow for 3 h. After 3 h the cells were pelleted for 10 min at 5000 rpm and rinsed with PBS twice. The cells were then

re-suspended in PBS with respective CdTe-2.4 in light and dark. After 6 h, resazurin sodium salt solution (Sigma Aldrich) was added and the fluorescence (485/610) was measured where an increase in red fluorescence was an indicator of cell viability.

5.5.11 Growth inhibition/enhancement analysis

To analyze the effect of treatment conditions, optical density measurements at late time points were evaluated. We used this as a metric for cell growth due to our treatment inducing multiple growth rates in cell populations, as the therapeutic takes effect. Growth inhibition, photo inhibition, and growth enhancement were defined as:

$$\text{Growth Inhibition} = 1 - \frac{OD_{L,trt}}{OD_{L,No\ trt}} \quad (\text{Equation 5.2})$$

$$\text{Growth Enhancement} = \frac{OD_{L,trt}}{OD_{L,No\ trt}} - 1 \quad (\text{Equation 5.3})$$

$$\text{Photo-Inhibition} = 1 - \frac{OD_{L,trt}}{OD_{D,trt}} \quad (\text{Equation 5.4})$$

where $OD_{L,trt}$ is the optical density in light in respective treatment, $OD_{L,No\ trt}$ is the optical density in light with no treatment, and $OD_{D,trt}$ is the optical density in dark in respective treatment. Raw growth curves can be seen in Figure 5.S12, Figure 5.S13, and Figure 5.S24.

5.5.12 Quantum yield (QY) determination

A stock solution of fluorescein isothiocyanate (FITC) was prepared by diluting 0.8 mg in 1 mL pH 11 water. This was subsequently diluted 50x to yield the reference solution. The quantum dot samples were filtered in the same manner as discussed previously and diluted 10x to yield solutions with absorbance at 475 nm between 0.03-0.05. The emission spectrum was measured on a Photon Technologies International fluorimeter for each solution starting at 485 nm using 475 nm excitation with three independent replicates for each sample (Figure 5.S14a-d).

Recorded intensities were corrected with a NIST calibration file to account for detector sensitivity. Quantum yield was calculated using (Equation 5.2, where Φ_X is the quantum yield of x, A_X is the absorbance of x, I_X is the measured intensity spectrum, and λ is the wavelength. Measured quantum yields range from 4-5(± 1)% in this size range with no significant size dependence.

$$\frac{\Phi_{QD}}{\Phi_{FITC}} = \frac{A_{FITC} \int_{\lambda_1}^{\lambda_2} I_{QD} \lambda d\lambda}{A_{CdTe} \int_{\lambda_1}^{\lambda_2} I_{FITC} \lambda d\lambda} \quad (\text{Equation 5.5})$$

Interactions with redox targets were probed by tracking fluorescence quantum yield upon the addition of electron and hole quenching small molecules. Emission was quenched by adding 2 μL of quencher solution to 100 μL of QD stock (quantum yield was within measurement error when 2 μL of water was added as a control). Silver nitrate (electron quencher), a 1:1 mixture of sodium sulfite and sodium sulfide (hole quenchers), and methylene blue (redox indicator) all exhibit concentration dependent quenching of the QD photoluminescence (Figure 5.S14e). With a high light fluence the photoluminescence quantum yield can recover over time as the quencher in solution is used up, and indicates that the interactions between QDs and redox targets are reversible (Figure 5.S14f-g, using 365 nm light, spectra recorded with an Ocean Optics USB 4000 detector).

5.5.13 2',7'-Dichlorofluorescin diacetate microscopy and flow cytometry

2',7'-dichlorofluorescin diacetate (DCF-DA or DCFH-DA, Sigma Aldrich D6883-50MG) was used to probe the oxidative species generated from CdTe-2.4 in cells. DCFH-DA, when exposed to oxidizing species is oxidized to fluorescent 2',7'-dichlorofluorescin³⁹ resulting in the green fluorescence. We treated a 1:100 dilution of *E. coli* MG1655 overnight culture in M9 with respective concentration CdTe-2.4 for 2 h in light and dark. We then added DCFH-DA to the cultures and allowed the reagent to react for 5 min. The sample was then diluted 1:10 into PBS and measured using a CyAn ADP Analyzer Cytometer (488/530) to evaluate the relative

fluorescence, and therefore oxidative species, in the treated cells. Images shown in Figure 5.3a were acquired using a Zeiss inverted microscope with a camera affixed to the eyepiece.

We treated a 1:100 dilution of *E. coli* MG1655 overnight culture in M9 with respective concentration CdTe-2.4 for 2 h in light and dark, followed by DCFH-DA addition. DCFH-DA, when exposed to oxidizing species such as ONOO⁻ and ·OH radicals is oxidized to fluorescent 2',7'-dichlorofluorescin³⁹ resulting in the green fluorescence. The cultures were incubated with DCFH-DA for 5 min. Samples for flow cytometry analysis were diluted 1:10 into PBS and measured using a CyAn ADP Analyzer Cytometer (488/530) to evaluate the relative fluorescence, and therefore oxidative species, in the treated cells. Samples were kept on ice throughout the procedure. From each sample 30,000 cells were counted. Flow cytometry data was analyzed using MATLAB and excel software.

5.5.14 Anaerobic cell culture

M9 media was bubbled with N₂ for 30 min (Airgas, prepurified) to remove dissolved oxygen. Overnight *E. coli* MG1655 cultures were pelleted for 10 min at 5000 rpm and resuspended in the N₂ bubbled M9. Cells were diluted 1:10 into N₂ bubbled M9 and respective quantum dot concentrations. The 96 well plate was sealed with a non-permeable gas film (AB-1170, Thermo-Fisher Scientific) that does not allow for gas exchange between wells or the environment to prevent oxygen from entering the cultures and maintenance of an anaerobic environment. The culture OD's were measured every hour as previously described. Results can be seen in Figure 5.S18.

5.5.15 Uptake bioassay of CdTe-2.4

E. coli MG1655 cells were diluted 1:10 from overnight into M9 with the respective concentration of quantum dot and grown in dark at 37°C for 1 h to allow for uptake. The cells were then pelleted for 10 min at 5000 rpm and rinsed in PBS twice to remove quantum dots in the media.

The cells were resuspended with a 1:10 dilution into M9 medium without quantum dots, total dilution from overnight being 1:100. Optical density was measured every hour as previously described. Results are shown in Figure 5.S21.

5.5.16 Mammalian cell culture

HEK 293T cells (American Type Culture Collection, CRL-3216) were recovered from freezer stocks in high glucose Dulbecco's Modified Eagle Medium (HyClone) supplemented with glutamine and fetal bovine serum (HyClone). Cultures were grown at 37°C in 5% CO₂ with controlled humidity. Cells were passaged at 80% confluence with 0.25% trypsin (HyClone) and seeding densities were calculated using a hemocytometer. HEK 293T cells were used between passages 11-20. Cells were stored in liquid nitrogen for long term storage.

Cells were seeded at 6,000 cells per well into a tissue culture treated 96-well plate (Cellstar). Media was supplemented with penicillin streptomycin solution to minimize the chance of contamination, however the penicillin streptomycin solution was omitted in co-culture studies. QD dilutions were made in sterile Dulbecco's modified phosphate buffered saline (dPBS) (HyClone). Images of these cells were acquired on an EVOS FL microscope after 24 h of treatment. Three replicate images were taken by randomly imaging different locations in each well. Representative images under all QD conditions are shown in Figure 5.S22. After imaging, Resazurin sodium salt solution (Sigma Aldrich) was added and the fluorescence was measured using a Tecan GENios with an excitation and emission wavelength of 485 nm and 610 nm respectively (Figure 5.S23). An increase in red fluorescence over time was used as an indicator of cell viability. The slope of the linear range of fluorescence was used as an evaluator of cell viability.

5.5.17 Co-culture experiment

Co-culture experiments were carried out with HEK 293T cells and *E. coli* DH5 α transformed with pFPV-mCherry plasmid. pFPV-mCherry was a gift from Olivia Steele-Mortimer (Addgene plasmid # 20956)⁴⁰. The pFPV-mCherry plasmid was used in these experiments for the constitutive production of fluorescent protein mCherry for imaging purposes. 9,000 HEK 293T cells were seeded per well into 96 well plates and allowed to grow for 36 h to reach 80% confluence. The 96 well plates were pretreated with 0.01% poly-L-lysine (Sigma Aldrich) for one hour and rinsed twice with dPBS prior to seeding. Separate 96 well plates were used for the light and dark conditions. pFPV-mCherry *E. coli* were grown for 16 h from a single colony under above described bacterial cell culture conditions and with 100 μ g/mL ampicillin sodium salt to maintain the plasmid. DMEM was removed from the HEK 293T cultures and supplemented with DMEM containing approximately 10^5 bacterial cells/mL, 100 μ g/mL ampicillin sodium salt, and respective quantum dots. Plates were then placed in an incubator with 5% CO₂ at 37°C for 24 h either illuminated or shielded from light with tin foil. Media and/or bacterial culture were removed from the wells, pelleted at 7,000 rpm for 5 min, and re-suspended in the same volume of dPBS.

Mammalian cells were then stained with the following procedure. Cells were washed twice with dPBS and fixed in 4% methanol free formaldehyde for 5 min. The cells were again rinsed twice with dPBS and treated with 0.1% triton x-100 for 3-5 min. The cells were then rinsed with dPBS two times. The cells were then stained with a 1x dilution of Phalloidin CruzFluor 488 Conjugate (Santa Cruz Biotechnology) for 20 min at room temperature. The cells were then rinsed twice with warm dPBS. The cells were then treated with 300 nM DAPI (Santa Cruz Biotechnology) for 5 min at room temperature. The cells were rinsed two final times with warm

dPBS and covered with tin foil to protect stains. All wash steps were carried out with pre-warmed 37°C dPBS.

5.5.18 Cyclic voltammetry measurements (C-V)

Cyclic voltammetry measurements were carried out in a three-electrode configuration (glassy carbon plate electrode, platinum wire electrode and Ag/AgCl (1M KCl) as working, counter, and reference electrode, respectively) using a Bio-Logic SP-200 Research Potentiostat. Briefly, phosphate buffered solution (pH=7.4) was used as an electrolyte and bubbled with air to observe peaks corresponding to superoxide and other ROS species. For C-V measurements with *E. coli* MG1655 cells, the solution was sonicated to lyse the cells (so membrane penetration of redox species was not a factor), then bubbled with Argon gas (to remove dissolved oxygen) for 10 minutes before starting the measurements. The typical scan rates ranged from 100 mV/sec to 1 V/sec. All the voltammograms were corrected using the NHE (normal hydrogen electrode) scale.

5.6 Supplementary Information

5.6.1 Supplementary discussion: role of ROS as the therapeutic mechanism of CdTe-2.4

The redox mechanism of action from CdTe-2.4 LARS was probed using several techniques. We introduced 2',7'-dichlorofluorescin diacetate (DCFH-DA) to cultures of *E. coli* MG1655 grown with and without CdTe-2.4 in light and dark. When exposed to oxidizing species DCFH-DA is oxidized to fluorescent 2',7'-dichlorofluorescin (DCFH) resulting in the green color observed in Figure 5.3a. From these images we see negligible fluorescence from the cells treated in dark compared to very clear responses from the light treated cultures, indicating a possible role of these reactive oxidative species in light-activated therapy^{10,11,13,14,41}. This observation was further quantified using flow cytometry (Figure 5.2f, Figure 5.S17) which shows that only those

cells exposed to light and CdTe-2.4 show significant increases in reactive oxidative species. CdTe-2.4 also has reduction and oxidation potentials which energetically align with half reactions associated with the generation of radicals from water and dissolved oxygen, broadly classified here as reactive oxidative species (ROS). The likely redox half reactions associated with generation of these oxidative species were identified ((Equation 5.6, (Equation 5.7, (Equation 5.8) ^{31,41}.



To further test the possible role of these oxidative species, we performed an anaerobic experiment (removing oxygen to prevent these reactions), and the photoeffect was strongly attenuated due to the removal of dissolved oxygen (Figure 5.S18). Since variation in light intensity due to absorption of light in tissues and complex media can attenuate the photo-generation of these LARS species, we evaluated the effect of light intensity on phototherapy (Figure 5.S19). The growth curves indicate that with 25 nM CdTe-2.4, a bactericidal effect can be expected up to 12.5% of the nominal incident light (Figure 5.S20). This light intensity dependence of growth rate and saturation of the oxidative stress supports the light-activated ROS generation as a plausible mechanism for therapeutic action. We also tested whether these LARS species need to be generated only inside the cells for the phototoxicity. The cells were allowed to incubate with the CdTe-2.4 in dark for 1 h, before being washed twice with PBS, to remove any particles not internalized or associated with the cells. We tested the growth of these washed cells in light and dark (Figure 5.S21) and found significant therapeutic effect. A combination of this uptake bioassay, along with the single cell microscopy and flow cytometry with DCFH dye indicates that while quantum dots are both inside and outside the cells, a significant photoeffect is maintained

following this treatment and the quantum dots are therapeutically active within the cells. Furthermore, since some reactive oxidative species can also be generated externally, and have several microsecond lifetimes (like superoxide), diffusion of uncharged ROS can also penetrate cells and generate toxic effects (Figure 5.S21)⁴².

We tested CdTe-2.4 on *E. coli* in LB, M9, M9 supplemented with riboflavin (a component in LB), and PBS (Figure 5.S10, Figure 5.1c, Figure 5.S11, Figure 5.S12, and Figure 5.S13). We added 4 times the riboflavin present in LB, as determined by fluorescence at 485/530, but no phototoxic effect was observed, ruling out any potential significant generation of ROS species from riboflavin in the observed phototherapy (Figure 5.S25). In all media, we observed significant phototoxicity confirming that the media was not responsible for the LARS phototoxicity.

5.6.2 Supplementary figures

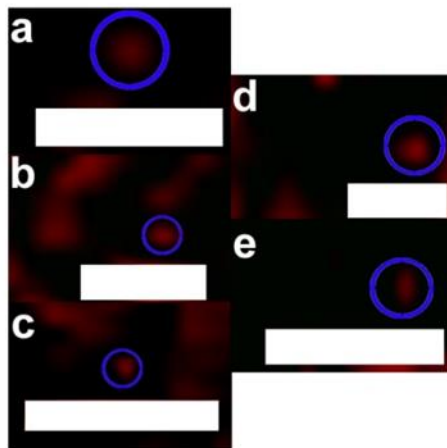


Figure 5.S5 STM images of a. CdSe-2.6, b. CdSe-2.4, c. CdTe-2.4, d. CdTe-2.2, e. CIS-1.6. Scale bars are 50 nm in each image. Individual QDs are circled in blue.

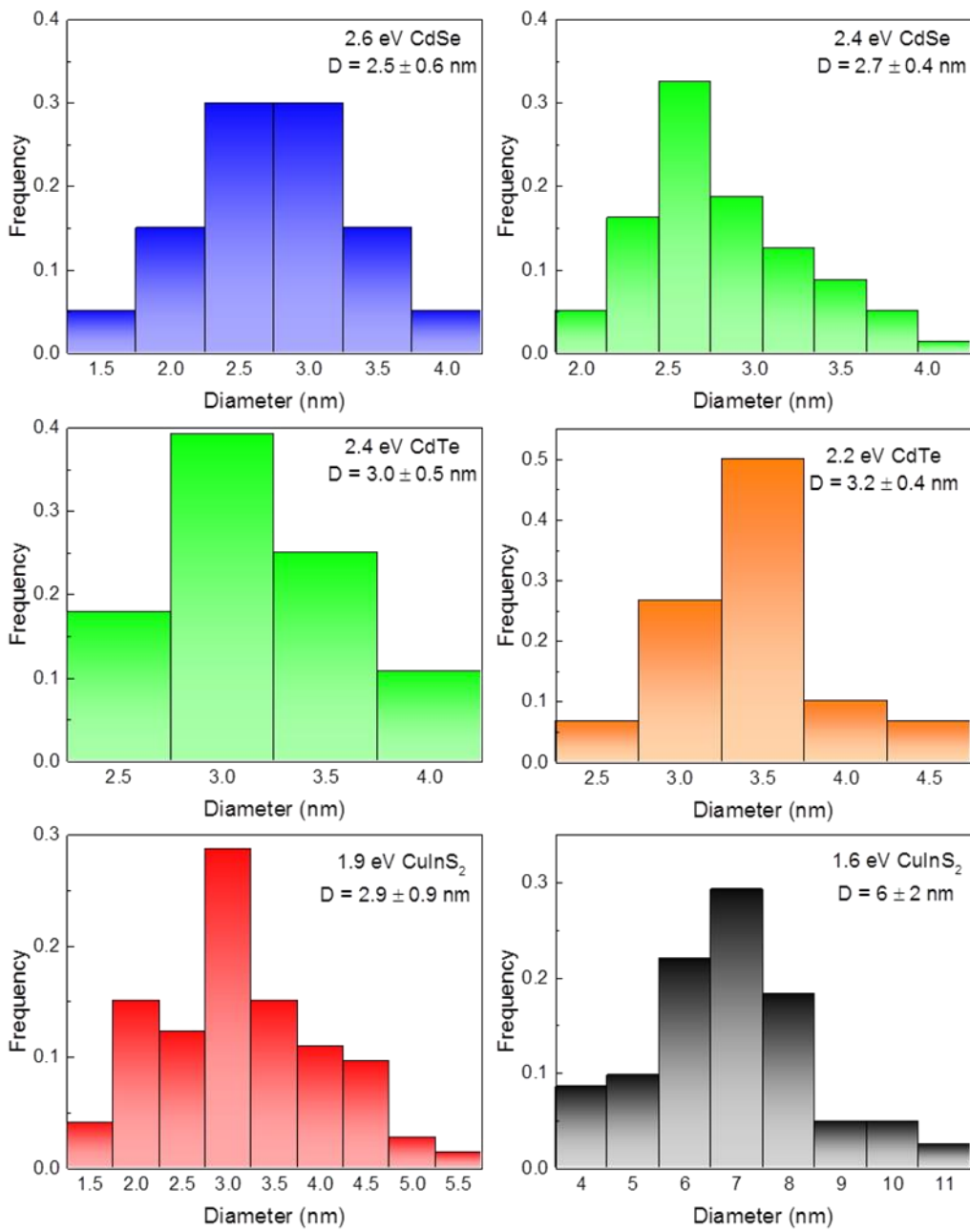


Figure 5.S6 Size distribution histograms of the respective quantum dots.

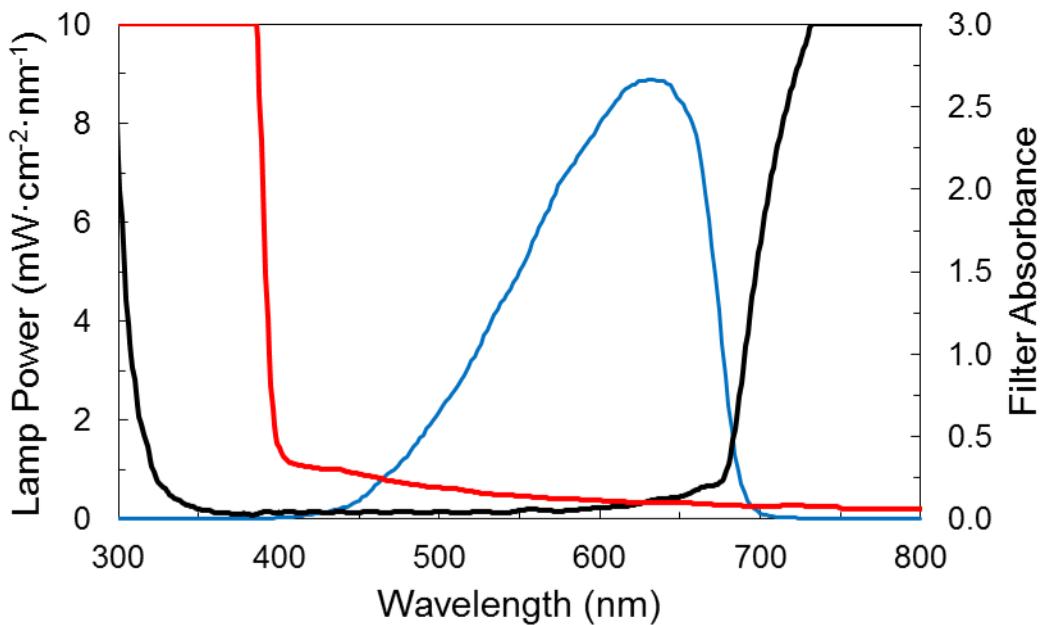


Figure 5.S7 Lamp emission spectrum (blue) and filter absorbance spectra (IR – black, UV – red) at 100% light intensity.

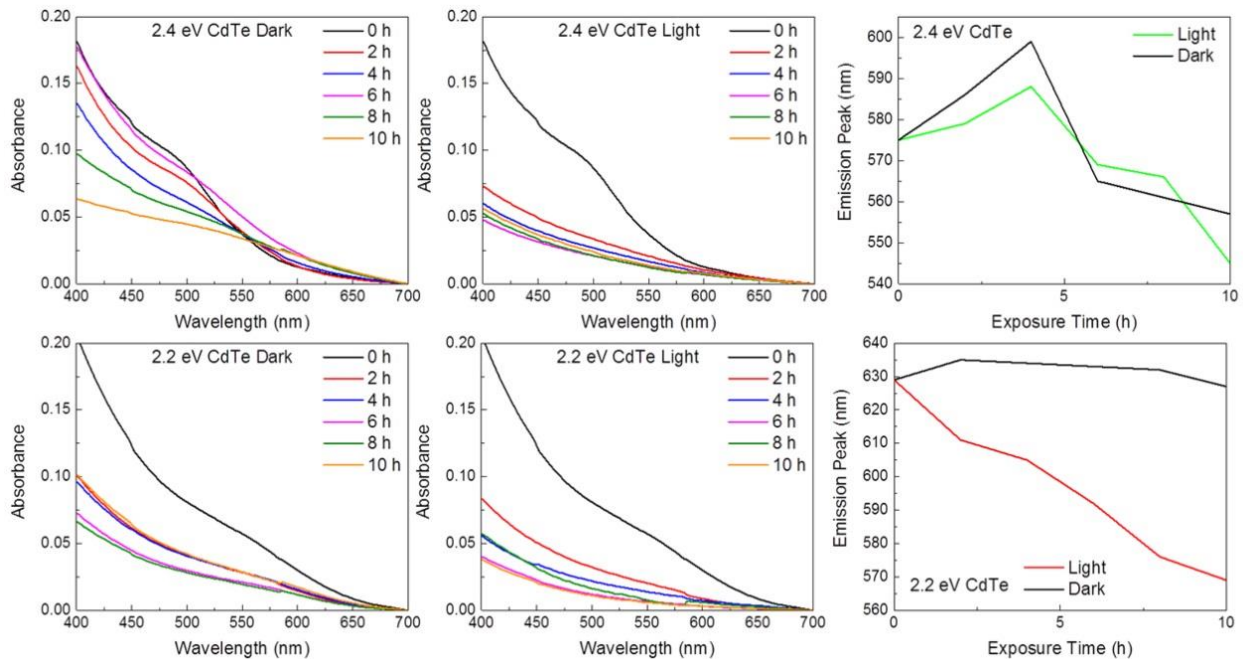


Figure 5.S8 Absorbance spectra of the CdTe quantum dots over time light and dark incubated at 37°C. On the right are plots tracking the peak position of the PL emission of the two sizes over time. The blue shift of the emission peak indicates formation of a CdO shell on the surface.

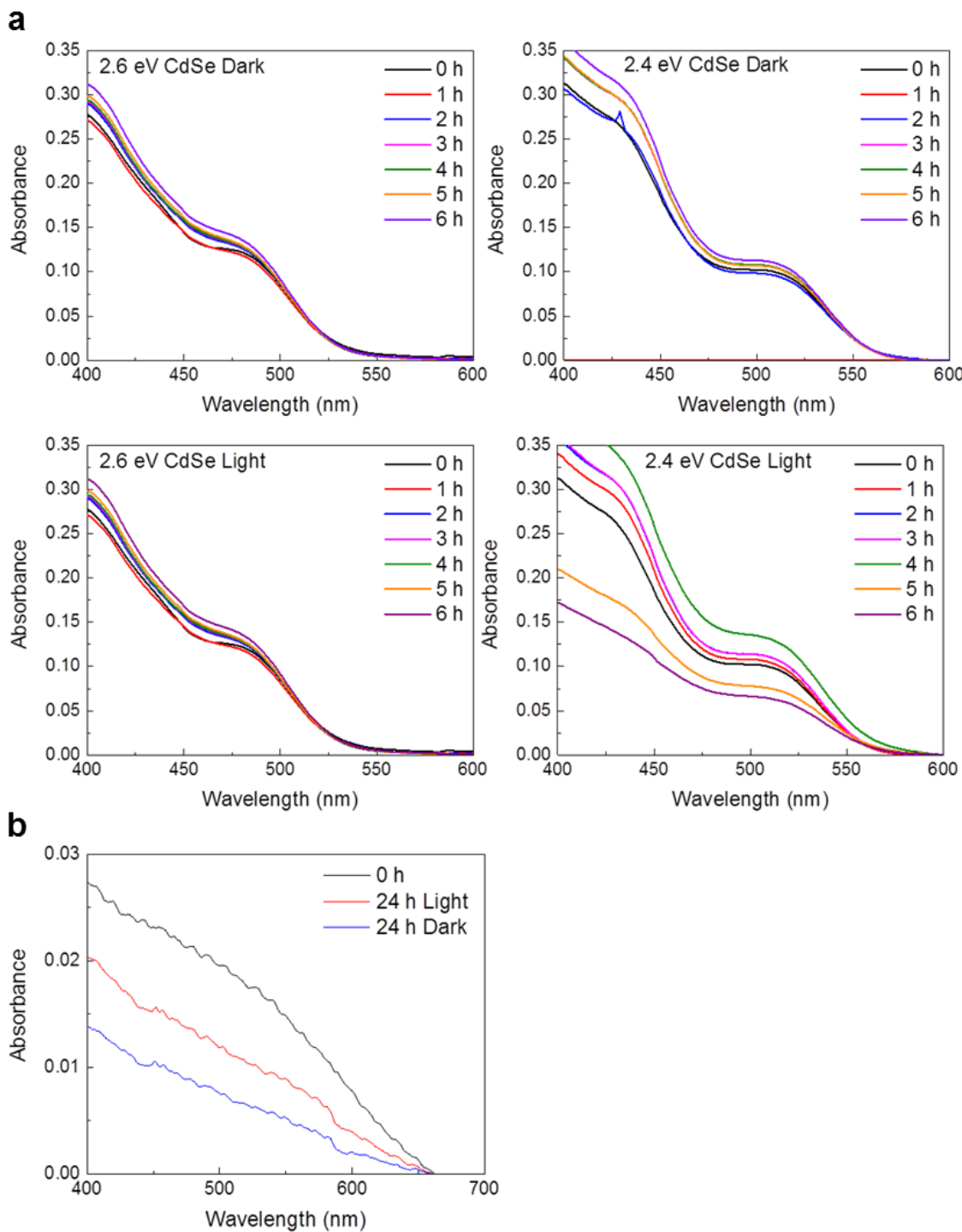


Figure 5.S9 CdSe stability. a. Changes in CdSe absorbance over time in light and dark incubated at 37°C in basic media (left) and PBS (right). b. Absorbance spectra after 24 hours of incubation of CIS-1.9 particles in PBS.

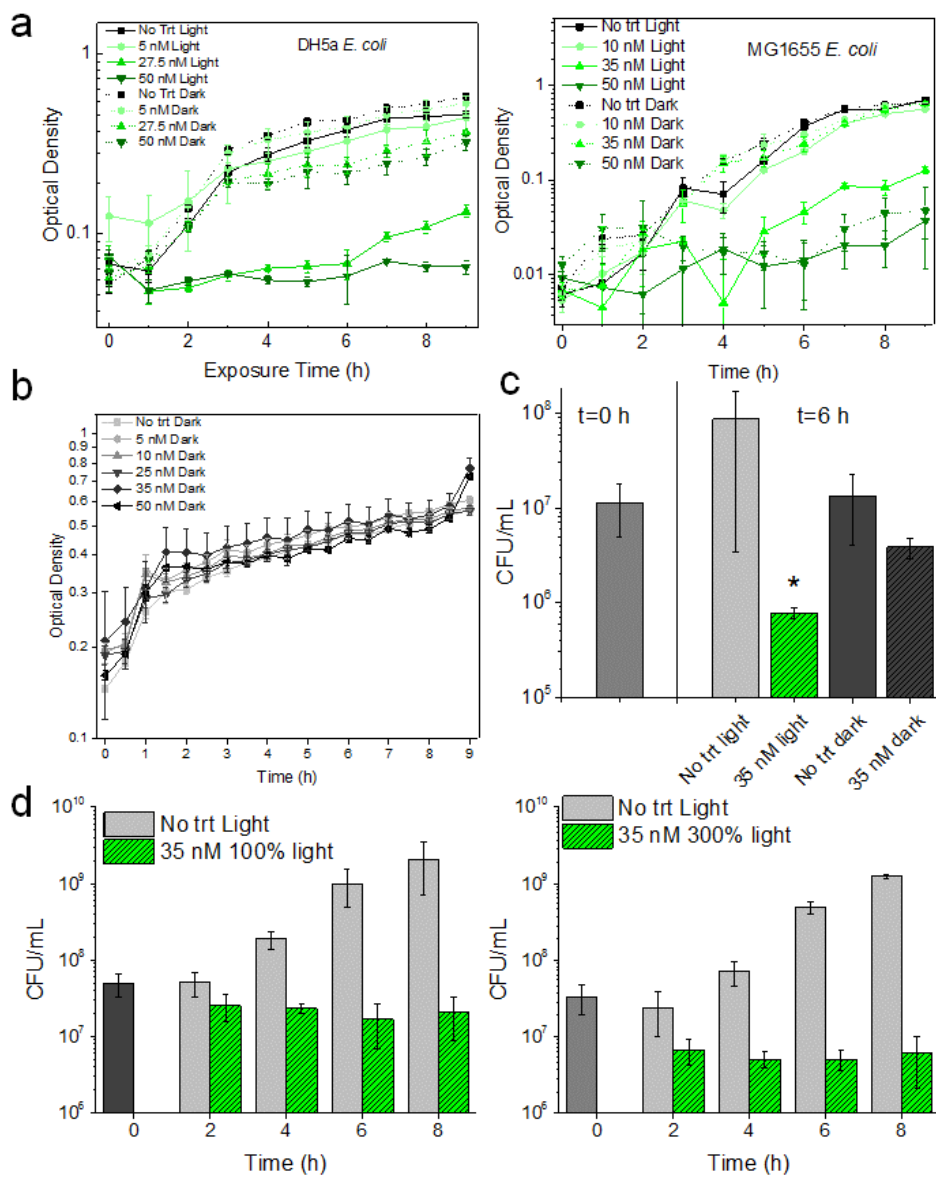


Figure 5.S10 Growth inhibition and CFU/mL with CdTe-2.4 in *E. coli*. a. Comparison of growth curves of *E. coli* DH5 α and *E. coli* MG1655 cultures to varying concentrations of CdTe-2.4 in presence of light and dark. b. Growth curves of *E. coli* DH5 α exposed to different concentrations of CdTe-2.4 in dark. c. Raw CFU/mL data with respective treatment for *E. coli* MG1655 in M9. The CFU/mL at time t=0 corresponds to 1:100 dilution from overnight culture. d. Time dependent CFU/mL of *E. coli* MG1655 in M9 in light with respective concentration of CdTe-2.4. Left panel is raw CFU/mL data with 100% light intensity and right panel is with 300% light intensity. The increase in light intensity increases the cell death from 35 nM CdTe-2.4 therapeutic. The CFU/mL at time t=0 corresponds to 1:100 dilution from overnight culture. The time dependent cell viability for 35 nM of the therapeutic and varying light intensity. Figure 5.S10d shows dependence of cell death on rate of LARS generation. We have also shown the dependence of the therapeutic action on concentration and light intensity in Figure 5.S20. Data shown are an average of three independent experiments (error bars are standard deviation from average values). All OD data is shown using a semi-log plot.

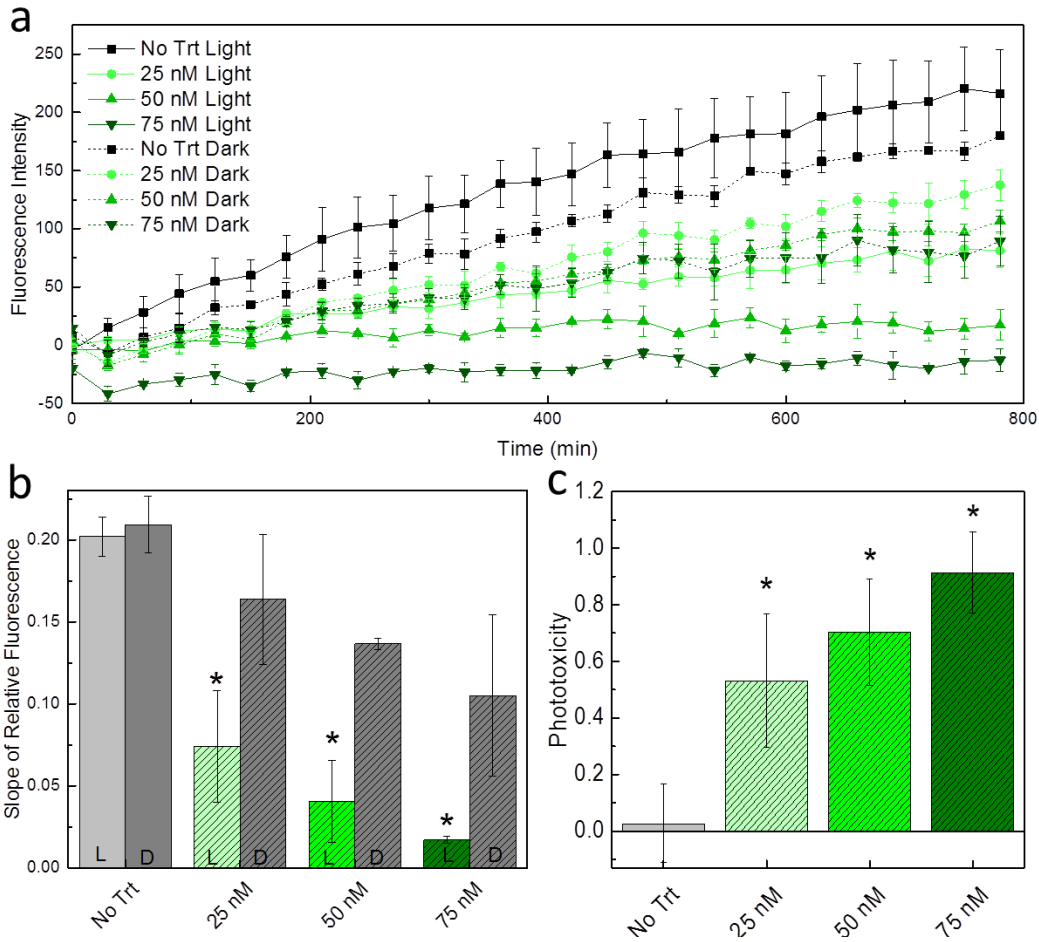


Figure 5.S11 Effect of CdTe-2.4 on cultures in PBS. a. Time dependent Resazurin fluorescence of *E. coli* MG1655 cultures in phosphate buffered saline exposed to CdTe-2.4 at various concentrations in light and dark. b. Slopes of the measured fluorescence during the initial linear phase, where bars labeled “L” were under light exposure and bars labeled “D” were in dark. c. Representation of the phototoxicity caused by CdTe-2.4 in PBS at various concentrations shown as 1-(slope of fluorescence in light/slope of fluorescence in dark). Data shown are an average of three independent experiments (error bars are standard deviation from average values).

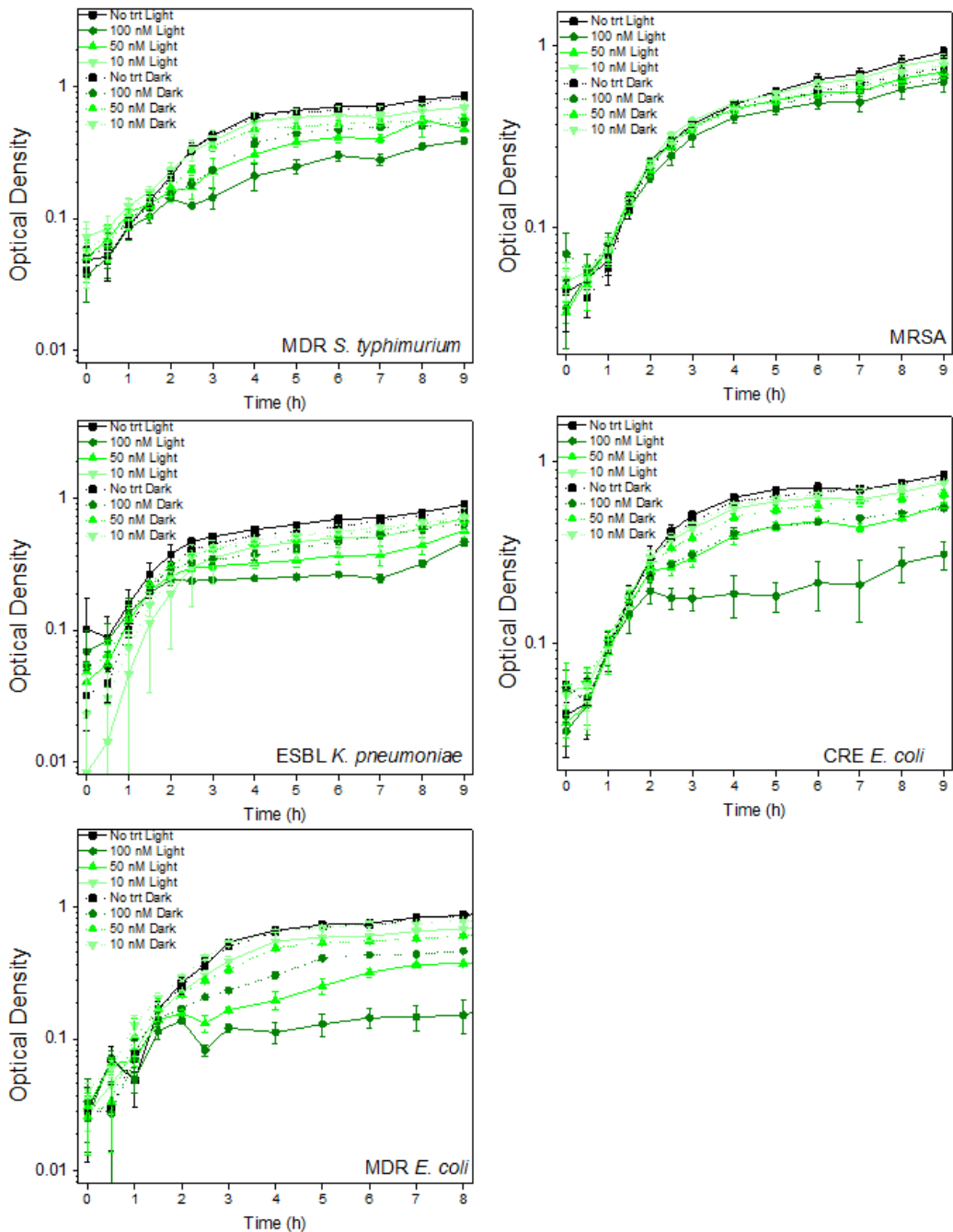


Figure 5.S12 Optical density of respective MDR strains exposed to CdTe-2.4 as a function of time and concentration. All OD data is shown using a semi-log plot.

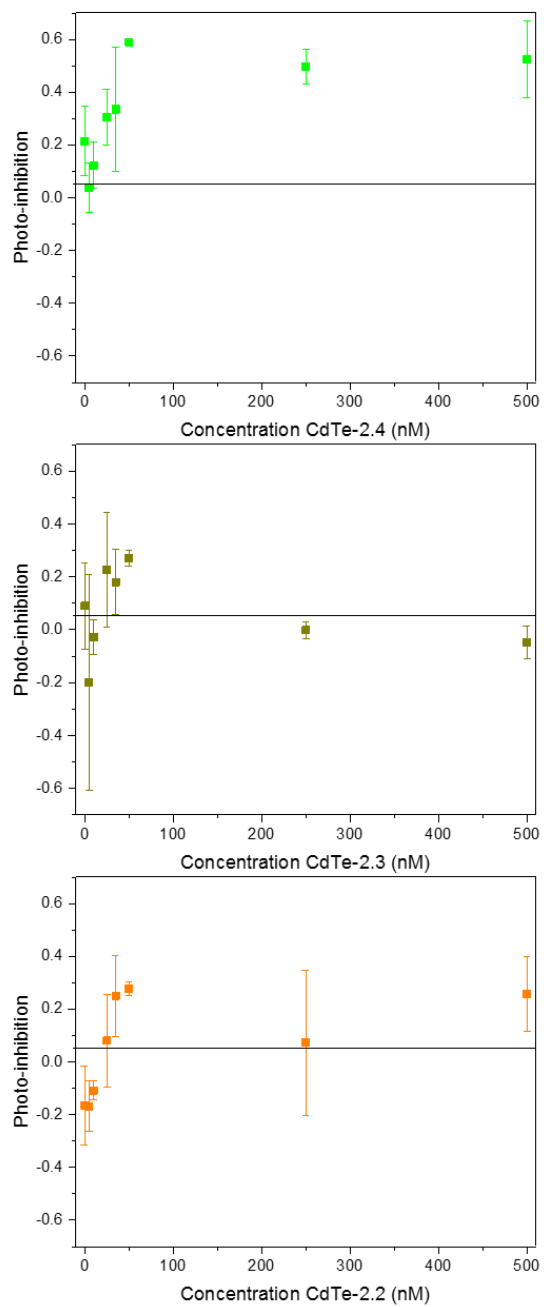


Figure 5.S13 Photo-inhibition (Equation 5.4) as a function of concentration for respective quantum dots in *E. coli* DH5 α . Optical density at 8 h was normalized to 0 h for this calculation of photo-inhibition because the starting OD's varied between conditions. Data shown are an average of three independent experiments (error bars are standard deviation from average values).

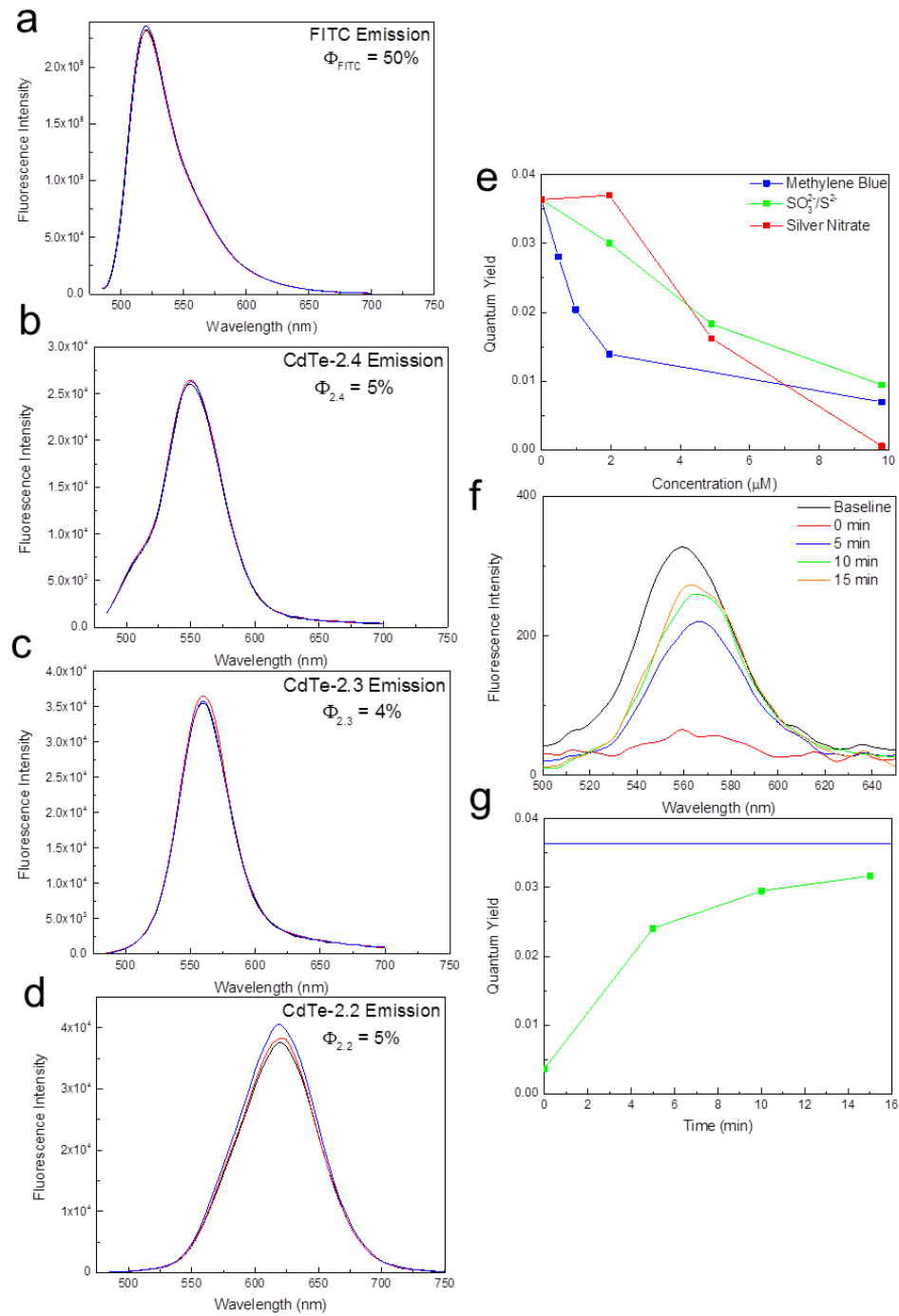


Figure 5.S14 Quantum yield evaluation. a-d. Fluorescence spectra of FITC and the CdTe quantum dots with 3 replicates per sample are shown. e. Quantum yield as a function of quencher concentration. f. Fluorescence spectra of dots exposed to the sulfite/sulfide quenchers at 500 nM over time while stimulated with UV radiation at 365 nm. g. Calculated quantum yield from the spectra shown in f. showing recovery against the nominal baseline (blue line).

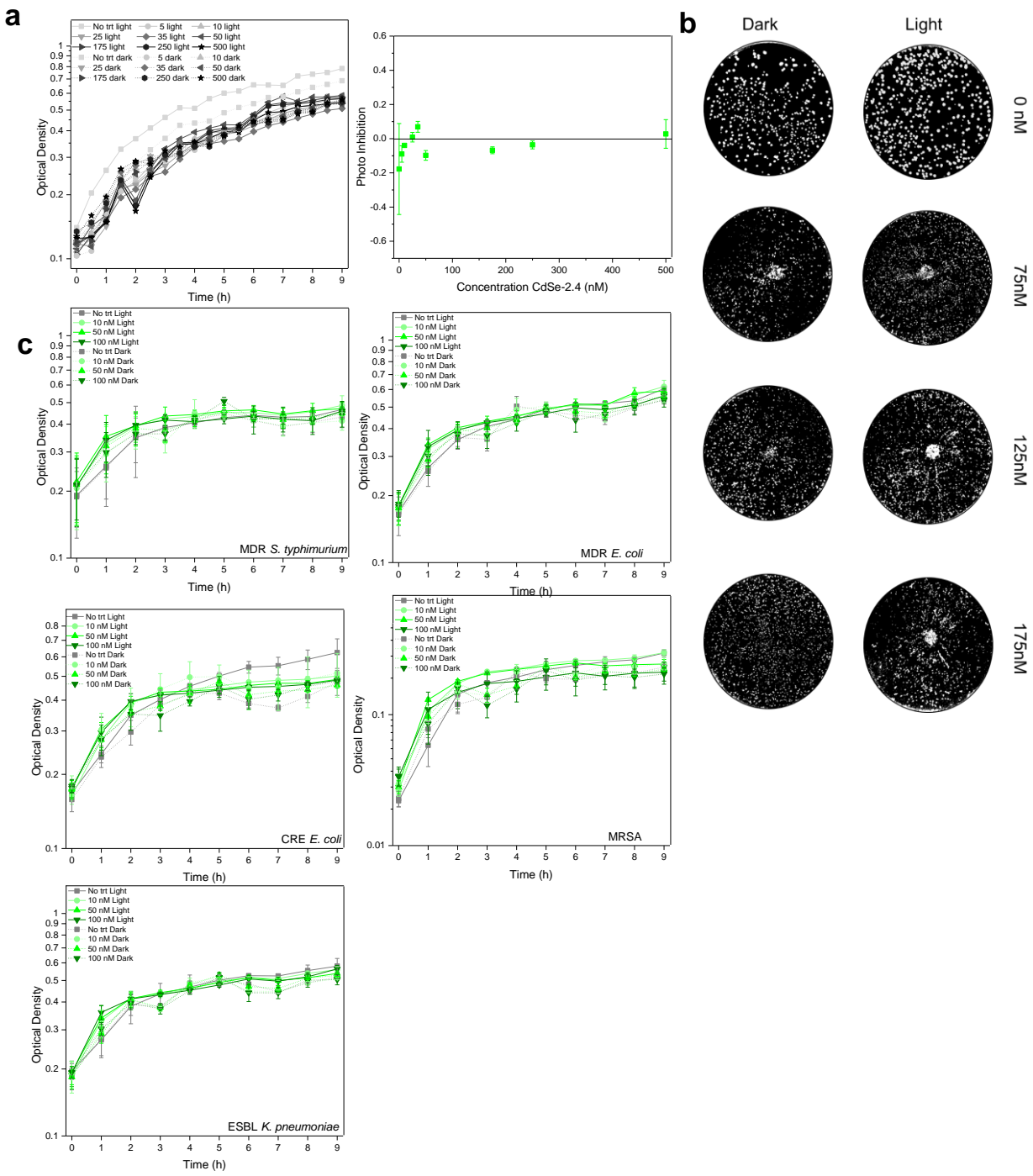


Figure 5.S15 Effect on CdSe-2.4 on bacterial growth. a. Optical density growth curves of *E. coli* DH5 α exposed to light or dark and different concentration of CdSe-2.4. b. *E. coli* DH5 α plated on solid LB medium after 7 h of exposure to CdSe-2.4 at respective concentrations. c. MDR strains in respective conditions demonstrating benign effect of CdSe-2.4. Data shown in (a, c) are an average of three independent experiments (error bars are standard deviation from average values). All OD data is shown using a semi-log plot.

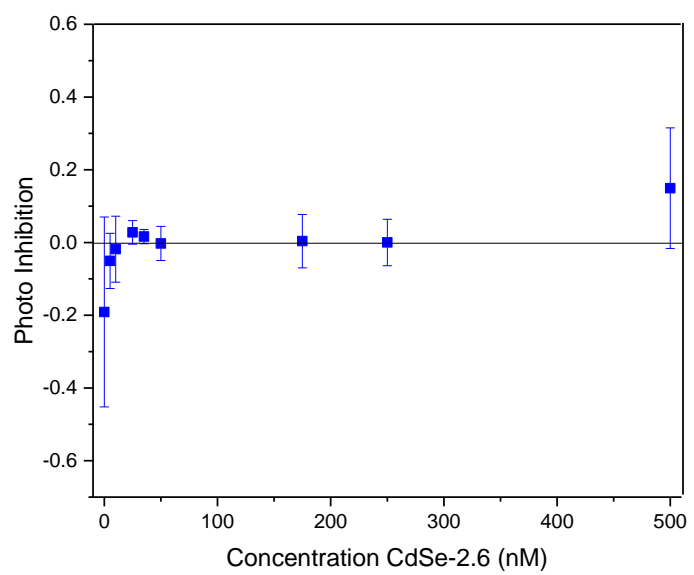


Figure 5.S16 Photo-inhibition as a function of concentration for CdSe-2.6 quantum dots in *E. coli* DH5 α . Data shown are an average of three independent experiments (error bars are standard deviation from average values).

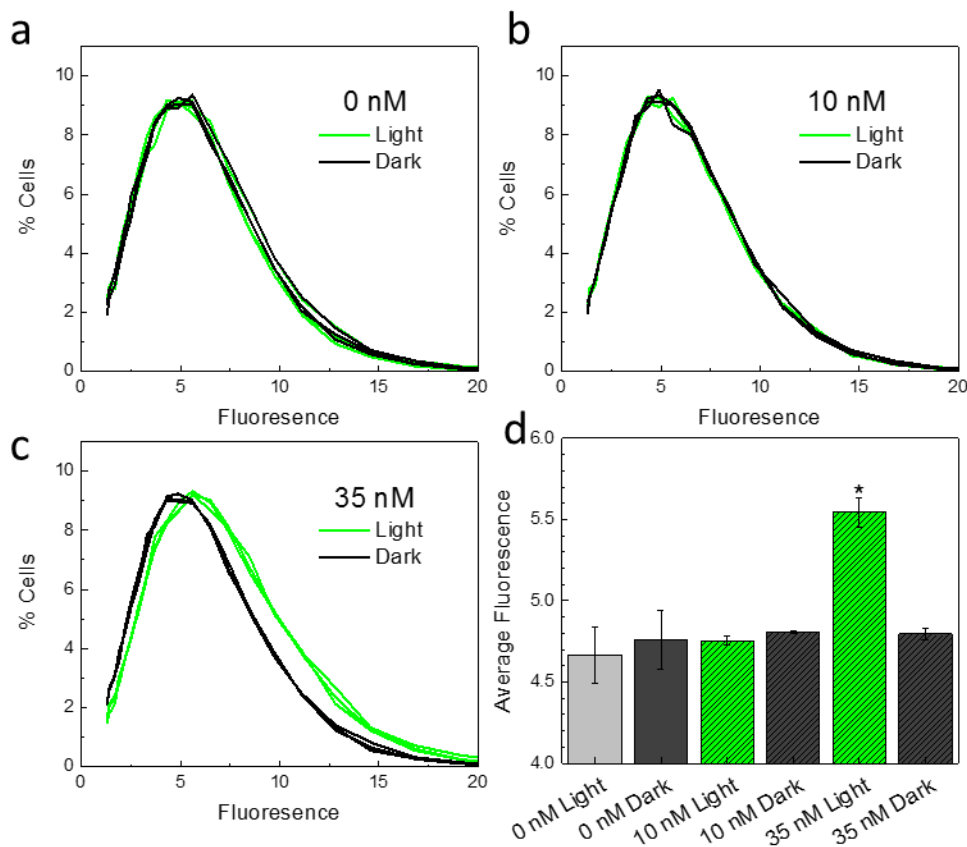


Figure 5.S17 Flow cytometry data for *E. coli* MG1655 in M9 medium treated with DCFH-DA and a. 0 nM, b. 10 nM, and c. 35 nM CdTe in light and dark with three biological replicates per sample and 30,000 cells per sample. The samples were treated with DCFH-DA to measure the generation of oxidative species from CdTe-2.4 in cells. DCFH-DA, when exposed to oxidizing species is oxidized to fluorescent DCFH resulting in the green fluorescence.³⁹ Flow cytometry was used to measure the green fluorescence of individual cells. d. Average fluorescence of each sample. Data shown are an average of three independent experiments (error bars are standard deviation from average values). Cells treated with 35 nM CdTe-2.4 in presence of light demonstrated significantly higher DCFH fluorescence ($p < 0.05$) compared to all other conditions shown.

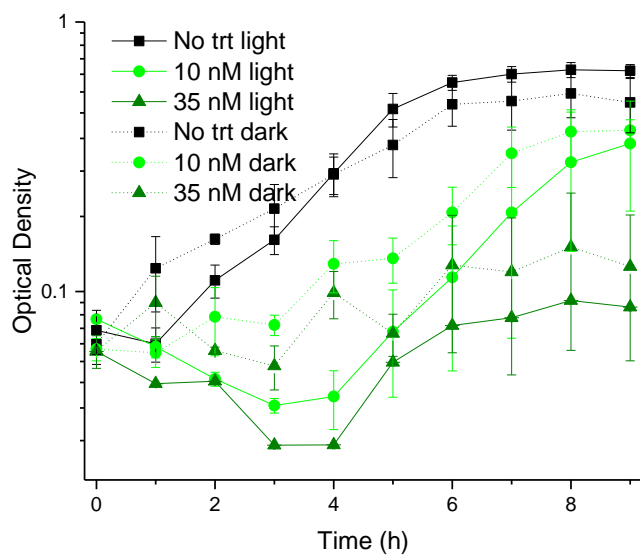


Figure 5.S18 Growth curves of *E. coli* MG1655 in M9 medium grown under anaerobic conditions. Data shown are an average of three independent experiments (error bars are standard deviation from average values). No significant difference ($p>0.05$) in growth in presence of CdTe-2.4 is observed between light and dark conditions. All OD data is shown using a semi-log plot.

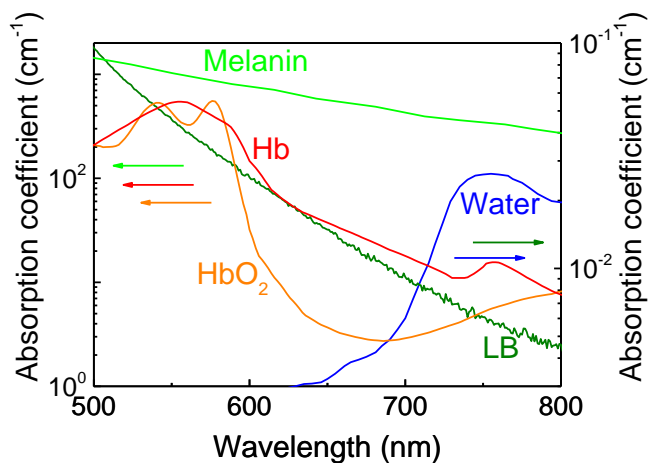


Figure 5.S19 Optical window evaluation. Absorption coefficient for various biological species (melanin, hemoglobin (Hb), oxyhemoglobin (HbO₂), water, complex media (LB)) demonstrating an optical window available for illumination and excitation of visible light activated quantum dots for phototherapy

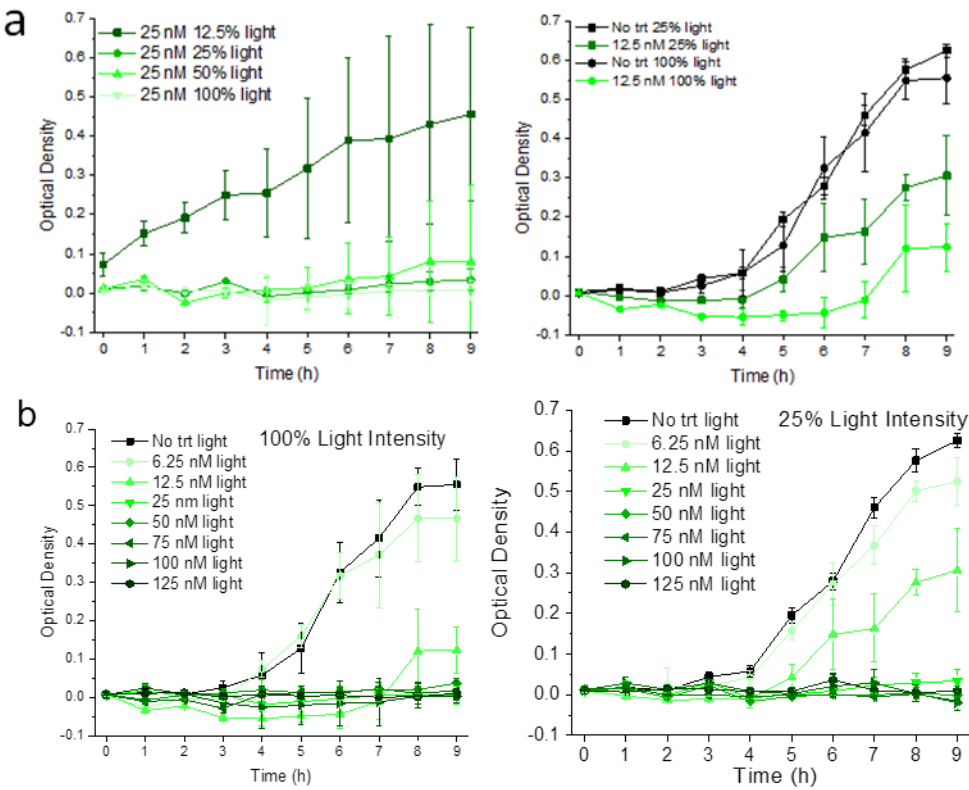


Figure 5.S20 Light flux effect on therapeutic intensity. a. Optical density of *E. coli* MG1655 in M9 with varying light intensity at 25 nM (left panel) and 12.5 nM (right panel). b. Optical density of *E. coli* MG1655 in M9 at 100% (left panel) and 25% (right panel) of nominal light intensity with no treatment and increasing CdTe-2.4 concentrations. Data shown are an average of three independent experiments (error bars are standard deviation from average values). Since the rate of cell death is proportional to the rate of LARS generation (above saturation), we see an exponential dependence on concentration, and linear dependence on the light intensity. Therefore, a small increase in CdTe-2.4 concentration can offset a reduction in light intensity for phototherapy applications. Optical density curves shown here are on a linear scale for clarity of effects at low OD.

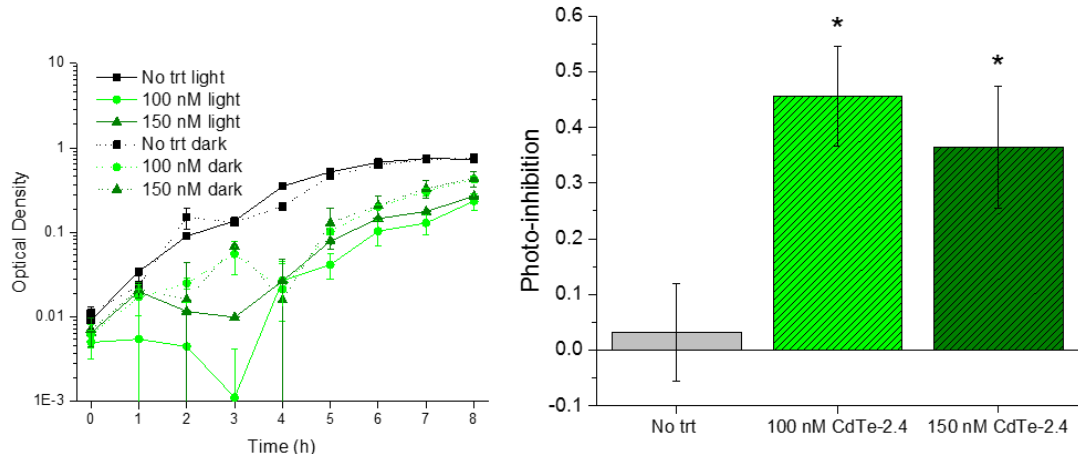


Figure 5.S21 *E. coli* MG1655 in M9 uptake bioassay with CdTe-2.4 showing significant photo-inhibition ($p<0.05$) from CdTe-2.4 even after removing the quantum dots from the media. The cells were removed from the QD media after 1 hour of incubation in dark and resuspended in fresh M9. These results indicate that the quantum dots are present inside the cells. Data shown in are an average of three independent experiments.

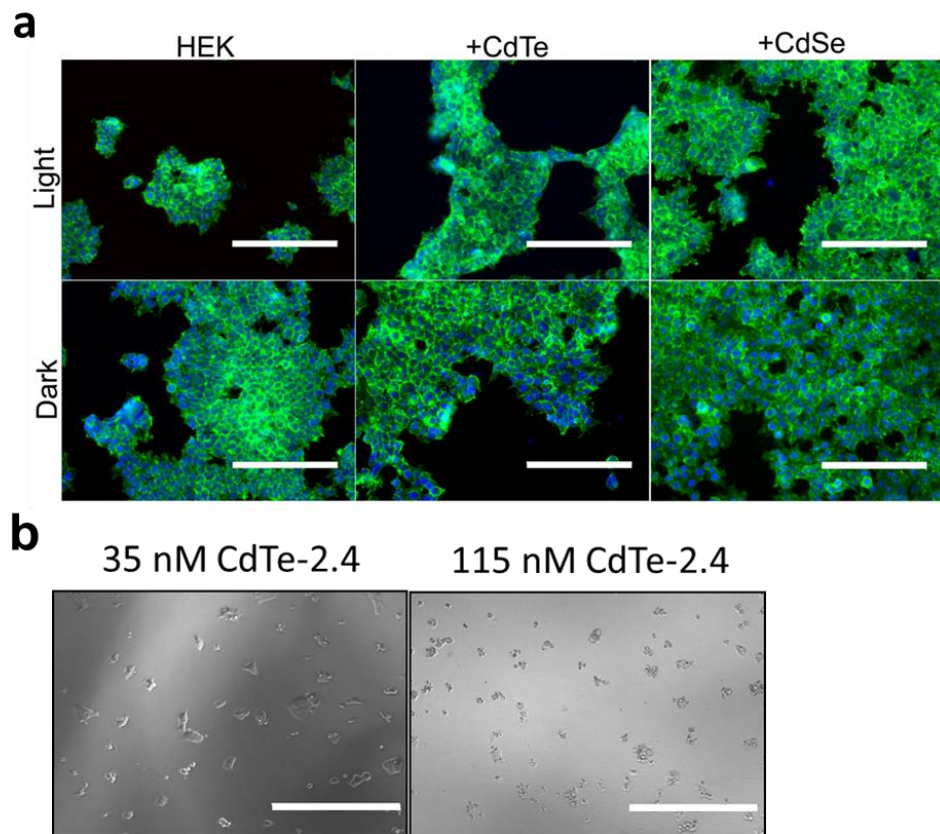


Figure 5.S22 HEK 293T monocultures. a. Images of a monoculture of HEK 293T cells after exposure to respective quantum dots. Concentrations are 35 nM for CdTe-2.4 and 100 nM for CdSe-2.4. b. HEK 293T cells in non-toxic (35 nM) and toxic (115 nM) concentrations of CdTe-2.4 which were used as morphological controls of healthy, adhered cells and un-healthy, non-adhered cells in our co-culture experiments (Life Technologies reference manual), respectively. Scale bars in all images are 200 μ m.

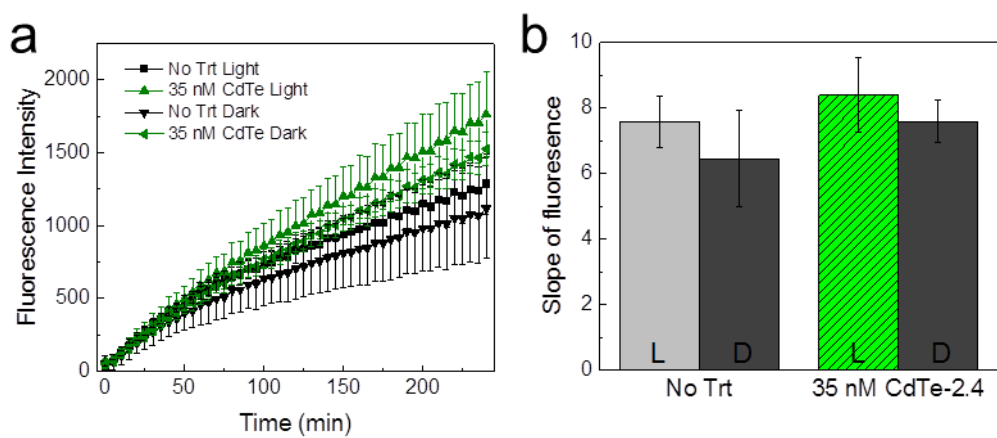


Figure 5.S23 HEK 293T health. a. Time dependent Resazurin fluorescence of HEK 293T cells exposed to CdTe-2.4 in light and dark. b. Slopes of the measured fluorescence during the initial linear phase, where bars labeled “L” were under light exposure and bars labeled “D” were in dark, showing no significant difference in cell viability between treated and untreated cells ($p>0.05$).

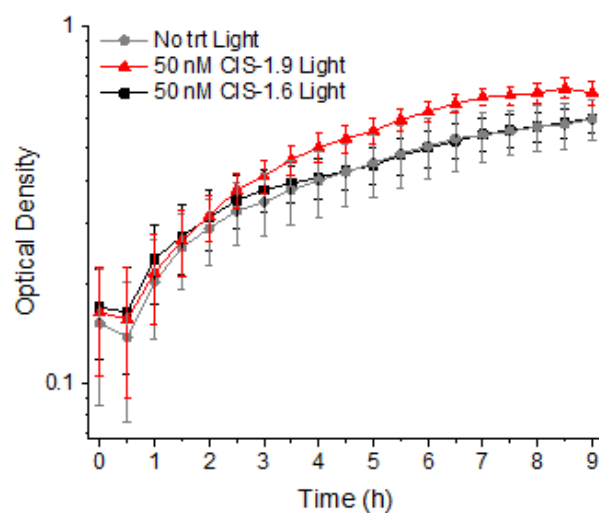


Figure 5.S24 Optical density of *E. coli* DH5 α in presence of respective treatment. All OD data is shown using a semi-log plot.

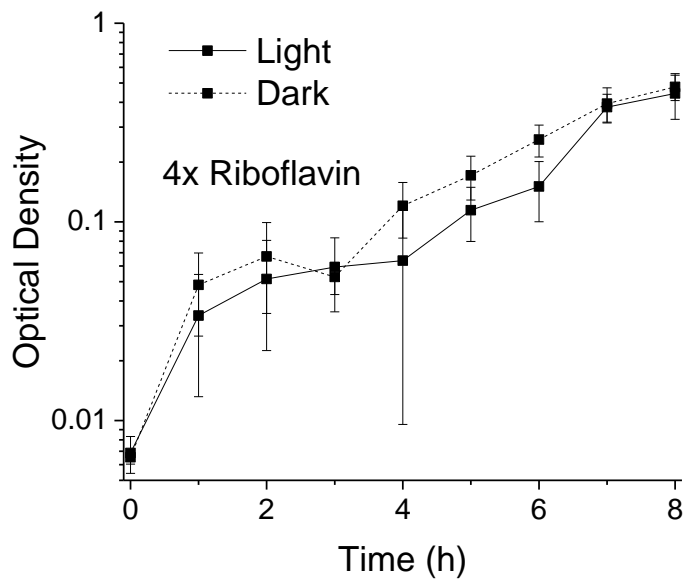


Figure 5.S25 Optical density curves of *E. coli* MG1655 in M9 media with riboflavin. Grown in light or dark with 4x the riboflavin content in LB medium as determined by fluorescence at 485/530 nm. All OD data is shown using a semi-log plot

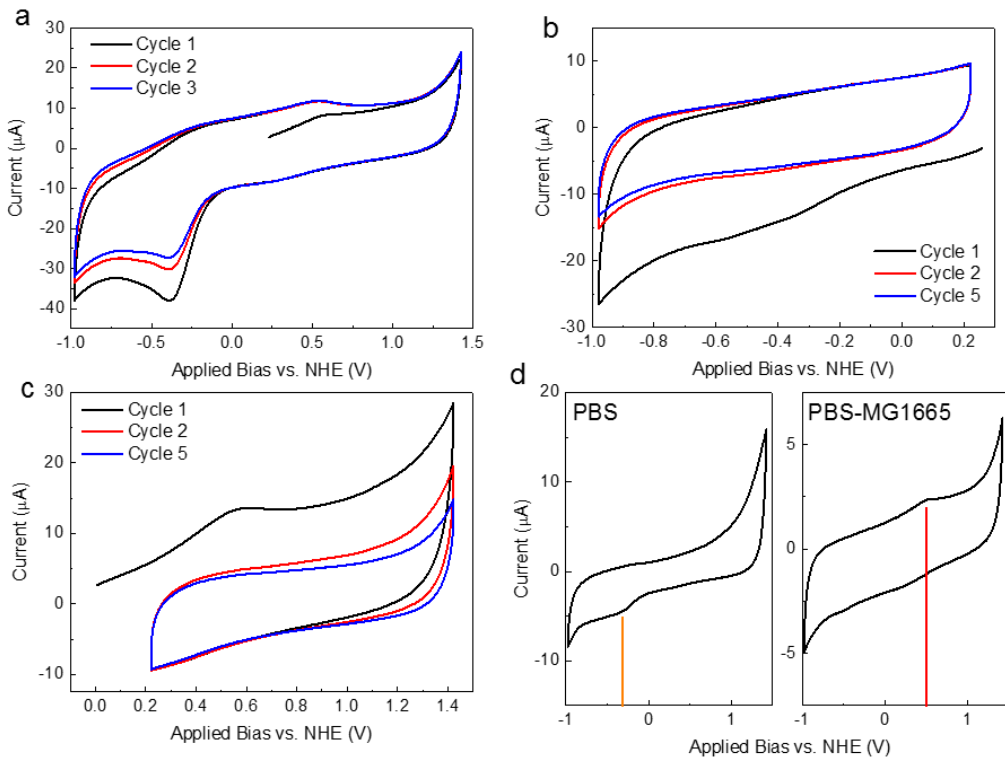


Figure 5.S26 Cyclin voltammograms confirming superoxide species from molecular oxygen.
 a. Cyclic voltammograms (C-Vs) of PBS bubbled with oxygen exhibiting decreased signal from the superoxide peak at -0.38 V with continued scans, due to consumption of dissolved oxygen. The broad peak centered ~+0.5V occurs due to formation of ROS species (see discussion on potential role of ROS species as LARS). b. Scans of PBS- *E. coli* MG1655 in the negative mode and c. scans of PBS- *E. coli* MG1655 in the positive mode, showing a loss of features with successive measurements, likely due to consumption of short lived superoxide and other ROS species. d. C-Vs of phosphate-buffered saline (PBS) solution and PBS with *E. coli* MG1655 bacteria with features marked. The superoxide peak in PBS is quenched on addition of *E. coli* MG1655 cells. Instead the ROS species result in the broad peak centered ~+0.5V.

5.7 Author Contributions

P.N. and A.C. conceived the idea. C.M.C. conducted cellular experiments and S.M.G. and J.A.M. performed material synthesis and characterization. N.E.M. prepared the clinical isolates and provided the samples. P.N., A.C., C.M.C. and S.M.G. analyzed the experimental data and wrote the paper. All the authors discussed the results and edited the manuscript.

5.8 References

- LeClerc, J. E., Li, B., Payne, W. L. & Cebula, T. a. High mutation frequencies among

- Escherichia coli and Salmonella pathogens. *Science* **274**, 1208–1211 (1996).
2. Chatterjee, A., Johnson, C. M., Shu, C.-C., *et al.* Convergent transcription confers a bistable switch in Enterococcus faecalis conjugation. *Proc. Natl. Acad. Sci. U. S. A.* **108**, 9721–6 (2011).
 3. Courtney, C. M. & Chatterjee, A. Sequence-Specific Peptide Nucleic Acid-Based Antisense Inhibitors of TEM-1 β -Lactamase and Mechanism of Adaptive Resistance. *ACS Infect. Dis.* **1**, 253–263 (2015).
 4. World Health Organization. *Global Tuberculosis Report*. (2012).
 5. United States Center for Disease Control. *Antibiotic Resistance Threats*. (2013).
 6. He, M., Miyajima, F., Roberts, P., *et al.* Emergence and global spread of epidemic healthcare-associated Clostridium difficile. *Nat. Genet.* **45**, 109–13 (2013).
 7. Chang, H.-H., Cohen, T., Grad, Y. H., *et al.* Origin and Proliferation of Multiple-Drug Resistance in Bacterial Pathogens. *Microbiol. Mol. Biol. Rev.* **79**, 101–116 (2015).
 8. Blair, J. M. A., Webber, M. A., Baylay, A. J., Ogbolu, D. O. & Piddock, L. J. V. Molecular mechanisms of antibiotic resistance. *Nat. Rev. Microbiol.* **13**, 42–51 (2015).
 9. Falagas, M. E. & Bliziotis, I. a. Pandrug-resistant Gram-negative bacteria: the dawn of the post-antibiotic era? *Int. J. Antimicrob. Agents* **29**, 630–636 (2007).
 10. Yu, B. P. Cellular defenses against damage from reactive oxygen species. *Physiol. Rev.* **74**, 139–162 (1994).
 11. Thannickal, V. J. & Fanburg, B. L. Reactive oxygen species in cell signaling. *Am. J. Physiol. Lung Cell. Mol. Physiol.* **279**, L1005–L1028 (2000).
 12. Imlay, J. A. The molecular mechanisms and physiological consequences of oxidative stress: lessons from a model bacterium. *Nat. Rev. Microbiol.* **11**, 443–54 (2013).
 13. Valko, M., Leibfritz, D., Moncol, J., *et al.* Free radicals and antioxidants in normal physiological functions and human disease. *Int. J. Biochem. Cell Biol.* **39**, 44–84 (2007).
 14. Apel, K. & Hirt, H. Reactive oxygen species: metabolism, oxidative stress, and signal transduction. *Annu. Rev. Plant Biol.* **55**, 373–399 (2004).
 15. Kohanski, M. a., Dwyer, D. J., Hayete, B., Lawrence, C. a. & Collins, J. J. A Common Mechanism of Cellular Death Induced by Bactericidal Antibiotics. *Cell* **130**, 797–810 (2007).
 16. Dwyer, D. J., Belenky, P. a, Yang, J. H., *et al.* Antibiotics induce redox-related physiological alterations as part of their lethality. *Proc. Natl. Acad. Sci. U. S. A.* **111**, E2100–9 (2014).

17. Sun, Q. C., Mundoor, H., Ribot, J. C., *et al.* Plasmon-enhanced energy transfer for improved upconversion of infrared radiation in doped-lanthanide nanocrystals. *Nano Lett.* **14**, 101–106 (2014).
18. Huang, X., El-Sayed, I. H., Qian, W. & El-Sayed, M. a. Cancer cell imaging and photothermal therapy in the near-infrared region by using gold nanorods. *J. Am. Chem. Soc.* **128**, 2115–2120 (2006).
19. Loo, C., Lowery, A., Halas, N., West, J. & Drezek, R. Immunotargeted nanoshells for integrated cancer imaging and therapy. *Nano Lett.* **5**, 709–711 (2005).
20. Connor, E. E., Mwamuka, J., Gole, A., Murphy, C. J. & Wyatt, M. D. Gold nanoparticles are taken up by human cells but do not cause acute cytotoxicity. *Small* **1**, 325–327 (2005).
21. Sun, Q.-C., Ding, Y., Goodman, S. M., H. Funke, H. & Nagpal, P. Copper plasmonics and catalysis: role of electron–phonon interactions in dephasing localized surface plasmons. *Nanoscale* **6**, 12450–12457 (2014).
22. Ipe, B. I., Lehnig, M. & Niemeyer, C. M. On the generation of free radical species from quantum dots. *Small* **1**, 706–9 (2005).
23. Rengifo-Herrera, J. a., Sanabria, J., Machuca, F., *et al.* A Comparison of Solar Photocatalytic Inactivation of Waterborne *E. coli* Using Tris (2,2'-bipyridine)ruthenium(II), Rose Bengal, and TiO₂. *J. Sol. Energy Eng.* **129**, 135 (2007).
24. Walker, G. C. Mutagenesis and inducible responses to deoxyribonucleic acid damage in *Escherichia coli*. *Microbiol. Rev.* **48**, 60–93 (1984).
25. Lu, Z., Li, C. M., Bao, H., Qiao, Y. & Toh, Y. Mechanism of Antimicrobial Activity of CdTe Quantum Dots. *Langmuir* **24**, 5445–5452 (2008).
26. Brayner, R., Ferrari-iliou, R., Brivois, N., *et al.* Toxicological Impact Studies Based on *Escherichia coli* Bacteria in Ultrafine ZnO Nanoparticles Colloidal Medium. *Nano Lett.* **6**, 866–870 (2006).
27. Medintz, I. L. & Mattoussi, H. Quantum dot-based resonance energy transfer and its growing application in biology. *Phys. Chem. Chem. Phys.* **11**, 17–45 (2009).
28. Lovrić, J., Bazzi, H. S., Cuie, Y., *et al.* Differences in subcellular distribution and toxicity of green and red emitting CdTe quantum dots. *J. Mol. Med.* **83**, 377–85 (2005).
29. Cho, S. J., Maysinger, D., Jain, M., *et al.* Long-Term Exposure to CdTe Quantum Dots Causes Functional Impairments in Live Cells. *Lamgmuir* **23**, 1974–1980 (2007).
30. The European Committee on Antimicrobial Susceptibility Testing. Breakpoint tables for interpretation of MICs and zone diameters. *Version 5.0* (2015).
31. Singh, V., Beltran, I. J. C., Ribot, J. C. & Nagpal, P. Photocatalysis deconstructed: Design

- of a new selective catalyst for artificial photosynthesis. *Nano Lett.* **14**, 597–603 (2014).
- 32. Tikhomirov, G., Hoogland, S., Lee, P. E., *et al.* DNA-based programming of quantum dot valency, self-assembly and luminescence. *Nat. Nanotechnol.* **6**, 485–90 (2011).
 - 33. Yu, W. W., Qu, L., Guo, W. & Peng, X. Experimental Determination of the Extinction Coefficient of CdTe, CdSe, and CdS Nanocrystals. *Chem. Mater.* **125**, 2854–2860 (2003).
 - 34. Panthani, M. G., Akhavan, V., Goodfellow, B., *et al.* Nanocrystal ‘Inks’ for Printable Photovoltaics. *J. Am. Chem. Soc.* **130**, 16770–16777 (2008).
 - 35. Booth, M., Brown, A. P., Evans, S. D. & Critchley, K. Determining the concentration of CuInS₂ quantum dots from the size-dependent molar extinction coefficient. *Chem. Mater.* **24**, 2064–2070 (2012).
 - 36. Zhu, Z.-J., Yeh, Y.-C., Tang, R., *et al.* Stability of quantum dots in live cells. *Nat. Chem.* **3**, 963–968 (2011).
 - 37. Jiong, M., Cnen, J. Y., Zhang, Y., *et al.* Photochemical instability of thiol-capped CdTe quantum dots in aqueous solution and living cells: Process and mechanism. *J. Phys. Chem. B* **111**, 12012–12016 (2007).
 - 38. Ma, J., Chen, J.-Y., Guo, J., *et al.* Photostability of thiol-capped CdTe quantum dots in living cells: the effect of photo-oxidation. *Nanotechnology* **17**, 2083–2089 (2006).
 - 39. Myhre, O., Andersen, J. M., Aarnes, H. & Fonnum, F. Evaluation of the probes 2',7'-dichlorofluorescin diacetate, luminol, and lucigenin as indicators of reactive species formation. *Biochem. Pharmacol.* **65**, 1575–1582 (2003).
 - 40. Drecktrah, D., Levine-Wilkinson, S., Dam, T., *et al.* Dynamic behavior of salmonella-induced membrane tubules in epithelial cells. *Traffic* **9**, 2117–2129 (2008).
 - 41. Valko, M., Izakovic, M., Mazur, M., Rhodes, C. J. & Telser, J. Role of oxygen radicals in DNA damage and cancer incidence. *Mol. Cell. Biochem.* **266**, 37–56 (2004).
 - 42. Rodgers, M. a. J. & Snowden, P. T. Lifetime of O₂ (1^Δg) in Liquid Water as Determined by Time-resolved Infrared Luminescence Measurements. *J. Am. Chem. Soc.* **104**, 5541–5543 (1982).

Chapter 6

Potentiating antibiotics in drug-resistant clinical isolates via stimuli-activated superoxide generation

Courtney C.M., Goodman, S.M., Nagy, T.A., Levy, M., Bhusal, P., Madinger, N.E., Detweiler, C.S., Nagpal, P., and Chatterjee, A. *Submitted.*

6.1 Abstract

The rise of multidrug-resistant (MDR) bacteria is a growing concern to global health and is exacerbated by the lack of new antibiotics^{1,2}. In order to treat already pervasive MDR infections, new classes of antibiotics or antibiotic adjuvants are needed. Recently reactive oxygen species (ROS) have been shown to play a role during antibacterial action, however, it is not yet understood whether ROS contributes directly or results as a byproduct of bacterial lethality in the presence of antibiotics. Here, we show a light-activated nanoparticle, designed to produce tunable flux of specific reactive oxygen species (ROS), superoxide, potentiates the activity of antibiotics in clinical MDR isolates of *Escherichia coli*, *Salmonella enterica*, and *Klebsiella pneumoniae*. Despite the high degree of antibiotic resistance in these isolates, we observed a synergistic interaction between both bactericidal and bacteriostatic antibiotics with varied mechanisms of action and our superoxide-producing nanoparticles in more than 75% of combinations. As a result of this potentiation, the effective antibiotic concentration of the clinical isolates was reduced up to 1000-fold below their respective sensitive/resistant breakpoint concentrations. Further, superoxide-generating nanoparticles in combination with ciprofloxacin reduced bacterial load in epithelial cells infected with *Salmonella enterica* serovar Typhimurium, and increased *Caenorhabditis elegans* survival upon infection with *Salmonella enterica* serovar Enteritidis,

compared to antibiotic alone. This demonstration highlights the ability to engineer superoxide generation to potentiate antibiotic activity and combat highly drug-resistant bacterial pathogens.

6.2 Introduction

The high-frequency of multidrug-resistant (MDR) bacterial infections and the lack of new antibiotics threaten the future of our healthcare system as we approach a post-antibiotic era¹. In 2013 antibiotic-resistant infections in the United States cost an estimated \$20 billion in direct healthcare costs and an additional \$35 billion in lost productivity². Enterobacteriaceae including carbapenem-resistant (CRE) *Escherichia coli* and extended spectrum β-lactamase (ESBL) producing *Klebsiella pneumoniae* (KPN) are severely antibiotic resistant and were recently designated priority 1 critical class bacterial pathogens in urgent need of effective antibiotics by the World Health Organization³. The gravity of the situation is highlighted by the fact that clinical isolates of these strains have up to 1000-fold higher 50% growth inhibition concentrations (GIC₅₀) of antibiotic relative to sensitive/resistant breakpoints recommended by Clinical Laboratory Standard Institute (CLSI), for a range of antibiotics with different mechanisms of actions (Figure 6.1a, Table 6.1). Such trends show the urgent need for development of new antimicrobials that can treat or potentiate current antibiotics against MDR bacteria. Here, we show the response of clinical isolates to multiple classes of antibiotics including a third-generation cephalosporin (ceftriaxone) that targets cell-wall synthesis and is bactericidal, a second-generation fluoroquinolone (ciprofloxacin) that inhibits DNA Topoisomerase II and is bactericidal, a lincosamide (clindamycin) and chloramphenicol, both of which target protein synthesis and are bacteriostatic, and an aminoglycoside (streptomycin) that targets protein synthesis and is bactericidal.

Recent studies indicate that the presence and level of reactive oxygen species (ROS) during antibiotic treatment can increase antibiotic lethality^{4–8}, affect the survival of persisters^{4,9}, and

contribute to the development of drug resistance¹⁰. ROS, including superoxide radical $\cdot\text{O}_2^-$, peroxide O_2^{2-} , and hydroxyl radicals $\cdot\text{OH}$, are present in bacteria at low levels during normal aerobic respiration, which can be mitigated by antioxidant defenses in bacteria including superoxide dismutase (SOD) and catalase. However, at elevated levels, ROS can overwhelm bacterial defenses and cause significant damage to DNA and iron-sulfur clusters and reduce metalloenzyme activity¹¹. Here we exploit this strategy by using an engineered quantum dot (QD) nanoparticle to produce intracellular superoxide to enhance our ability to inhibit clinical MDR bacteria. We show that engineered production of intracellular superoxide leads to robust potentiation of both bactericidal and bacteriostatic antibiotics in a range of clinical MDR bacteria despite their high level of resistance. Our work sheds light on the current debate regarding whether ROS contributes directly or results as a byproduct of bacterial lethality in the presence of antibiotics^{4-7,9,12}, and provides evidence for the former.

QDs are nanoparticles made of semi-conducting materials that, when illuminated with light, generate excited electrons and holes across their nominal energy bandgap¹³, which are then available, at energy levels specific to the engineered QDs size and material, for reduction and oxidation (redox) reactions (Figure 6.1b). Unlike photodynamic therapy which uses light-activation of different dyes and small molecules to produce non-specific ROS¹⁴, engineered QDs with tailored redox potentials allow for the generation of desired ROS that can perturb the cellular redox environment¹⁵. Since superoxide has been shown to be the principle initial species with relatively longer radical lifetime and diffusion lengths and can give rise to a variety of physiologically relevant primary and secondary reactive oxygen/nitrogen species¹⁶, we developed a specific ROS perturbation approach using superoxide radicals. In bacteria, superoxide disrupts enzyme iron-sulfur clusters resulting in an increased free ferrous iron pool¹⁷. This free iron further

localizes at DNA, proteins, and lipids allowing Fenton chemistry to occur within the diffusion lengths of hydroxyl radical for increased deleterious effects from ROS species¹⁸. Furthermore, it was recently shown that enhancing endogenous production of superoxide and peroxide in *E. coli* by single gene deletions potentiated antibiotic activity¹⁹ yet this study was constrained by the level of superoxide generation biologically possible in *E. coli*. Here, we create a platform for potentiating antibiotic activity without genetic manipulation, with concentration and stimuli-dependent control of superoxide generation by designing a stimuli-responsive nanoparticle to produce specific ROS superoxide.

6.3 Results and Discussion

6.3.1 Confirmation of intracellular superoxide production

We designed a cadmium telluride QD with a bandgap energy of 2.4 eV (CdTe-2.4) whose oxidation potential is tuned for superoxide production from molecular oxygen (Figure 6.S4). The design of this nanoparticle is detailed in Chapter 5. The ROS produced by CdTe-2.4 upon illumination were measured using electron paramagnetic resonance (EPR) spectroscopy. To identify short-lived radical species produced by CdTe-2.4, we used 5,5-dimethyl-1-pyrroline N-oxide (DMPO), a spin trapping reagent, whose resonance double bonds react with oxygen-centered radicals to form more stable radical adducts (Figure 6.1c, left). These adducts were then exposed to a varied external magnetic field to measure characteristic energy differences of unpaired electron spins^{20,21}. We measured CdTe-2.4 suspensions with and without illumination to identify adducts produced via their a characteristic EPR spectra^{13,22} (see 6.5 Materials and Methods). In dark, CdTe-2.4 produced negligible unpaired spins or radical adducts, values were subtracted from the illuminated CdTe-2.4 spectra before analysis (Figure 6.S4). With illumination, CdTe-2.4 has

characteristic superoxide and hydroxyl signals (Figure 6.1c, middle). Immediately following photoexcitation, a dominant signal is observed from superoxide radical (Figure 6.1c, right). As time progresses, the superoxide radicals dismutate to form hydroxyl radicals in solution and the EPR

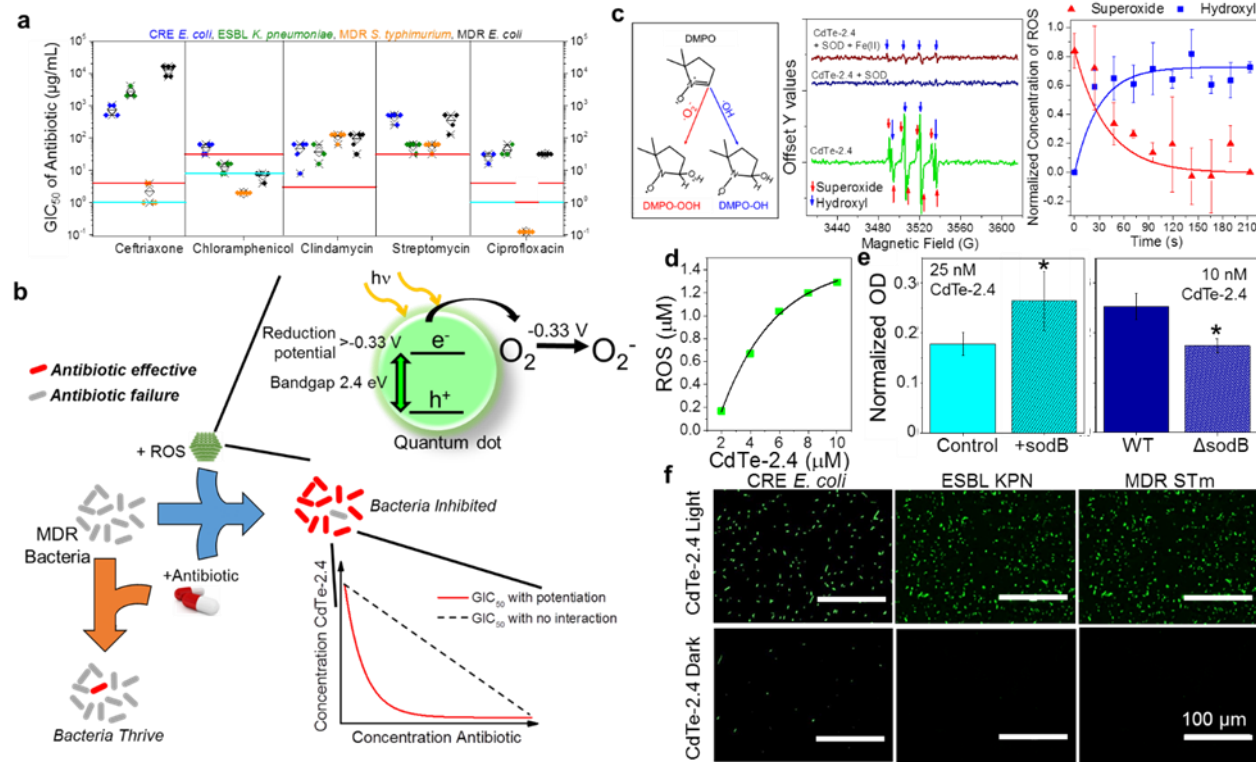


Figure 6.1 Light-activated QDs engineered to produce superoxide in MDR isolates. a. Characterization of MDR clinical isolates used in the study showing the high level of resistance to different classes of antibiotics. The graph shows sensitive (blue line)/resistant (red line) breakpoint minimum inhibitory concentration values based on 2017 CLSI guidelines where applicable, filled diamonds are biological replicates, and the open diamond symbol represents the average of the replicates. *Salmonella enterica* has a separate ciprofloxacin CLSI breakpoint value as shown. b. Schematic showing MDR clinical patient isolates can be inhibited with previously ineffective concentrations of antibiotics by adding superoxide-producing CdTe-2.4 which potentiates the antibiotic activity. c. DMPO superoxide or hydroxyl adducts identified and measured by EPR (left). Confirmation of superoxide production from CdTe-2.4 by signal quenching upon addition of superoxide dismutase (middle). Hydroxyl signal is observed upon addition of iron as Fenton chemistry occurs in solution. Production of superoxide by CdTe-2.4 and subsequent dismutation to hydroxyl species as a function of time measured using EPR (right). d. Concentration dependence of ROS production from CdTe-2.4 measured using EPR. Dark CdTe-2.4 spectra are subtracted from sample before analysis for panels c and d. e. Evidence of superoxide production by CdTe-2.4 *in vitro*. Overexpression (left, 25 nM CdTe-2.4) or deletion of *sodB* (right, 10 nM CdTe-2.4) in *E. coli* reduced or increased inhibitory effect of CdTe-2.4 respectively, compared to control or wildtype (WT) strain. f. Micrographs of respective MDR bacterial clinical isolates treated with 100 nM CdTe-2.4 in light or dark and treated with DCFH-DA demonstrating the presence of light activated oxidative species *in vitro*.

adducts observed are predominantly hydroxyl (see 6.6.1 Supplementary discussion: EPR confirmation of superoxide). We hypothesized that if the CdTe-2.4 was only producing superoxide then addition of superoxide dismutase (SOD), an enzyme specific to dismutation of superoxide to hydrogen peroxide²³, should eliminate EPR signal of superoxide, and as a consequence hydroxyl radical as well. Indeed, with addition of SOD, the EPR signal for both superoxide and hydroxyl radical is quenched confirming direct production of superoxide from CdTe-2.4 (Figure 6.1c, middle). Further, we argued that addition of Fe (II) should provide a pathway for hydrogen peroxide to dismute to hydroxyl radical following Fenton chemistry. As expected, with addition of Fe (II) to SOD and CdTe-2.4, we observe a recovery of hydroxyl radical signal. We further demonstrated that with the same illumination, increased quantities of ROS were produced with higher CdTe-2.4 concentrations (Figure 6.1d). These data indicate that illumination of CdTe-2.4 generates concentration- and stimuli-dependent superoxide radicals, which allows us to controllably increase the flux of superoxide in bacteria.

We investigated CdTe-2.4 superoxide generation intracellularly, by studying the response of an *E. coli* superoxide dismutase B (*sodB*) deletion strain, as well as *E. coli* overexpressing *sodB* to treatment with CdTe-2.4. SodB mitigates oxidative species within *E. coli* by converting superoxide radicals to benign molecular oxygen or hydrogen peroxide²³. We found that with addition of CdTe-2.4, there is significant growth inhibition in the *sodB* deletion strain when compared to wildtype (BW25113) while the overexpression of *sodB* in *E. coli* had reduced growth inhibition relative to control (*E. coli* MG1655 with pZE21MCS plasmid). These results indicate that SodB can modulate the phototoxic effects of CdTe-2.4 and further supports that superoxide radical stress is the antibacterial mechanism (Figure 6.1e, Figure 6.S5). These data also suggest that CdTe-2.4 particles produce ROS intracellularly given the small size of CdTe-2.4 (Figure

6.S4), that SodB is an established cytosolic enzyme specific to superoxide, and that under physiological conditions superoxide radical does not cross Gram-negative cellular membranes²⁴.

After confirming superoxide production by CdTe-2.4 upon illumination, we investigated whether light-activated CdTe-2.4 activates an ROS sensor, 2,7- dichlorofluorescin diacetate (DCFH-DA), in three Gram-negative MDR clinical isolates: a carbapenem-resistant (CRE) *E. coli*, an ESBL-producing strain of *K. pneumoniae*, and an MDR strain of *Salmonella enterica* serovar Typhimurium (STm). Exposure to light-activated CdTe-2.4 stimulates conversion of DCFH-DA to a green fluorescent product (Figure 6.1f) consistent with oxidation by ROS²⁵. These results further indicate that light activated CdTe-2.4 particles increase intracellular ROS.

6.3.2 Superoxide-producing CdTe-2.4 potentiates small molecule antibiotics in MDR clinical isolates

Given that CdTe-2.4 produces intracellular superoxide in Gram-negative pathogens, we hypothesized that it would increase bacterial inhibition when used in combination with antibiotics. We performed checkerboard style assays with the set of bactericidal (ceftriaxone, ciprofloxacin, and streptomycin) and bacteriostatic (clindamycin and chloramphenicol) antibiotics of varied mechanisms of action mentioned above and CdTe-2.4 (12.5, 25, or 50 nM). Five concentrations of each antibiotic were tested for every strain and were determined specific to the isolate's antibiotic GIC₅₀ to survey concentrations above and below the sensitive/resistant breakpoint and antibiotic GIC₅₀ (Figure 6.1a, Figure 6.S6, Figure 6.S7, Figure 6.S8, Figure 6.S9, Figure 6.S10, and Table 6.2); totaling 480 unique treatment conditions measured in biological triplicates. All four clinical isolates had increased sensitivity to one or more antibiotics in the presence of light-activated CdTe-2.4 superoxide generation (Figure 6.2a, Figure 6.S11, Figure 6.S12, Figure 6.S13, Figure 6.S14, Figure 6.S15, and Figure 6.S16).

We evaluated the combinatorial nature of antibiotic and CdTe-2.4 using the Bliss Independence model²⁶. The S parameter dictates deviation from no interaction and is defined as

$$S = \left(\frac{OD_{AB}}{OD_0} \right) \times \left(\frac{OD_{QD}}{OD_0} \right) - \left(\frac{OD_{AB,QD}}{OD_0} \right) \quad (\text{Equation 6.1})$$

where OD_{AB} is the optical density (OD) at 8 h in only antibiotic, OD₀ is the OD at 8 h in no treatment, OD_{QD} is the OD at 8 h in only CdTe-2.4, and OD_{AB,QD} is the OD at 8 h in combination of antibiotic and CdTe-2.4 (Figure 6.2b)²⁶. Combinations were removed from analysis if the OD of bacteria in either monotherapy did not reach 0.1 by 8 h. We observed synergy (S>0) between antibiotics and CdTe-2.4 in 76.4% of all combinations tested (n=271) (Figure 6.2b, c and Figure 6.S17). With both bactericidal and bacteriostatic antibiotics, the degree of potentiation increased (S>>0) with increasing doses of CdTe-2.4, highlighting that antibiotic potentiation can improve with higher superoxide flux (Figure 6.2c). The few combinations where antagonism was observed (S<0) were typically when the monotherapy concentration was ineffective; consistent with previous studies demonstrating that the type and strength of antibiotic interactions are dose-dependent²⁷ (Figure 6.S17). The distribution of S-values across all conditions was significantly greater than 0 as indicated by a right-tailed t-test ($p<0.001$) (Figure 6.2c). The synergistic effect results in the antibiotic GIC₅₀ of many clinical isolates dropping below the sensitive/resistant breakpoint values of antibiotic with addition of CdTe-2.4 (Figure 6.2d). In cases of streptomycin treated ESBL *K. pneumoniae* and MDR *S. Typhimurium*, the GIC₅₀ goes to 100-fold below the breakpoint demonstrating a strong potentiation of antibiotic activity. These data indicate that

superoxide potentiates both bactericidal and bacteriostatic antibiotics with a broad range of mechanisms across diverse Gram-negative pathogens.

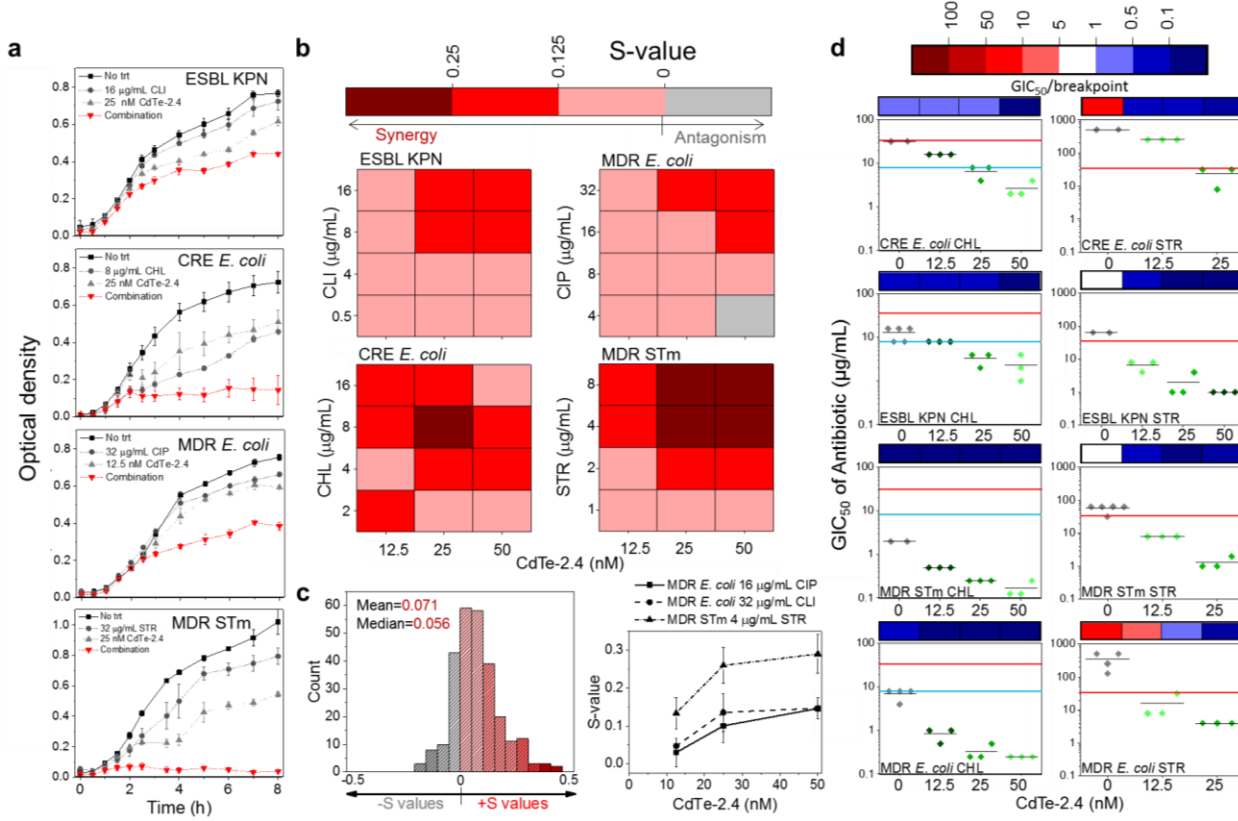


Figure 6.2 QDs potentiate antibiotic activity and lower antibiotic GIC₅₀ values. a. Growth curves of strains under mono- or combinatorial treatment demonstrating increased growth inhibition upon combination of antibiotic and CdTe-2.4. b. Evaluation of CdTe-2.4 and antibiotic synergistic interaction using the Bliss Independence model. S>0 (red scale) indicates a synergistic interaction where S>0 value is higher deviation from no interaction between treatments. S<0 indicates antagonistic interaction (gray scale). c. Histogram of S-values for all combinations of antibiotic and CdTe-2.4 across all clinical isolates tried in this investigation, n=271 (left). The S-value distribution average is significantly higher than 0 confirmed by a right-tailed t-test ($p<0.05$). Demonstration of increased potentiation of antibiotic activity with increasing CdTe-2.4 concentration (right). At constant antibiotic concentration, addition of greater CdTe-2.4, increases the S-value and the interaction towards a more synergistic relationship. S-values shown in panels B and C are the average of three biological replicates. d. GIC₅₀ of respective antibiotic with addition of CdTe-2.4 at various concentrations. The addition of CdTe-2.4 potentiates the activity of antibiotics to allow for successful inhibition of 50% or greater at or below sensitive (blue line)/resistant (red line) breakpoint values. The effect is seen as a sharp decrease in GIC₅₀ corresponding with increased addition of CdTe-2.4.

6.2.3 CdTe-2.4 and antibiotic inhibition of *Salmonella enterica* infected epithelial cells and nematodes

To establish whether CdTe-2.4 potentiates antibiotic activity not only in broth but also during infection, we investigated a tissue culture and an animal model system. Intestinal epithelial cells are infected by *Salmonella enterica* in gut-associated and systemic infections, are permissive for uncontrolled *S. enterica* growth in culture, and have little endogenous or inducible ROS activity²⁸. To test whether CdTe-2.4 potentiates ciprofloxacin, we infected HeLa cells (epithelial cells) with *Salmonella enterica* serovar Typhimurium (strain SL1344 expressing GFP from the chromosome²⁹) (Figure 6.3a), treated with mono- or combinatorial therapy and then lysed the HeLa cells after 18 hours of infection to enumerate intra-epithelial colony forming units (CFU). All CdTe-2.4 concentrations used were minimally-lethal to HeLa cells as determined by a lactate dehydrogenase release assay (Figure 6.S18). CdTe-2.4 significantly reduced CFU at concentrations of 80 nM and higher, suggesting CdTe-2.4 could be a useful monotherapy for intracellular infection (Figure 6.3b, $p<0.05$). Ciprofloxacin has high efficacy against SL1344 and for combinatorial experiments was set at 0.06125 µg/mL, which alone reduced bacterial load 50-fold (Figure 6.3b). Incubation of infected HeLa cells with a dosage range of CdTe-2.4 in combination with 0.06125 µg/mL ciprofloxacin significantly reduced recoverable bacteria compared to ciprofloxacin treatment alone (Figure 6.3c, d, $p<0.05$), highlighting the ability of CdTe-2.4 to increase the sensitivity of intracellular bacteria to antibiotic therapy. To establish whether CdTe-2.4 may potentiate antibiotics in an animal model of gut colonization and killing, we used the nematode *Caenorhabditis elegans*.

First, we screened 46 clinical isolates of *K. pneumoniae*, *E. coli*, and *S. enterica* species for high mortality of *C. elegans* (Figure 6.S20) and selected a *S. Enteritidis* isolate. We then transferred

mature *C. elegans* to sparse lawns of control *E. coli* OP50 (standard *C. elegans* food) or the MDR clinical isolate of *S. Enteritidis* and incubated for 3 days. Infected worms were then transferred to S medium under illumination and were dosed with respective treatments every 24 hours. After 4

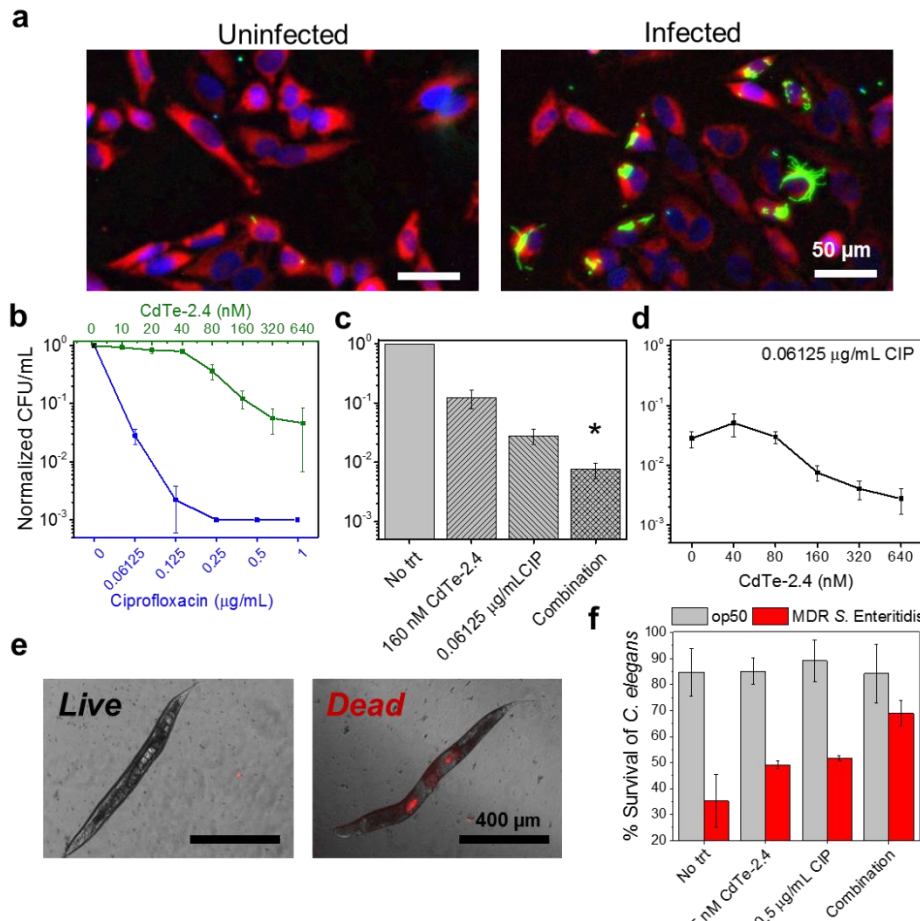


Figure 6.3 Increased inhibition of bacteria in infection models with addition of stimuli-activated ROS. a. Micrographs of uninfected and *S. Typhimurium* infected HeLa cells (composite images: red is Mitotracker (mitochondrial voltage indicator), blue is DAPI for nuclei, and green is GFP-expressing SL1344 *S. Typhimurium*). b. Effect of monotherapies on *S. Typhimurium* load (CFU/mL) (top axis CdTe-2.4 and bottom axis ciprofloxacin) in *S. Typhimurium*-infected HeLa cells. c. Addition of CdTe-2.4 to ciprofloxacin treatment significantly reduces intracellular *S. Typhimurium* (CFU/mL) compared to antibiotic alone. d. Reduction in *S. Typhimurium* CFU in HeLa cells as a function of adding CdTe-2.4 in the presence of constant ciprofloxacin concentration. CFU/mL data shown are the average of three biological replicates and is represented and analyzed as normalized to no treatment due to infection variability between biological replicates (Figure 6.S19). e. SYTOX orange viability stain used to determine live and dead *C. elegans*. f. Survival of *C. elegans* infected with *S. Enteritidis* with mono- and combinatorial therapy. The percent survival of *C. elegans* with combination therapy is higher than monotherapy and no treatment. n=2 biological replicates comprised of >28 nematodes per condition per biological replicate.

days of treatment in the presence of light, *C. elegans* were stained with SYTOX orange viability dye and live nematodes were enumerated (Figure 6.3e). Only $35\pm10\%$ of untreated, *S. Enteritidis*-infected *C. elegans* survived infection. Monotherapy treatment with ciprofloxacin ($0.5 \mu\text{g/mL}$) or CdTe-2.4 (75 nM) increased survival to $51.5\pm1.0\%$ and $49.2\pm1.6\%$, respectively. However, combinatorial therapy led to a $69\pm5.0\%$ survival rate of infected worms (Figure 6.3f). This increase in survival rate over monotherapy ($p=0.076$ compared to antibiotic only and $p=0.063$ compared to CdTe-2.4 only) demonstrates that CdTe-2.4 in combination with an antibiotic protects nematodes from bacterial killing.

6.4 Conclusions

In conclusion, we established that superoxide generation potentiates bactericidal and bacteriostatic antibiotics against range of MDR Gram-negative clinical isolates despite their high drug-resistance. We highlight the ability to engineer stimuli-responsive nanoparticles to produce specific ROS of interest, namely superoxide. We show that combinatorial treatment inhibits MDR clinical isolates to levels where the antibiotic GIC₅₀ is below the clinical sensitive/resistant breakpoint, and in some cases 1000-fold lower. The synergy observed in our study provides new insight into superoxide's impact on bactericidal and bacteriostatic antibiotic lethality. The demonstration of combinatorial therapy out-performing antibiotic monotherapy in two different infection models, epithelial cell and nematode gut infection, further highlights the potential to improve antibiotic efficacy with addition of superoxide generation. The wide variety of tunable nanomaterial parameters including size, reduction and oxidation potentials, and surface moieties provides the opportunity to engineer tools to control redox perturbation for mitigating multidrug-resistance and improving antibiotic efficacy.

6.5 Materials and Methods

6.5.1 Quantum dot synthesis and characterization

CdTe-2.4 quantum dots were synthesized and filtered for experiments as described in Courtney et al. 2016¹⁵. Size distribution analysis of the utilized particles was obtained from transmission electron micrographs (Figure 6.S4) using ImageJ ($d = 2.8 \pm 0.3$ nm). Images were acquired using a Phillips CM 100 TEM at 80 kV acceleration. Samples were prepared using Cu-Formvar grids which were made hydrophilic using a glow-discharge plasma treatment.

6.5.2 Culture conditions

For non-clinical isolate bacterial growth liquid lysogeny broth (LB) (2% LB Sigma Aldrich L3022) or solid LB (2% LB, 1.5% agar (214010)) was used for all experiments. For clinical isolate growth liquid cation adjusted Mueller Hinton broth (CAMHB) (Becton, Dickinson and Company 212322) or solid CAMHB (1.5% agar). Dulbecco modified Eagle medium (DMEM) (Sigma-Aldrich, St. Louis, MO) supplemented with fetal bovine serum (10%), l-glutamine (2 mM), sodium pyruvate (1 mM), beta-mercaptoethanol (50 µM), HEPES (10 mM) was used for HeLa infection assays and maintenance. All cells were incubated at 37°C during growth. HeLa infection studies were carried out with 5% CO₂ and liquid bacterial cultures were grown with shaking at 225 rpm. Worms were grown on solid nematode growth medium (NGM) (2.3% N1000 powder (US Biological), 25 mM phosphate buffer, 1 mM CaCl₂, 1 mM MgSO₄) for propagation and during infection. Worms were grown in liquid S medium (1 L S Basal (0.585% NaCl, 0.1% K₂HPO₄, 0.6% KH₂PO₄, 5 mg/L cholesterol), 10 mL 1 M potassium citrate, 10 mL trace metals solution, 3 mL 1 M CaCl₂, 3 mL 1 M MgSO₄), during treatment.

6.5.3 Bacterial strains

Clinical strains were obtained from Dr. Nancy Madinger at the University of Colorado Anschutz medical campus and were stored in 10% glycerol at -80°C for long term storage. Biological replicates were started in liquid media from individual, single colonies off of solid plates and grown for 16 h before beginning experiments. Optical density was measured with a Tecan GENios at 562 nm with a bandwidth of 35 nm. All bacterial strains used are in Table 6.1 and Table 6.3.

6.5.4 Cloning of sodB overexpression plasmid

The SodB gene, including the RBS, was cloned from the *E. coli* MG1655 genome and inserted to the BamHI and MluI sites of the pZE21MCS plasmid (Expressys, Germany) for expression in *E. coli* by the P_{LtetO-1} promoter. The control plasmid was the pZE21MCS plasmid in *E. coli* MG1655 without insert. Plasmids were cloned into chemically competent *E. coli* MG1655 and maintained with 25 µg/mL kanamycin.

6.5.5 GIC₅₀ measurement

Overnight cultures of clinical isolates were diluted to a 0.5 McFarland standard in media with respective test concentration of antibiotic. Cultures were grown for 24 h in 384 well microplates. After 24 h of growth, Resazurin sodium salt (Sigma Aldrich) solution was added and the reaction was monitored for fluorescence measuring every 5 min for 4 h at 37°C with 225 rpm shaking using 485/610 nm filters. The slope of Resazurin fluorescence was used as a quantitative measure of cell metabolism. The GIC₅₀ was determined as the lowest concentration of antibiotic which caused a 50% or greater reduction in slope compared to the same biological replicate in no treatment. GIC₅₀'s were compared to sensitive/resistant breakpoints from 2016-2017 CLSI guidelines or literature^{30,31} shown in Table 6.4.

6.5.6 Combinatorial experiments

Five antibiotic concentrations were chosen for each strain so that the levels tested would be below the GIC₅₀, near the CLSI or defined breakpoint, and near the GIC₅₀. Concentrations tested for each strain can be seen in Table 6.2 with breakpoints shown in Table 6.4. Concentrations of CdTe-2.4 were held constant for all strains at 12.5, 25, and 50 nM. Using these metrics, three biological replicates were tested from each strain with fifteen combination test conditions as well as monotherapy controls and a no treatment condition. Clinical strains were diluted 1:100 from overnight into test condition. Optical density was measured every 30 min for the first 3 h and every hour subsequently until 8 h. The optical density at 8 h normalized to no treatment was used in the Bliss Independence model²⁶ to determine the combinatorial effect. We used optical density at 8 h instead of growth rate because of the two phase growth many of our conditions demonstrated which yielded multiple growth rates. The optical density at 8 h was normalized to account for difference in starting cell viability and biological replicate colony variation.

6.5.7 *Caenorhabditis elegans* infection experiments

C. elegans CF512 [(fer-15(b26; fem-1(hc17)] were used for infection experiments. CF512 do not replicate when grown at 25°C to allow for control of the worm count and determination of live and dead populations from starting t=0. *Escherichia coli* op50 was used as both the food source prior to infection and as the control strain during infection experiments. During the treatment phase of infection experiments worms were suspended in standard liquid S medium and all wash steps were carried out with standard M9 buffer³². NGM plates were seeded with *E. coli* op50 or MDR strains by plating 100 µL of overnight culture onto NGM and incubating at 37°C for 8 h. Worms were chunked onto NGM plates seeded with *E. coli* op50 and allowed to grow for 10-14 days at 15°C to allow for egg production. The eggs were then collected using NaOH and bleach and

transferred to NGM and incubated at 25°C. After 24 h, hatched worms were transferred to NGM seeded with op50 and grown at 25°C to allow for adult worms to grow without reproduction for 48 h. Adult worms were collected and washed twice before being transferred to NGM seeded with infection strains. Infection on solid plates was carried out for 3 days. After infection, worms were collected and washed three times (30 s at 600xg) before being transferred to S medium, with respective treatment condition in 100 µL cultures in 96 well plates at 25°C to limit reproduction. Every 24 h, worms were monitored for morphology and media was changed to refresh CdTe and antibiotic. At the end of the treatment period worms were stained with 0.5 µM SYTOX orange (Thermo Fisher Scientific S11368) for 30 min prior to imaging and counting. Images were acquired and counting was performed using an EVOS FL microscope and analyzed using ImageJ. 46 clinical isolates were screened to choose the *Salmonella enterica* serovar Enteritidis strain used in experiments (S48, Figure 6.S20).

6.5.8 Electron paramagnetic resonance spectroscopy

For all EPR measurements we used CW X-band EPR spectroscopy. Quantum dot samples were prepared for EPR measurements by filtering as described above and re-suspended in pH 11 water. 100 µL of this solution was then mixed with 1 µL of DMPO (Dojindo) and sequestered from light exposure. Quartz capillaries were filled with the CdTe-DMPO mixture and measured in a Bruker Elexsys E 500 spectrometer equipped with an SHQE resonator. Exposure to ambient light was greatly minimized by preparing and recording every measurement in a dark room. A dark background was measured for each sample which consisted of the average of 10 scans using a 200 G scan range (0.05 G resolution) centered on 3515 G with a microwave attenuation of 16 dB and power of 5W and was subtracted from the light signal as negligible (Figure 6.S4). Time dependent scans were conducted over the same 200G scan range (20.48 seconds) with a 100 ms

delay between scans. The SiO₂ E' defect was present in all measurements but was subtracted out during analysis as part of the dark signal. The sample was then exposed to 9 mW/cm² white light and immediately re-measured to obtain the photo-activated spectrum. For confirmation of superoxide production conditions were as follows: 10vol% DMSO in DDW, 1-2 mg of the SOD (Sigma) enzyme in 100 μL DDW, or the degassed water was prepared by bubbling nitrogen through DDW for 1 h. Each spectrum, containing multiple species was simulated using the SpinFit module of the Bruker Xepr software (version 2.6 b 149) to identify the radical adducts. The initial fit parameters were: DMPO-OH: a_N = 14.90 G and a_H^β = 14.93 G, DMPO-OOH: a_N = 14.2 G, a_H^β = 11.4 G, and a_H^{γ1} = 1.2 G. Provided a fixed and known active sample volume in each capillary, the concentration of DMPO adducts was calculated from the total number of spins detected using Bruker SpinFit software. This software-reported concentration corresponded to the ROS generated multiplied by the number of capillaries in the cavity. Concentrations of ROS species are reported in the main text for one capillary. Data in Figure 6.1b (middle) are time dependent EPR scan and successive scans were each saved as slices and we averaged the results of the SpinFit from three replicate experiments. Data in Figure 6.1b right shows 10 successive scan was averaged to minimize error.

6.5.9 2, 7'-dichlorofluorescin diacetate imaging

Respective strain was diluted 1:10 from overnight into CAMHB and treated with respective concentration of CdTe-2.4 for 1 h in dark or light. Cells were pelleted and re-suspended in PBS with DCFH-DA and incubated for 5 min before cells were imaged on glass slides with coverslips on an EVOS FL microscope. Images were processed identically for all conditions using ImageJ.

6.5.10 Gentamicin protection assays

HeLa cells were seeded at 1.0×10^4 cells per well in 96-well tissue culture plates and grown for 24 hours. *Salmonella enterica* serovar Typhimurium wild-type strain SL1344 with chromosomal *rpsM::GFP*²⁹ was grown overnight, diluted 1:10 and grown for four hours in LB prior to infections. Streptomycin antibiotic selection was used at 30 µg/mL. *S. Typhimurium* in Gibco PBS was added at a multiplicity of infection of 30:1 (bacteria:HeLa) and centrifuged for five minutes at $500 \times g$. After 45 minutes cells were incubated for a further 1.25 hours at 37°C in fresh medium supplemented with gentamicin (40 µg/mL) to kill extracellular bacteria. Medium was then exchanged for medium with treatment conditions supplemented with 40 µg/mL gentamicin to inhibit extracellular bacterial growth. At 18 h post-infection the wells were washed 3x with 300 µL PBS and cells were lysed with 30 µL 0.1% Triton X-100 for 15 min at room temperature. After 15 min, 270 µL PBS was added to each well (serving as 100-fold dilution), serially diluted, plated onto 2% LB, 1.5% agar, and 40 µg/mL streptomycin, and then incubated at 37°C for 16 h to enumerate colony forming units per milliliter. For staining and imaging, wells were stained with 100 nM MitoTracker followed by fixation with 16% PFA for 15 min. Wells were then washed 2x with PBS, stained with DAPI for 20 min, washed 2x with PBS, and stored in 100 µL 90% glycerol, 1x PBS before imaging and/or storage at 4C in dark. Images were acquired using an EVOS FL microscope and analyzed using ImageJ.

6.5.11 LDH cytotoxicity assay

HeLa cells were seeded as above. Cells were treated with respective conditions and incubated for 18 h. 50 µL of supernatant was used to determine lactate dehydrogenase release as a measure of cytotoxicity using the Pierce LDH cytotoxicity assay kit. Cells lysed with the supplied lysis buffer served as a positive control.

6.5.12 Error and significance analysis

Error is represented as standard deviation between technical replicates or standard error of the mean for biological replicates. Significance is defined as $p < 0.05$ and denoted by an asterisk (*) unless otherwise stated.

6.6 Supplementary Information

6.6.1 Supplementary discussion: EPR confirmation of superoxide

Since our observed EPR spectra show both superoxide and hydroxyl radical adducts in solution with photoexcited CdTe-2.4 and we know that CdTe-2.4 should be unable to directly produce hydroxyl radical due to the energetic position of its valence band (Figure 6.1b)¹⁵, we conducted further studies to confirm the tuning of CdTe-2.4 to produce superoxide. We tracked the EPR signal following the light activation of CdTe-2.4 suspension in water, and quantified the signal from each radical as a function of time after the initial light stimulation (Figure 6.S4). Immediately following photoexcitation, the observed signal showed the characteristic peaks of DMPO-OOH and DMPO-OH adducts indicating the presence of both superoxide and hydroxyl radicals at early time points (Figure 6.1c). As time progresses, the fraction of superoxide decreases such that 1-2 min after light exposure, superoxide is present in minimal amounts. Correspondingly, there is an increasing signal contribution from hydroxyl adducts. Since CdTe-2.4 is engineered to produce superoxide, we hypothesized that the observation of hydroxyl DMPO-OH adducts was due to either formation of hydroxyl radicals free in solution by the dismutation of superoxide radicals or due to spontaneous direct conversion of DMPO-OOH to the more stable DMPO-OH.

Using pseudo-first order kinetics for the dismutation and quenching of radicals, due to excess reactants, a simplified kinetics of the superoxide dismutation and measurement of respective superoxide and hydroxyl adducts can be modeled as:

$$\frac{d[O_2^- \cdot]_t}{dt} = [O_2^- \cdot]_{t=0} - k_1[O_2^- \cdot]_t - k_3[O_2^- \cdot]_t + k_4[DMPO-OOH] \quad (\text{Equation 6.2})$$

$$\frac{d[OH \cdot]_t}{dt} = k_1[O_2^- \cdot]_t - k_2[OH \cdot]_t - k_5[OH \cdot]_t + k_6[DMPO-OH] \quad (\text{Equation 6.3})$$

$$\frac{d[DMPO-OOH]}{dt} = k_3[O_2^- \cdot]_t - k_4[DMPO-OOH] \quad (\text{Equation 6.4})$$

$$\frac{d[DMPO-OH]}{dt} = k_5[OH \cdot]_t - k_6[DMPO-OH] \quad (\text{Equation 6.5})$$

where k_1 is pseudo-first order dismutation rate of superoxide radical to hydroxyl, k_2 is pseudo-first order quenching rate of hydroxyl radical, k_3 and k_5 are respective rates of superoxide and hydroxyl adduct formation with DMPO (assuming excess DMPO in solution), and k_4 and k_6 are respective rates of DMPO adduct disintegration to respective radicals in solution. Since k_4 , $k_6 \ll k_1$, k_2 , k_3 , k_5 and $k_1, k_2 > k_3, k_5$ ³³⁻³⁶, the pseudo-first order kinetics simplifies to observable DMPO adduct kinetics in our experiments:

$$\frac{d[DMPO-OOH]}{dt} = [DMPO-OOH]_{t=0} - k_4[DMPO-OOH] \quad (\text{Equation 6.6})$$

$$\frac{d[DMPO-OH]}{dt} = [DMPO-OH]_{t=0} + f * k_4[DMPO-OOH] - k_6[DMPO-OH] \quad (\text{Equation 6.7})$$

Since superoxide adduct on disintegration to superoxide free-radical can dismute to give hydroxyl radicals and a fraction of which will form the DMPO-OH adduct observed in our measurements (our measurements indicate $k_4 > k_6$).

To probe whether the DMPO-OH adduct is formed from the dismutation of the DMPO-OOH adduct or from superoxide free radicals in solution we repeated the experiment in the presence of dimethyl sulfoxide (DMSO). Hydroxyl radicals can attack the sulfur of DMSO and release methyl radicals into solution, which can then be detected by DMPO. Immediately after light stimulation of CdTe-2.4 QDs in 10% DMSO, we observed characteristic features of DMPO-CH₃ in the acquired spectra, which become a dominant species over time at the expense of DMPO-

OH and DMPO-OOH (Figure 6.S21). This clearly indicates that hydroxyl radicals are formed freely in solution and that the observed DMPO-OH adducts are not due to conversion of DMPO-OOH.

We further investigated the hypothesis that superoxide radicals are formed first, and further dismute to generate hydroxyl radical by repeating the EPR experiment for CdTe-2.4 in presence of the superoxide scavenging enzyme superoxide dismutase (SOD). SOD oxidizes the superoxide radicals to molecular oxygen and should stop the formation of DMPO adducts and cause diminished EPR signal. Immediately following light-activation in the presence of SOD enzyme we observed a strong attenuation (~95% decrease) in spectral intensity as compared to in the absence of SOD. After 8 min the signal is nearly undetectable (Figure 6.S21). As both superoxide and hydroxyl radical signals were diminished, it can be concluded that the hydroxyl radicals are formed through a dismutation pathway starting from superoxide, and not through the direct oxidation of water via the photogenerated hole from CdTe-2.4. This observation is also confirmed using cyclic voltammetry measurements, where cycling CdTe-2.4 through complete redox cycles shows peaks corresponding to superoxide and hydroxyl radicals (Figure 6.S21). However, direct hole injection into CdTe-2.4 does not lead to the broad peak attributed to hydroxyl radicals, and removing the redox half-cycle for formation of superoxide radical leads to rapid decay in the hydroxyl peak.

The simplest route of superoxide formation would involve the direct electron transfer from CdTe-2.4 to dissolved oxygen. To test superoxide radical formation from oxygen as the primary step we partially removed dissolved oxygen by degassing the water used in filtration and resuspension of CdTe-2.4 by bubbling nitrogen through it for 90 min. As in the presence of SOD, the initial radical signal was strongly attenuated under the same measurement conditions, thus

confirming the initial radical source as oxygen (~80% decrease, Figure 6.S21). The experimental results confirm that CdTe-2.4 is tuned to produce superoxide radicals which are likely formed first after interaction of oxygen and over time dismute in solution to hydroxyl radicals.

6.6.2 Supplementary figures

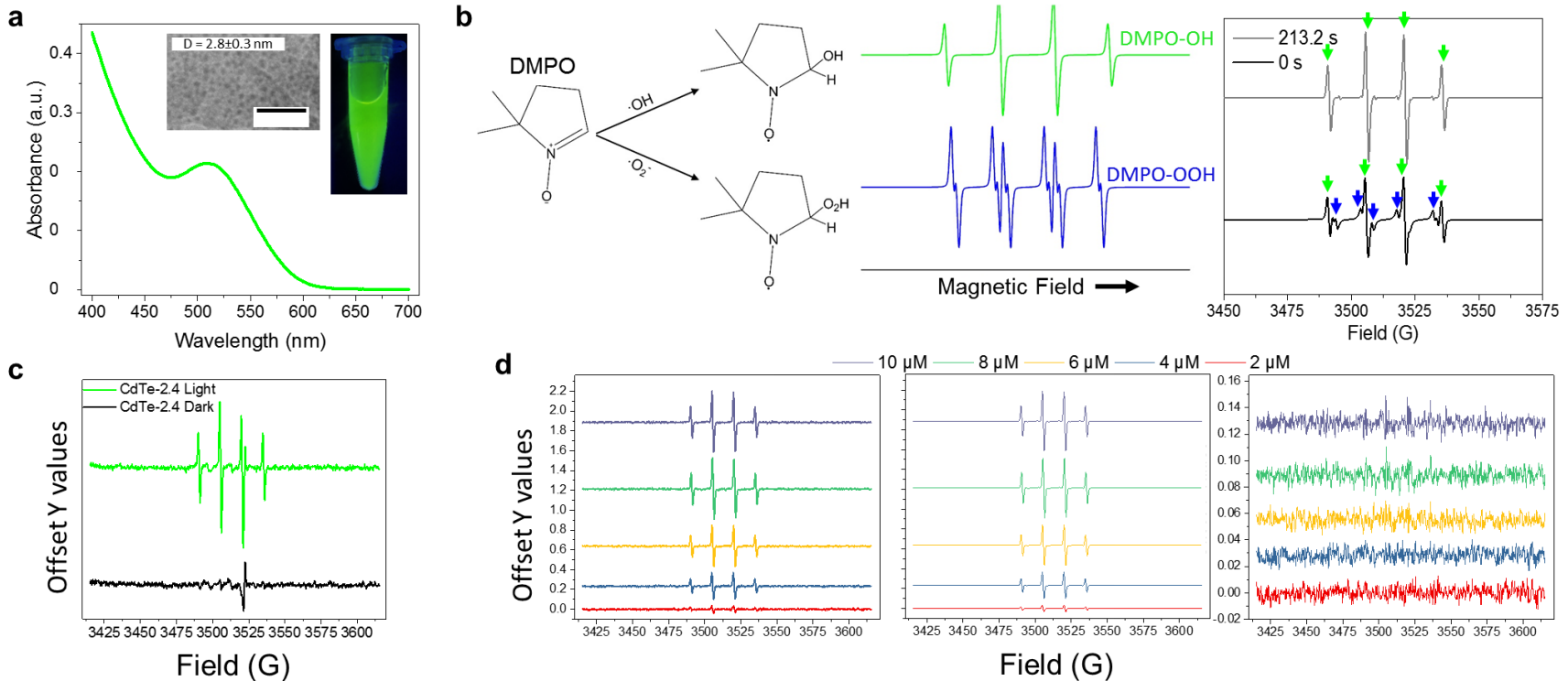


Figure 6.S4 Quantum Dot Characterization and EPR analysis. a. Absorbance of CdTe-2.4 stock after filtering, prior to experiment and dilution. Inset is TEM of CdTe-2.4 (left) and an image of CdTe-2.4 QD stock illuminated with ultraviolet light (right). b. EPR spectroscopy species signatures for identification of superoxide and hydroxyl radicals using DMPO as the spin trap (left). EPR spectroscopy with CdTe-2.4 in light with time showing clear production of superoxide (blue dots) and hydroxyl radicals (green dots) at early time points and dismutation to a hydroxyl dominated signal at 213 s (right). c. EPR spectra for 4 μM CdTe-2.4 in dark and with 60 s of white light illumination showing the negligible dark signal and SiO₂ E' defect. In all other EPR data presented the dark signal is subtracted from the light signal. d. EPR spectra (left), SpinFit for radical adducts used to calculate ROS concentrations (middle), and residuals for the SpinFit (right) used to calculated concentration correlation between CdTe-2.4 and ROS production. Offset Y values are shown to highlight that the residuals are small compared to the spectra and the SpinFit of the spectra.

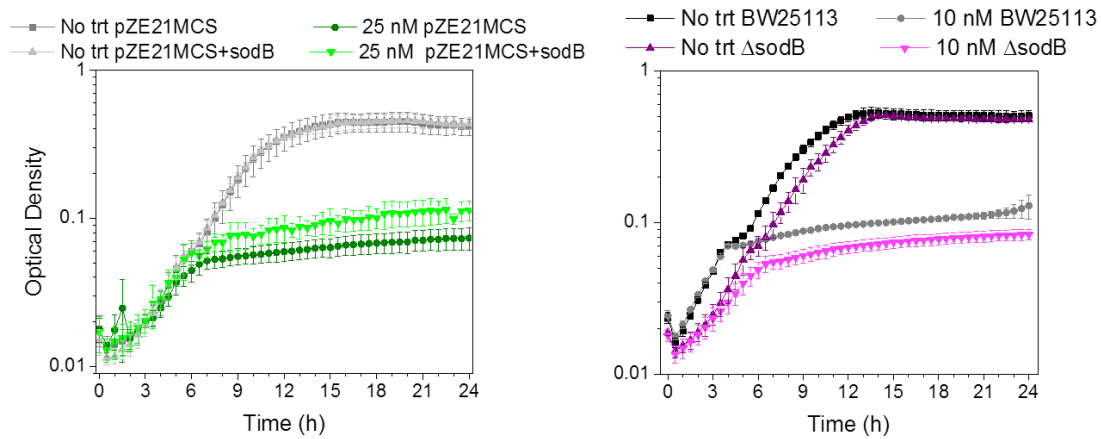


Figure 6.S5 Growth curves for *sodB* deletion and overexpression constructs. Growth curve of *E. coli* MG1655 carrying control plasmid (pZE21MCS) or plasmid overexpressing *sodB* (pZE21MCS+sodB) subjected to no treatment (No trt) and treatment with CdTe-2.4 at 25 nM (left). Growth curve of Keio collection wild type BW25113 and *sodB* deletion strains (Δ sodB) with respective treatment (right).

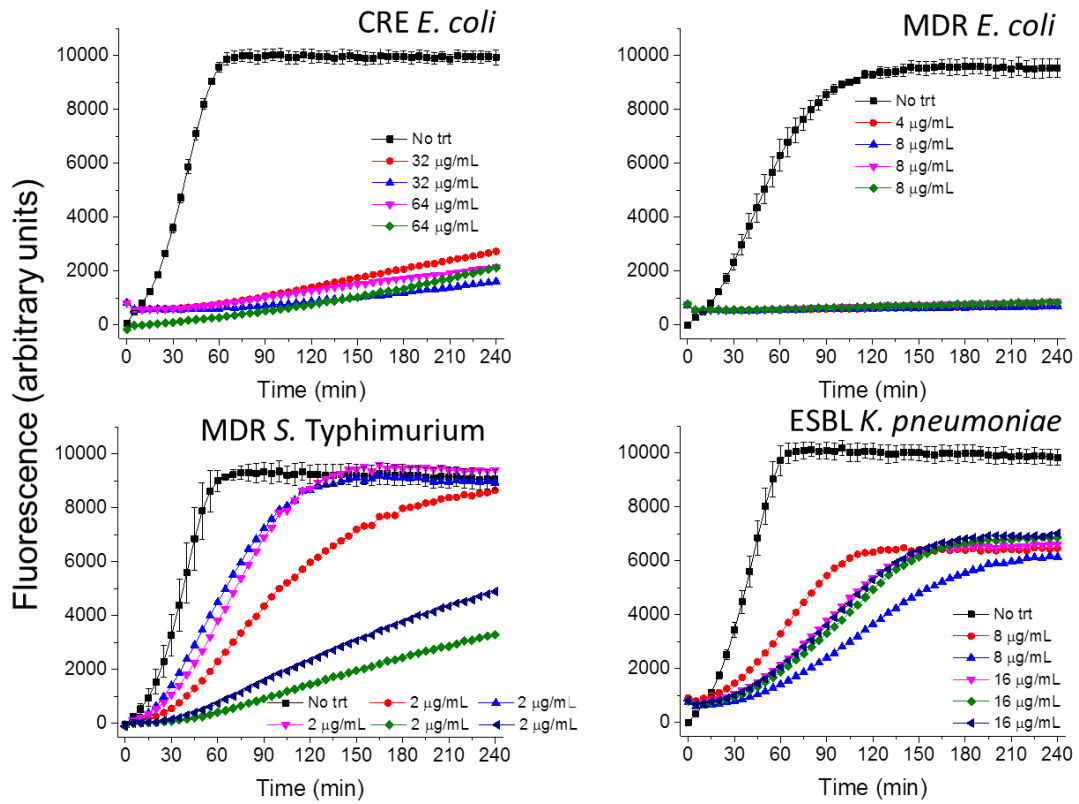


Figure 6.S6 Chloramphenicol GIC₅₀. Resazurin curves for respective strains at GIC₅₀ with labeled concentrations of chloramphenicol. Due to heterogeneity between replicates, we show each biological replicate separately. No treatment is the average of three biological replicates. GIC₅₀ is determined by ratio of slope between treatment and no treatment (≤ 0.5) in the linear region of the curve. The corresponding data is shown in Figure 6.1a (see 6.5 Materials and Methods).

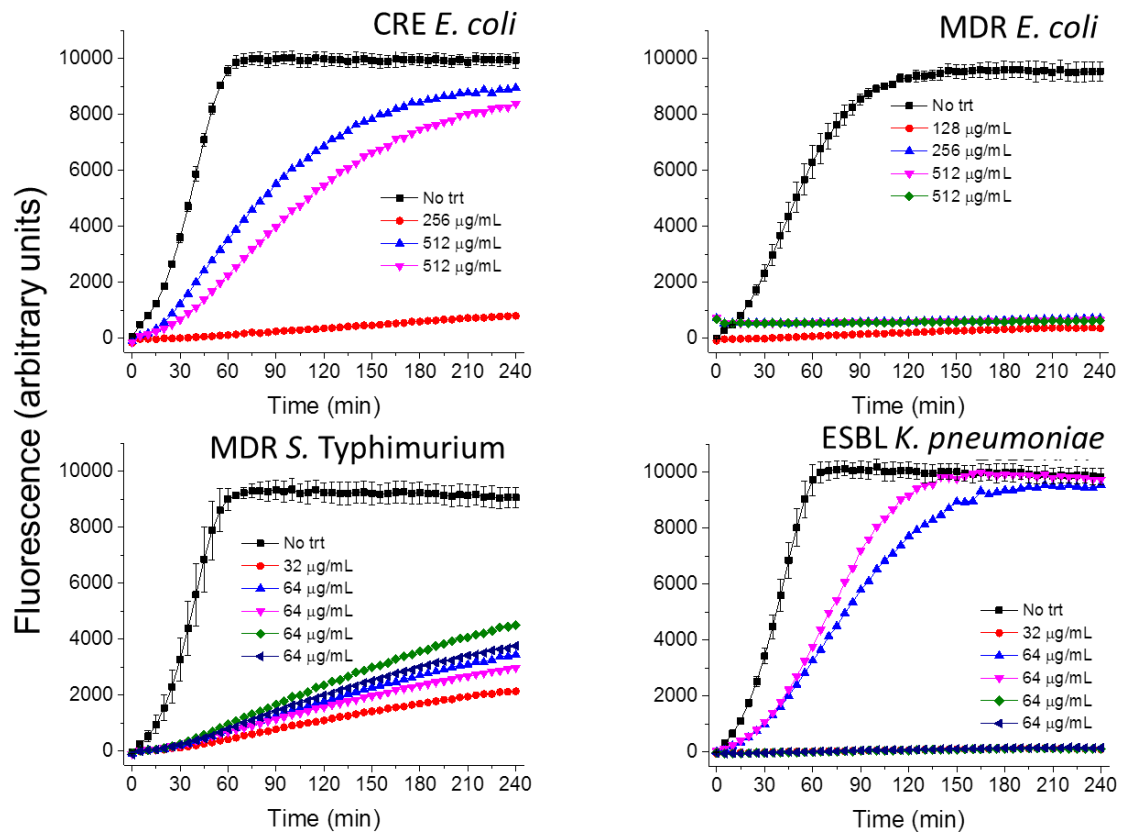


Figure 6.S7 Streptomycin GIC₅₀. Resazurin curves for respective strains at GIC₅₀ with labeled concentrations of streptomycin. Due to heterogeneity between replicates, we show each biological replicate separately. No treatment is the average of three biological replicates. GIC₅₀ is determined by ratio of slope between treatment and no treatment (≤ 0.5) in the linear region of the curve. The corresponding data is shown in Figure 6.1a (see 6.5 Materials and Methods).

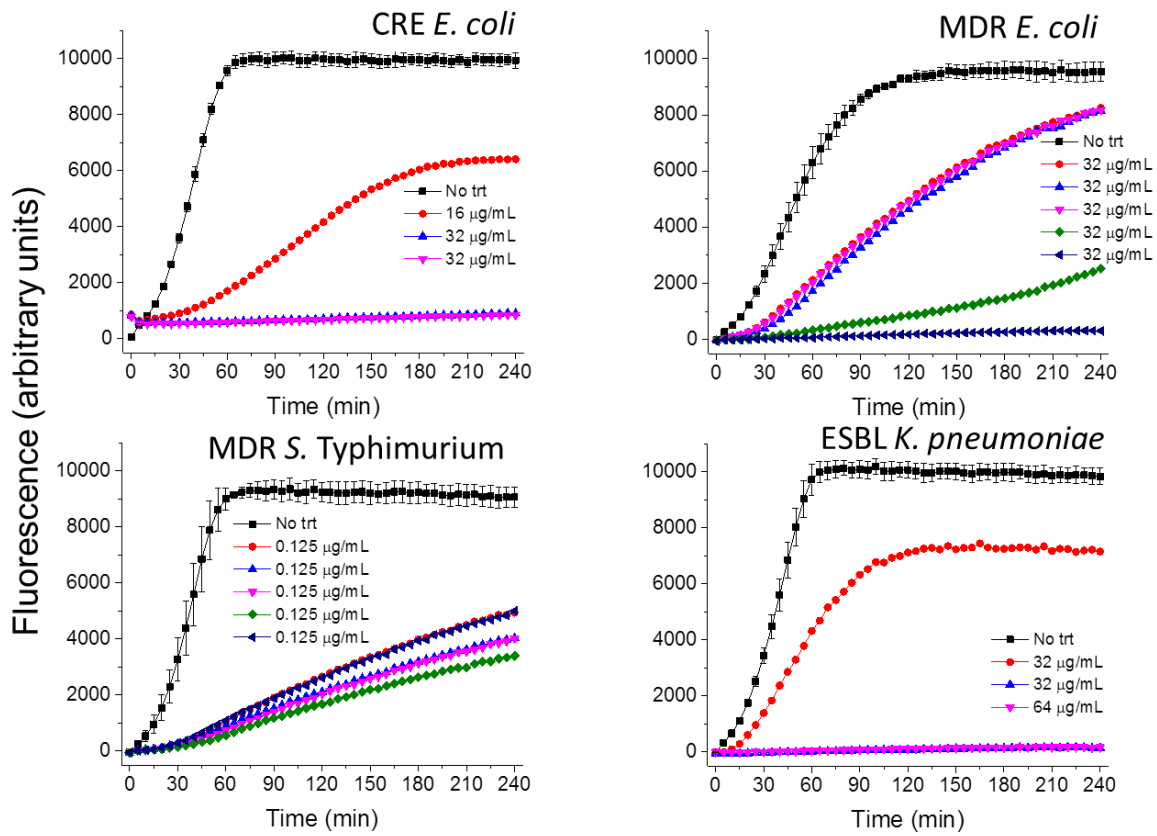


Figure 6.S8 Ciprofloxacin GIC₅₀. Resazurin curves for respective strains at GIC₅₀ with labeled concentrations of ciprofloxacin. Due to heterogeneity between replicates, we show each biological replicate separately. No treatment is the average of three biological replicates. GIC₅₀ is determined by ratio of slope between treatment and no treatment (≤ 0.5) in the linear region of the curve. The corresponding data is shown in Figure 6.1a (see 6.5 Materials and Methods).

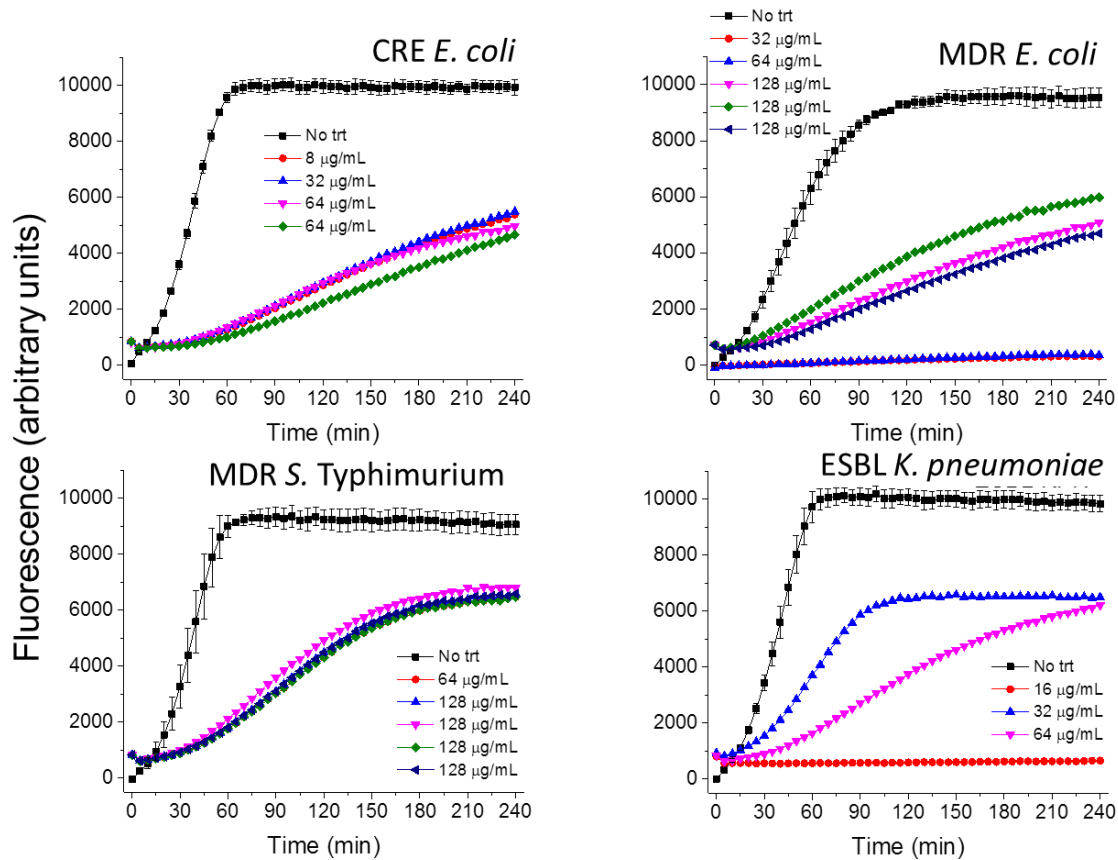


Figure 6.S9 Clindamycin GIC₅₀. Resazurin curves for respective strains at GIC₅₀ with labeled concentrations of clindamycin. Due to heterogeneity between replicates, we show each biological replicate separately. No treatment is the average of three biological replicates. GIC₅₀ is determined by ratio of slope between treatment and no treatment (≤ 0.5) in the linear region of the curve. The corresponding data is shown in Figure 6.1a (see 6.5 Materials and Methods).

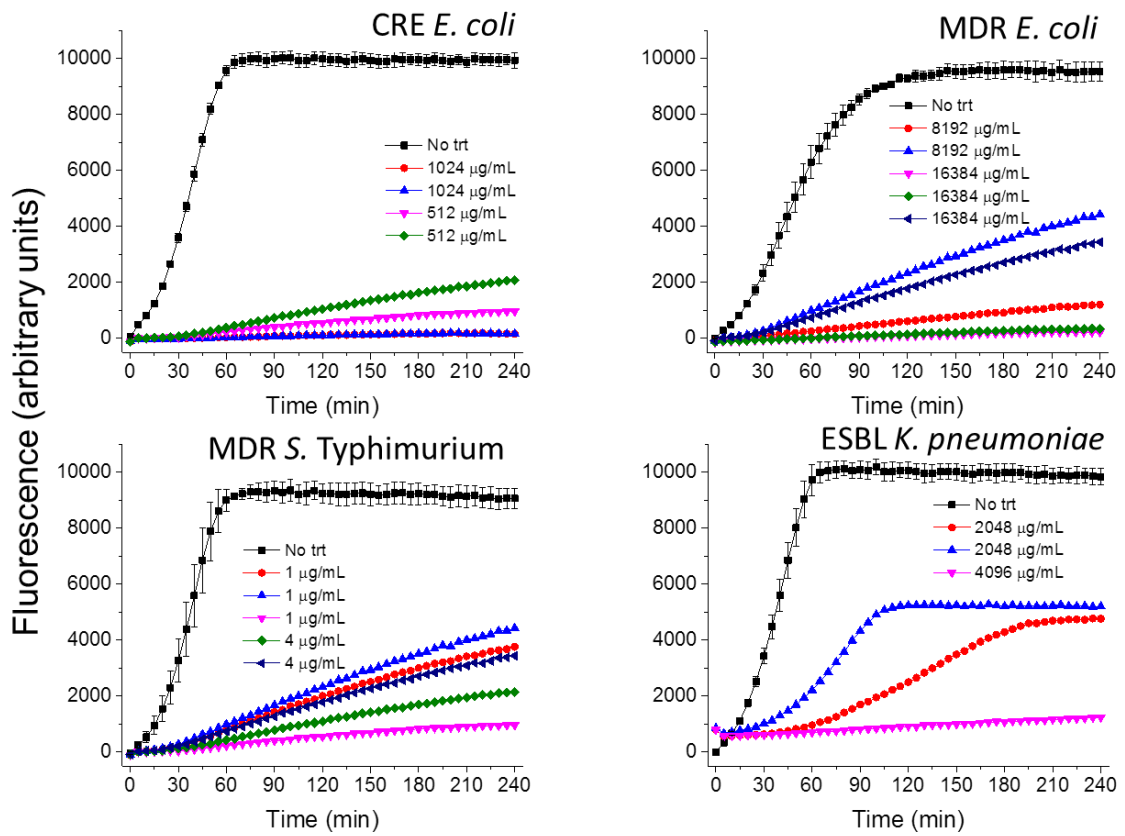


Figure 6.S10 Ceftriaxone GIC₅₀. Resazurin curves for respective strains at GIC₅₀ with labeled concentrations of ceftriaxone. Due to heterogeneity between replicates, we show each biological replicate separately. No treatment is the average of three biological replicates. GIC₅₀ is determined by ratio of slope between treatment and no treatment (≤ 0.5) in the linear region of the curve. The corresponding data is shown in Figure 6.1a (see 6.5 Materials and Methods).

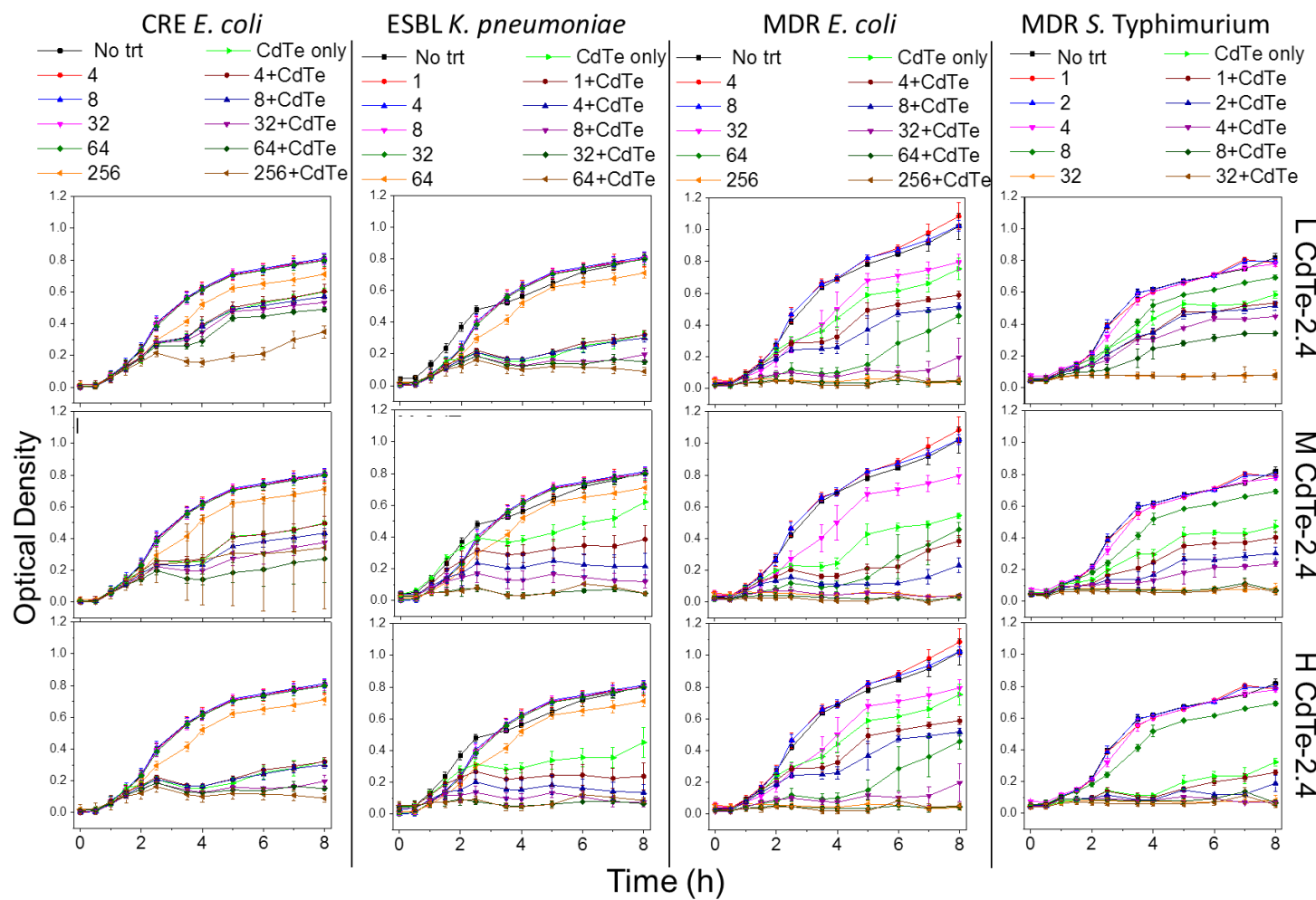


Figure 6.S11 Growth curve of clinical strains subjected to treatment with different concentrations of streptomycin and CdTe-2.4. For CdTe-2.4 concentrations: L (low level) is 12.5 nM, M (medium level) is 25 nM, and H (high level) is 50 nM. Concentrations of streptomycin are shown in legend as values in $\mu\text{g/mL}$. Data are the average of three biological replicates.

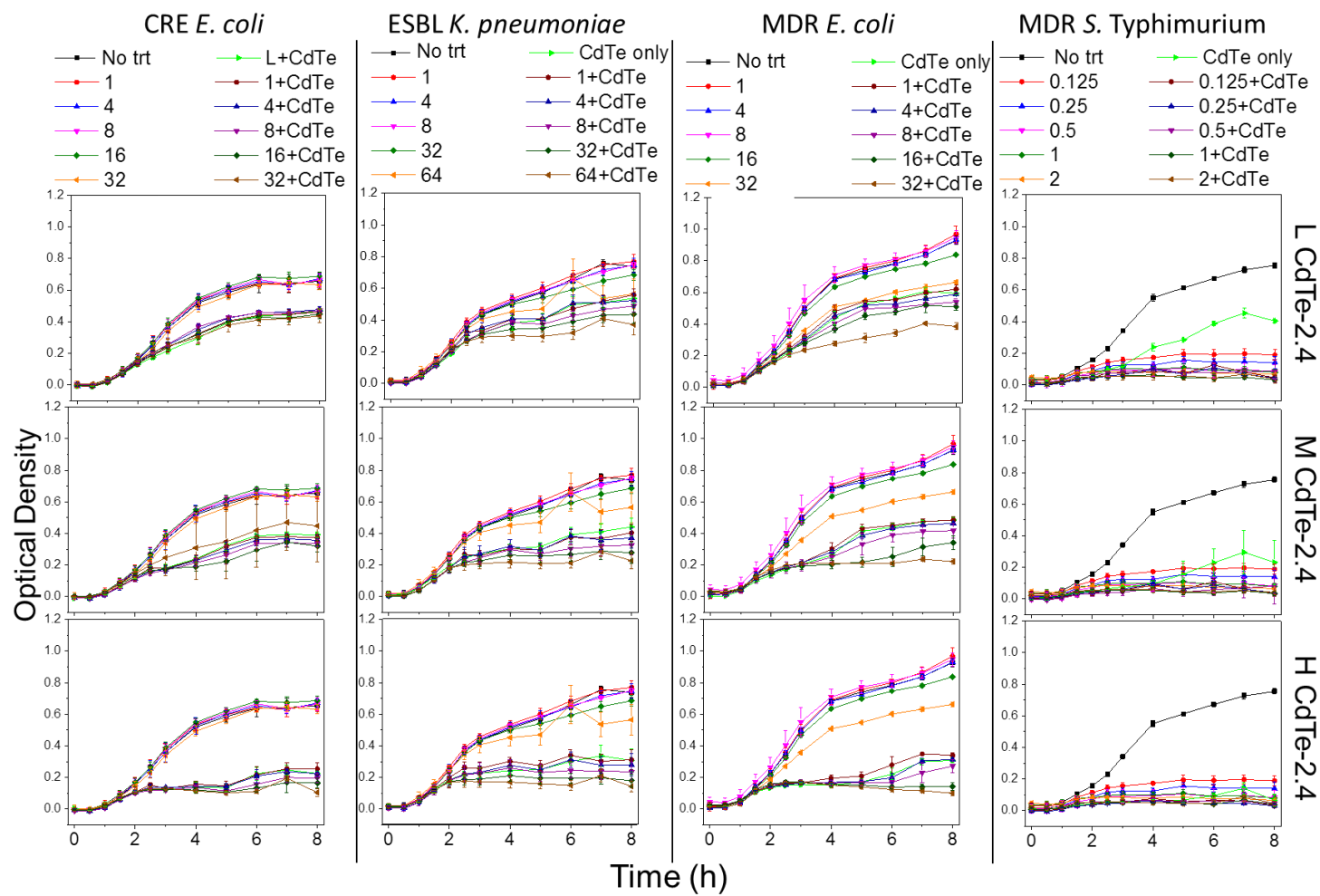


Figure 6.S12 Growth curve of clinical strains subjected to treatment with different concentrations of ciprofloxacin and CdTe-2.4. For CdTe-2.4 concentrations: L (low level) is 12.5 nM, M (medium level) is 25 nM, and H (high level) is 50 nM. Concentrations of ciprofloxacin are shown in legend as values in $\mu\text{g/mL}$. Data are the average of three biological replicates.

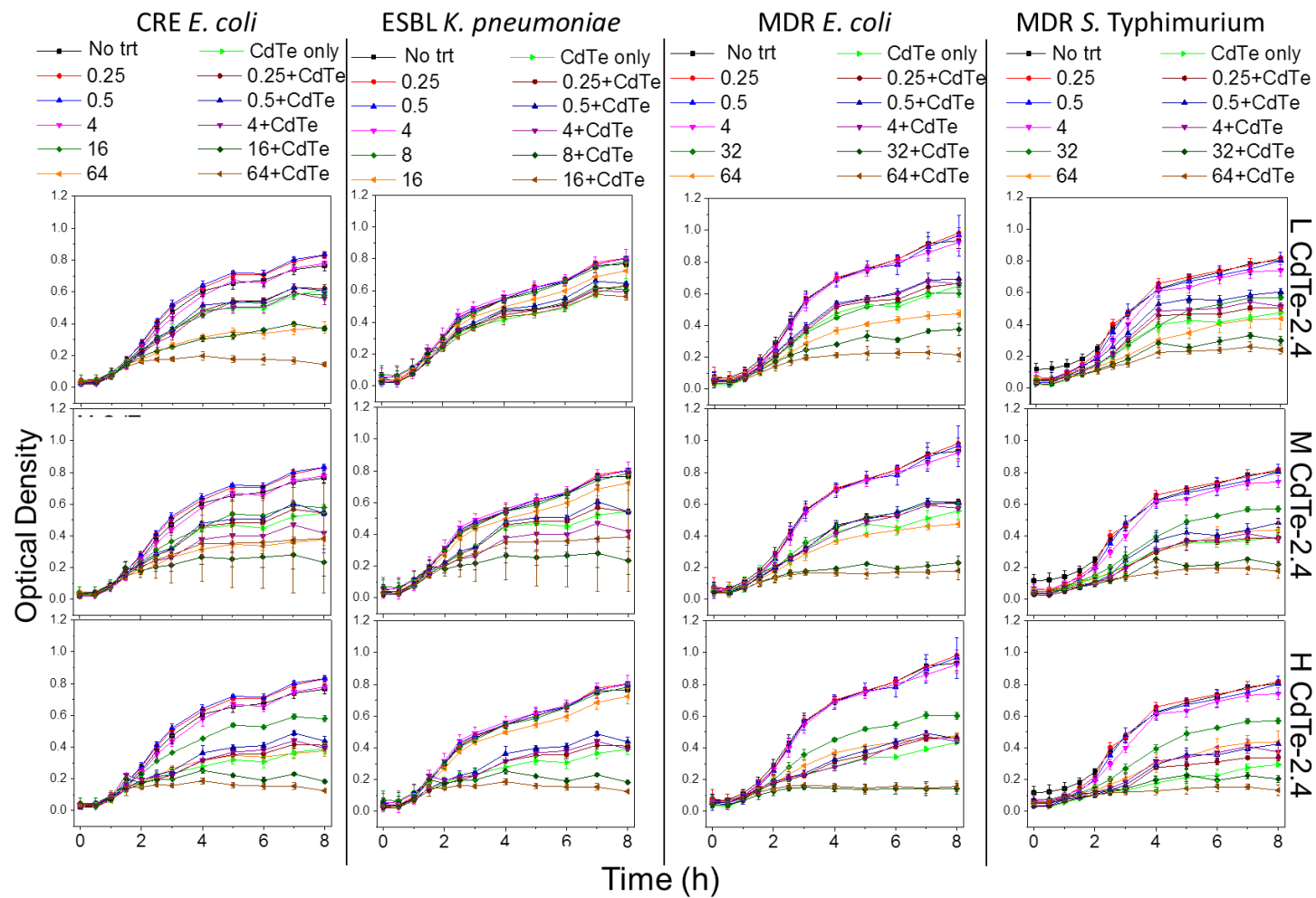


Figure 6.S13 Growth curve of clinical strains subjected to treatment with different concentrations of clindamycin and CdTe-2.4. For CdTe-2.4 concentrations: L (low level) is 12.5 nM, M (medium level) is 25 nM, and H (high level) is 50 nM. Concentrations of clindamycin are shown in legend as values in $\mu\text{g}/\text{mL}$. Data are the average of three biological replicates.

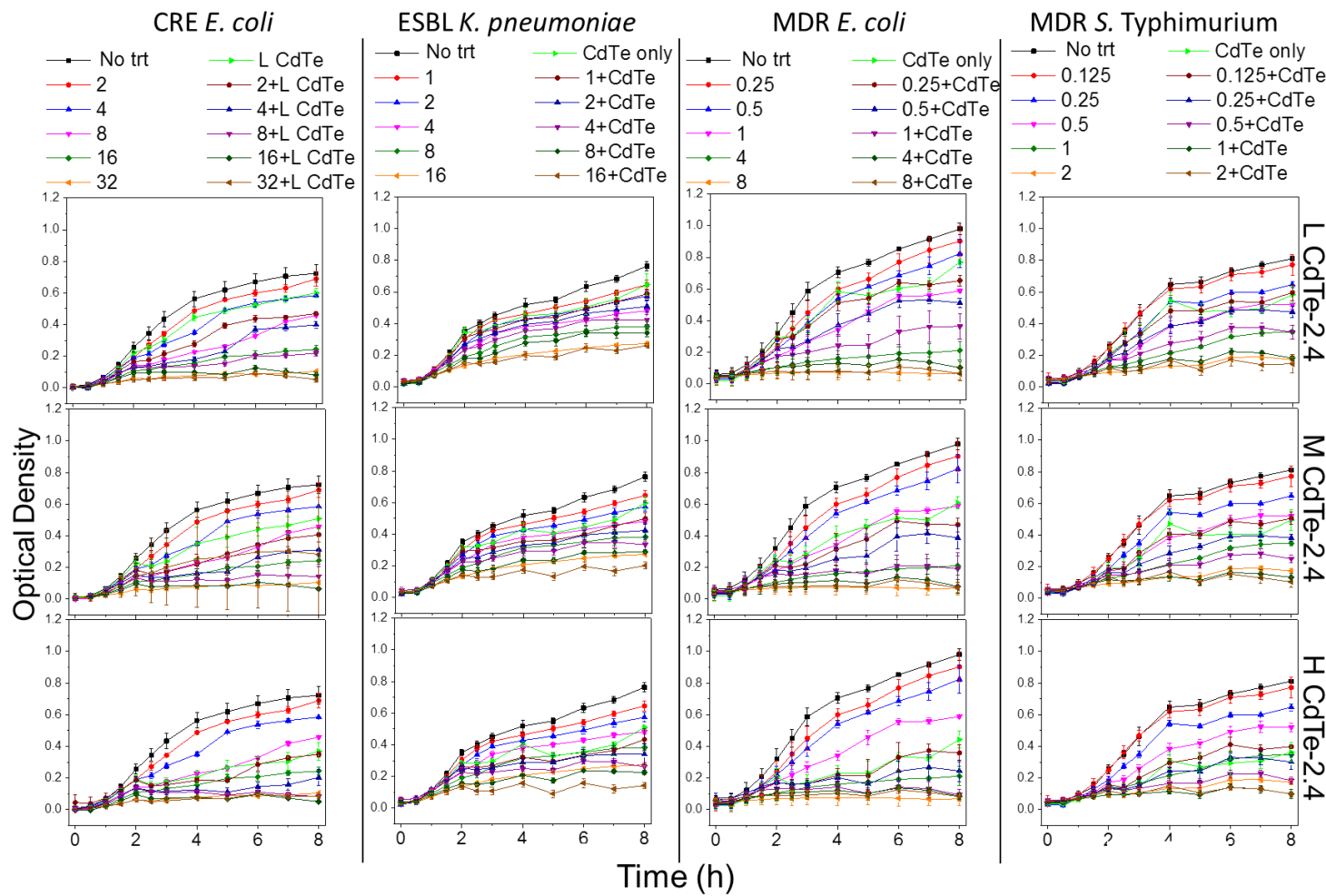


Figure 6.S14 Growth curve of clinical strains subjected to treatment with different concentrations of chloramphenicol and CdTe-2.4. For CdTe-2.4 concentrations: L (low level) is 12.5 nM, M (medium level) is 25 nM, and H (high level) is 50 nM. Concentrations of chloramphenicol are shown in legend as values in $\mu\text{g}/\text{mL}$. Data are the average of three biological replicates.

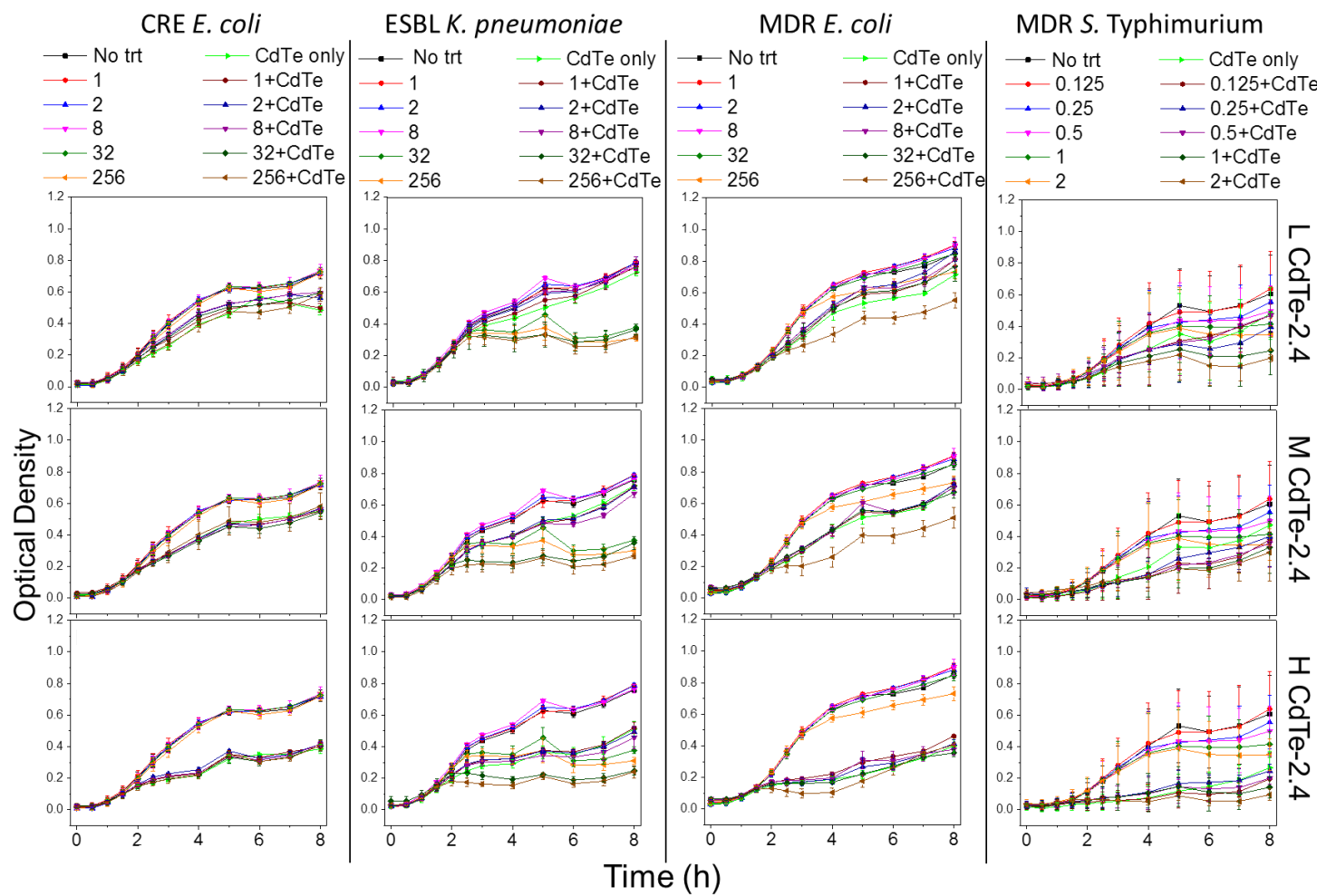


Figure 6.S15 Growth curve of clinical strains subjected to treatment with different concentrations of ceftriaxone and CdTe-2.4. For CdTe-2.4 concentrations: L (low level) is 12.5 nM, M (medium level) is 25 nM, and H (high level) is 50 nM. Concentrations of ceftriaxone are shown in legend as values in $\mu\text{g}/\text{mL}$. Data are the average of three biological replicates.

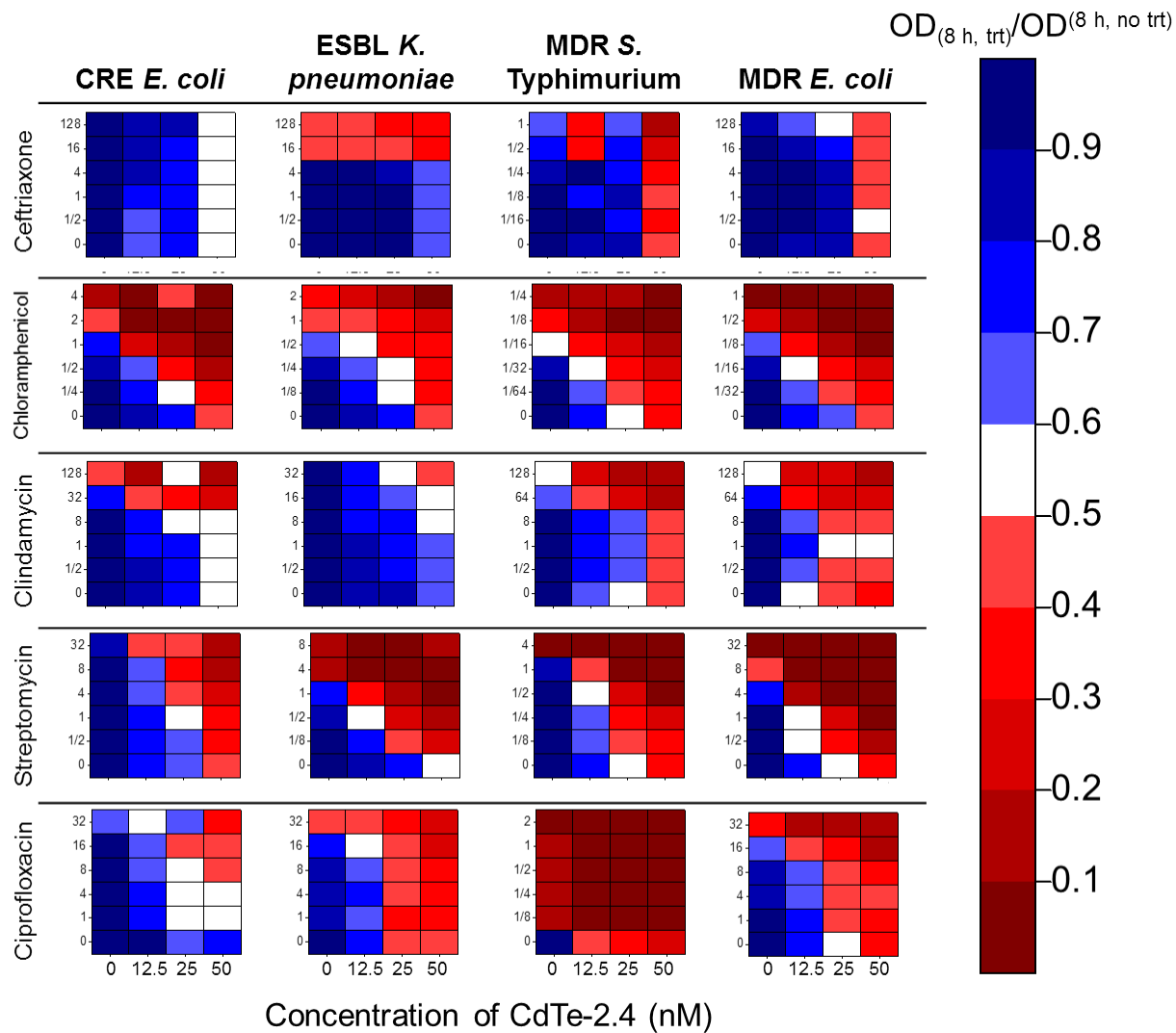


Figure 6.S16 Effect of antibiotics in combination with CdTe-2.4. Combinatorial effect on MDR clinical strains with multiple antibiotics showing the broad range applicability of CdTe-2.4. Y axis values are tested concentration/antibiotic breakpoint concentration for each strain and color map values are optical density (OD) at 8 h in respective treatment normalized to OD at 8 h in no treatment.

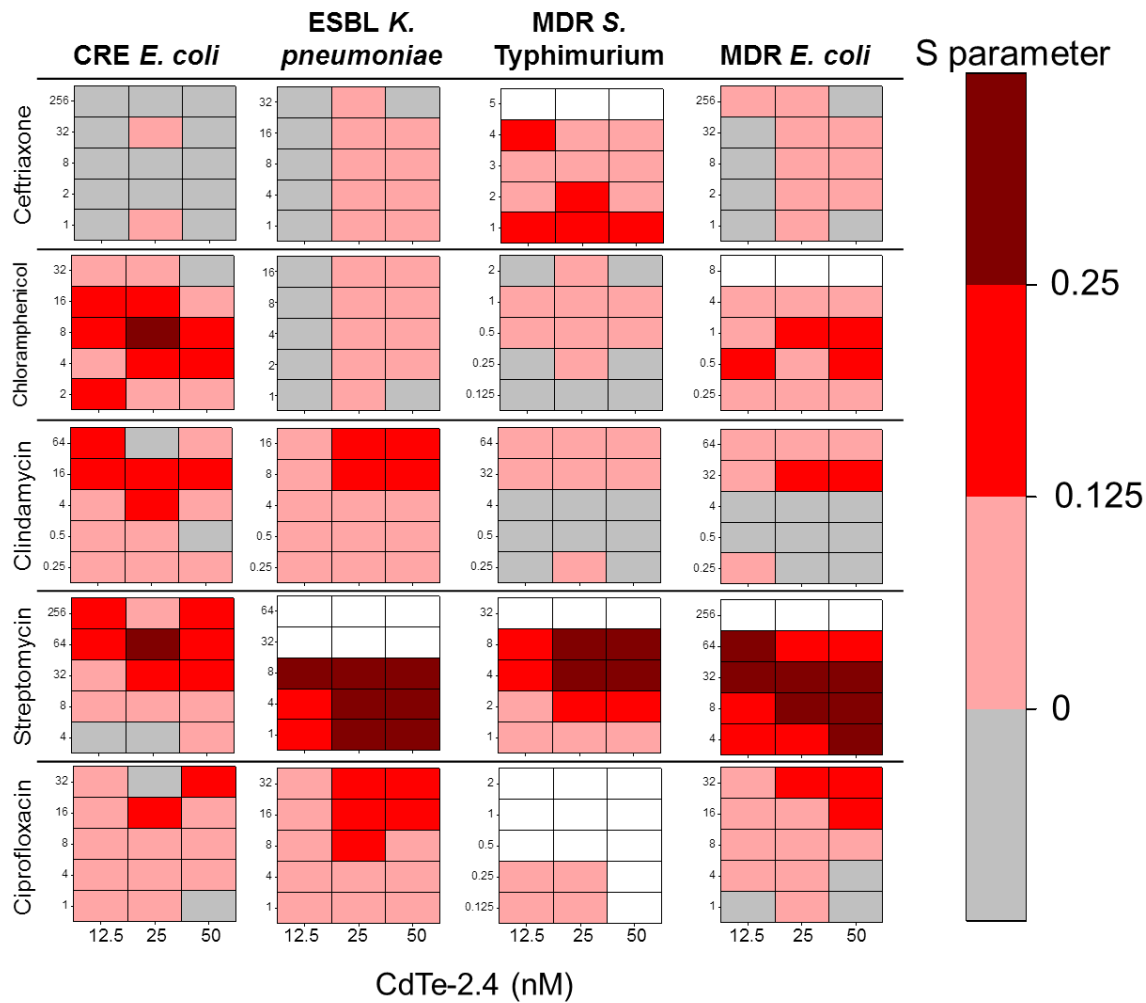


Figure 6.S17 S parameter heat maps for combinations of CdTe-2.4 and antibiotics. S parameter, $S = (OD_{AB}/OD_0)(OD_{QD}/OD_0) - (OD_{AB,QD}/OD_0)$, where OD_{AB} is the optical density (OD) at 8 h in only antibiotic treatment, OD_0 is the OD at 8 h in no treatment, OD_{QD} is the OD at 8 h in only CdTe-2.4 treatment, and $OD_{AB, QD}$ is the OD at 8 h in combination of antibiotic and CdTe-2.4 treatment, heat maps grouped by strain and antibiotic. Y axis is antibiotic concentration ($\mu\text{g/mL}$). White represents a missing value for cases where the monotherapy treatment yielded a OD at 8 h that was less than 0.1. n=3 for each representation. It is notable that most antagonistic interactions observed occur at low monotherapy concentrations.

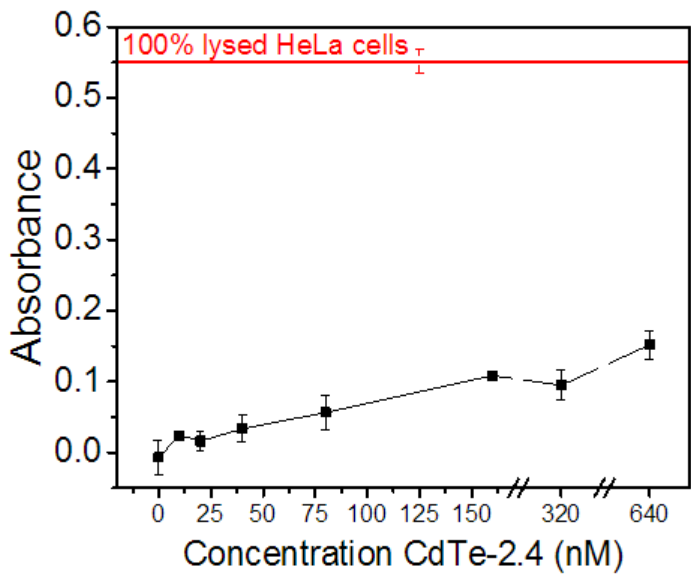


Figure 6.S18 LDH assay results for HeLa cells under CdTe-2.4 treatment. CdTe-2.4 was minimally-lethal to HeLa cells as demonstrated by the low LDH assay absorbance with increasing CdTe-2.4 concentration compared to the 100% lysed cell control. Data shown are the average of three biological replicates.

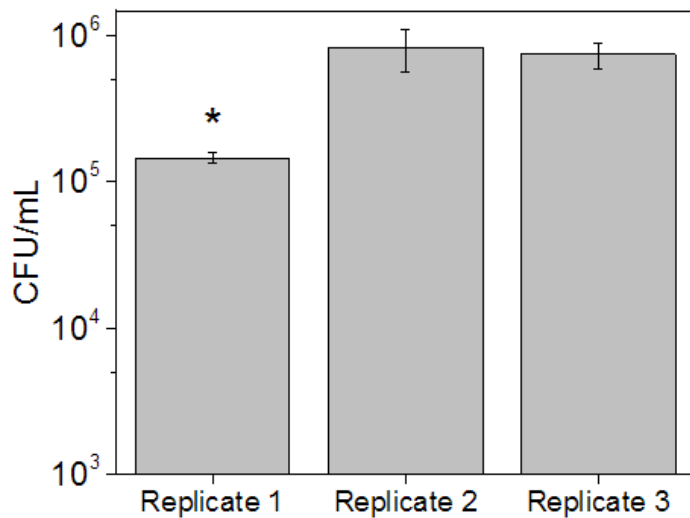


Figure 6.S19 Raw CFU/mL data for gentamicin protection assay. Raw colony forming units per milliliter (CFU/mL) for SL1344 in no treatment samples across biological replicates in gentamicin protection assay. CFU/mL data comparing treatments is normalized to no treatment in **Figure 6.3b-d** because the level of HeLa infection across biological replicates was statistically different for replicate 1 compared to 2 and 3. Data shown are the average of 4 technical replicates per biological replicate.

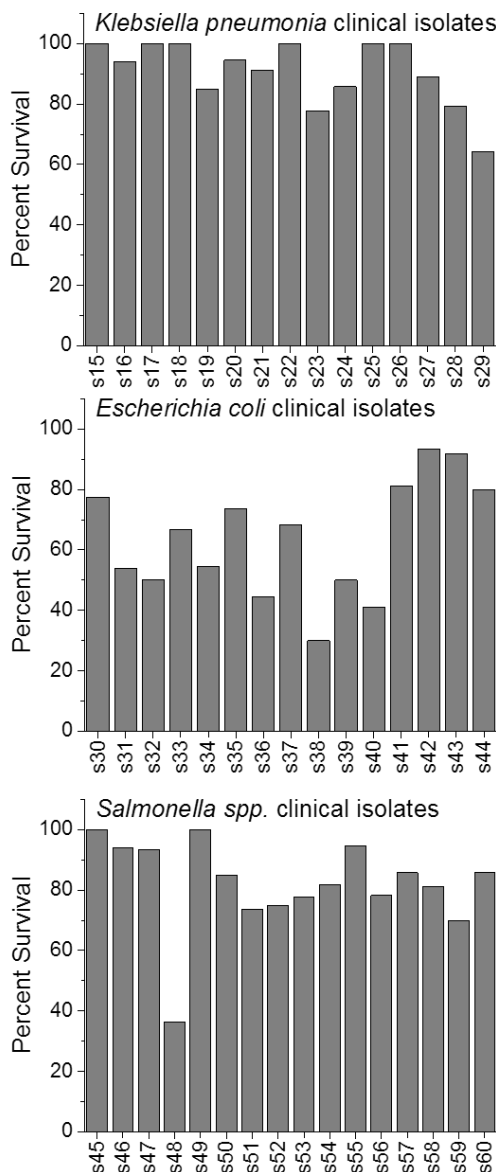


Figure 6.S20 Clinical strain screen for pathogen of *C. elegans*. 46 MDR strains from the University of Colorado Anschutz campus were screened to find effective pathogens that cause *C. elegans* death. n>10 nematodes for all samples. Nematodes were counted using SYTOX dye after 3 days of no treatment in S medium. S. Enteritidis corresponds to strain S48.

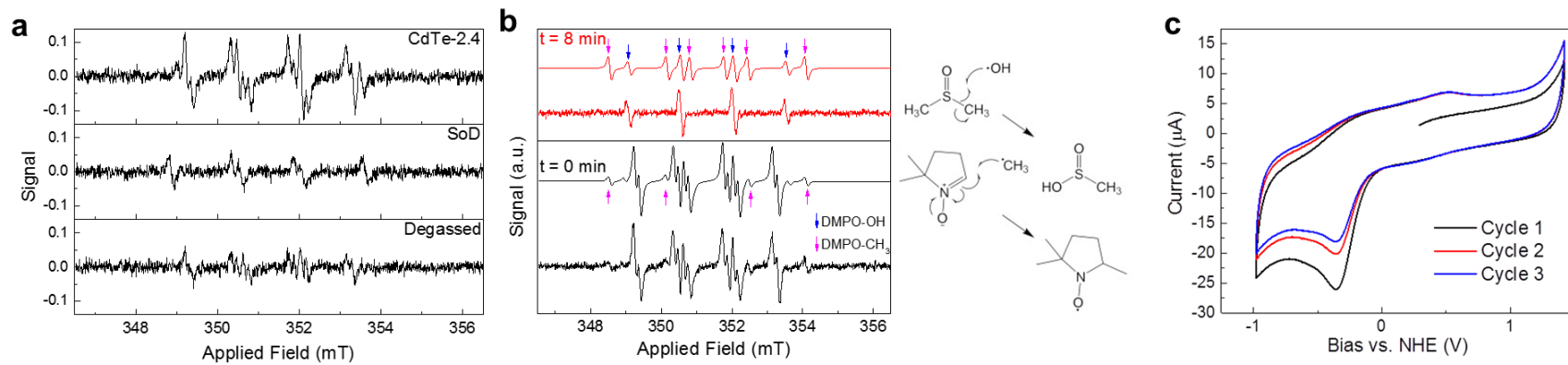


Figure 6.S21 CdTe-2.4 superoxide production. a. Attenuating radical signal through the addition of the enzyme superoxide dismutase or removing dissolved oxygen. The top curve shows nominal CdTe-2.4 EPR spectra on light illumination, middle curve reduced radical adducts upon addition of SOD, and bottom curve reduced number of radicals produced by removing dissolved oxygen. b. Measured (bottom) and simulated (top) EPR spectra of illuminated CdTe-2.4 in the presence of 10vol% DMSO initially (0 min) and over time (after 8 min). The spectra show clear peaks attributed to methyl free radical adduct. The radical interconversion mechanism is shown on the right. c. Cyclic voltammograms (CVs) of phosphate-buffered saline (PBS) solutions exhibiting decreased superoxide signal (-0.38 V) with successive scans, due to consumption of dissolved oxygen.

6.6.3 Supplementary Tables

Table 6.1 Details for clinical isolates used in the study. All strains were selected for the high resistance to multiple antibiotics and MDR *S. Enteritidis* was selected through a screen of strains for its lethality in the infection of *C. elegans* (Figure 6.S20). All strains were isolated from a *Homo sapiens* host by the University of Colorado Hospital and are part of the University of Colorado Hospital Clinical Microbiology Laboratory culture collection.

Sample Name	CRE <i>Escherichia coli</i>	ESBL <i>Klebsiella pneumoniae</i>	MDR <i>Salmonella enterica</i> serovar Typhimurium	MDR <i>Escherichia coli</i>	MDR <i>Salmonella enterica</i> serovar Enteritidis
Organism	Escherichia coli	<i>Klebsiella pneumoniae</i>	<i>Salmonella enterica</i> serovar Typhimurium	Escherichia coli	<i>Salmonella enterica</i> serovar Enteritidis
Host disease	asthma	Urinary tract infection (UTI)	bacteremia, GI source	end-stage liver disease, bacteremia	diarrhea
Isolation source	rectal swab	urine	blood	blood	blood
Host description	asthma exacerbation	UTI	rheumatoid arthritis on immunosuppression		enterocolitis
Host disease outcome	recovery	recovery	recovery	deceased	recovered
Host health state	stable	stable	critical	critical	stable

Table 6.2 Concentrations of antibiotics tested ($\mu\text{g/mL}$) for each clinical isolate bacterial strain in combination therapy.

	CRE <i>E. coli</i>	ESBL <i>K. pneumoniae</i>	MDR <i>S. typhimurium</i>	MDR <i>E. coli</i>
Ceftriaxone	1, 2, 8, 32, 256	1, 2, 8, 32, 256	0.125, 0.25, 0.5, 1, 2	1, 2, 8, 32, 256
Streptomycin	4, 8, 32, 64, 256	1, 4, 8, 32, 64	1, 2, 4, 8, 32	4, 8, 32, 64, 256
Clindamycin	0.25, 0.5, 4, 16, 64	0.25, 0.5, 4, 8, 16	0.25, 0.5, 4, 32, 64	0.25, 0.5, 4, 32, 64
Chloramphenicol	2, 4, 8, 16, 32	1, 2, 4, 8, 16	0.125, 0.25, 0.5, 1, 2	0.25, 0.5, 1, 4, 8
Ciprofloxacin	1, 4, 8, 16, 32	1, 4, 8, 16, 32	0.125, 0.25, 0.5, 1, 2	1, 4, 8, 16, 32

Table 6.3 Non-clinically isolated *Escherichia coli* strains used in studies.

Name in text	Description	Source/Strain Information
Control	MG1655 <i>E. coli</i> transformed with pZE21MCS	<i>E. coli</i> MG1655 (ATCC700926) Plasmid obtained from Expressys
+sodB	<i>E. coli</i> MG1655 transformed with pZE21MCS + <i>sodB</i> , cloned from MG1655 genome, between mluI and bamHI sites	Primers ordered from IDT Forward primer: GGATCCGGATCCATGTCATTGAAATTACCTGC Reverse primer: ACCGTACGCGTTATGCAGCGAGATTTCG
WT (BW25113)	<i>E. coli</i> Keio collection parent strain	From Coli Genetic Stock Center (CGSC)
ΔsodB	<i>sodB</i> Keio knockout strain from BW25113	CGSC JW1648-1
<i>E. coli</i> Op50	<i>C. elegans</i> food source	Caenorhabditis Genetics Center
SL1344 with GFP	<i>Salmonella enterica</i> serovar Typhimurium with chromosomal <i>rpsM::GFP</i>	Vazquez-Torres, A. et al. ²⁹

Table 6.4 Sensitive/resistant breakpoints used for determining resistance of clinical strains. 2016-2017 CLSI breakpoints³⁷ were used when available.

	Sensitive	Resistant
Ceftriaxone	1	4
Chloramphenicol	8	32
Clindamycin	Data not available	3.2 ³⁰
Streptomycin	Data not available	32 ³¹
Ciprofloxacin (<i>E. coli</i> and KPN)	1	4
Ciprofloxacin (<i>Salmonella enterica</i>)	0.06	1

6.7 Author Contributions

C.M.C. conducted clinical isolate drug-resistant characterization, confirmation of superoxide in bacteria, combinatorial studies, and *C. elegans* experiments. S.M.G and M.L. performed EPR spectroscopy. P.B. performed cloning of *sodB* overexpression construct. T.A.N. and C.M.C. performed the HeLa infection experiments. N.E.M. provided the clinical isolates. A.C., C.M.C., P.N., analyzed the experimental data. T.A.N., C.S.D., C.M.C. and A.C. analyzed HeLa infection data. A.C., C.M.C., and P.N. wrote the paper. All the authors discussed the results and edited the manuscript.

6.8 References

1. Alanis, A. J. Resistance to antibiotics: Are we in the post-antibiotic era? *Arch. Med. Res.* **36**, 697–705 (2005).
2. United States Center for Disease Control. *Antibiotic Resistance Threats*. (2013).
3. Tacconelli, E. & Magrini, N. *Global priority list of antibiotic-resistant bacteria to guide research, discovery, and development of new antibiotics*. (2017).
4. Grant, S. S., Kaufmann, B. B., Chand, N. S., Haseley, N. & Hung, D. T. Eradication of bacterial persisters with antibiotic-generated hydroxyl radicals. *Proc. Natl. Acad. Sci. U. S. A.* **109**, 12147–12152 (2012).
5. Dwyer, D. J., Kohanski, M. a, Hayete, B. & Collins, J. J. Gyrase inhibitors induce an oxidative damage cellular death pathway in Escherichia coli. *Mol. Syst. Biol.* **3**, 91 (2007).
6. Dwyer, D. J., Belenky, P. a, Yang, J. H., *et al.* Antibiotics induce redox-related physiological alterations as part of their lethality. *Proc. Natl. Acad. Sci. U. S. A.* **111**, E2100–9 (2014).
7. Kottur, J. & Nair, D. T. Reactive Oxygen Species Play an Important Role in the Bactericidal Activity of Quinolone Antibiotics. *Angew. Chemie* **55**, 2397–2400 (2016).
8. Liu, X., Marrakchi, M., Jahne, M., Rogers, S. & Andreescu, S. Real-time investigation of antibiotics-induced oxidative stress and superoxide release in bacteria using an electrochemical biosensor. *Free Radic. Biol. Med.* **91**, 25–33 (2016).
9. Wu, Y., Vulić, M., Keren, I. & Lewis, K. Role of oxidative stress in persister tolerance. *Antimicrob. Agents Chemother.* **56**, 4922–6 (2012).

10. Kohanski, M. A., DePristo, M. A. & Collins, J. J. Sublethal Antibiotic Treatment Leads to Multidrug Resistance via Radical-Induced Mutagenesis. *Mol. Cell* **37**, 311–320 (2010).
11. Imlay, J. A. The molecular mechanisms and physiological consequences of oxidative stress: lessons from a model bacterium. *Nat. Rev. Microbiol.* **11**, 443–54 (2013).
12. Liu, Y. & Imlay, J. A. Cell Death from Antibiotics Without the Involvement of Reactive Oxygen Species. *Science* **339**, 2010–2013 (2013).
13. Ipe, B. I., Lehnig, M. & Niemeyer, C. M. On the generation of free radical species from quantum dots. *Small* **1**, 706–9 (2005).
14. Dai, T., Huang, Y.-Y. & Hamblin, M. R. Photodynamic therapy for localized infections – state of the art. *Photodiagnosis Photodyn Ther.* **6**, 170–188 (2009).
15. Courtney, C. M., Goodman, S. M., McDaniel, J. a., *et al.* Photoexcited quantum dots for killing multidrug-resistant bacteria. *Nat. Mater.* **15**, 485–588 (2016).
16. Vatansever, F., de Melo, W. C. M. A., Avci, P., *et al.* Antimicrobial strategies centered around reactive oxygen species - bactericidal antibiotics, photodynamic therapy, and beyond. *FEMS Microbiol. Rev.* **37**, 955–989 (2013).
17. Keyer, K. & Imlay, J. Superoxide accelerates DNA damage by elevating free-iron levels. *Proc. Natl. Acad. Sci. U. S. A.* **93**, 13635–13640 (1996).
18. Keyer, K., Strohmeier Gort, A. & Imlay, J. A. Superoxide and the Production of Oxidative DNA Damage. *J. Bacteriol.* **177**, 6782–6790 (1995).
19. Brynildsen, M. P., Winkler, J. a, Spina, C. S., MacDonald, I. C. & Collins, J. J. Potentiating antibacterial activity by predictably enhancing endogenous microbial ROS production. *Nat. Biotechnol.* **31**, 160–165 (2013).
20. Bhattacharjee, S. Reactive oxygen species and oxidative burst: Roles in stress, senescence and signal transduction in plants. *Curr. Sci.* **89**, 1113–1121 (2005).
21. Buettner, G. R. & Mason, R. P. Spin-Trapping Methods for Detecting Superoxide and Hydroxyl Free Radicals in Vitro and in Vivo. *Methods Enzymol.* **186**, 127–133 (1990).
22. Harbour, J. R. & Hair, M. L. Superoxide generation in the photolysis of aqueous cadmium sulfide dispersions. Detection by spin trapping. *J. Phys. Chem.* **81**, 1791–1793 (1977).
23. Storz, G., Tartaglia, L. a., Farr, S. B. & Ames, B. N. Bacterial defenses against oxidative stress. *Trends Genet.* **6**, 363–368 (1990).
24. Korshunov, S. S. & Imlay, J. A. A potential role for periplasmic superoxide dismutase in blocking the penetration of external superoxide into the cytosol of Gram-negative bacteria. *Mol. Microbiol.* **43**, 95–106 (2002).

25. Scott, J. A., Homcy, C. J., Khaw, B.-A. & Rabito, C. A. Quantitation of Intracellular Oxidation in a Renal Epithelial Cell Line. *Free Radic. Biol. Med.* **4**, 79–83 (1988).
26. Hegreness, M., Shoresh, N., Damian, D., Hartl, D. & Kishony, R. Accelerated evolution of resistance in multidrug environments. *Proc. Natl. Acad. Sci. U. S. A.* **105**, 13977–81 (2008).
27. Berenbaum, M. C., Yu, V. L. & Felegie, T. P. Synergy with double and triple antibiotic combinations compared. *J. Antimicrob. Chemother.* **12**, 555–563 (1983).
28. Van der Heijden, J., Bosman, E. S., Reynolds, L. A. & Finlay, B. B. Direct measurement of oxidative and nitrosative stress dynamics in *Salmonella* inside macrophages. *Proc. Natl. Acad. Sci. U. S. A.* **112**, 560–5 (2015).
29. Vazquez-Torres, A., Jones-Carson, J., Bäumler, A., *et al.* Extraintestinal dissemination of *Salmonella* by CD18-expressing phagocytes. *Nature* **401**, 804–808 (1999).
30. Fass, R. J., Rotilie, C. A. & Prior, R. B. Interaction of clindamycin and gentamicin in vitro. *Antimicrob. Agents Chemother.* **6**, 582–587 (1974).
31. Sunde, M. & Norström, M. The genetic background for streptomycin resistance in *Escherichia coli* influences the distribution of MICs. *J. Antimicrob. Chemother.* **56**, 87–90 (2005).
32. Stiernagle, T. in *Wormbook*, ed Maintenance of *C. elegans*. (2005). doi:Available at: doi/10.1895/wormbook.1.7.1, <http://www.wormbook.org>.
33. Gray, B. & Carmichael, A. J. Kinetics of superoxide scavenging by dismutase enzymes and manganese mimics determined by electron spin resonance. *Biochem J* **281**, 795–802 (1992).
34. Cohen, G. & Heikkila, R. E. The Generation of Hydrogen-Peroxide, Superoxide Radical, and Hydroxyl Radical by 6-Hydroxydopamine, Dialuric Acid, and Related Cytotoxic Agents. *J. Biol. Chem.* **249**, 2447–2452 (1974).
35. Mohammad, M., Y.Khan, a., Subhani, M. S., *et al.* Kinetics and electrochemical studies on superoxide. *Res. Chem. Intermed.* **27**, 259–267 (2001).
36. Afanas'ev, I. B. *Superoxide Ion Chemistry and Biological Implications*. **1**, (CRC Press, 1989).
37. CLSI M100 S27:2017-Performance Standards for Antimicrobial Susceptibility Testing; 27th Edition. 62–71 (2017). Available at: <http://em100.edaptivedocs.info/dashboard.aspx>.

Chapter 7

Escherichia coli transcriptomic response to superoxide generation from cadmium telluride quantum dots

Courtney, C.M., Eller, K.A., Levy, M., Erickson, K.E., Goodman, S.M., Nagpal, P., Chatterjee, A. *In preparation.*

7.1 Abstract

Nanomaterials have been extensively used in the biomedical field and have garnered attention as antimicrobial agents. We demonstrated the design of light-activated cadmium telluride quantum dot with a bandgap of 2.4 eV (CdTe-2.4), specifically tuned for superoxide production in Chapters 5 and 6. We showed that CdTe-2.4 inhibits of multidrug-resistant bacteria (MDR) and highlighted the tunability of the antibiotic nanoparticles by demonstrating the benign nature of cadmium selenide quantum dots with the same 2.4 eV bandgap (CdSe-2.4). Here we investigate the transcriptome response of *Escherichia coli* to CdTe-2.4 and CdSe-2.4 quantum dots with and without activation by illumination to elucidate the toxic effect of illuminated CdTe-2.4. We find that activation of CdTe-2.4 generates overall high variability in gene expression compared to CdSe-2.4 activation. Activated CdTe-2.4 specifically alters genes involved in anaerobic nitrogen metabolism, leading us to believe *E. coli* is forced to search for alternate electron acceptors causing induced anaerobiosis. CdTe-2.4 activation also resulted in over expression of amino acid synthesis related genes possibly as a protection or protein repair mechanism. Additionally, we observed altered expression of genes related to high pH and heat shock possibly indicating oxidative stress induced cross-protection. These results provide new insight into CdTe-2.4 antibacterial activity and the effect of superoxide on *E. coli*.

7.2 Introduction

Responding to the imminent threat of multidrug-resistant bacteria requires the development of new antibiotics. Nanoparticles, such as those made of silver¹, silica², zinc oxide, and titanium dioxide³, have shown antibacterial efficacy attributed to non-specific reactive oxygen species (ROS), electrostatic interactions, and cell wall disruption⁴. While these nonspecific antibacterial effects could be desirable, the ability to tune and customize nanomaterial properties for specific therapeutic effects make them of interest for the rational design of antibiotics.

We previously demonstrated the design of light-activated cadmium telluride quantum dots with a bandgap of 2.4 eV (CdTe-2.4) and reduction potential tuned for inhibiting MDR bacteria via superoxide generation from dissolved, molecular oxygen^{5,6}. Quantum dots (QDs) are nanoparticles made of semi-conducting materials which have narrow “molecule-like”, tunable reduction and oxidation potentials attributed to quantum confinement. When excited across their bandgap, QDs produce excited electrons and subsequent holes available at their tuned redox potentials for interaction in biological environments. We previously compared the antibacterial effect of CdTe-2.4, with and without activation by illumination with visible light, to cadmium selenide quantum dots with a bandgap of 2.4 eV (CdSe-2.4), with and without activation, to confirm that the antibacterial activity of CdTe-2.4 was due to its tuned reduction potential for superoxide production rather than its bandgap or presence of cadmium⁵. In this study, we define the different effects between antibacterial CdTe-2.4 and benign CdSe-2.4, with and without activation, using transcriptome analysis of *Escherichia coli* under treatment.

Transcriptome analysis can yield insightful data on cellular response to stress because it measures the level of every gene being expressed in *E. coli* at the time of collection. A deeper understanding of the response of bacteria to not only the quantum dot but the excitation of the

quantum dot of interest can help guide future design of rationally designed nanoparticles for antimicrobial applications. Additionally, it is often hard to decouple the effect of ROS from their producer but in our system, superoxide generation can be decoupled from the material by comparison of CdTe-2.4 with and without illumination. In this comparison, the only difference in stress for the bacteria should be the excited electrons being transferred to oxygen converting it to superoxide. Previously, transcriptomic analysis of Ag, TiO₂, ZnO, CdS, and CdTe nanoparticles in green alga *Chlamydomonas reinhardtii* revealed changes in gene expression for photosynthetic systems, elevated global stress response (ZnO), cell wall and flagellar activity (Ag), and proteasome inhibition (TiO₂ and ZnO)⁷. Two sizes of glutathione (GSH) capped CdTe were also previously investigated using microarray analysis in *E. coli* and it was found that CdTe treatment alters gene expression related to stress, respiration, transcription, metabolism, and transport⁸. While this previous study seeks to answer the difference between two sizes of CdTe, it does not distinguish the effects of light activation versus effects solely from introducing metal nanoparticles into biological systems. We sought to independently characterize these effects by comparing transcriptome analysis of CdTe-2.4 and CdSe-2.4 both with and without illumination.

7.3 Results and Discussion

7.3.1 Characterization of CdTe-2.4 and CdSe-2.4

To highlight the difference between CdTe-2.4 and CdSe-2.4, we performed *E. coli* culture analysis and ROS production characterization using spectroscopy. CdTe-2.4 and CdSe-2.4 were steriley synthesized and filtered to remove precursors and reaction solution. Particles were tested in *E. coli* MG1655 with illumination at 10-50 nM to demonstrate the significant growth inhibition from CdTe-2.4 with respect to (wrt) no treatment and CdSe-2.4 (Figure 7.1a). We then used electron paramagnetic resonance (EPR) spectroscopy with addition of 5,5-dimethyl-1-pyrroline

N-oxide (DMPO) for spin trapping to measure radical species production by CdTe-2.4 and CdSe-2.4. CdTe-2.4 and CdSe-2.4 spectra were collected with and without illumination to demonstrate the light activated ROS production by CdTe-2.4. Here we show primarily hydroxyl radical signal from CdTe-2.4 due to dismutation of superoxide in solution⁶ and significantly less signal from CdSe-2.4 (Figure 7.1b). These results reiterate the difference between CdTe-2.4 and CdSe-2.4 both in effect on cellular growth and ROS production.

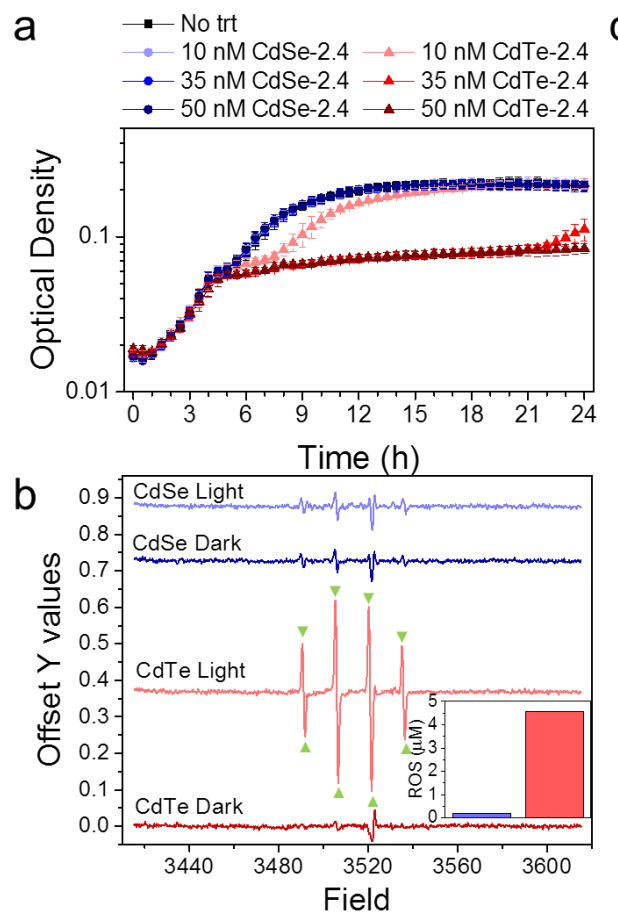


Figure 7.1 Comparison of CdTe-2.4 and CdSe-2.4 in *E. coli* and EPR spectroscopy and RNA-seq workflow. a. Growth curves of *E. coli* MG1655 with CdTe-2.4 or CdSe-2.4 compared to a no treatment (No trt) control under illumination. CdSe-2.4 has negligible effect on growth while CdTe-2.4 significantly stunts bacterial growth. b. EPR spectroscopy of CdSe-2.4 and CdTe-2.4 with and without illumination demonstrating light-activated ROS production by CdTe-2.4 compared to CdSe-2.4. Inset bar graph shows quantification of ROS, in light with dark subtracted, where CdTe-2.4 generates over 20-times more ROS compared to CdSe-2.4. Green triangles indicate hydroxyl radical signal. c. RNA-seq workflow from culture to differential expression and variability analysis of transcriptome. Five conditions were sampled in biological duplicate. The concentration of CdTe-2.4 and CdSe-2.4 was 10 nM.

7.3.2 Bioinformatic analysis workflow

To next evaluate the effect of CdTe-2.4 treatment and illumination on the transcriptome of *E. coli* MG1655, we treated two biological replicates with five conditions: 10 nM CdTe-2.4 and light or dark, 10 nM CdSe-2.4 and light or dark, or no treatment (Figure 7.1c). We grew the cells in M9 salts media (0.4% glucose) until they reached exponential phase and extracted RNA from the cell pellet. We then performed DNase treatment and subsequent library preparation was performed in the University of Colorado BioFrontiers Institute Next Generation sequencing facility for RNAtag-Seq⁹. The ten samples were multiplexed (Table 7.3) and sequencing was performed on an Illumina HiSeq with 1x50 reads in three lanes (Table 7.4). Bioinformatics analysis was conducted on the University of Colorado BioFrontiers Institute computing core. Samples were de-multiplexed (Table 7.5) and trimmed for adapters, minimum length, and quality (Table 7.6). Reads were then aligned to *E. coli* MG1655 genome and the coverage of RNA-seq was sufficiently high to use for differential expression analysis in all samples¹⁰ (Table 7.7). We then used HTSeq-count¹¹ and DESeq¹² to generate count tables and determine differential expression or evaluate variability in expression (Table 7.9). Significance in differential expression was defined with a 95% confidence interval.

7.3.3 Differential expression analysis

Differential expression analysis was conducted for eight different comparisons. Gene ontology (GO) was characterized and analysis of statistical overrepresentation by GO classifications were tabulated using DAVID¹³ and PANTHER¹⁴ (Table 7.1). Differential expression analysis determines which genes had significantly different expression in one condition wrt another. We first looked at DE genes in CdTe-2.4 in illumination (CdTe Light) wrt no treatment and found significant overrepresentation of only one pathway, amide ligase activity, including upregulation of *asnA*, *asnB*, and *puuA*. DE genes by GO classification were clustered in

to classical and nitrogen metabolism, metal binding, iron, periplasmic space or signaling, nucleotide binding, cell membrane, and transcription regulation (Figure 7.2a). There were five DE genes with greater than 2 log₂ fold change in expression: *zntA*, *tusA*, *metR*, *zraP*, and *glnK*. Consistent with previous reports⁸, *zntA*, a metal efflux pump, and *znuA*, a zinc influx pump, were

Table 7.1 Statistical overrepresentation in GO classification of differentially expressed genes between conditions by molecular function, biological process, and cellular component.

	# genes	Statistically overrepresented GO classifications
CdTe Light wrt No trt	49	Amide ligase activity
CdTe Dark wrt No trt	125	Electron carrier activity Oxidoreductase activity Respiratory electron transport chain Aerobic and anaerobic respiration NarGHI complex Cytochrome complex Intrinsic component of cytoplasmic side of plasma membrane
CdSe Light wrt No trt	127	None
CdSe Dark wrt No trt	216	None
CdTe Light wrt CdTe Dark	31	None
CdSe Light wrt CdSe Dark	166	Ribosomal subunit/Cytosolic ribosome
CdTe Light wrt CdSe Light	119	None
CdTe Dark wrt CdSe Dark	320	None

overexpressed in CdTe Light probably as a characteristic response to metal nanoparticles inside cells. Indeed, a Venn diagram of DE genes in CdTe Light and CdTe-2.4 without illumination (CdTe Dark) with respect to (wrt) no treatment shows metal-binding or transport genes: *zntA*, *feoC*, *zraP*, *afuC*, and *znuA* as DE (Figure 7.2b). This led us to examine DE genes in CdTe Light wrt CdTe Dark to evaluate non-material related effects.

There were no statistically overrepresented GO classes within the CdTe Light wrt CdTe Dark DE genes however the DE genes could be clustered into GO classes involving 4Fe-4S iron clusters and oxidoreductase, proton transport and cell membrane, transcription regulation, and ATP/nucleotide binding. Within the 4Fe-4S and oxidoreductase cluster, *ynfF*, *ynfG*, *narH* and *hycE* were all downregulated. Within transcription regulation *fis* and *appY* had reduced and *yeeY* and *yafQ* had increased expression in CdTe Light. *fis* is a nucleoid-associated DNA bending factor which has been shown to have a regulatory effect on 21% of *E. coli*'s genome¹⁵ including genes involved in stress response, transport, motility, and chemotaxis¹⁶ indicating different stress applied by CdTe Light compared to CdTe Dark. Within the proton transport and cell membrane *codB*, *plaP*, *yhbE*, *ynfF*, *yfhR*, and *narH* had reduced expression and *nhaA*, *betA*, *psiE*, *yjcC*, and *mdtM* were overexpressed. *nhaA* and *mdtM* are both Na⁺:H⁺ antiporters which play a role in pH homeostasis corresponding with previous studies demonstrating altered pH in *E. coli* during oxidative stress and overlap of genes involved in pH regulation and oxidative stress^{17,18}.

We next performed DE analysis of CdTe Light wrt CdSe-2.4 with illumination (CdSe Light) to observe transcriptome effects of ROS production by CdTe-2.4 compared to the significantly reduced level of ROS and negligible growth inhibition by CdSe-2.4. There were 119 DE genes in CdTe Light wrt CdSe Light highlighting the different responses to the two illuminated nanoparticles. Seventeen genes were DE and had a log2 fold change in expression greater than 2: *paaY*, *insD4*, *ydhW*, *ldtE*, *yebE*, *yebF*, *pssA*, *yfiM*, *kgtP*, *rrfG*, *rrlG*, *yhjC*, *dut*, *recF*, *dnaN*, *hemD*, and *yihU*. There were no significantly overrepresented classes of genes but the genes clustered by GO classification into transcription regulation, ATP/nucleotide binding, zinc related genes, and cell membrane and transport.

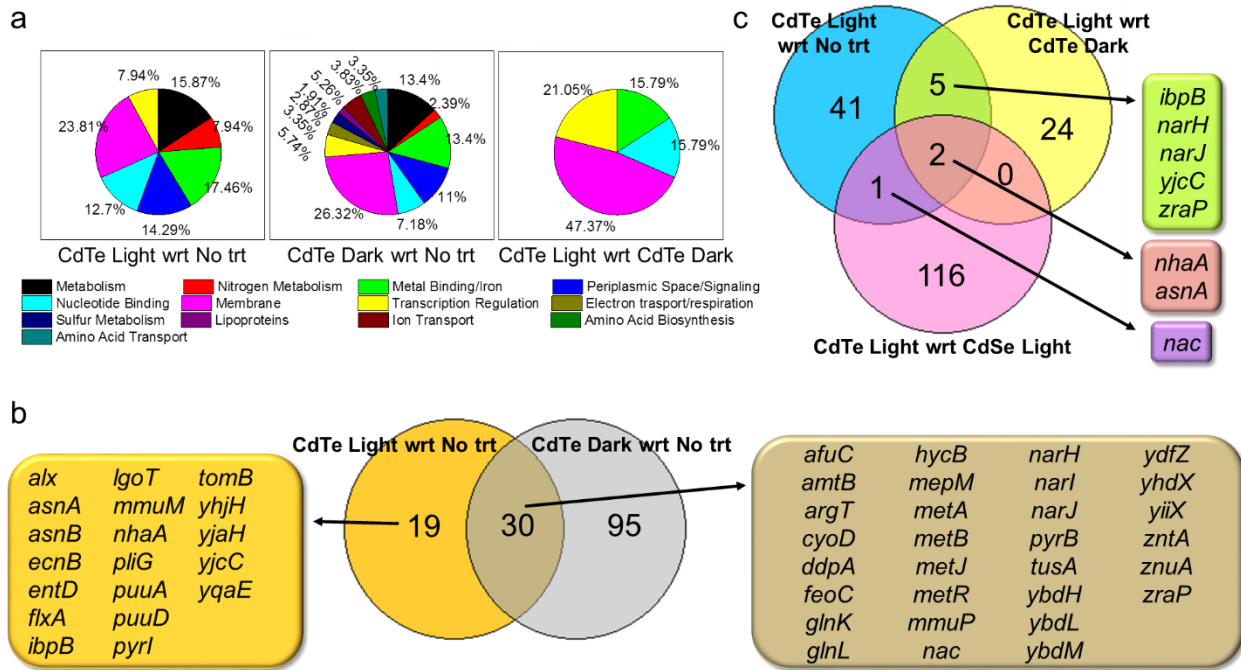


Figure 7.2 Differentially expressed genes within and between conditions. a. DE genes between conditions: CdTe Light wrt no treatment (left), CdTe Dark wrt no treatment (middle), and CdTe Light wrt CdTe Dark (right) grouped by GO classifications into pie charts by function/pathway/cellular component. b. Venn diagram of DE genes in respective comparisons to highlight genes common and unshared by CdTe Light and CdTe Dark wrt no treatment. Left gene list corresponds to the 19 DE genes only in CdTe Light wrt no treatment and gene list to the right corresponds to the 30 DE genes found in both CdTe Light and CdTe Dark wrt no treatment. c. Venn diagram of DE genes in respective comparisons to highlight genes that were DE in CdTe Light wrt three other conditions: no treatment, CdTe Dark, and CdSe Light. Gene lists are color coded to the overlap section they belong.

To elucidate the different response of *E. coli* in CdTe Light wrt no treatment, CdTe Dark, and CdSe Light, we generated a Venn diagram of DE genes in each comparison (Figure 7.2c). Two genes were significantly upregulated in all three comparisons: *nhaA*, a $\text{Na}^+:\text{H}^+$ antiporter discussed above, and *asnA* for asparagine synthetase A. *asnA* has been shown to be essential for *mazEF*-mediated cell death¹⁹ and was upregulated in bactericidal killing by small molecule antibiotics²⁰. *nac*, nitrogen assimilation control gene²¹, was significantly upregulated commonly in CdTe Light wrt no treatment and CdSe Light. Five genes were DE in CdTe Light wrt no treatment and CdTe Dark: *ibpB*, *narH*, *narJ*, *yjcC*, and *zraP*. *ibpB*, a heat shock inducible chaperone, was similarly upregulated under hydrogen peroxide stress²² which *E. coli* would likely

experience during CdTe-2.4 treatment due to superoxide dismutation and Fenton chemistry inside the cell.

7.3.4 Differentially variable gene expression analysis

Interestingly the least number of DE genes was observed for comparisons of CdTe Light wrt to no treatment, CdSe Light, or CdTe Dark (Table 7.8 and Table 7.9). Based on previous studies which showed gene expression variability contributing to stress response and adaptation^{23–25}, we looked at the variability within biological replicates in each condition. Variability was determined by first calculating the coefficient of variation (CV) (standard deviation divided by the mean) of gene expression between replicates in the same condition. To compare CV and determine significance, Δ CV was calculated between conditions for each gene. Significantly different variability was defined as a Δ CV greater than two standard deviations from the mean of Δ CV for the comparison.

We calculated Δ CV for CdTe Light wrt no treatment, CdTe Dark, and CdSe Light and CdSe Light wrt CdSe Dark. Positive Δ CV values indicate more variability in gene expression while negative Δ CV values indicate less variability in gene expression. For CdTe Light wrt no treatment, there were genes with both lower and higher variability related to the cell membrane. Less variable genes were also related to the electron transport chain and metal binding while more variable genes were in transcriptional regulation, nucleotide binding, periplasmic space/signaling, lipoproteins, and metabolism (Figure 7.3a). Histograms of Δ CV for CdTe Light wrt CdTe Dark and CdSe Light wrt CdSe Dark highlight an increase in gene expression variability in CdTe-2.4 treatment with illumination compared to CdSe-2.4 (Figure 7.3b). There were 24 shared genes that were more variable in both CdTe Light and CdSe light wrt the dark conditions and no shared genes

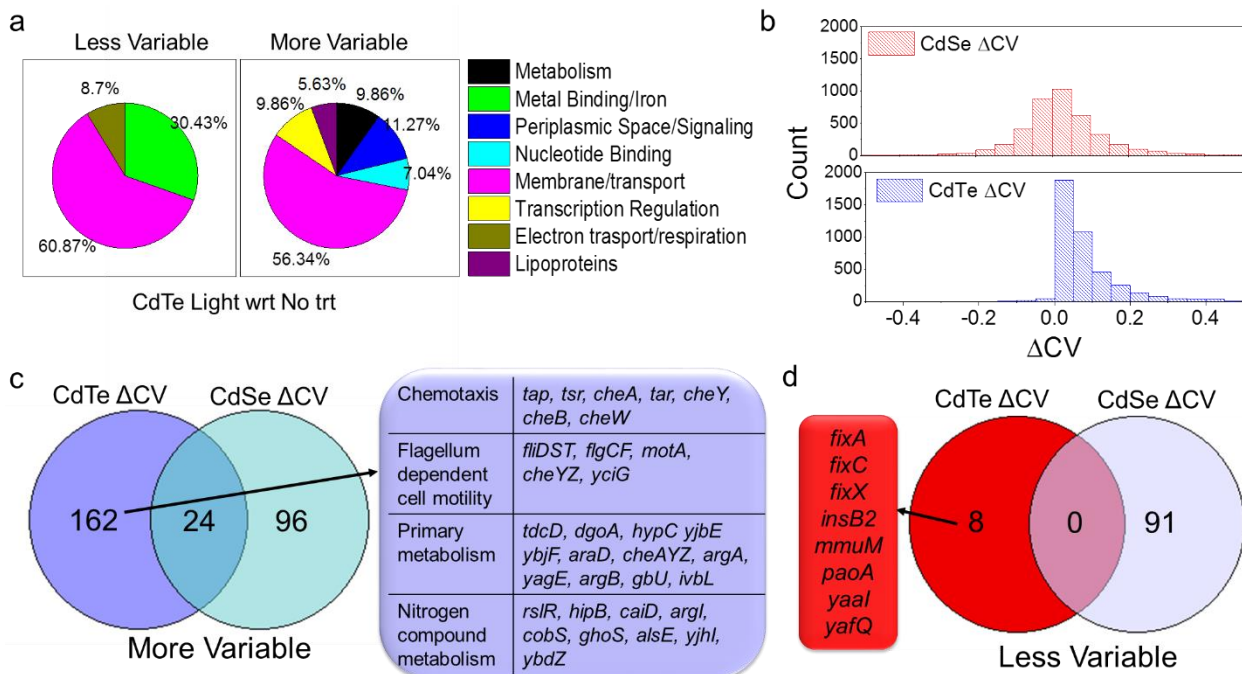


Figure 7.3 Gene expression variability within conditions highlights genes and pathways of interest. a. Genes with significantly lower (left) and higher (right) variability in CdTe Light wrt no treatment grouped by function/pathway/cellular component classifications into pie charts. b. Histogram of the change in coefficient of variation (ΔCV) for all genes CdSe Light wrt CdSe Dark (CdSe ΔCV , top) or CdTe Light wrt CdTe Dark (CdTe ΔCV , bottom). A positive ΔCV indicates more variable in light compared to dark and a negative ΔCV indicates less variable in light compared to dark. c. Venn diagram of genes that were significantly more variable in CdSe ΔCV and CdTe ΔCV highlighting common genes in list to right. d. Venn diagram of genes that were significantly less variable in CdSe ΔCV and CdSe ΔCV highlight no shared genes.

that were less variable (Figure 7.3c, d). There were 162 genes that were only more variable in CdTe-2.4 treatment which had statistical overrepresentation by GO classification of catalytic activity, chemotaxis, flagellum-dependent cell motility, and primary and nitrogenous metabolic processes. Interestingly, of the 8 genes that were less variable in CdTe, three were related to anaerobic carnitine metabolism.

We then examined ΔCV in CdTe Light wrt CdSe Light. We used GO classification to identify statistically overrepresented classes of genes among the more and less variable genes in CdTe Light wrt no treatment, CdTe Dark, and CdSe Light (Figure 7.4). GO classes were statistically overrepresented as more variable in CdTe Light wrt CdTe Dark and CdSe Light

including catalytic activity, chemotaxis, flagellum-dependent cell motility, and metabolic processes (Table 7.2). There were 25 genes with high variability in CdTe Light wrt to the other three conditions (Figure 7.4a). *soxS*, a regulator of the superoxide response regulon, which typically has increased expression with superoxide stress²⁶, was significantly more variable in CdTe Light compared to the other conditions (Figure 7.4a). The large variability within CdTe Light replicates (814 and 1604 base expression in CdTe Light) prevented differential expression

Table 7.2 Statistical overrepresentation in GO classification by molecular function, biological process, and cellular component of less or more variable genes in CdTe Light wrt condition.

Condition	# genes	CdTe Light genes less variable	# genes	CdTe Light genes more variable
No trt	102	Catalytic Activity/Binding Metabolic processes Cytoplasmic/Intracellular parts	106	Cytoplasmic/Intracellular part Cellular biosynthetic processes
CdTe Dark	8	Respiratory electron transport chain Carnitine metabolic processes	186	Catalytic Activity Chemotaxis Flagellum-dependent cell motility Metabolic processes
CdSe Light	1	<i>fixX</i> - carnitine metabolism	218	Ion binding Catalytic Activity Chemotaxis Flagellum-dependent cell motility Metabolic processes Cellular biosynthetic processes Cell projection Cytoplasmic/Intracellular parts

call for *soxS* ($padj=0.174$) even though both levels were higher than that of other conditions (183 and 158 no treatment, 186 and 170 CdSe Light, and 274 and 514 in CdTe Dark base expression). *soxS* was not more variable or DE in CdSe Light wrt CdSe Dark confirming negligible superoxide

production of CdSe-2.4. *fliF*, *fliP*, and *motB* play a role in flagellar assembly and were all more variable in CdTe Light compared to the other three conditions. *nrfC* and *nrfD* additionally were more variable and are involved in anaerobic electron transport chain as components of formate-dependent nitrite reductase.

All genes that were significantly more variable in CdTe Light wrt CdTe Dark were also more variable in CdTe Light wrt CdSe Light potentially suggesting these genes, while variable, are a somewhat coordinated response to stress. Only one gene, *lpp*, which codes for the major lipoprotein and is required for stabilization of the bacterial cell envelope, was more variable in CdTe Light wrt no treatment and CdSe Light. One gene, *fixX*, shared lower variability in CdTe Light wrt CdTe Dark and CdSe Light (Figure 7.4b). *fixX*, as mentioned above, is for anaerobic carnitine metabolism.

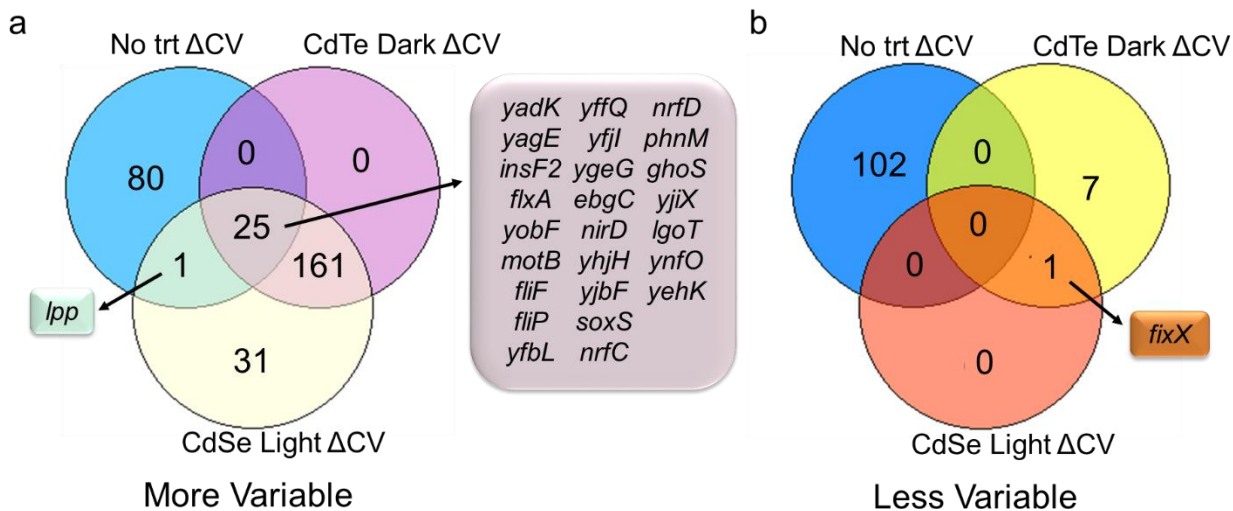


Figure 7.4 Comparison of genes with significantly higher or lower variability in CdTe Light. Significantly more (a) and less (b) variable genes in CdTe Light wrt to different conditions. Gene lists are color coded to the overlay section they belong.

7.3.5 Small regulatory map of gene expression and variability changes in CdTe Light

Through our comparisons of conditions, we found that both regulators and downstream genes demonstrated DE and significant changes in expression variability. We sought to

demonstrate this by mapping a small portion of the genes discussed above in their regulatory network (Figure 7.5). We highlighted above the variability in *soxS* and here show that while *soxS* was more variable in CdTe Light, downstream gene *ompN* was less variable ((Figure 7.5, box 1). We further show the opposite effect where *nac*, nitrogen assimilation control regulator, was DE up and downstream gene *cadB* was significantly more variable in CdTe Light wrt CdTe Dark and CdSe Light and significantly less variable wrt No treatment highlighting unique variability characteristics ((Figure 7.5, box 2). There were a number of global regulators highlighted through analysis ((Figure 7.5, boxed in turquoise), *crp* a cAMP receptor protein and general regulator, *fis*

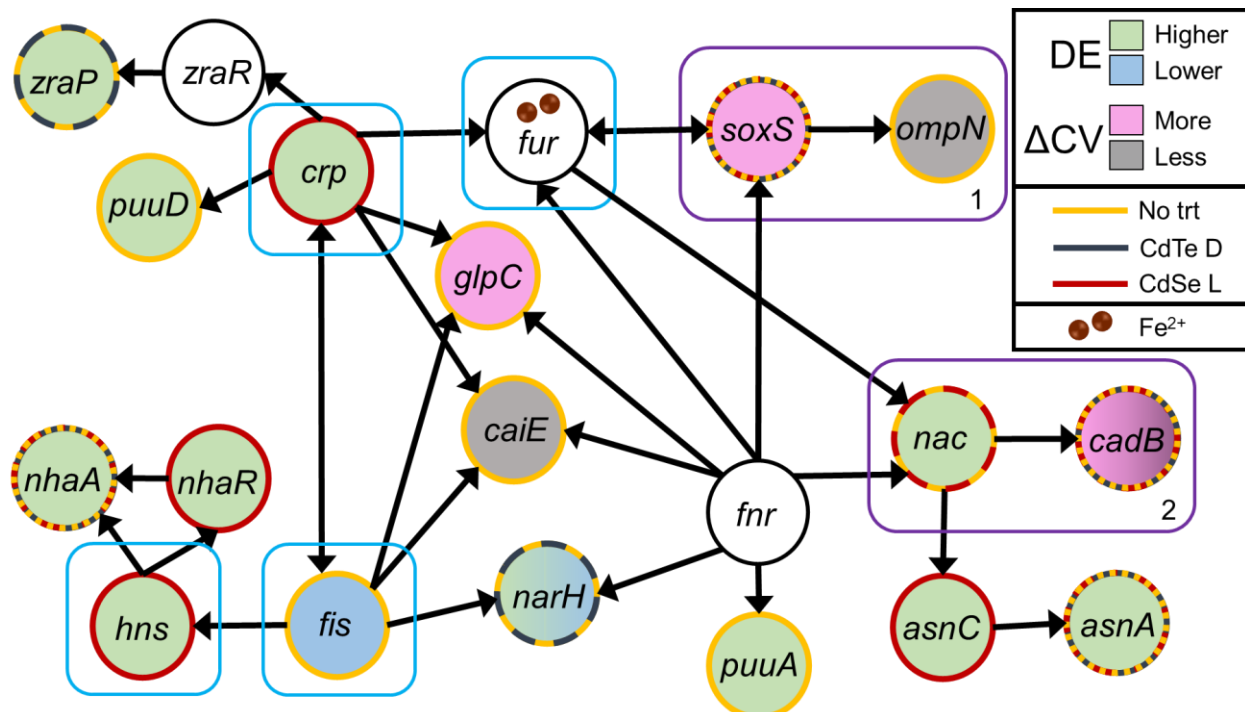


Figure 7.5 Network of genes with differential or significantly changed variability in expression with CdTe Light. Subset of genes to demonstrate connectivity and expression relationships in CdTe Light wrt treatment is shown by outline code. Genes with no color were not significantly DE or changed in variability in CdTe Light. Genes with color are coded by their expression: DE higher expression (green), DE lower expression (blue), and significantly more (pink) and less (grey) variable. Arrows indicate the direction of regulation and only direct regulation was considered. We highlight two relationships in box 1 and 2 showing that while regulator *soxS* was more variable in CdTe Light, downstream gene *ompN* was less variable and conversely *nac* was DE higher in CdTe Light and resulted in more variable expression of downstream *cadB*. We further use turquoise boxes to highlight major transcription factors involved in the network and demonstrate the high connectivity between observed gene expression changes. Regulatory relationships were used from Eco Cyc Regulatory Overview tool^{46,47}.

inversion stimulation factor and regulator of rRNA, tRNA, and other genes, *hns* which regulates two fimbrial operons and other genes, and *fur* for iron regulation and pH sensing²⁷. We include *fur* even though it did not have altered expression in our study because it is activated post-transcriptionally by the binding of two ferrous iron ions²⁸ which would be present in an increased free iron pool resulting superoxide stress from disruption of bacterial iron clusters²⁹. The large regulatory footprint of the regulators is demonstrated by their number of direct regulatees: *crp* 197, *fis* 76, *hns* 24, and *fur* 21 genes.

7.4 Conclusions

Throughout analysis of DE genes and significant changes to gene variability, a number of trends arose. Throughout our analysis, we observed changes to nitrogen metabolism. Asparagine synthetase gene, *asnA*, was one of two genes with significantly higher expression in CdTe Light wrt no treatment, CdTe Dark, and CdSe Light. Additionally, nitrogen assimilation regulator, *nac*, was differentially upregulated in CdTe Light wrt no treatment and CdSe Light. NAC activates operons to supply *E. coli* with ammonium, the nitrogen source in our minimal media, or glutamate. Furthermore, *amtB*, encoding an ammonium transporter was upregulated in CdTe Light compared to no treatment. It has been shown that supplementation of media with amino acids protects bacteria from oxidative stress³⁰. These trends together indicate possibly an increase in amino acid production which is linked to stress response via protein degradation repair, potentially from hydroxyl radical damage, or requirement of amino acids to synthesize protection proteins^{31,32}. In the same vein, *lpp*, which encodes murein lipoprotein had increased expression in CdTe Light wrt CdSe Light and more variability in CdTe Light wrt no treatment and CdSe Light possibly indicating a lipid repair mechanism in response to hydroxyl damage or as a mechanism to reduce permeability of the cell membrane to prevent transport of toxins into the cell³³.

Interestingly *asnA* was also significantly upregulated during bactericidal antibiotic killing, which was attributed to ROS-mediated toxicity²⁰. It was also shown that *Mycobacterium tuberculosis* mutants lacking *asnA* are ultimately attenuated in macrophages and mice³⁴. Further links suggest the balance of asparagine, tryptophan, and arginine amino acids may be important in host-pathogen interactions³⁵. These findings indicate new avenues for rationally designed antibiotics. Since amino acids are vital for the host and pathogen, targeting proteins which utilize these compounds would be difficult to distinguish between host and pathogen effects. Therefore depleting genes in bacteria for amino acid utilization with sequence-specific antibiotics like those shown in Chapters 3 and 4 could be useful in understanding and disrupting this unique interface.

Furthermore, nitrogen metabolism genes were differentially upregulated in the *narGHIJ* pathway in CdTe Light compared to no treatment and CdTe Dark. This pathway is repressed by oxygen and is usually only expressed in anaerobic or nitrate-rich conditions³⁶, the media used in this study does not have nitrate. While we were not cultured in anaerobic conditions, it is reasonable that molecular oxygen was limited intracellularly because it is used as an electron acceptor for CdTe-2.4 superoxide generation potentially depleting it for metabolic use and normal aerobic metabolism. Altered expression of the *nar*, *cai*, and *fix* operons could be indicative of *E. coli* trying to generate alternate electron acceptors for metabolism.

We also observed a number of gene expression changes related to motility. We observed differentially lower expression of *fliZ* in CdTe Light wrt to CdSe Light. Additionally, *flxA* was DE lower in CdTe Light wrt no treatment and had significantly higher variability in CdTe Light wrt no treatment, CdTe Dark, and CdSe Light. High variability was also observed in CdTe Light for *fliZCDSTFHJOP* wrt CdTe Dark, *fliZACDSTFHJKOP* wrt CdSe Light, and *fliFP* wrt no treatment. Further, high variability was also observed in *flgNCFHKL* wrt CdSe Light and *flgCFKL*

wrt CdTe Dark. *motB* was additionally more variable in CdTe Light wrt no treatment, CdTe Dark, and CdSe Light. This large degree of gene expression changes seen in motility can be explained by two different possible mechanisms: cellular efforts for energy or protein conservation to mitigate oxidative stress or cross-protection behavior, as demonstrated by motility changes under high pH conditions^{18,37}. In previous adaptation studies to low levels of activated CdTe-2.4 performed in our lab, we have observed a tolerant mutant state arising from a loss of function mutation in *hdfR*³⁸, a regulator of the flhDC flagellar class II operon. This adapted mutant was shown to have an increased NADPH/NADP+ ratio providing energy conservation and an increase in possible antioxidant activity by NADPH³⁹.

We additionally measured altered expression of genes generally thought to have changed expression under pH stress⁴⁰ such as significantly higher expression of *alx* in CdTe Light wrt no treatment but not DE in CdTe Dark wrt no treatment (Fig. 1b) and higher *nhaA* expression in CdTe Light wrt no treatment, CdTe Dark, and CdSe Light (Fig. 1c) both corresponding to high pH stress. Interestingly, high pH stress response has been shown to be similar to heat shock, the SOS response, and the CpxP envelope stress response¹⁸. Correspondingly, we also observed higher expression in CdTe Light wrt to CdTe Dark and no treatment and high variability in CdTe Light wrt to CdTe Dark and CdSe Light for *ipbB*, a small heat shock protein, possibly further evidence of the strong link between oxidative, pH, and heat stress. *ipbB* was also upregulated during ampicillin antibiotic treatment³³ which has been shown to function, in part, by ROS mediated activity²⁰.

In conclusion, in this study we aimed to differentiate the response of *E. coli* to activated CdTe-2.4 quantum dots from their unactivated counterpart. We compared this response to that of light activated and unactivated, non-toxic CdSe-2.4 quantum dots. We demonstrate significantly

higher variability in gene expression in response to superoxide stress shown by high expression variability between activated and non-activated CdTe-2.4 treatment compared to activated and non-activated CdSe-2.4. Additionally, we find that genes with altered expression or variability are related to amino acid abundance, likely for protection or protein repair, induced anaerobic metabolism, and altered expression high pH and heat shock associated genes. Further studies need to be conducted to determine if the altered variability in gene expression is directly related to adaptation. Possible gene targets for investigating the impact of more variable genes are the 25 genes that were significantly more variable in CdTe Light wrt no treatment, CdTe Dark, and CdSe Light (Figure 7.4). There were a number of genes with unknown function potentially suggesting they have been overlooked previously due to high variability and lack of differential expression. These results outline the response to activated superoxide generation, removing materials effects, and suggest possible targets for future studies to develop a deeper understanding oxidative stress and its toxic mechanism.

7.5 Materials and Methods

7.5.1 Quantum dot synthesis

Cadmium telluride and cadmium selenide dots were synthesized following methods in Courtney et al. 2016⁵. Particles were synthesized steriley and filtered prior to use in studies. Particles were filtered using 3 kDa Pall Nanosep devices that were first sterilized, following manufacturer's instructions, with 70% ethanol. Dots were stored at pH≥11 for stability.

7.5.2 RNA extraction cell growth conditions

Escherichia coli MG1655 (ATCC700926) was plated streaked from freezer stock onto lysogeny broth, agar plates (2% LB, 1.5% agar). Two individual colonies were selected and grown

overnight in M9 minimum medium (1x M9 minimal media salts solution (MP Biomedicals), 2.0 mM MgSO₄, 0.1 mM CaCl₂, and 0.4% glucose). Cells were then diluted 1:100 into fresh M9 with respective treatment/illumination. Nanoparticle concentration was held at 10 nM for both CdSe and CdTe. The conditions, collected in biological duplicates, were as follows: No trt, 10 nM CdTe-2.4 with illumination, 10 nM CdTe-2.4 in dark, 10 nM CdSe-2.4 with illumination, and 10 nM CdSe-2.4 in dark. The cells were treated for 5 h after which the OD was 0.3-0.6 and 1 mL of culture was pelleted by centrifugation at 4,000 rpm for 10 min.

7.5.3 Electron paramagnetic resonance (EPR) spectroscopy.

CdTe and CdSe quantum dot samples filtered as described above prior to spectroscopy. 100 uL aliquots of respective quantum dot were mixed with 1 uL of the spin trapping agent DMPO (Dojindo) and wrapped in foil to eliminate exposure to light. Three quartz capillaries were filled with the quantum dot, DMPO mixture and measured in a Bruker Elexsys E 500 spectrometer (SHQE resonator) using a microwave attenuation of 16 dB, power of 5W, and operated in a dark room. After tuning the machine, a measurement was taken in dark and subtracted from post-illumination spectra. This protocol eliminated the minimal effects of ambient light exposure and the omnipresent SiO₂ E'. The sample was then exposed to 60 seconds of white light (9 mW/cm²) and immediately remeasured. Both dark and light measurements consisted of 10 consecutive scans (20.48 s each) over a range of 200 G (0.05 G resolution) centered on 3515 G. Presence of DMPO adducts was confirmed using Bruker's SpinFit software to fit measured spectra to the following parameters: DMPO-OH: a_n= 14.90 G and a_{ii}^b= 14.93 G, DMPO-OOH: a_n= 14.2 G, a_{ii}^b= 11.4 G, and a_{ii}^{g1}=1.2 G.

7.5.4 EPR to determine ROS concentration

Quantification of ROS present from the EPR spectra was done using SpinFit (Bruker). Dark spectra were subtracted from those after illumination, and the resulting spectra were fitted to the parameters detailed above. With the EPR software, the spectra were then double integrated to yield a count of spins detected from DMPO-ROS adducts. Radical concentrations were then calculated using the known active volume consistent across all samples.

7.5.5 RNA sample prep.

Cell pellets described above were treated with Qiagen RNAProtect and flash frozen in a dry ice, ethanol bath for storage at -80C. RNA was then extracted using Thermo Scientific GeneJET RNA Purification Kit. The RNA was then treated with Thermo Scientific TURBO DNA-free kit following the rigorous digestion protocol. Library preparation of the 10 samples (two biological replicates of 5 conditions) was done according to Shishkin et al⁹ with barcodes shown in Table 7.3. Sequencing was performed as 1x50, stranded, on 3 lanes in an Illumina HiSeq at the BioFrontiers Next Generation Sequencing facility at the University of Colorado Boulder (Table 7.4).

7.5.6 RNA-seq data processing

All data processing was done with resources on the University of Colorado BioFrontiers Institute computing core. The three lanes were demultiplexed individually using fastq-multx in ea-utils v1.1.2⁴¹ (Table 7.5) and then trimmed using TRIMOMATIC v0.32⁴². Trimmomatic was run to trim/remove reads for Illumina adapters, quality, and minimum length. Reads were trimmed to remove leading or trailing low quality (below quality 3) or “N” bases and further a 4-bp sliding window was used with trimming occurring when the average quality per base dropped below 15. Reads were also removed if the length was <25 bp. Trimmomatic results are shown in Table 7.6.

The sample files from the three lanes were then merged to obtain 10 fastq files, one for each sample. The fastq files were then run through Rockhopper^{43,44} to determine the rRNA which was 3-4% for each sample showing high rRNA depletion during library prep. The fastq files were then aligned using Bowtie2 v2.2.3⁴⁵ to *Escherichia coli* MG1655 index (Escherichia_coli_str_k_12_substr_mg1655.GCA_000005845.2.30 from NCBI) with sensitive settings. Results of alignment are shown in Table 7.7. We then generated bam files from the Bowtie2 sam files using samtools v0.1.18. We then used htseq-count v0.6.1¹¹ to generate count tables for the 10 samples. Count tables were merged into one text file and differential expression analysis between conditions, using pooled replicates, was performed using DESeq v3.4¹².

7.6 Supplementary Information

7.6.1 Supplementary tables

Table 7.3 Barcodes used for multiplexing of samples.

Sample #	Sample Name	Barcode #	Barcode Seq
1	No trt 1	RNA5	ACCTGAT
2	No trt 2	RNA15	ATGCTCT
3	CdTe-2.4 L1	RNA21	CAGCTTT
4	CdTe-2.4 L2	RNA22	CCAGTCT
5	CdTe-2.4 D1	RNA27	CCTTAGT
6	CdTe-2.4 D2	RNA33	GGCAACT
7	CdSe-2.4 L1	RNA37	TTTGCT
8	CdSe-2.4 L2	RNA38	TAATCAT
9	CdSe-2.4 D1	RNA49	TGACATT
10	CdSe-2.4 D2	RNA53	TTCCCGT

Table 7.4 Run statistics for HiSeq sequencing of RNA samples. The 3 lanes contained the same library of multiplexed samples.

Lane	Yield (Mbases)	% PF	# Reads	% of >= Q30 Bases (PF)	Mean Quality (PF)	Score
3	6,533	100	128,088,415	88.8	35.73	
4	6,567	100	128,765,639	89.01	35.81	
5	6,293	100	123,397,070	88.56	35.7	

Table 7.5 Demultiplexing results.

Sample #	Sample Name	Lane 3	Lane 4	Lane 5	# reads per sample (millions)
1	No trt 1	6,860,424	6,883,347	6,264,888	20.0
2	No trt 2	8,143,522	8,041,316	7,666,731	23.9
3	CdTe-2.4 L1	8,408,816	8,233,336	8,019,770	24.7
4	CdTe-2.4 L2	8,766,447	8,664,717	8,113,537	25.5
5	CdTe-2.4 D1	10,699,036	10,738,819	9,911,969	31.3
6	CdTe-2.4 D2	9,689,110	9,726,608	9,057,189	28.5
7	CdSe-2.4 L1	8,156,986	8,046,894	7,375,464	23.6
8	CdSe-2.4 L2	12,958,195	12,812,001	12,215,854	38.0
9	CdSe-2.4 D1	13,850,320	13,758,053	12,983,134	40.6
10	CdSe-2.4 D2	7,825,475	7,845,098	7,374,061	23.0
Mismatched 26.6%		32,730,084	34,015,450	34,414,473	101.2

Table 7.6 Results of TRIMMOMATIC trimming for adapters, quality, and length.

Lane.sample #	Surviving %	Dropped %
3.1	98.62	1.38
3.2	98.59	1.41
3.3	98.53	1.47
3.4	98.76	1.24
3.5	98.64	1.36
3.6	98.86	1.14
3.7	98.49	1.51
3.8	98.93	1.07
3.9	98.79	1.21
3.10	98.63	1.37
4.1	98.76	1.24
4.2	98.71	1.29
4.3	98.66	1.34
4.4	98.85	1.15
4.5	98.75	1.25
4.6	98.96	1.04
4.7	98.65	1.35
4.8	99.04	0.96
4.9	98.92	1.08
4.10	98.78	1.22
5.1	98.68	1.32
5.2	98.71	1.29
5.3	98.6	1.4
5.4	98.83	1.17
5.5	98.71	1.29
5.6	98.97	1.03
5.7	98.57	1.43
5.8	99.01	0.99
5.9	98.89	1.11
5.10	98.74	1.26

Table 7.7 Results of alignment using Bowtie2.

Sample	# reads	% aligned 0 times	% aligned exactly 1 time	% aligned >1 times	Overall alignment rate
No trt 1	19,647,633	4.00	89.56	6.44	96.00
No trt 2	23,421,420	4.45	89.54	6.00	95.55
CdTe-2.4 L1	24,209,734	4.04	90.43	5.53	95.96
CdTe-2.4 L2	25,166,285	4.61	89.77	5.62	95.39
CdTe-2.4 D1	30,824,849	4.48	89.51	6.01	95.52
CdTe-2.4 D2	28,028,853	3.94	89.79	6.27	96.06
CdSe-2.4 L1	23,149,189	4.63	89.29	6.09	95.37
CdSe-2.4 L2	37,322,197	4.93	88.88	6.20	95.07
CdSe-2.4 D1	39,904,668	4.25	89.85	5.90	95.75
CdSe-2.4 D2	22,655,238	4.15	89.55	6.29	95.85

Table 7.8 Calculated differentially expressed genes and log2 fold change in expression, with 95% confidence interval.

CdTe Light wrt No trt		CdTe Dark wrt No trt				CdTe Light wrt CdTe Dark		CdTe Light wrt CdSe Light			
nhaA	1.301	aceE	-0.767	mepM	1.114	nhaA	0.928	nhaA	1.311	csiE	0.751
mmuP	1.535	aceF	-0.941	znuA	1.227	yafQ	0.739	nhaR	0.741	hcaT	0.730
mmuM	0.868	lpd	-0.631	znuC	0.742	betA	0.652	gluQ	0.686	hcaR	1.608
afuC	1.094	metI	1.086	zinT	2.022	codB	-0.627	gloB	0.729	srmB	-1.132
cyoD	-0.762	metN	1.574	yodB	0.967	appY	-0.798	ykfA	1.350	yfiE	-1.254
glnK	2.002	mmuP	1.337	shmA	-0.680	narH	-0.850	ecpD	0.697	yfiF	-0.789
amtB	1.637	afuC	0.938	cbl	1.113	narJ	-0.787	ecpC	0.838	trxC	-1.461
tomB	0.784	betA	-0.712	nac	1.431	pyrF	-0.645	ecpB	0.705	yfiP	-1.747
entD	-1.257	cyoE	-1.071	hisD	-1.670	ynfF	-0.770	ykgG	1.442	pka	-1.923
ybdH	0.949	cyoD	-1.110	hisB	-0.970	ynfG	-0.736	yahK	1.141	pssA	-2.057
ybdL	1.439	cyoC	-0.811	hisH	-0.582	ydhR	0.735	lon	0.599	yfiM	-2.226
ybdM	1.113	cyoB	-0.553	yohK	-0.943	astA	-0.881	acrB	-0.608	kgtP	-2.029
asnB	0.886	glnK	1.563	yeiE	-0.628	ynjD	-0.676	sfmD	-0.632	rffG	-2.461
pliG	1.362	amtB	1.535	yfaD	0.812	yodD	0.821	insF3	-1.761	rrlG	-2.362
narH	1.044	copA	-0.630	yfbS	-0.672	plaP	-0.627	renD	-1.458	gltW	-1.728
narJ	1.054	borD	0.661	argT	0.729	yeeY	0.629	emrE	-1.197	ratB	-0.699
narI	1.244	cusC	1.241	cysU	0.573	yfaD	-0.956	ybcK	-0.612	rnlA	-0.647
puuA	0.820	entH	-1.234	cysP	0.869	purM	-0.616	ybcH	0.681	rnlB	-0.593
puuD	1.002	cstA	-0.890	stpA	0.820	yfhR	-0.776	nagA	0.868	argQ	1.627
ddpA	1.133	ybdH	0.673	hycB	-1.156	raiA	0.855	nagB	0.916	mutH	1.068
ydfZ	1.925	ybdL	1.670	hycA	-1.000	hycE	-0.701	nagE	0.952	ygdQ	0.929
flxA	-1.055	ybdM	1.014	mazF	0.781	yhbE	-0.604	glnS	1.153	xdhC	0.929
mepM	1.073	sdhB	-0.613	yghG	1.220	fis	-0.641	chiP	0.644	speB	0.943
znuA	1.075	sucA	-0.940	pppA	0.845	yhjY	0.861	modA	0.843	yggR	0.827
nac	1.219	sucB	-0.640	hybO	-0.670	ibpB	1.554	glnQ	0.770	ygiV	0.895
argT	1.116	sucC	-0.629	yhbQ	-0.625	asnA	0.960	glnP	1.862	folB	0.677
yqaE	1.210	ybiO	0.690	yhbU	-1.400	zraP	1.205	macB	-0.603	yhbP	-0.613
hycB	-1.288	glnQ	1.039	yhdX	1.361	yjaB	-0.945	hspQ	0.904	lptA	0.976
alx	0.984	glnP	0.647	yhdY	1.392	psiE	0.694	lolD	0.979	mreB	-0.612
yhdX	1.026	yliE	0.926	rpsQ	-0.579	yjcC	0.944	hns	1.052	rpsM	-0.808
feoC	-0.971	yliF	0.923	rpmC	-0.570	mdtM	0.651	tdk	1.137	gspI	0.848

zntA	3.040	yliI	-0.612	feoB	-1.349			adhE	0.719	crp	0.767
tusA	2.544	dmsC	1.016	feoC	-0.861			ydaQ	0.678	yhfZ	0.951
yhjH	-1.204	ycbJ	-0.624	yhhX	-0.588			paaY	-2.237	yhhY	0.762
ibpB	1.609	elyC	-0.671	zntA	2.888			insD4	-2.684	yhjC	2.072
asnA	1.461	hyaD	0.720	tusA	2.426			insC4	-1.159	yhjD	1.331
metR	2.311	hyaE	0.828	yhhQ	1.001			ynbD	0.847	dfp	1.110
glnL	0.736	hyaF	0.689	nikA	-1.033			yddK	1.494	dut	2.260
yiiX	0.964	cbdB	0.578	nikE	0.800			hipB	0.948	gyrB	-1.453
metJ	1.336	narG	0.624	nikR	0.694			ynfH	0.777	recF	-2.657
metB	1.745	narH	1.890	mdtF	0.816			rnt	0.856	dnaN	-2.714
yjaH	1.045	narJ	1.837	lldD	-0.711			ydhW	2.728	dnaA	-1.139
zraP	2.281	narI	1.616	metR	1.333			ydhV	1.823	asnC	0.960
metA	1.877	yciW	0.585	glnG	0.936			ydhZ	1.038	asnA	1.283
yjcC	1.278	yncJ	0.769	glnL	0.826			pykF	1.078	viaA	1.308
pyrI	-0.822	bdm	-0.938	glnA	0.676			lpp	1.074	hemX	0.835
pyrB	-0.931	ddpB	1.065	fdoI	-0.746			ldtE	2.310	hemD	2.076
lgoT	-0.952	ddpA	1.016	fdoH	-0.601			sufE	0.978	yigB	1.513
ecnB	0.861	yddA	-1.083	sbp	1.230			ydiR	0.859	spf	1.295
		ydfZ	0.985	yiiX	0.603			manY	0.826	yihL	1.155
		ynfF	0.905	metJ	0.668			yobD	0.805	yihU	-2.277
		ynfG	0.834	metB	1.511			yebW	-0.598	malK	1.102
		ynfH	0.705	metF	1.446			yebE	2.654	yjbL	1.889
		dmsD	0.608	zraP	1.073			yebF	3.625	melR	1.297
		astD	1.190	metA	1.841			aspS	1.096	melA	1.032
		astA	1.811	nrfG	0.974			fliZ	-0.844	yjdF	0.755
		astC	1.554	crfC	-0.914			nac	0.867	yjfL	1.371
		ydjY	-1.437	frdB	-1.317			alkB	0.755	yjff	-0.660
		ynjC	0.715	pyrB	-0.578			ubiX	-0.694	idnD	0.861
		ynjD	1.004	fecB	-0.652			ypfJ	0.709		
		yeaG	0.783	fecA	-0.603						
		yeaH	1.000	yjjP	-0.859						
		yeaI	0.966								

Table 7.9 Additional calculated differentially expressed genes and log2 fold change in expression, with 95% confidence interval.

CdSe Light wrt No trt		CdSe Dark wrt No trt			CdTe Dark wrt CdSe Dark						CdSe Light wrt CdSe Dark				
yagJ	1.228	aceE	-1.134	insD6	1.054	nhaA	0.521	recE	0.503	pka	-1.588	aceE	1.057	yeiS	-0.849
ecpE	-0.650	aceF	-1.389	insC6	0.876	leuA	-0.357	racC	0.684	pssA	-1.653	aceF	1.156	yejL	0.440
ykgG	-0.874	lpd	-1.075	wcaN	-1.106	ilvI	-0.362	ompN	0.622	yfiM	-1.769	lpd	0.703	yejM	0.448
yajC	-0.869	acnB	-0.939	wcaM	-0.609	ilvH	-0.402	pfo	0.372	kgtP	-1.939	acnB	0.714	glpB	-0.475
secD	-0.883	cueO	-0.783	wcaG	-0.653	aceF	0.449	feaR	-1.024	rrfG	-1.983	cueO	0.767	nuoA	-0.622
secF	-0.588	gcd	-1.063	wcaC	-0.822	lpd	0.444	paaX	-0.532	rrlG	-1.901	gcd	0.721	ubiX	0.508
cyoD	1.257	ykfl	0.976	gatZ	0.727	acnB	0.587	paaY	-2.499	gltW	-1.752	gluQ	-0.552	purF	0.745
cyoC	1.189	ecpE	-1.700	fbaB	0.721	gcd	0.640	insD4	-2.707	rrsG	-0.745	ykfA	-0.672	nupC	-0.453
insE3	2.728	ecpD	-1.180	yehC	-0.788	fhuA	-0.384	insC4	-1.499	rluD	-0.584	perR	-0.469	gcvR	0.478
nohD	-0.703	ecpC	-0.957	sanA	1.030	dapD	-0.326	opgD	-0.768	bamD	-0.407	yagJ	0.942	hcaC	-1.158
envY	-0.821	ecpB	-0.835	yeiS	1.188	dinJ	0.366	ydcH	-0.920	ypjF	-0.388	ecpE	1.047	yphC	-0.978
ybeD	0.737	yajC	-2.014	yejM	-0.777	lafU	-0.394	rimL	-1.641	emrA	0.592	ecpD	0.806	yphD	-0.850
nagA	-0.784	secD	-2.214	gcvR	-0.737	ecpE	0.988	yddK	-0.597	hycH	0.518	ecpB	0.481	yphE	-0.909
nagB	-0.906	secF	-1.794	hyfH	1.127	ecpD	0.934	sad	-0.577	cysC	0.395	ykgG	-0.809	recN	0.718
nagE	-1.109	yajD	-1.370	hyfI	1.094	ecpC	0.881	yneJ	-0.569	yqeE	-0.399	secF	1.204	bamE	0.763
glnS	-1.307	tsx	-0.995	hcaC	1.639	ecpB	0.858	yneK	-0.584	gudD	-0.370	yajD	0.912	yfjM	0.914
chiP	-1.199	cyoD	1.777	srmB	0.947	yahK	0.920	ydfR	0.381	mutH	1.703	tsx	0.604	rnlA	0.825
chiQ	-0.801	cyoC	1.581	yfiE	0.738	yajC	0.942	essQ	0.392	ygdQ	0.675	acrB	0.644	scpA	-0.818
fur	-0.726	cyoA	-0.604	yfiF	1.093	secD	1.105	cspF	0.402	pbl	-0.377	tesA	-0.495	exbD	0.624
modF	1.062	acrB	-0.665	trxC	1.270	secF	0.983	ynfC	-0.428	insD8	-0.464	sfmC	-0.919	yqhD	0.627
modE	0.820	cysS	0.684	yfiP	1.979	yajD	0.817	uidB	-0.392	ygeQ	0.658	insE3	2.886	ftsP	0.782
acrZ	0.792	ybcI	1.046	pka	2.083	tsx	0.650	ydhI	0.493	xdhC	0.532	insF3	2.469	plsC	0.835
modA	-0.739	sfmC	1.054	pssA	2.089	ribD	0.426	valV	0.854	ygfF	-0.377	renD	2.295	parC	0.627

moaC	0.815	sfmD	0.626	yfiM	2.153	cyoA	0.409	valW	1.033	scpA	-0.893	emrE	1.730	mqsR	-0.466
moaD	0.658	insF3	-1.118	kgtP	1.583	sfmC	-0.447	ydhR	1.023	speA	-0.348	quuD	-1.233	agaD	0.515
smtA	0.922	renD	-1.519	rrfG	0.826	sfmD	-0.533	ydhW	2.379	exbB	-0.704	insH2	-1.353	agaI	0.536
mukF	0.886	emrE	-1.229	rllG	0.900	argU	0.627	ydhV	2.107	ftsP	0.452	nmpC	-1.076	yraH	0.607
mukE	0.840	ybeD	0.910	rluD	0.803	insE3	1.400	ydhY	0.608	ttdB	-0.352	essD	-1.179	yraI	0.530
mukB	0.842	metU	0.609	bamD	0.963	insF3	1.431	ydhZ	0.748	ygjP	0.376	ybcW	-0.502	yraJ	0.579
ldtD	0.987	glnW	0.636	raiA	0.929	renD	1.637	pykF	1.233	alx	1.010	nohD	-0.549	yraK	0.497
ycbK	0.762	nagC	-0.677	ypjC	0.702	emrE	1.508	lpp	1.471	yhaK	0.364	tafD	-1.060	yraR	0.652
ycbL	0.598	nagA	-0.915	ppdA	1.435	ybcK	0.417	ldtE	2.678	yhaB	0.951	ybcY	-1.057	yhbO	0.632
aspC	0.636	nagB	-1.094	thyA	1.085	ninE	0.604	sufE	1.035	ftsH	-0.580	tafX	-0.787	yhbP	0.581
rutA	-0.982	nagE	-1.783	mutH	-1.440	ybcO	0.533	ydiT	-0.397	mreB	-0.494	appY	-0.723	yhbQ	0.652
ymgC	1.153	glnS	-2.165	kduD	0.727	quuD	-1.314	ydiU	0.757	ileU	-0.379	ompT	-0.721	yhbS	0.567
ycgG	0.998	chiP	-1.727	scpC	-1.054	insH2	-1.516	ydiV	0.405	rpsN	2.046	envY	-0.696	yhbU	0.500
narJ	0.794	chiQ	-1.028	yqhA	-0.602	nmpC	-1.152	katE	-0.407	rplE	1.653	citC	0.722	yrbL	-1.016
oppA	-0.934	fur	-0.977	yqhD	-0.643	essD	-1.266	nadE	-0.365	rplIX	1.120	citA	0.516	mreB	0.398
paaY	2.016	fldA	-0.924	ftsP	-0.938	nohD	-0.465	cho	-0.335	rpsS	-1.181	nagE	0.671	yhdY	-0.768
insD4	2.675	valZ	-0.681	plsC	-0.881	tafD	-0.854	astC	0.561	rplB	-0.782	glnS	0.855	rplQ	0.459
insC4	1.652	galE	0.726	tdcA	1.286	ybcY	-0.965	yeaC	-0.422	rplW	-0.819	chiP	0.525	rpoA	0.585
ynbB	-1.272	modF	1.341	agaD	-0.660	tafX	-1.086	gapA	1.007	rplD	-0.620	ybgK	0.559	rpsD	0.594
rimL	-1.093	modE	1.033	agaI	-0.651	appY	-0.999	yeaD	1.266	gspA	-0.637	sucA	-0.540	rpsN	1.959
pqqL	-1.472	acrZ	0.747	yraH	-0.652	ompT	-1.046	yeaE	0.585	gspC	-0.675	galM	-1.056	rplE	1.504
lsrC	0.646	modA	-0.695	yraI	-0.617	envY	-0.763	mipA	0.673	gspJ	-0.419	moaC	-0.447	rplIX	0.810
sad	0.712	moaA	0.817	yraJ	-0.627	cusB	-0.388	manZ	0.443	gspK	0.402	glnH	-0.560	rpsS	-1.014
mdtK	-0.966	moaC	1.260	yraR	-0.676	citC	0.613	yebE	3.108	hofO	0.452	rhtA	-0.549	rplB	-1.102
ydhS	1.003	moaD	1.001	yhbO	-0.723	citA	0.662	yebF	3.784	yhhY	0.970	ybjL	-0.583	rplW	-1.220

ydhW	-3.816	ybjO	0.580	yhbP	-0.598	ybeD	-0.499	yebG	1.414	yhhZ	0.942	helD	0.606	rplD	-1.160
ydhV	-2.607	ltaE	-0.707	yhbQ	-0.665	ubiF	-0.376	purT	0.789	yrhA	0.642	opgG	-0.717	gspA	-1.021
ydhY	-0.927	smtA	0.806	ftsH	0.708	glnX	-0.382	cheY	1.395	ugpC	-0.359	phoQ	0.571	gspC	-0.874
ydhZ	-1.221	mukF	0.776	yrbL	0.853	metU	-0.399	tar	-0.406	ugpE	-0.381	ymgA	-1.087	slyD	-0.713
pykF	-1.000	mukE	0.888	mtgA	0.940	glnW	-0.419	fliA	-0.387	hdeD	0.461	ariR	-1.063	yhfK	0.591
ldtE	-2.684	mukB	0.954	yhdX	0.750	nagC	0.383	fliC	-0.438	yhjJ	-0.526	ymgC	-0.866	yhfY	0.745
sufE	-0.982	ldtD	1.130	yhdY	0.821	nagA	0.911	fliD	-0.371	yhjR	0.591	ycgM	-0.515	hofQ	0.560
sufS	-1.073	ycbK	0.873	rpsN	0.841	nagB	1.081	cobS	0.495	bcsE	0.553	ycgV	-0.738	yrhA	0.811
ydiE	0.763	ycbL	0.643	rplE	0.772	nagE	1.341	insC6	-0.620	yiaF	0.351	hns	0.593	pitA	-0.536
gapA	0.921	aspC	0.653	rpsS	0.903	glnS	1.552	yeeP	-0.511	yiaM	-0.485	ychE	0.798	selA	0.531
yeaD	1.158	ompF	0.691	rplB	1.329	chiP	0.787	flu	-0.466	yibG	-0.988	feaR	-0.986	yibA	0.429
yeaX	-0.888	rutA	-0.818	rplW	1.618	chiQ	0.389	yeeR	-0.499	waaG	0.445	opgD	-0.684	yibQ	0.523
tsaB	-1.627	flgL	-0.731	rplD	1.315	fldA	0.422	cpsB	0.495	gyrB	-0.909	ydcH	-0.947	dfp	-0.820
yoaA	-1.598	pepT	-0.734	gspB	1.067	ybfL	-0.395	wcaH	0.529	recF	-2.024	rimL	-1.654	gyrB	0.700
yoaB	-1.771	phoQ	-0.662	gspA	1.434	sucA	-0.567	wcaG	0.354	dnaN	-1.813	yddK	-1.154	recF	1.142
pabB	-1.580	ymgA	1.458	gspC	1.204	galM	-0.756	wcaF	-0.486	dnaA	-0.673	cspF	0.499	dnaN	1.180
nudL	-1.618	ariR	2.379	gspK	-0.739	modE	-0.386	wcaE	-1.240	pstB	-0.380	pntA	-0.524	dnaA	0.803
manZ	-0.674	ymgC	2.016	slyD	1.032	acrZ	-0.316	yegI	0.454	rbsD	-0.568	rsxA	-0.535	asnC	-0.600
yobD	-0.753	ycgG	1.449	argD	-0.806	modA	0.430	yegP	0.530	trpT	-0.410	lhr	-0.475	ilvL	-0.849
yebW	0.641	dhaR	1.038	pabA	-1.072	uvrB	-0.351	yehC	0.634	ilvD	0.451	gapA	0.813	ilvM	-1.074
holE	-1.427	ycgV	1.121	yhfY	-0.929	ybhK	-0.449	yohJ	-0.396	wzzE	0.445	yeaD	1.194	yihO	-1.412
yobB	-1.235	kdsA	-0.705	yhgF	0.554	moaA	-0.390	yohK	-0.673	hemD	0.920	purT	0.665	yihP	-1.277
yebE	-3.092	hns	-0.825	glgP	-0.655	moaC	-0.334	cdd	-0.910	rhtB	-0.495	cheY	1.327	yihR	-0.923
yebF	-3.816	ychE	-1.183	yhhZ	-1.130	ybhQ	0.414	sanA	-1.351	pldB	-0.559	fliZ	1.038	fpr	-0.834
yebG	-1.660	oppA	-1.405	yrhA	-1.353	bssR	-0.397	rtn	0.536	spf	0.570	fliA	0.663	yijF	-0.516

ruvA	-0.684	oppB	-0.756	pitA	0.567	dacC	-0.399	yejA	0.423	yihL	0.870	fliG	0.462	ppc	0.563
cheY	1.956	paaY	2.204	yiaL	0.932	potI	-0.347	yejB	0.356	yihM	-0.512	insD6	-0.917	yjbL	-0.613
motA	1.045	insD4	2.691	nepI	0.652	ybjO	-0.400	yejE	0.427	yihU	-1.954	insC6	-0.843	nrfE	-0.536
flhC	0.978	insC4	1.714	ivbL	1.015	macB	-0.420	rsuA	0.427	fpr	-1.156	yeeP	-0.741	nrfF	-0.824
purF	0.642	ynbB	-1.300	emrD	0.698	ycaN	0.403	ccmF	-0.431	glpX	-1.098	wcaN	1.128	nrfG	-0.739
cvpA	0.807	yncG	0.761	gyrB	0.663	ycaI	-0.428	ccmD	-0.433	metB	-0.417	wcaM	0.718	cadC	-0.715
folC	1.087	yddK	1.582	recF	1.278	ssuA	0.403	ccmC	-0.452	yijF	-0.380	wcaG	0.441	epmB	-0.506
hyfH	0.744	pqqL	-1.114	dnaN	1.213	hspQ	0.915	emrK	-0.323	gldA	-0.626	wcaE	-1.309	ppa	-1.078
hyfI	0.656	sad	1.152	dnaA	0.551	appA	-0.876	yfdE	-0.393	pflD	0.390	wcaC	0.456	sgcC	3.342
yphA	-0.700	yneJ	1.022	asnC	0.603	cspH	0.406	ypeC	0.404	ppc	-0.372	sanA	-1.078	fimC	0.484
srmB	0.853	yneK	0.834	viaA	1.589	rutD	-0.426	ligA	0.732	zraR	0.450				
yfiE	0.894	cspB	-0.703	kup	1.796	opgG	-0.968	cysU	0.583	rrlE	0.446				
yfiF	0.975	cspF	-0.710	rbsD	0.812	hinT	0.451	ucpA	0.524	malF	-0.400				
trxC	1.167	rsxA	0.659	ilvM	0.841	lpoB	0.542	murR	0.642	yjbJ	-0.441				
yfiP	1.755	ydhS	1.343	ilvD	-0.644	ldtC	-0.372	eutE	0.451	nrfE	-0.651				
pka	1.853	ydhT	1.474	yigB	2.041	mdf	-0.349	gcvR	0.759	nrfF	-0.765				
pssA	1.798	ydhX	-0.704	rhtB	0.636	ycfT	-0.339	bcp	0.465	nrfG	-0.769				
yfiM	1.930	ydhW	-3.815	yihL	-1.159	pepT	0.422	hyfE	-0.458	basR	-0.560				
kgtP	1.440	ydhV	-3.118	ompL	0.896	ymgA	-0.834	hyfI	-0.645	eptA	-0.499				
rrfG	1.175	ydhY	-1.182	yihO	1.334	ariR	-0.488	purN	-0.345	melR	1.329				
rrlG	1.363	ydhZ	-0.882	yihP	1.539	ymgD	1.081	yfgM	-0.404	melA	0.766				
recN	0.955	ldtE	-2.603	yihR	1.109	ycgM	-0.829	trmJ	0.476	epmB	-0.474				
bamE	0.740	sufE	-0.947	yihU	1.468	dhaR	-0.476	hcaC	-0.818	frdC	0.677				
ratB	0.807	yeaX	-0.768	kdgT	-0.637	ycgV	-0.620	yphB	-1.307	yjeM	-0.835				
ratA	0.992	yoaB	-1.437	cpxA	-0.605	ychF	-0.436	yphC	-1.153	tamB	0.820				

Table 7.10 Genes that were significantly more variable or less variable in the first listed condition compared to respective second condition in pair. Significance was determined if the difference in coefficient of variation between the two populations was more than 2 standard deviations outside the average CV for that comparison.

CdTe Light wrt No trt		CdTe Light wrt CdTe Dark			CdTe Light wrt CdSe Light			CdSe Light wrt CdSe Dark	
More	Less	More	More con't	Less	More	More con't	Less	More	Less
fixC	mokC	caiD	yhdU	yaal	caiD	hyfC	fixX	fixC	carB
yadK	caiE	caiT	yhdV	fixA	caiT	glnB		ppdD	yaau
yagE	rclA	araD	nirD	fixC	folA	yfjI		yadL	yahC
insF2	yahC	ppdD	yhfU	fixX	araD	yqaE		yadM	codB
ybbY	cynS	yadK	yhfX	yafQ	ppdD	nrdH		yafT	insD1
allD	mhpC	yadV	hofP	mmuM	yadK	srlA		rayT	tauA
ylbF	glnK	yafT	hofN	insB2	yadM	srlB		rclB	glnK
sfmC	hyi	rayT	feoA	paoA	yadV	hypC		ybbW	insF3
sfmZ	ybbW	phoE	insB5		cdaR	casA		rusA	ybcW
quuD	ninE	yagE	ugpB		yaeF	fucP		ybdO	nohD
cusF	rusA	paoD	hdeA		yafT	argA		ybeU	modA
cusB	fepA	rclB	yhjH		rayT	ygeG		ybfP	modB
citE	citF	rclR	yiaL		phoE	ygeH		ybfC	modC
citD	ybeT	insD1	yiaM		yagE	ygeI		ybhI	ybhA
pagP	ybfC	insF2	yiaO		yagH	scpB		ybhM	moaA
cspE	ybfD	insF3	sgbU		paoD	yghS		ssuA	moaB
acrZ	ybiX	ninE	ivbL		rclB	insD9		ymcE	moaD
ycaD	fiu	ybcO	ibpB		rclR	ttdA		opgC	moaE
yccE	cspD	nohD	yidB		insD1	ttdB		ymfM	dmsA
rutC	rutE	ybeR	yieL		insF2	ebgC		narH	dmsB
csgC	pgaD	insH4	bglG		glxR	ygiI		tpr	dmsC
ymgC	fhuE	ybgD	yihM		glxK	ygiJ		osmB	elfD
pspA	croE	bioD	yihQ		sfpH	yhaL		ycjP	rutC
ycjO	ymfR	ymcE	frvA		insF3	tdcD		ycjW	rutB

ynaE	iraM	insF4	rhaS		ninE	tdcB		kilR	ymfI
uspF	ycgZ	flgC	argC		ybcO	tdcR		ydaG	ariR
paaA	ycgY	flgF	argB		insH2	agaD		ydaS	yciI
patD	ycjN	flgK	yjbE		nohD	yhdU		ynaE	ycjO
ydcC	sieB	flgL	yjbF		ybeR	yhdV		paaA	ycjU
dosC	ompN	ycfT	yjbL		insH4	nirD		paaE	ralR
rzpQ	paaE	ymfJ	yjbM		ybgD	nirC		paaG	ydaT
hokD	paaI	ymfQ	soxS		bioD	yhfU		paaI	ddpX
relE	insI3	ycgZ	nrfC		cspH	yhfX		insI3	ydeR
flxA	ynbA	ariR	nrfD		ymcE	hofP		yncH	lsrB
ydfD	pptA	chaB	alsE		insF4	hofN		ydcC	tfaQ
uidC	ydeS	yciG	phnM		yceJ	feoA		ydeM	relB
ydhC	ydfO	ralR	yjcZ		flgN	insB5		ydfK	dicC
lpp	ydfR	sieB	yjdI		flgC	ugpB		ydfO	ynfE
astE	rem	ydaG	ghoS		flgF	hdeA		ynfN	ynfF
yeaI	ydfB	paaB	cadB		flgH	gadA		essQ	ynfG
yobF	ydhZ	paaI	yjfL		flgK	yhjH		ydhZ	ynfH
motB	ydiL	insI3	ulaB		flgL	yiaL		yeaI	dmsD
fliF	astC	sra	chpS		ycfT	yiaM		yeaR	ydhL
fliP	yoaG	safA	argI		xisE	yiaO		yedK	ydhW
zinT	torY	ydeQ	holC		ymfJ	sgbU		hisL	yoaG
psuG	wcaH	hipB	yjhI		ymfQ	yicN		wcaA	cheA
napD	yegJ	ydfO	yjiX		ycgZ	ivbL		wzb	motB
glpC	yegK	rem	tsr		ariR	ibpB		yehA	motA
yfbL	yegR	flxA	lgoT		chaB	yidB		yehE	cbl
yfcG	yehL	dicC	dgoA		yciG	yieL		ccmC	wcaB
yfdF	cirA	ydiL	ybdZ		ralR	bglG		elaD	rcnR
yffO	atoA	ydjO	ydaE		sieB	yihM		yfcR	psuK
yffQ	yfbM	ydjZ	ynfO		ydaG	yihQ		yfcS	yfcQ
yphC	yfbN	ydjJ	yehK		paaB	frvA		yfdN	eutP
yfjI	yfdN	yobF	ybfK		paal	rhaS		yfdE	ssrA

yfjJ	yfdT	torY	yciZ		insI3	argC		yfdY	alpA
ypjK	yfeK	cheZ	ydgU		sra	argB		yffN	casB
ypjF	eutJ	cheY	sgrT		safA	yjbE		yffQ	ygcW
gabP	hyfA	cheB	azuC		ydeQ	yjbF		eutE	ygeG
ygcG	pheL	cheR	ibsD		hipB	yjbL		eutS	gcvP
ppdA	nrdH	tap	ilvX		ydfO	yjbM		yfhR	cmtA
ygeG	nrdI	tar	ynbG		rem	soxS		mltF	hybB
ygeY	srlA	cheW	yoel		flxA	nrfC		yfjY	hybA
uacT	hycG	cheA	yohP		dicC	nrfD		yqaE	hybO
yqiH	ygeI	motB	yqeL		lpp	alsE		ygaV	yghW
ebgC	ygeW	motA	mgtL		ydiL	phnM		nrdH	insD9
yhaB	cmtB	fliZ			ydjO	yjcZ		srlA	higA
agaC	yghR	fliC			ydjZ	yjdI		ygcG	tdcR
yraI	ygjI	fliD			ydjI	ghoS		ppdA	yraH
yhcA	alx	fliS			ydjJ	cadB		yqeJ	yhcC
nirD	tdcR	fliT			yobF	yjfL		yqeK	yhdU
yhfL	yhaC	fliF			torY	ulaB		ygeH	yhdY
nikE	agaV	fliH			cheZ	chpS		ygeI	insB5
yhjH	yhbT	fliI			cheY	argI		idi	livJ
yhjR	insH18	fliJ			cheB	holC		endA	arsR
yiaB	yhdU	fliO			cheR	yjhI		yghD	lyxK
yiaK	yhdV	fliP			tap	nanC		ygiL	bglG
lyxK	yhdZ	cobS			tar	yjiX		yqiH	ilvL
sgbH	yhfU	wcaL			cheW	tsr		tdcB	sbp
yiaW	hofO	wcaC			cheA	lgoT		agaC	phnG
tnaC	insB5	wcaB			motB	dgoA		yhdJ	yjfL
yigG	yiaM	yegL			motA	ybdZ		bfd	chpS
frvX	sgbU	yehL			fliZ	ydaE		hofN	insI4
frwB	yiaV	ccmD			fliA	ynfO		yhhZ	yjhI
yjbF	yihR	napB			fliC	yehK		yiaL	ybdD
soxS	kdgT	yfbL			fliD	yjhX		yiaM	ydaF

nrfC	yjbE	yfbM			fliS	ybfK		yiaW	ydgU
nrfD	yjbL	yfcR			fliT	yciZ		yigF	ytcA
nrfF	yjbM	yfcV			fliF	ydgU		yigG	sgrT
phnM	phnH	yfdR			fliH	sgrT		yiiF	ykgR
ghoS	phnD	yffN			fliI	azuC		frvA	yqcG
bsmA	cadB	yffQ			fliJ	ibsD		fsaB	
yjgN	ulaC	eutM			fliK	ilvX		frwB	
idnK	yjiY	eutT			fliO	ynbG		argC	
yjiX	frlC	eutQ			fliP	yoel		arpA	
lgoT	kdpF	eutP			cobS	yohP		nrfF	
glcE	gnsA	hyfC			wcaL	yqeL		phnM	
ymiA	yneM	glnB			wcaC	mgtL		phnJ	
ynfO	psaA	yfjI			wcaB			phnH	
yehK	ibsA	yqaE			yegL			phnF	
ytcA	yohP	srlA			yehL			yjfI	
ykgR	yqeL	srlB			yehP			ulaA	
ymiB		hypC			ccmD			yjfZ	
yoaK		casA			napB			idnK	
yqfG		fucP			yfbL			fimA	
shoB		argA			yfbM			fimC	
		ygeG			yfbN			fimD	
		ygeI			yfcR			fimF	
		yghS			yfcV			fimG	
		insD9			yfdR			yjiH	
		ttdA			oxc			yaeP	
		ttdB			yfdX			ylcG	
		ebgC			yffN			yciX	
		ygjI			yffP			yecJ	
		ygjJ			yffQ			ymgJ	
		yhaL			eutN			yjbS	
		tdcD			eutM			yoel	

		tdcB			eutT			yqeL	
		tdcR			eutQ			yqfG	
		agaD			eutP			shoB	

7.7 Author Contributions

M.L. collected EPR spectra, S.M.G., M.L., and C.M.C. synthesized nanoparticles, and K.E.E. advised on bioinformatic analysis. C.M.C. performed all other experiments and RNA-seq data processing and analysis

7.8 References

1. Kim, J. S., Kuk, E., Yu, K. N., *et al.* Antimicrobial effects of silver nanoparticles. *Nanomedicine Nanotechnology, Biol. Med.* **3**, 95–101 (2007).
2. Hetrick, E. M., Shin, J. H., Paul, H. S. & Schoenfisch, M. H. Anti-biofilm efficacy of nitric oxide-releasing silica nanoparticles. *Biomaterials* **30**, 2782–2789 (2009).
3. Jin, T., Sun, D., Su, J. Y., Zhang, H. & Sue, H.-J. Antimicrobial efficacy of zinc oxide quantum dots against Listeria monocytogenes, Salmonella Enteritidis, and Escherichia coli O157:H7. *J. Food Sci.* **74**, M46–52 (2009).
4. Hajipour, M. J., Fromm, K. M., Ashkarraan, A. A., *et al.* Antibacterial properties of nanoparticles. *Trends Biotechnol.* **30**, 499–511 (2012).
5. Courtney, C. M., Goodman, S. M., McDaniel, J. a., *et al.* Photoexcited quantum dots for killing multidrug-resistant bacteria. *Nat. Mater.* **15**, 485–588 (2016).
6. Courtney, C. M., Goodman, S. M., Nagy, T., *et al.* Potentiating antibiotics in drug-resistant clinical isolates via stimuli-activated superoxide generation. *Submitted*
7. Simon, D. F., Domingos, R. F., Hauser, C., *et al.* Transcriptome Sequencing (RNA-seq) Analysis of the Effects of Metal Nanoparticle Exposure on the Transcriptome of Chlamydomonas reinhardtii. *Appl. Environ. Microbiol.* **79**, 4774–4785 (2013).
8. Monrás, J. P., Collao, B., Molina-quiroz, R. C., *et al.* Microarray analysis of the Escherichia coli response to CdTe-GSH Quantum Dots: understanding the bacterial toxicity of semiconductor nanoparticles. *BMC Genomics* **15**, 1–13 (2014).
9. Shishkin, A. a, Giannoukos, G., Kucukural, A., *et al.* Simultaneous generation of many RNA-seq libraries in a single reaction. *Nat. Methods* **12**, 323–325 (2015).
10. Haas, B. J., Chin, M., Nusbaum, C., Birren, B. W. & Livny, J. How deep is deep enough for RNA-Seq profiling of bacterial transcriptomes? *BMC Genomics* **13**, 734 (2012).
11. Anders, S., Pyl, P. T. & Huber, W. HTSeq-A Python framework to work with high-throughput sequencing data. *Bioinformatics* **31**, 166–169 (2015).

12. Anders, S., Huber, W., Nagalakshmi, U., *et al.* Differential expression analysis for sequence count data. *Genome Biol.* **11**, 1–12 (2010).
13. Huang, D. W., Lempicki, R. a & Sherman, B. T. Systematic and integrative analysis of large gene lists using DAVID bioinformatics resources. *Nat. Protoc.* **4**, 44–57 (2009).
14. Thomas, P. D., Campbell, M. J., Kejariwal, A., Mi, H. & Karlak, B. PANTHER: A Library of Protein Families and Subfamilies Indexed by Function. *Genome Res.* **13**, 2129–2141 (2003).
15. Finkel, S. E. & Johnson, R. C. The Fis protein: it's not just for DNA inversion anymore. *Mol. Microbiol.* **6**, 3257–3265 (1992).
16. Brondsted, L. & Atlung, T. Effect of growth conditions on expression of the acid phosphatase (cyx- appA) operon and the appY gene, which encodes a transcriptional activator of *Escherichia coli*. *J. Bacteriol.* **178**, 1556–1564 (1996).
17. Baatout, S., De Boever, P. & Mergeay, M. Physiological changes induced in four bacterial strains following oxidative stress. *Appl. Biochem. Microbiol.* **42**, 369–377 (2006).
18. Maurer, L. M., Yohannes, E., Bondurant, S. S., Radmacher, M. & Slonczewski, J. L. pH Regulates Genes for Flagellar Motility, Catabolism, and Oxidative Stress in *Escherichia coli* K-12. *J. Bacteriol.* **187**, 304–319 (2005).
19. Kolodkin-Gal, I., Hazan, R., Gaathon, A., Carmeli, S. & Engelberg-Kulka, H. A linear pentapeptide is a quorum-sensing factor required for mazEF-mediated cell death in *Escherichia coli*. *Science* **318**, 652–655 (2007).
20. Kohanski, M. a., Dwyer, D. J., Hayete, B., Lawrence, C. a. & Collins, J. J. A Common Mechanism of Cellular Death Induced by Bactericidal Antibiotics. *Cell* **130**, 797–810 (2007).
21. Muse, W. B. & Bender, R. A. The nac (Nitrogen Assimilation Control) Gene from *Escherichia coli*. *J. Bacteriol.* **180**, 1166–1173 (1998).
22. Zheng, M., Wang, X., Templeton, L. J., *et al.* DNA Microarray-Mediated Transcriptional Profiling of the *Escherichia coli* Response to Hydrogen Peroxide. *J. Bacteriol.* **183**, 4562–4570 (2001).
23. Courtney, C. M. & Chatterjee, A. Sequence-Specific Peptide Nucleic Acid-Based Antisense Inhibitors of TEM-1 β -Lactamase and Mechanism of Adaptive Resistance. *ACS Infect. Dis.* **1**, 253–263 (2015).
24. Erickson, K. E., Otoupal, P. B. & Chatterjee, A. Gene Expression Variability Underlies Adaptive Resistance in Phenotypically Heterogeneous Bacterial Populations. *ACS Infect. Dis.* **1**, 555–567 (2016).
25. Sánchez-Romero, M. A. & Casadesús, J. Contribution of phenotypic heterogeneity to adaptive antibiotic resistance. *Proc. Natl. Acad. Sci. U. S. A.* **111**, 355–60 (2014).
26. Wu, J. & Weiss, B. Two-stage induction of the soxRS (superoxide response) regulon of *Escherichia coli*. *J. Bacteriol.* **174**, 3915–3920 (1992).
27. Babu, M. M. & Teichmann, S. A. Evolution of transcription factors and the gene regulatory network in *Escherichia coli*. *Nucleic Acids Res.* **31**, 1234–1244 (2003).

28. Troxell, B. & Hassan, H. M. Transcriptional regulation by Ferric Uptake Regulator (Fur) in pathogenic bacteria. *Front. Cell. Infect. Microbiol.* **3**, 59 (2013).
29. Keyer, K. & Imlay, J. Superoxide accelerates DNA damage by elevating free-iron levels. *Proc. Natl. Acad. Sci. U. S. A.* **93**, 13635–13640 (1996).
30. Boehm, D. E. Oxygen and toxicity inhibition of amino acid biosynthesis. *Nature* **262**, 418–420 (1976).
31. Jozefczuk, S., Klie, S., Catchpole, G., *et al.* Metabolomic and transcriptomic stress response of Escherichia coli. *Mol. Syst. Biol.* **6**, 364 (2010).
32. Bearson, B. L., Lee, I. S. & Casey, T. A. Escherichia coli O157 : H7 glutamate- and arginine-dependent acid-resistance systems protect against oxidative stress during extreme acid challenge. *Microbiology* **155**, 805–812 (2009).
33. Kaldalu, N., Mei, R. & Lewis, K. Killing by Ampicillin and Ofloxacin Induces Overlapping Changes in Escherichia coli Transcription Profile. *Antimicrob. Agents Chemother.* **48**, 890–896 (2004).
34. Gouzy, A., Larrouy-Maumus, G., Bottai, D., *et al.* Mycobacterium tuberculosis Exploits Asparagine to Assimilate Nitrogen and Resist Acid Stress during Infection. *PLoS Pathog.* **10**, (2014).
35. Olive, A. J. & Sassetti, C. M. Metabolic crosstalk between host and pathogen: sensing, adapting and competing. *Nat. Rev. Microbiol.* **14**, 221–234 (2016).
36. Bonnefoy, V. & Demoss, J. A. Nitrate reductases in Escherichia coli. *Antonie Van Leeuwenhoek* **47**–56 (1994).
37. Dragosits, M., Mozhayskiy, V., Quinones-Soto, S., Park, J. & Tagkopoulos, I. Evolutionary potential, cross-stress behavior and the genetic basis of acquired stress resistance in Escherichia coli. *Mol. Syst. Biol.* **9**, 1–13 (2013).
38. Reynolds, T. S., Courtney, C. M., Erickson, K. E., *et al.* ROS Mediated Selection for Increased NADPH Availability in Escherichia coli. *Submitted*
39. Kirsch, M. & de Groot, H. NAD(P)H, a directly operating antioxidant? *Faseb J.* **15**, 1569–1574 (2001).
40. Shimizu, K. Regulation Systems of Bacteria such as Escherichia coli in Response to Nutrient Limitation and Environmental Stresses. *Metabolites* **4**, 1–35 (2013).
41. Aronesty, E. Comparison of Sequencing Utility Programs. *Open Bioinforma. J.* **7**, 1–8 (2013).
42. Bolger, A. M., Lohse, M., Usadel, B., *et al.* Trimmomatic: A flexible trimmer for Illumina sequence data. *Bioinformatics* **30**, 2114–2120 (2014).
43. Tjaden, B. De novo assembly of bacterial transcriptomes from RNA-seq data. *Genome Biol.* **16**, 1 (2015).
44. McClure, R., Balasubramanian, D., Sun, Y., *et al.* Computational analysis of bacterial RNA-Seq data. *Nucleic Acids Res.* **41**, 1–16 (2013).
45. Langmead, B., Trapnell, C., Pop, M. & Salzberg, S. Ultrafast and memory-efficient

- alignment of short DNA sequences to the human genome. *Genome Biol.* **10**, (2009).
46. Salgado, H., Santos-Zavaleta, A., Gama-Castro, S., *et al.* The comprehensive updated regulatory network of Escherichia coli K-12. *BMC Bioinformatics* **7**, 5 (2006).
47. Keseler, I. M., Mackie, A., Peralta-Gil, M., *et al.* EcoCyc: Fusing model organism databases with systems biology. *Nucleic Acids Res.* **41**, 605–612 (2013).

Chapter 8

Conclusions and Future Directions

8.1 Summary of key findings

The inherent ability of bacteria to develop antibiotic resistance and the lack of new antibiotics has led to the current antibiotic resistance crisis. We are fast approaching the post-antibiotic era of medicine if nothing is done to combat the problem. In this work, we show efforts focused on the rational design of antibiotics for mitigation of the already pervasive antibiotic resistant bacteria. We directly applied the two technologies investigated in this work, antisense RNA-inhibitors and superoxide generating nanoparticles, to multidrug-resistant (MDR) clinical isolates and demonstrated their individual efficacy and combinatorial activity with small-molecule antibiotics as potentiators and adjuvants. Our key findings of this work are:

1. The rational design of antibiotics allows for expansion of the antibiotic arsenal to include targets in non-traditional antibiotic pathways
2. Rationally designed antibiotics can act as potentiators and adjuvants in combination with small-molecule antibiotics, combining traditional and non-traditional antibiotic target pathways
3. Predictive homology allows for design of sequence-specific, broad-pathogen antisense antibiotics
4. Nanoparticles can be tuned for specific production of superoxide and the flux is controllable with concentration and illumination intensity
5. Superoxide generation potentiates both bacteriostatic and bactericidal antibiotics

6. Low-level nanoparticle superoxide generation causes transcriptome-wide gene expression variability and specifically changes expression related to amino acid synthesis, nitrogen and anaerobic metabolism, and stress response

8.2 Thesis Conclusions

Antisense RNA-inhibitors have a number of advantages for use as antimicrobials. The sequence specificity allows not only for ease of design against any gene of interest but also for potential alleviation of detrimental side effects from broad-range activity. In this work, we used peptide nucleic acid (PNA) RNA-inhibitors to target resistance-conferring gene TEM-1 β -lactamase (Chapter 3) and essential genes across six different bacterial pathways (Chapter 4). Four of these PNA were designed in non-traditional antibiotic pathways to investigate circumvention of the already pervasive antibiotic resistance mechanisms in the clinical isolates tested. We showed that PNA re-sensitized drug-resistant *Escherichia coli* by targeting TEM-1 β -lactamase and studied the mechanism of resistance to this combination. We further designed a set of six PNAs for essential genes in *E. coli* four of which have predicted homology in *Klebsiella pneumoniae* and *Salmonella enterica*. While we designed the PNA with predictive homology to drug-sensitive, non-pathogenic bacterial genomes, we tested the efficacy of the PNA against MDR clinical isolates. We found that 54% of predicted targets and respective PNA were effective at significantly inhibiting bacterial growth and further that the antisense PNA demonstrated adjuvant or potentiator activity with small-molecule antibiotics.

As a second inquisition for rationally design therapeutics, we focused on engineering a controllable, superoxide generating nanoparticle. We focused on the material design and efficacy of the nanoparticle as a monotherapy (Chapter 5) as well as its behavior as a potentiator in combination with small molecule antibiotics against MDR clinical isolates (Chapter 6). We

demonstrated that the superoxide antibacterial effect is specific to the tuned energy properties of our designed nanoparticle and not material effects. We further showed that the degree of antibacterial activity can be controlled with concentration or light-flux dependence. The designed superoxide generating nanoparticle potentiated antibiotic activity in clinical isolates despite their high level of antibiotic resistance. Additionally, this potentiation was not dependent on the antibiotic mechanism of action and was observed across clinical isolates of *E. coli*, *K. pneumoniae*, and *S. enterica*. To the best of our knowledge, this is the first demonstration of reactive oxygen species acting in synergy with bacteriostatic small molecule antibiotics. As an additional investigation, we showed increased bacterial inhibition of *S. enterica* serovar Typhimurium in infected epithelial cells and increased survival of nematodes with *S. enterica* serovar Enteritidis gut-infection upon combination of superoxide generating nanoparticles with ciprofloxacin.

With successful inhibition of multiple clinical isolates, we sought to better understand the mechanism of action of the superoxide generating nanoparticles by performing a transcriptome-wide analysis in *E. coli* with activated nanoparticles (Chapter 7). We designed the study to remove material effects and examine only the effect of nanoparticle activation and superoxide generation. We found significantly higher gene expression variability with nanoparticle activation. The most significant changes in both variability and differential expression were to genes in motility, primary and nitrogen metabolism, and amino acid synthesis. We also measured changes in gene expression for stress response to high pH and heat shock, potentially indicating a cross-protection state.

8.4 Future Directions

By far, the biggest advantage of antisense-mediated RNA-inhibition is the freedom to not spend time asking how to hit a target but the ability to just ask what to target. While preventing

translation of proteins is one approach, currently available antibiotics only target bacterial ribosomal RNA¹ leaving a wealth of other RNA molecules as possible targets which antisense inhibition is poised to study. Non-coding RNA immediately stand out as potential targets because of the role they play in regulation of systems from virulence in *Shigella flexneri*² to processes as core to bacterial growth as the transition from exponential to stationary phase³. Additionally, small non-coding RNAs have garnered attention for their coordination of bacterial adaptation⁴ further suggesting they could be interesting targets for mitigating antibiotic resistance.

Based on our findings in Chapter 4, we are motivated to develop a bioinformatic approach to antisense-PNA design. Our success with the small initial study of six PNA and three species of Enterobacteriaceae can be expanded for future avenues. The large, ever-expanding databases of sequencing data could be incorporated into a design tool allowing for sequence specific antimicrobials to be created across a broad range of organisms. There are a few additional pieces of information needed to create this type of design tool. While antisense-PNA characteristically have significantly reduced binding upon a single target sequence mismatch⁵, we did find in our own studies some unexplained inhibitory effects that were not predicted by sequencing. Perhaps a more thorough understanding of off-target binding or interactions is necessary for implementing a bioinformatic approach. This type of binding study could incorporate both traditional approaches such as gel shift assays and also systematic target point mutations and evaluation of efficacy. Without a complete understanding of PNAs off-target binding it would be near-impossible to create a tool which predicts successful antimicrobial PNA design especially when considering preventing off-target effects to the host. Furthermore, not every organism has a defined set of essential genes making it difficult to predict the effectiveness or relevance of gene targets across

organisms. Antisense-PNA screens across genes in diverse pathogens could be useful to define essential gene sets for non-model organisms.

We see specific delivery as the largest barrier to PNA therapeutic use and future studies should focus on optimizing an agent for delivery. In order to maintain the desired specificity of RNA-inhibitors, the strength of delivery needs to remain in balance with the antisense molecule uniqueness to prevent off-target effects. Specificity for bacterial species could potentially be incorporated into an optimized delivery agent to further minimize chances of off-target activity. Antimicrobial peptides (AMPs), especially those natively expressed by the host of interest, could be promising delivery agents as their activity is largely attributed to passive permeabilization of bacterial membranes garnering not only its own antimicrobial activity but also possibly aiding in transport of PNA. While eukaryotic produced AMPs are typically broad-range in their activity, bacteriocins, AMPs naturally produced by bacteria, are more often species specific making them interesting candidates to control off-target effects while increasing transport by passive permabilization⁶.

To further develop superoxide generating nanoparticles for therapeutic applications, there are a number of considerations for further studies. In this thesis, we focused on cadmium chalcogenides nanoparticles excitable by visible light however the mechanism of action is translatable to other materials since it is energy level dependent. While visible light excitation could be applied for treating surfaces infections, such as burns, or for localized treatment, designing nanoparticles which excite with other wavelengths of energy could expand the antibiotic nanoparticle applications. The biological optical window allows for near-infrared light to penetrate deep into tissue or nanoparticles could be designed for excitation with highly penetrating ultrasound waves. For applications in human health, it would be ideal to transition to more

biocompatible materials such as titanium dioxide nanoparticles. With a wealth of dopants available for tuning energy levels, there are likely many materials which could be investigated and modified. Additionally, conjugating biomarkers to nanoparticles for specific targeting and/or delivery would be advantageous for treating infections. Localizing the superoxide flux from nanoparticles to the pathogen could also reduce toxicity concerns for host cells. All of these modifications, while maintaining the same mechanism-of-action, would expand the possible applications of the technology.

While we have shown a wealth of evidence to support that superoxide is inside of bacterial cells during treatment (Chapter 6) and that the nanoparticles are physically associated with the bacterial cells (Chapter 5), an in-depth study on the localization of the nanoparticles in different model systems would deepen our understanding of their activity. We have begun efforts to use STORM microscopy in conjunction with 3D-resolving phase masks (Double Helix Optics) to image CdTe-2.4 in *E. coli*. We could also explore avenues into electron microscopy. These techniques would be interesting to apply to bacteria alone and infected mammalian cells. The use of super-resolution imaging would also allow up to answer questions about morphology changes due to superoxide flux. Further, nanoparticle biodispersion should eventually be done in murine models to further development of an antimicrobial agent.

Given, redox homeostasis is of interest across broad applications from infectious disease to metabolic engineering, the implications of our findings with superoxide generating nanomaterials are far reaching. While we tuned our nanoparticle for superoxide production, the redox levels could be altered for energy transfer to other biological molecules of interest. In chapter 5, we showed both inhibition and proliferation of growth using nanoparticles highlighting its potential utility in tuning bacterial phenotype. In work not shown in this thesis, we adapted *E. coli*

to low-level superoxide generating nanoparticles to select for an *E. coli* mutants with higher NADPH/NADP⁺ ratio, enabling higher cofactor availability for the production of 3-hydroxypropionic acid⁷.

Moving forward, one of our primary interests focuses on the roles that redox and transition metals play during microbial pathogenesis and virulence⁸. Redox balance has been shown to be important during virulence or pathogenicity for a variety of deleterious microorganisms including malaria-causing *Plasmodium*⁹ and diverse fungal pathogens¹⁰ indicating more avenues for investigating redox perturbing nanoparticles. The link between redox disruption and metal homeostatic balance is well established given that transition metals, including iron, zinc, and manganese, are required nutrients for bacteria and levels and storage of metals directly govern bacterial response to oxidative stress¹¹. During host-pathogen interactions, metal balance plays a crucial role as part of nutritional immunity, when the host actively withhold nutrients to prevent bacterial colonization¹², or metal intoxication, when the host actively overwhelms the pathogen with excess metals¹¹. Bacterial evasion of nutritional immunity via metal homeostatic processes in bacteria has been shown to be important for *Salmonella enterica*'s ability to cause persistent infection of macrophage cells¹³ and for *Neisseria meningitidis* infection of the human host¹⁴. We find host response of both excess and limitation of metals as further evidence that disruption of metal balance via redox perturbation is important for further study in fighting microorganisms.

For this work, we have demonstrated combinatorial antibiotic approaches which have shown efficacy and various degrees of synergistic interactions. Many combinations of synthetic, rationally design antibiotic agents and small molecule antibiotics were effective even with the clinical isolates high degree of antibiotic resistance against the small molecule antibiotic. The idea of combinatorial antibiotics is not new and has been examined in clinical and academic

investigations of antibiotic efficacy^{15–17}. Combinations of small molecule antibiotics are currently limited by risks of toxicity due to side-effects¹⁸. Markedly with sequence-specific RNA-inhibitors, we see the ability to expand combinatorial treatment to include multiple, even tens of targets into one antibiotic agent with a toxicity profile that would be concentration dependent only on one chemical species, the RNA-inhibitor. We envision a number of interesting avenues for investigation including a cocktail of antibiotic agents and anti-adaptation factors or anti-virulence agents and creating rational combinations of antagonistic and synergistic agents to combat the development of resistance¹⁹.

8.5 Concluding Remarks

Throughout my thesis work, one idea that I first came across in Chait et al. 2012²⁰ remains in my mind: “what counters antibiotic resistance in nature?” This idea is rooted in antibiotic resistance spreading and evolving rapidly due to the introduction of clinical antibiotics^{21,22,20} (Figure 8.1). The antibiotic crisis and lack of control over antibiotic resistance resulted from our ability to control infection. By creating an environment that is toxic to bacteria using antibiotics, we encourage evolution and adaptation to select for the most-fit, resistant bacterium. Adaptation needs to be controlled and manipulated to find a state where resistance is selected against to prevent

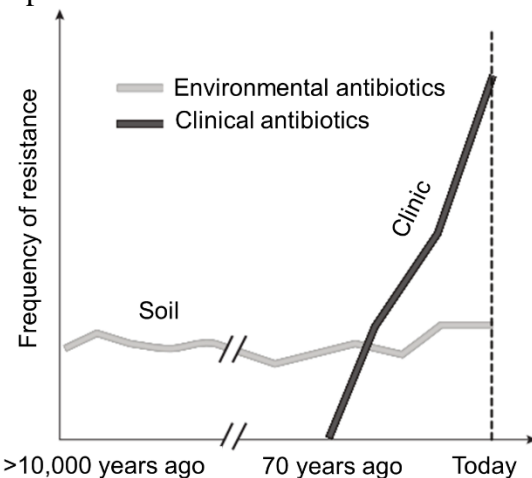


Figure 8.1. Schematic of antibiotic resistance frequency trend in soil environment compared to clinical application of antibiotics. Figure from Chait et al. 2012 Nature Chemical Biology²⁰.

further antibiotic resistance. Based on our findings in this work, rational design can be effective for creating antibiotic agents against a specific microbial process or target of interest. This ability expedites investigation and evaluation of potential antibiotic targets or combinations and enables tight control over the specific microbial process being targeted. Imaginably, rational development of antibiotics will allow for fine-tuned control over emerging antibiotic resistance and can aid in preventing the post-antibiotic era.

8.6 References

1. Hong, W., Zeng, J. & Xie, J. Antibiotic drugs targeting bacterial RNAs. *Acta Pharm. Sin. B* **4**, 258–265 (2014).
2. Giangrossi, M., Prosseda, G., Tran, C. N., *et al.* A novel antisense RNA regulates at transcriptional level the virulence gene icsA of *Shigella flexneri*. *Nucleic Acids Res.* **38**, 3362–75 (2010).
3. Repoila, F. & Darfeuille, F. Small regulatory non-coding RNAs in bacteria: physiology and mechanistic aspects. *Biol. cell* **101**, 117–31 (2009).
4. Repoila, F., Majdalani, N. & Gottesman, S. Small non-coding RNAs, co-ordinators of adaptation processes in *Escherichia coli*: The RpoS paradigm. *Mol. Microbiol.* **48**, 855–861 (2003).
5. Hyrup, B. & Nielsen, P. E. Peptide Nucleic Acids (PNA): Synthesis, Properties and Potential Applications. *Bioorg. Med. Chem.* **4**, 5–23 (1996).
6. Hassan, M., Kjos, M., Nes, I. F., Diep, D. B. & Lotfipour, F. Natural antimicrobial peptides from bacteria: characteristics and potential applications to fight against antibiotic resistance. *J. Appl. Microbiol.* **113**, 723–36 (2012).
7. Reynolds, T. S., Courtney, C. M., Erickson, K. E., *et al.* ROS Mediated Selection for Increased NADPH Availability in *Escherichia coli*. *Submitted*
8. Palmer, L. D. & Skaar, E. P. Transition Metals and Virulence in Bacteria. *Annu. Rev. Genet.* **50**, 67–91 (2016).
9. Kehr, S., Sturm, N., Rahlf, S., Przyborski, J. M. & Becker, K. Compartmentation of redox metabolism in malaria parasites. *PLoS Pathog.* **6**, (2010).
10. Jacobson, E. S. & Jacobson, E. S. Pathogenic Roles for Fungal Melanins Pathogenic Roles for Fungal Melanins. *Clin. Microbiol. Rev.* **13**, 708–717 (2000).
11. Chandrangsu, P., Rensing, C. & Helmann, J. D. Metal homeostasis and resistance in bacteria. *Nat. Rev. Microbiol.* Advanced Online Publication (2017).
12. Hood, M. I. & Skaar, E. P. Nutritional immunity: transition metals at the pathogen-host interface. *Nat. Rev. Microbiol.* **10**, 525–537 (2012).

13. Nagy, T. A., Moreland, S. M., Andrews-Polymenis, H. & Detweiler, C. S. The ferric enterobactin transporter fep is required for persistent salmonella enterica serovar typhimurium infection. *Infect. Immun.* **81**, 4063–4070 (2013).
14. Stork, M., Grijpstra, J., Bos, M. P., *et al.* Zinc Piracy as a Mechanism of Neisseria meningitidis for Evasion of Nutritional Immunity. *PLoS Pathog.* **9**, (2013).
15. Kohanski, M. a, Dwyer, D. J. & Collins, J. J. How antibiotics kill bacteria: from targets to networks. *Nat. Rev. Microbiol.* **8**, 423–435 (2010).
16. Tängdén, T., Hickman, R. a., Forsberg, P., *et al.* Evaluation of double- and triple-antibiotic combinations for VIM- and NDM-producing klebsiella pneumoniae by in vitro time-kill experiments. *Antimicrob. Agents Chemother.* **58**, 1757–1762 (2014).
17. Toussaint, K. a & Gallagher, J. C. β -Lactam/ β -Lactamase Inhibitor Combinations: From Then to Now. *Ann. Pharmacother.* **49**, 86–98 (2015).
18. Tängdén, T. Combination antibiotic therapy for multidrug-resistant Gram-negative bacteria. *Ups. J. Med. Sci.* **9734**, 149–153 (2014).
19. Chait, R., Craney, A. & Kishony, R. Antibiotic interactions that select against resistance. *Nature* **446**, 668–671 (2007).
20. Chait, R., Vetsigian, K. & Kishony, R. What counters antibiotic resistance in nature? *Nat. Chem. Biol.* **8**, 2–5 (2012).
21. United States Center for Disease Control. *Antibiotic Resistance Threats*. (2013).
22. Bush, K. Proliferation and significance of clinically relevant β -lactamases. *Ann. N. Y. Acad. Sci.* **1277**, 84–90 (2013).

Chapter 9

Bibliography

- Afanas'ev, I. B. *Superoxide Ion Chemistry and Biological Implications*. **1**, (CRC Press, 1989).
- Al Mamun, A. A. M., Lombardo, M.-J., Shee, C., *et al.* Identity and function of a large gene network underlying mutagenic repair of DNA breaks. *Science* **338**, 1344–1348 (2012).
- Alanis, A. J. Resistance to antibiotics: Are we in the post-antibiotic era? *Arch. Med. Res.* **36**, 697–705 (2005).
- Albrecht, M., Sharma, C. M., Reinhardt, R., Vogel, J. & Rudel, T. Deep sequencing-based discovery of the Chlamydia trachomatis transcriptome. *Nucleic Acids Res.* **38**, 868–77 (2010).
- Anders, S., Huber, W., Nagalakshmi, U., *et al.* Differential expression analysis for sequence count data. *Genome Biol.* **11**, 1–12 (2010).
- Anders, S., Pyl, P. T. & Huber, W. HTSeq-A Python framework to work with high-throughput sequencing data. *Bioinformatics* **31**, 166–169 (2015).
- André, G., Even, S., Putzer, H., *et al.* S-box and T-box riboswitches and antisense RNA control a sulfur metabolic operon of Clostridium acetobutylicum. *Nucleic Acids Res.* **36**, 5955–69 (2008).
- Apel, K. & Hirt, H. Reactive oxygen species: metabolism, oxidative stress, and signal transduction. *Annu. Rev. Plant Biol.* **55**, 373–399 (2004).
- Arnoldini, M., Vizcarra, I. A., Peña-Miller, R., *et al.* Bistable Expression of Virulence Genes in *Salmonella* Leads to the Formation of an Antibiotic-Tolerant Subpopulation. *PLoS Biol.* **12**, e1001928 (2014).
- Aronesty, E. Comparison of Sequencing Utility Programs. *Open Bioinforma. J.* **7**, 1–8 (2013).
- Arraiano, C. M., Andrade, J. M., Domingues, S., *et al.* The critical role of RNA processing and degradation in the control of gene expression. *FEMS Microbiol. Rev.* **34**, 883–923 (2010).
- Avery, S. V. Molecular targets of oxidative stress. *Biochem. J.* **434**, 201–10 (2011).
- Baatout, S., De Boever, P. & Mergeay, M. Physiological changes induced in four bacterial strains following oxidative stress. *Appl. Biochem. Microbiol.* **42**, 369–377 (2006).

- Baba, T., Ara, T., Hasegawa, M., *et al.* Construction of Escherichia coli K-12 in-frame, single-gene knockout mutants: the Keio collection. *Mol. Syst. Biol.* **2**, 1–11 (2006).
- Babu, M. M. & Teichmann, S. A. Evolution of transcription factors and the gene regulatory network in Escherichia coli. *Nucleic Acids Res.* **31**, 1234–1244 (2003).
- Bankevich, A., Nurk, S., Antipov, D., *et al.* SPAdes: a new genome assembly algorithm and its applications to single-cell sequencing. *J. Comput. Biol.* **19**, 455–477 (2012).
- Barbosa, T. M. & Levy, S. B. Differential expression of over 60 chromosomal genes in Escherichia coli by constitutive expression of MarA. *J. Bacteriol.* **182**, 3467–3474 (2000).
- Battesti, A., Majdalani, N. & Gottesman, S. The RpoS-mediated general stress response in Escherichia coli. *Annu. Rev. Microbiol.* **65**, 189–213 (2011).
- Bearson, B. L., Lee, I. S. & Casey, T. A. Escherichia coli O157 : H7 glutamate- and arginine-dependent acid-resistance systems protect against oxidative stress during extreme acid challenge. *Microbiology* **155**, 805–812 (2009).
- Beaume, M., Hernandez, D., Farinelli, L., *et al.* Cartography of methicillin-resistant S. aureus transcripts: detection, orientation and temporal expression during growth phase and stress conditions. *PLoS One* **5**, e10725 (2010).
- Beaumont, H. J. E., Gallie, J., Kost, C., Ferguson, G. C. & Rainey, P. B. Experimental evolution of bet hedging. *Nature* **462**, 90–93 (2009).
- Bendtsen, K. M., Erdosy, J., Csiszovszki, Z., *et al.* Direct and indirect effects in the regulation of overlapping promoters. *Nucleic Acids Res.* **39**, 6879–85 (2011).
- Bennett, C. F. & Swayze, E. E. RNA targeting therapeutics: molecular mechanisms of antisense oligonucleotides as a therapeutic platform. *Annu. Rev. Pharmacol. Toxicol.* **50**, 259–293 (2010).
- Bérdy, J. Thoughts and facts about antibiotics: Where we are now and where we are heading. *J. Antibiot. (Tokyo)* **65**, 441–441 (2012).
- Berenbaum, M. C., Yu, V. L. & Felegie, T. P. Synergy with double and triple antibiotic combinations compared. *J. Antimicrob. Chemother.* **12**, 555–563 (1983).
- Berteaux, N., Aptel, N., Cathala, G., *et al.* A novel H19 antisense RNA overexpressed in breast cancer contributes to paternal IGF2 expression. *Mol. Cell. Biol.* **28**, 6731–45 (2008).
- Bhattacharjee, S. Reactive oxygen species and oxidative burst: Roles in stress, senescence and signal transduction in plants. *Curr. Sci.* **89**, 1113–1121 (2005).

- Bjedov, I., Tenaillon, O., Gérard, B., *et al.* Stress-induced mutagenesis in bacteria. *Science* **300**, 1404–1409 (2003).
- Blair, J. M. A., Webber, M. A., Baylay, A. J., Ogbolu, D. O. & Piddock, L. J. V. Molecular mechanisms of antibiotic resistance. *Nat. Rev. Microbiol.* **13**, 42–51 (2015).
- Blanchard, C., Barnett, P., Perlmutter, J. & Dunman, P. M. Identification of *Acinetobacter baumannii* Serum-Associated Antibiotic Efflux Pump Inhibitors. *Antimicrob. Agents Chemother.* **58**, 6360–6370 (2014).
- Blumberg, P. M. & Strominger, J. L. Interaction of penicillin with the bacterial cell: penicillin-binding proteins and penicillin-sensitive enzymes. *Bacteriol. Rev.* **38**, 291–335 (1974).
- Boehm, D. E. Oxygen and toxicity inhibition of amino acid biosynthesis. *Nature* **262**, 418–420 (1976).
- Bognar, A. L., Osborne, C., Shane, B., Singer, S. C. & Ferone, R. Folylpoly- γ -glutamate synthetase-dihydrofolate synthetase. *J. Biol. Chem.* **260**, 5625–5630 (1985).
- Bolger, A. M., Lohse, M., Usadel, B., *et al.* Trimmomatic: A flexible trimmer for Illumina sequence data. *Bioinformatics* **30**, 2114–2120 (2014).
- Bonnefoy, V. & Demoss, J. A. Nitrate reductases in *Escherichia coli*. *Antonie Van Leeuwenhoek* 47–56 (1994).
- Booth, M., Brown, A. P., Evans, S. D. & Critchley, K. Determining the concentration of CuInS₂ quantum dots from the size-dependent molar extinction coefficient. *Chem. Mater.* **24**, 2064–2070 (2012).
- Bordoy, A. E., Varanasi, U. S., Courtney, C. M. & Chatterjee, A. Transcriptional Interference in Convergent Promoters as a Means for Tunable Gene Expression. *ACS Synth. Biol.* **5**, 1331–1341 (2016).
- Brantl, S. Antisense-RNA regulation and RNA interference. *Biochim. Biophys. Acta* **1575**, 15–25 (2002).
- Brantl, S. Regulatory mechanisms employed by cis-encoded antisense RNAs. *Curr. Opin. Microbiol.* **10**, 102–9 (2007).
- Brayner, R., Ferrari-iliou, R., Brivois, N., *et al.* Toxicological Impact Studies Based on *Escherichia coli* Bacteria in Ultrafine ZnO Nanoparticles Colloidal Medium. *Nano Lett.* **6**, 866–870 (2006).
- Brink, A. J., Coetzee, J., Clay, C. G., *et al.* Emergence of New Delhi metallo- β -lactamase (NDM-1) and *Klebsiella pneumoniae* carbapenemase (KPC-2) in South Africa. *J. Clin. Microbiol.* **50**, 525–527 (2012).

- Brondsted, L. & Atlung, T. Effect of growth conditions on expression of the acid phosphatase (cyx- appA) operon and the appY gene, which encodes a transcriptional activator of *Escherichia coli*. *J. Bacteriol.* **178**, 1556–1564 (1996).
- Brunel, C., Marquet, R., Romby, P. & Ehresmann, C. RNA loop-loop interactions as dynamic functional motifs. *Biochimie* **84**, 925–944 (2002).
- Brynildsen, M. P., Winkler, J. a, Spina, C. S., MacDonald, I. C. & Collins, J. J. Potentiating antibacterial activity by predictably enhancing endogenous microbial ROS production. *Nat. Biotechnol.* **31**, 160–165 (2013).
- Buettner, G. R. & Mason, R. P. Spin-Trapping Methods for Detecting Superoxide and Hydroxyl Free Radicals in Vitro and in Vivo. *Methods Enzymol.* **186**, 127–133 (1990).
- Buffie, C. G. & Pamer, E. G. Microbiota-mediated colonization resistance against intestinal pathogens. *Nat Rev Immunol* **13**, 790–801 (2013).
- Burnett, J. C. & Rossi, J. J. RNA-based therapeutics: current progress and future prospects. *Chem. Biol.* **19**, 60–71 (2012).
- Bush, K. & Jacoby, G. a. Updated functional classification of β-lactamases. *Antimicrob. Agents Chemother.* **54**, 969–76 (2010).
- Bush, K. Proliferation and significance of clinically relevant β-lactamases. *Ann. N. Y. Acad. Sci.* **1277**, 84–90 (2013).
- Callen, B. P., Shearwin, K. E. & Egan, J. B. Transcriptional Interference between Convergent Promoters Caused by Elongation over the Promoter. *Mol. Cell* **14**, 647–656 (2004).
- Chait, R., Craney, A. & Kishony, R. Antibiotic interactions that select against resistance. *Nature* **446**, 668–671 (2007).
- Chait, R., Shrestha, S., Shah, A. K., Michel, J. B. & Kishony, R. A differential drug screen for compounds that select against antibiotic resistance. *PLoS One* **5**, 1–8 (2010).
- Chait, R., Vetsigian, K. & Kishony, R. What counters antibiotic resistance in nature? *Nat. Chem. Biol.* **8**, 2–5 (2012).
- Chandrangsu, P., Rensing, C. & Helmann, J. D. Metal homeostasis and resistance in bacteria. *Nat. Rev. Microbiol.* Advanced Online Publication (2017).
- Chang, H.-H., Cohen, T., Grad, Y. H., *et al.* Origin and Proliferation of Multiple-Drug Resistance in Bacterial Pathogens. *Microbiol. Mol. Biol. Rev.* **79**, 101–116 (2015).

- Chatterjee, A., Cook, L. C. C., Shu, C.-C., *et al.* Antagonistic self-sensing and mate-sensing signaling controls antibiotic-resistance transfer. *Proc. Natl. Acad. Sci. U. S. A.* **110**, 7086–90 (2013).
- Chatterjee, A., Drews, L., Mehra, S., *et al.* Convergent transcription in the butyrolactone regulon in *Streptomyces coelicolor* confers a bistable genetic switch for antibiotic biosynthesis. *PLoS One* **6**, e21974 (2011).
- Chatterjee, A., Johnson, C. M., Shu, C.-C., *et al.* Convergent transcription confers a bistable switch in *Enterococcus faecalis* conjugation. *Proc. Natl. Acad. Sci. U. S. A.* **108**, 9721–6 (2011).
- Chen, J., Sun, M., Hurst, L. D., Carmichael, G. G. & Rowley, J. D. Genome-wide analysis of coordinate expression and evolution of human cis-encoded sense-antisense transcripts. *Trends Genet.* **21**, 322–6 (2005).
- Chen, J., Sun, M., Kent, W. J., *et al.* Over 20% of human transcripts might form sense-antisense pairs. *Nucleic Acids Res.* **32**, 4812–20 (2004).
- Chiang, S. M. & Schellhorn, H. E. Regulators of oxidative stress response genes in *Escherichia coli* and their functional conservation in bacteria. *Arch. Biochem. Biophys.* **525**, 161–169 (2012).
- Cho, S. J., Maysinger, D., Jain, M., *et al.* Long-Term Exposure to CdTe Quantum Dots Causes Functional Impairments in Live Cells. *Lamgmuir* **23**, 1974–1980 (2007).
- CLSI M100 S27:2017-Performance Standards to Antimicrobial Susceptibility Testing; 27th Edition. 62–71 (2017). Available at: <http://em100.edaptivedocs.info/dashboard.aspx>.
- Cohen, G. & Heikkila, R. E. The Generation of Hydrogen-Peroxide, Superoxide Radical, and Hydroxyl Radical by 6-Hydroxydopamine, Dialuric Acid, and Related Cytotoxic Agents. *J. Biol. Chem.* **249**, 2447–2452 (1974).
- Coiras, M., López-Huertas, M. R., Pérez-Olmeda, M. & Alcamí, J. Understanding HIV-1 latency provides clues for the eradication of long-term reservoirs. *Nat. Rev. Microbiol.* **7**, 798–812 (2009).
- Connor, E. E., Mwamuka, J., Gole, A., Murphy, C. J. & Wyatt, M. D. Gold nanoparticles are taken up by human cells but do not cause acute cytotoxicity. *Small* **1**, 325–327 (2005).
- Cook, L., Chatterjee, A., Barnes, A., *et al.* Biofilm growth alters regulation of conjugation by a bacterial pheromone. *Mol. Microbiol.* **81**, 1499–1510 (2011).
- Cotter, P. A., Chepuri, V., Gennis, R. B. & Gunsalus, R. P. Cytochrome o (cyoABCDE) and d (cydAB) Oxidase Gene Expression in *Escherichia coli* Is Regulated by Oxygen, pH, and the fnr Gene Product. *J. Bacteriol.* **172**, 6333–6338 (1990).

- Courtney, C. & Chatterjee, A. cis-Antisense RNA and Transcriptional Interference: Coupled Layers of Gene Regulation. *J. Gene Ther.* **2**, 1–9 (2014).
- Courtney, C. M. & Chatterjee, A. Sequence-Specific Peptide Nucleic Acid-Based Antisense Inhibitors of TEM-1 β -Lactamase and Mechanism of Adaptive Resistance. *ACS Infect. Dis.* **1**, 253–263 (2015).
- Courtney, C. M., Goodman, S. M., McDaniel, J. a., et al. Photoexcited quantum dots for killing multidrug-resistant bacteria. *Nat. Mater.* **15**, 485–588 (2016).
- Courtney, C. M., Goodman, S. M., Nagy, T., et al. Potentiating antibiotics in drug-resistant clinical isolates via stimuli-activated superoxide generation. *Submitted*
- Crampton, N., Bonass, W. a, Kirkham, J., Rivetti, C. & Thomson, N. H. Collision events between RNA polymerases in convergent transcription studied by atomic force microscopy. *Nucleic Acids Res.* **34**, 5416–25 (2006).
- Dai, T., Huang, Y.-Y. & Hamblin, M. R. Photodynamic therapy for localized infections – state of the art. *Photodiagnosis Photodyn Ther.* **6**, 170–188 (2009).
- Das, U. & Shuman, S. 2'-Phosphate cyclase activity of RtcA: a potential rationale for the operon organization of RtcA with an RNA repair ligase RtcB in Escherichia coli and other bacterial taxa. *Rna* **19**, 1355–1362 (2013).
- Davies, J. & Davies, D. Origins and evolution of antibiotic resistance. *Microbiol. Mol. Biol. Rev.* **74**, 417–433 (2010).
- Davies, J. Where have all the antibiotics gone? *Can. J. Infect. Dis. Med. Microbiol.* **17**, 287–290 (2006).
- Dornenburg, J. E., Devita, A. M., Palumbo, M. J. & Wade, J. T. Widespread antisense transcription in Escherichia coli. *MBio* **1**, e00024–10 (2010).
- Dragosits, M., Mozhayskiy, V., Quinones-Soto, S., Park, J. & Tagkopoulos, I. Evolutionary potential, cross-stress behavior and the genetic basis of acquired stress resistance in Escherichia coli. *Mol. Syst. Biol.* **9**, 1–13 (2013).
- Drawz, S. M., Papp-Wallace, K. M. & Bonomo, R. A. New β -lactamase inhibitors: a therapeutic renaissance in an MDR world. *Antimicrob. Agents Chemother.* **58**, 1835–1846 (2014).
- Drecktrah, D., Levine-Wilkinson, S., Dam, T., et al. Dynamic behavior of salmonella-induced membrane tubules in epithelial cells. *Traffic* **9**, 2117–2129 (2008).
- Dryselius, R., Aswasti, S. K., Rajarao, G. K., Nielsen, P. E. & Good, L. The translation start codon region is sensitive to antisense PNA inhibition in Escherichia coli. *Oligonucleotides* **13**, 427–33 (2003).

- Dühring, U., Axmann, I. M., Hess, W. R. & Wilde, A. An internal antisense RNA regulates expression of the photosynthesis gene *isiA*. *Proc. Natl. Acad. Sci. U. S. A.* **103**, 7054–8 (2006).
- Durand, S. & Storz, G. Reprogramming of Anaerobic Metabolism by the FnrS Small RNA. *Mol. Microbiol.* **75**, 1215–123122 (2010).
- Dwyer, D. J., Belenky, P. a, Yang, J. H., *et al.* Antibiotics induce redox-related physiological alterations as part of their lethality. *Proc. Natl. Acad. Sci. U. S. A.* **111**, E2100–9 (2014).
- Dwyer, D. J., Kohanski, M. a, Hayete, B. & Collins, J. J. Gyrase inhibitors induce an oxidative damage cellular death pathway in *Escherichia coli*. *Mol. Syst. Biol.* **3**, 91 (2007).
- Egholm, M., Buchardt, O., Christensen, L., *et al.* PNA hybridizes to complementary oligonucleotides obeying the Watson-Crick hydrogen-bonding rules. *Nature* **365**, 566–568 (1993).
- Erickson, K. E., Otoupal, P. B. & Chatterjee, A. Gene Expression Variability Underlies Adaptive Resistance in Phenotypically Heterogeneous Bacterial Populations. *ACS Infect. Dis.* **1**, 555–567 (2016).
- Falagas, M. E. & Bliziotis, I. a. Pandrug-resistant Gram-negative bacteria: the dawn of the post-antibiotic era? *Int. J. Antimicrob. Agents* **29**, 630–636 (2007).
- Fass, R. J., Routilie, C. A. & Prior, R. B. Interaction of clindamycin and gentamicin in vitro. *Antimicrob. Agents Chemother.* **6**, 582–587 (1974).
- Fernández, L., Breidenstein, E. B. M. & Hancock, R. E. W. Creeping baselines and adaptive resistance to antibiotics. *Drug Resist. Updat.* **14**, 1–21 (2011).
- Filiatrault, M. J., Stodghill, P. V, Bronstein, P. A., *et al.* Transcriptome analysis of *Pseudomonas syringae* identifies new genes, noncoding RNAs, and antisense activity. *J. Bacteriol.* **192**, 2359–72 (2010).
- Finkel, S. E. & Johnson, R. C. The Fis protein: it's not just for DNA inversion anymore. *Mol. Microbiol.* **6**, 3257–3265 (1992).
- Fleming, A. On the antibacterial action of cultures of a penicillium, with special reference to their use in the isolation of *B. influenzae*. *Br. J. Exp. Pathol.* **10**, 226–236 (1929).
- Fozo, E. M., Hemm, M. R. & Storz, G. Small toxic proteins and the antisense RNAs that repress them. *Microbiol. Mol. Biol. Rev.* **72**, 579–89 (2008).
- Franch, T., Petersen, M., Wagner, E. G., Jacobsen, J. P. & Gerdes, K. Antisense RNA regulation in prokaryotes: rapid RNA/RNA interaction facilitated by a general U-turn loop structure. *J. Mol. Biol.* **294**, 1115–25 (1999).

- Garneau, J. E., Dupuis, M.-È., Villion, M., *et al.* The CRISPR/Cas bacterial immune system cleaves bacteriophage and plasmid DNA. *Nature* **468**, 67–71 (2010).
- Georg, J. & Hess, W. R. cis-antisense RNA, another level of gene regulation in bacteria. *Microbiol. Mol. Biol. Rev.* **75**, 286–300 (2011).
- Georg, J., Voss, B., Scholz, I., *et al.* Evidence for a major role of antisense RNAs in cyanobacterial gene regulation. *Mol. Syst. Biol.* **5**, 305 (2009).
- Gerdes, K. & Wagner, E. G. H. RNA antitoxins. *Curr. Opin. Microbiol.* **10**, 117–24 (2007).
- Ghosal, A., Vitali, A., Stach, J. E. M. & Nielsen, P. E. Role of SbmA in the Uptake of Peptide Nucleic Acid (PNA)-Peptide Conjugates in *E. coli*. *ACS Chem. Biol.* **8**, 360–367 (2013).
- Giangrossi, M., Prosseda, G., Tran, C. N., *et al.* A novel antisense RNA regulates at transcriptional level the virulence gene icsA of *Shigella flexneri*. *Nucleic Acids Res.* **38**, 3362–75 (2010).
- Gonzalez, R., Tao, H., Purvis, J. E., *et al.* Gene array-based identification of changes that contribute to ethanol tolerance in ethanologenic *Escherichia coli*: comparison of KO11 (parent) to LY01 (resistant mutant). *Biotechnol. Prog.* **19**, 612–623 (2003).
- Good, L. & Nielsen, P. E. Antisense inhibition of gene expression in bacteria by PNA targeted to mRNA. *Nat. Biotechnol.* **16**, 355–358 (1998).
- Good, L. & Nielsen, P. E. Inhibition of translation and bacterial growth by peptide nucleic acid targeted to ribosomal RNA. *Proc. Natl. Acad. Sci. U. S. A.* **95**, 2073–2076 (1998).
- Good, L., Awasthi, S. K., Dryselius, R., Larsson, O. & Nielsen, P. E. Bactericidal antisense effects of peptide-PNA conjugates. *Nat. Biotechnol.* **19**, 360–364 (2001).
- Gouzy, A., Larrouy-Maumus, G., Bottai, D., *et al.* Mycobacterium tuberculosis Exploits Asparagine to Assimilate Nitrogen and Resist Acid Stress during Infection. *PLoS Pathog.* **10**, (2014).
- Grant, S. S., Kaufmann, B. B., Chand, N. S., Haseley, N. & Hung, D. T. Eradication of bacterial persisters with antibiotic-generated hydroxyl radicals. *Proc. Natl. Acad. Sci. U. S. A.* **109**, 12147–12152 (2012).
- Gray, B. & Carmichael, A. J. Kinetics of superoxide scavenging by dismutase enzymes and manganese mimics determined by electron spin resonance. *Biochem J* **281**, 795–802 (1992).
- Greger, I. H., Aranda, A. & Proudfoot, N. Balancing transcriptional interference and initiation on the GAL7 promoter of *Saccharomyces cerevisiae*. *Proc. Natl. Acad. Sci. U. S. A.* **97**, 8415–8420 (2000).

- Güell, M., van Noort, V., Yus, E., *et al.* Transcriptome Complexity in a Genome-Reduced Bacterium. *Science* **326**, 1268–1271 (2009).
- Gullerova, M. & Proudfoot, N. J. Cohesin complex promotes transcriptional termination between convergent genes in *S. pombe*. *Cell* **132**, 983–95 (2008).
- Gupta, S. K., Padmanabhan, B. R., Diene, S. M., *et al.* ARG-annot, a new bioinformatic tool to discover antibiotic resistance genes in bacterial genomes. *Antimicrob. Agents Chemother.* **58**, 212–220 (2014).
- Haas, B. J., Chin, M., Nusbaum, C., Birren, B. W. & Livny, J. How deep is deep enough for RNA-Seq profiling of bacterial transcriptomes? *BMC Genomics* **13**, 734 (2012).
- Hajipour, M. J., Fromm, K. M., Ashkarran, A. A., *et al.* Antibacterial properties of nanoparticles. *Trends Biotechnol.* **30**, 499–511 (2012).
- Han, Y., Lin, Y. B., An, W., *et al.* Orientation-dependent regulation of integrated HIV-1 expression by host gene transcriptional readthrough. *Cell Host Microbe* **4**, 134–46 (2008).
- Harbour, J. R. & Hair, M. L. Superoxide generation in the photolysis of aqueous cadmium sulfide dispersions. Detection by spin trapping. *J. Phys. Chem.* **81**, 1791–1793 (1977).
- Hassan, M., Kjos, M., Nes, I. F., Diep, D. B. & Lotfipour, F. Natural antimicrobial peptides from bacteria: characteristics and potential applications to fight against antibiotic resistance. *J. Appl. Microbiol.* **113**, 723–36 (2012).
- Hatamoto, M., Ohashi, A. & Imachi, H. Peptide nucleic acids (PNAs) antisense effect to bacterial growth and their application potentiality in biotechnology. *Appl. Microbiol. Biotechnol.* **86**, 397–402 (2010).
- He, M., Miyajima, F., Roberts, P., *et al.* Emergence and global spread of epidemic healthcare-associated Clostridium difficile. *Nat. Genet.* **45**, 109–13 (2013).
- Hegreness, M., Shores, N., Damian, D., Hartl, D. & Kishony, R. Accelerated evolution of resistance in multidrug environments. *Proc. Natl. Acad. Sci. U. S. A.* **105**, 13977–81 (2008).
- Hendriksen, R. S., Joensen, K. G., Lukwesa-Musyani, C., *et al.* Extremely drug-resistant *Salmonella enterica* Serovar Senftenberg infections in patients in Zambia. *J. Clin. Microbiol.* **51**, 284–286 (2013).
- Hernández, J. a, Muro-Pastor, A. M., Flores, E., *et al.* Identification of a furA cis antisense RNA in the cyanobacterium *Anabaena* sp. PCC 7120. *J. Mol. Biol.* **355**, 325–34 (2006).
- Hernández, S. B., Cota, I., Ducret, A., Aussel, L. & Casadesús, J. Adaptation and preadaptation of *Salmonella enterica* to bile. *PLoS Genet.* **8**, (2012).

- Hetrick, E. M., Shin, J. H., Paul, H. S. & Schoenfisch, M. H. Anti-biofilm efficacy of nitric oxide-releasing silica nanoparticles. *Biomaterials* **30**, 2782–2789 (2009).
- Hobbs, E. C., Yin, X., Paul, B. J., Astarita, J. L. & Storz, G. Conserved small protein associates with the multidrug efflux pump AcrB and differentially affects antibiotic resistance. *Proc. Natl. Acad. Sci. U. S. A.* **109**, 16696–16701 (2012).
- Hong, W., Zeng, J. & Xie, J. Antibiotic drugs targeting bacterial RNAs. *Acta Pharm. Sin. B* **4**, 258–265 (2014).
- Hongay, C. F., Grisafi, P. L., Galitski, T. & Fink, G. R. Antisense transcription controls cell fate in *Saccharomyces cerevisiae*. *Cell* **127**, 735–45 (2006).
- Hood, M. I. & Skaar, E. P. Nutritional immunity: transition metals at the pathogen-host interface. *Nat. Rev. Microbiol.* **10**, 525–537 (2012).
- Huang, D. W., Lempicki, R. a & Sherman, B. T. Systematic and integrative analysis of large gene lists using DAVID bioinformatics resources. *Nat. Protoc.* **4**, 44–57 (2009).
- Huang, X., El-Sayed, I. H., Qian, W. & El-Sayed, M. a. Cancer cell imaging and photothermal therapy in the near-infrared region by using gold nanorods. *J. Am. Chem. Soc.* **128**, 2115–2120 (2006).
- Hyrup, B. & Nielsen, P. E. Peptide Nucleic Acids (PNA): Synthesis, Properties and Potential Applications. *Bioorg. Med. Chem.* **4**, 5–23 (1996).
- Imlay, J. A. Cellular defenses against superoxide and hydrogen peroxide. *Annu. Rev. Biochem.* **77**, 755–776 (2011).
- Imlay, J. a. Pathways of oxidative damage. *Annu. Rev. Microbiol.* **57**, 395–418 (2003).
- Imlay, J. A. The molecular mechanisms and physiological consequences of oxidative stress: lessons from a model bacterium. *Nat. Rev. Microbiol.* **11**, 443–54 (2013).
- Ipe, B. I., Lehnig, M. & Niemeyer, C. M. On the generation of free radical species from quantum dots. *Small* **1**, 706–9 (2005).
- Jacobson, E. S. & Jacobson, E. S. Pathogenic Roles for Fungal Melanins Pathogenic Roles for Fungal Melanins. *Clin. Microbiol. Rev.* **13**, 708–717 (2000).
- Jansen, G., Lee, A. Y., Epp, E., et al. Chemogenomic profiling predicts antifungal synergies. *Mol. Syst. Biol.* **5**, 338 (2009).
- Jen, C.-H., Michalopoulos, I., Westhead, D. R. & Meyer, P. Natural antisense transcripts with coding capacity in *Arabidopsis* may have a regulatory role that is not linked to double-stranded RNA degradation. *Genome Biol.* **6**, R51 (2005).

- Jin, H., Vacic, V., Girke, T., Lonardi, S. & Zhu, J.-K. Small RNAs and the regulation of cis-natural antisense transcripts in Arabidopsis. *BMC Mol. Biol.* **9**, 6 (2008).
- Jin, T., Sun, D., Su, J. Y., Zhang, H. & Sue, H.-J. Antimicrobial efficacy of zinc oxide quantum dots against Listeria monocytogenes, Salmonella Enteritidis, and Escherichia coli O157:H7. *J. Food Sci.* **74**, M46–52 (2009).
- Jiong, M., Cnen, J. Y., Zhang, Y., et al. Photochemical instability of thiol-capped CdTe quantum dots in aqueous solution and living cells: Process and mechanism. *J. Phys. Chem. B* **111**, 12012–12016 (2007).
- Johnson, C. M., Haemig, H. H. A., Chatterjee, A., et al. RNA-Mediated Reciprocal Regulation between Two Bacterial Operons Is RNase III Dependent. *MBio* **2**, (2011).
- Johnson, C. M., Manias, D. A., Haemig, H. A. H., et al. Direct evidence for control of the pheromone-inducible prgQ operon of Enterococcus faecalis plasmid pCF10 by a countertranscript-driven attenuation mechanism. *J. Bacteriol.* **192**, 1634–42 (2010).
- Johnson, E. & Srivastava, R. Volatility in mRNA secondary structure as a design principle for antisense. *Nucleic Acids Res.* **41**, 1–10 (2012).
- Johnson, M., Zaretskaya, I., Raytselis, Y., et al. NCBI BLAST: a better web interface. *Nucleic Acids Res.* **36**, 5–9 (2008).
- Jozefczuk, S., Klie, S., Catchpole, G., et al. Metabolomic and transcriptomic stress response of Escherichia coli. *Mol. Syst. Biol.* **6**, 364 (2010).
- Kaldalu, N., Mei, R. & Lewis, K. Killing by Ampicillin and Ofloxacin Induces Overlapping Changes in Escherichia coli Transcription Profile. *Antimicrob. Agents Chemother.* **48**, 890–896 (2004).
- Karsi, A. & Lawrence, M. L. Broad host range fluorescence and bioluminescence expression vectors for Gram-negative bacteria. *Plasmid* **57**, 286–95 (2007).
- Katayama, S., Tomaru, Y., Kasukawa, T., et al. Antisense transcription in the mammalian transcriptome. *Science* **309**, 1564–6 (2005).
- Kawano, M., Aravind, L. & Storz, G. An antisense RNA controls synthesis of an SOS-induced toxin evolved from an antitoxin. *Mol. Microbiol.* **64**, 738–54 (2007).
- Kehr, S., Sturm, N., Rahlf, S., Przyborski, J. M. & Becker, K. Compartmentation of redox metabolism in malaria parasites. *PLoS Pathog.* **6**, (2010).
- Keseler, I. M., Mackie, A., Peralta-Gil, M., et al. EcoCyc: Fusing model organism databases with systems biology. *Nucleic Acids Res.* **41**, 605–612 (2013).

- Keyer, K. & Imlay, J. Superoxide accelerates DNA damage by elevating free-iron levels. *Proc. Natl. Acad. Sci. U. S. A.* **93**, 13635–13640 (1996).
- Keyer, K., Strohmeier Gort, A. & Imlay, J. A. Superoxide and the Production of Oxidative DNA Damage. *J. Bacteriol.* **177**, 6782–6790 (1995).
- Kim, J. S., Kuk, E., Yu, K. N., et al. Antimicrobial effects of silver nanoparticles. *Nanomedicine Nanotechnology, Biol. Med.* **3**, 95–101 (2007).
- Kiran, D. & Sriranganathan, N. The antimicrobial effect of anti-dnaK peptide nucleic acids on multidrug resistant strains of Escherichia coli and Salmonella enterica serovar Typhimurium. *Bios* **85**, 48–56 (2014).
- Kirsch, M. & de Groot, H. NAD(P)H, a directly operating antioxidant? *Faseb J.* **15**, 1569–1574 (2001).
- Kiyosawa, H., Mise, N., Iwase, S., Hayashizaki, Y. & Abe, K. Disclosing hidden transcripts: mouse natural sense-antisense transcripts tend to be poly(A) negative and nuclear localized. *Genome Res.* **15**, 463–74 (2005).
- Kiyosawa, H., Yamanaka, I., Osato, N., Kondo, S. & Hayashizaki, Y. Antisense transcripts with FANTOM2 clone set and their implications for gene regulation. *Genome Res.* **13**, 1324–34 (2003).
- Kohanski, M. a., Dwyer, D. J. & Collins, J. J. How antibiotics kill bacteria: from targets to networks. *Nat. Rev. Microbiol.* **8**, 423–435 (2010).
- Kohanski, M. A., DePristo, M. A. & Collins, J. J. Sublethal Antibiotic Treatment Leads to Multidrug Resistance via Radical-Induced Mutagenesis. *Mol. Cell* **37**, 311–320 (2010).
- Kohanski, M. a., Dwyer, D. J., Hayete, B., Lawrence, C. a. & Collins, J. J. A Common Mechanism of Cellular Death Induced by Bactericidal Antibiotics. *Cell* **130**, 797–810 (2007).
- Koizumi, Y. & Iwami, S. Mathematical modeling of multi-drugs therapy: a challenge for determining the optimal combinations of antiviral drugs. *Theor. Biol. Med. Model.* **11**, 41 (2014).
- Kole, R., Krainer, A. R. & Altman, S. RNA therapeutics: beyond RNA interference and antisense oligonucleotides. *Nat. Rev. Drug Discov.* **11**, 125–140 (2012).
- Kolodkin-Gal, I., Hazan, R., Gaathon, A., Carmeli, S. & Engelberg-Kulka, H. A linear pentapeptide is a quorum-sensing factor required for mazEF-mediated cell death in Escherichia coli. *Science* **318**, 652–655 (2007).
- Kong, Y., Yao, H., Ren, H., et al. Imaging tuberculosis with endogenous β -lactamase reporter enzyme fluorescence in live mice. *Proc. Natl. Acad. Sci. U. S. A.* **107**, 12239–44 (2010).

- Korshunov, S. S. & Imlay, J. A. A potential role for periplasmic superoxide dismutase in blocking the penetration of external superoxide into the cytosol of Gram-negative bacteria. *Mol. Microbiol.* **43**, 95–106 (2002).
- Kottur, J. & Nair, D. T. Reactive Oxygen Species Play an Important Role in the Bactericidal Activity of Quinolone Antibiotics. *Angew. Chemie* **55**, 2397–2400 (2016).
- Krinke, L. & Wulff, D. L. OOP RNA, produced from multicopy plasmids, inhibits lambda cII gene expression through an RNase III-dependent mechanism. *Genes Dev.* **1**, 1005–1013 (1987).
- Kroger, C., Dillon, S. C., Cameron, A. D., et al. The transcriptional landscape and small RNAs of *Salmonella enterica* serovar Typhimurium. *Proc. Natl. Acad. Sci. U. S. A.* **109**, E1277–86 (2012).
- Kurupati, P., Tan, K. S. W., Kumarasinghe, G. & Poh, C. L. Inhibition of gene expression and growth by antisense peptide nucleic acids in a multiresistant β -lactamase-producing *Klebsiella pneumoniae* strain. *Antimicrob. Agents Chemother.* **51**, 805–811 (2007).
- Langmead, B., Trapnell, C., Pop, M. & Salzberg, S. Ultrafast and memory-efficient alignment of short DNA sequences to the human genome. *Genome Biol.* **10**, (2009).
- Laxminarayan, R., Malani, A., Howard, D. & Smith, D. L. *Extending the cure: policy responses to the growing threat of antibiotic resistance.* (Resources for the Future, 2007).
- LeClerc, J. E., Li, B., Payne, W. L. & Cebula, T. a. High mutation frequencies among *Escherichia coli* and *Salmonella* pathogens. *Science* **274**, 1208–1211 (1996).
- Lee, E.-J. & Groisman, E. a. An antisense RNA that governs the expression kinetics of a multifunctional virulence gene. *Mol. Microbiol.* **76**, 1020–33 (2010).
- Lewis, K. Persister cells, dormancy and infectious disease. *Nat. Rev. Microbiol.* **5**, 48–56 (2007).
- Lewis, K. Platforms for antibiotic discovery. *Nat. Rev. Drug Discov.* **12**, 371–87 (2013).
- Liao, S. M., Wu, T. H., Chiang, C. H., Susskind, M. M. & McClure, W. R. Control of gene expression in bacteriophage P22 by a small antisense RNA. I. Characterization in vitro of the Psar promoter and the sar RNA transcript. *Genes Dev.* **1**, 197–203 (1987).
- Little, J. W. & Mount, D. W. The SOS Regulatory System of *Escherichia coli*. *Cell* **29**, 11–22 (1982).
- Liu, J. M., Livny, J., Lawrence, M. S., et al. Experimental discovery of sRNAs in *Vibrio cholerae* by direct cloning, 5S/tRNA depletion and parallel sequencing. *Nucleic Acids Res.* **37**, e46 (2009).

- Liu, X., Marrakchi, M., Jahne, M., Rogers, S. & Andreescu, S. Real-time investigation of antibiotics-induced oxidative stress and superoxide release in bacteria using an electrochemical biosensor. *Free Radic. Biol. Med.* **91**, 25–33 (2016).
- Liu, Y. & Imaly, J. A. Cell Death from Antibiotics Without the Involvement of Reactive Oxygen Species. *Science* **339**, 2010–2013 (2013).
- Livermore, D. M. β -lactamase-mediated resistance and opportunities for its control. *J. Antimicrob. Chemother.* **41**, 25–41 (1998).
- Loo, C., Lowery, A., Halas, N., West, J. & Drezek, R. Immunotargeted nanoshells for integrated cancer imaging and therapy. *Nano Lett.* **5**, 709–711 (2005).
- Lovrić, J., Bazzi, H. S., Cuie, Y., et al. Differences in subcellular distribution and toxicity of green and red emitting CdTe quantum dots. *J. Mol. Med.* **83**, 377–85 (2005).
- Lu, Z., Li, C. M., Bao, H., Qiao, Y. & Toh, Y. Mechanism of Antimicrobial Activity of CdTe Quantum Dots. *Langmuir* **24**, 5445–5452 (2008).
- Ma, J., Chen, J.-Y., Guo, J., et al. Photostability of thiol-capped CdTe quantum dots in living cells: the effect of photo-oxidation. *Nanotechnology* **17**, 2083–2089 (2006).
- Magistri, M., Faghihi, M. A., St Laurent, G. & Wahlestedt, C. Regulation of chromatin structure by long noncoding RNAs: focus on natural antisense transcripts. *Trends Genet.* **28**, 389–96 (2012).
- Magnet, S., Smith, T., Zheng, R., Nordmann, P. & Blanchard, J. S. Aminoglycoside Resistance Resulting from Tight Drug Binding to an Altered Aminoglycoside Acetyltransferase. *Antimicrob. Agents Chemother.* **47**, 1577–1583 (2003).
- Marin, V. L., Roy, S. & Armitage, B. a. Recent advances in the development of peptide nucleic acid as a gene-targeted drug. *Expert Opin. Biol. Ther.* **4**, 337–348 (2004).
- Marshall, L. & White, R. J. Non-coding RNA production by RNA polymerase III is implicated in cancer. *Nat. Rev. Cancer* **8**, 911–4 (2008).
- Mason, E., Henderson, M. W., Scheller, E. V., Byrd, M. S. & Cotter, P. a. Evidence for phenotypic bistability resulting from transcriptional interference of bvgAS in *Bordetella bronchiseptica*. *Mol. Microbiol.* **90**, 716–733 (2013).
- Massé, E., Escorcí, F. E. & Gottesman, S. Coupled degradation of a small regulatory RNA and its mRNA targets in *Escherichia coli*. *Genes Dev.* **17**, 2374–2383 (2003).
- Maurer, L. M., Yohannes, E., Bondurant, S. S., Radmacher, M. & Slonczewski, J. L. pH Regulates Genes for Flagellar Motility, Catabolism, and Oxidative Stress in *Escherichia coli* K-12. *J. Bacteriol.* **187**, 304–319 (2005).

- McClure, R., Balasubramanian, D., Sun, Y., *et al.* Computational analysis of bacterial RNA-Seq data. *Nucleic Acids Res.* **41**, 1–16 (2013).
- Medintz, I. L. & Mattoussi, H. Quantum dot-based resonance energy transfer and its growing application in biology. *Phys. Chem. Chem. Phys.* **11**, 17–45 (2009).
- Meng, J., Da, F., Ma, X., *et al.* Antisense Growth Inhibition of Methicillin-Resistant *Staphylococcus aureus* by Locked Nucleic Acid Conjugated with Cell-Penetrating Peptide as a Novel FtsZ Inhibitor. *J. Am. Chem. Soc.* **59**, 914–922 (2015).
- Merrikh, H., Ferrazzoli, A. E., Bougdour, A., Olivier-Mason, A. & Lovett, S. T. A DNA damage response in *Escherichia coli* involving the alternative sigma factor, RpoS. *Proc. Natl. Acad. Sci. U. S. A.* **106**, 611–6 (2009).
- Milletti, F. Cell-penetrating peptides: Classes, origin, and current landscape. *Drug Discov. Today* **17**, 850–860 (2012).
- Misra, S. & Crosby, M. Annotation of the *Drosophila melanogaster* euchromatic genome: a systematic review. *Genome Biol.* **3**, 1–22 (2002).
- Mitschke, J., Georg, J., Scholz, I., *et al.* An experimentally anchored map of transcriptional start sites in the model cyanobacterium *Synechocystis* sp. PCC6803. *Proc. Natl. Acad. Sci. U. S. A.* **108**, 2124–9 (2011).
- Moghimi, S. M., Hunter, A. C. & Murray, J. C. Nanomedicine: current status and future prospects. *FASEB J.* **19**, 311–30 (2005).
- Mohammad, M., Y.Khan, a., Subhani, M. S., *et al.* Kinetics and electrochemical studies on superoxide. *Res. Chem. Intermed.* **27**, 259–267 (2001).
- Mondhe, M., Chessher, A., Goh, S., Good, L. & Stach, J. E. M. Species-selective killing of bacteria by antimicrobial peptide-PNAs. *PLoS One* **9**, e89082 (2014).
- Monrás, J. P., Collao, B., Molina-quiroz, R. C., *et al.* Microarray analysis of the *Escherichia coli* response to CdTe-GSH Quantum Dots: understanding the bacterial toxicity of semiconductor nanoparticles. *BMC Genomics* **15**, 1–13 (2014).
- Montange, R. K. & Batey, R. T. Riboswitches: emerging themes in RNA structure and function. *Annu. Rev. Biophys.* **37**, 117–33 (2008).
- Monti, L., Cinquetti, R., Guffanti, A., *et al.* In silico prediction and experimental validation of natural antisense transcripts in two cancer-associated regions of human chromosome 6. *Int. J. Oncol.* **34**, 1099–108 (2009).
- Murakami, K., Ono, T., Viducic, D., *et al.* Role for rpoS gene of *Pseudomonas aeruginosa* in antibiotic tolerance. *FEMS Microbiol. Lett.* **242**, 161–167 (2005).

- Muse, W. B. & Bender, R. A. The nac (Nitrogen Assimilation Control) Gene from Escherichia coli. *J. Bacteriol.* **180**, 1166–1173 (1998).
- Mwangi, M. M., Wu, S. W., Zhou, Y., *et al.* Tracking the in vivo evolution of multidrug resistance in *Staphylococcus aureus* by whole-genome sequencing. *Proc. Natl. Acad. Sci. U. S. A.* **104**, 9451–6 (2007).
- Myhre, O., Andersen, J. M., Aarnes, H. & Fonnum, F. Evaluation of the probes 2',7'-dichlorofluorescin diacetate, luminol, and lucigenin as indicators of reactive species formation. *Biochem. Pharmacol.* **65**, 1575–1582 (2003).
- Nagy, T. A., Moreland, S. M., Andrews-Polymenis, H. & Detweiler, C. S. The ferric enterobactin transporter fep is required for persistent salmonella enterica serovar typhimurium infection. *Infect. Immun.* **81**, 4063–4070 (2013).
- Napolitano, R., Janel-Bintz, R., Wagner, J. & Fuchs, R. P. All three SOS-inducible DNA polymerases (Pol II, Pol IV and Pol V) are involved in induced mutagenesis. *EMBO J.* **19**, 6259–6265 (2000).
- Neidig, A., Yeung, A. T. Y., Rosay, T., *et al.* TypA is involved in virulence, antimicrobial resistance and biofilm formation in *Pseudomonas aeruginosa*. *BMC Microbiol.* **13**, 77 (2013).
- Nicolas, P., Mader, U., Dervyn, E., *et al.* Condition-Dependent Transcriptome Reveals High-Level Regulatory Architecture in *Bacillus subtilis*. *Science* **335**, 1103–1106 (2012).
- Nielsen, P. E. Peptide nucleic acids as antibacterial agents via the antisense principle. *Expert Opin. Investig. Drugs* **10**, 331–341 (2001).
- Nielsen, P. E., Egholm, M., Berg, R. H. & Buchardt, O. Sequence-selective recognition of DNA by strand displacement with a thymine-substituted polyamide. *Science* **254**, 1497–500 (1991).
- Nikravesh, A., Dryselius, R., Faridani, O. R., *et al.* Antisense PNA accumulates in Escherichia coli and mediates a long post-antibiotic effect. *Mol. Ther.* **15**, 1537–42 (2007).
- Oh, E., Zhang, Q. & Jeon, B. Target optimization for peptide nucleic acid (PNA)-mediated antisense inhibition of the CmeABC multidrug efflux pump in *Campylobacter jejuni*. *J. Antimicrob. Chemother.* **69**, 375–80 (2014).
- Okazaki, Y., Furuno, M., Kasukawa, T. & Adachi, J. Analysis of the mouse transcriptome based on functional annotation of 60,770 full-length cDNAs. *Nature* **420**, 563–573 (2002).
- Okusu, H. & Nikaido, H. AcrAB efflux pump plays a major role in the antibiotic resistance phenotype of *Escherichia coli* multiple-antibiotic-resistance (Mar) mutants. *J. Bacteriol.* **178**, 306–308 (1996).

- Olive, A. J. & Sasse, C. M. Metabolic crosstalk between host and pathogen: sensing, adapting and competing. *Nat. Rev. Microbiol.* **14**, 221–234 (2016).
- Opdyke, J. A., Fozo, E. M., Hemm, M. R. & Storz, G. RNase III participates in GadY-dependent cleavage of the gadX-gadW mRNA. *J. Mol. Biol.* **406**, 29–43 (2011).
- Palmer, A. C., Ahlgren-Berg, A., Egan, J. B., Dodd, I. B. & Shearwin, K. E. Potent transcriptional interference by pausing of RNA polymerases over a downstream promoter. *Mol. Cell* **34**, 545–55 (2009).
- Palmer, A. C., Egan, J. B. & Shearwin, K. E. Transcriptional interference by RNA polymerase pausing and dislodgement of transcription factors. *Transcription* **2**, 9–14 (2011).
- Palmer, L. D. & Skaar, E. P. Transition Metals and Virulence in Bacteria. *Annu. Rev. Genet.* **50**, 67–91 (2016).
- Panthani, M. G., Akhavan, V., Goodfellow, B., *et al.* Nanocrystal ‘Inks’ for Printable Photovoltaics. *J. Am. Chem. Soc.* **130**, 16770–16777 (2008).
- Phillips, G. J. & Silhavy, T. J. The *E. coli* *ffh* gene is necessary for viability and efficient protein export. *Nature* **359**, 744–746 (1992).
- Prescott, E. M. & Proudfoot, N. J. Transcriptional collision between convergent genes in budding yeast. *Proc. Natl. Acad. Sci. U. S. A.* **99**, 8796–8801 (2002).
- Queenan, A. M. & Bush, K. Carbapenemases: the versatile β-lactamases. *Clin. Microbiol. Rev.* **20**, 440–458 (2007).
- Rengifo-Herrera, J. a., Sanabria, J., Machuca, F., *et al.* A Comparison of Solar Photocatalytic Inactivation of Waterborne *E. coli* Using Tris (2,2'-bipyridine)ruthenium(II), Rose Bengal, and TiO₂. *J. Sol. Energy Eng.* **129**, 135 (2007).
- Repoila, F. & Darfeuille, F. Small regulatory non-coding RNAs in bacteria: physiology and mechanistic aspects. *Biol. cell* **101**, 117–31 (2009).
- Repoila, F., Majdalani, N. & Gottesman, S. Small non-coding RNAs, co-ordinators of adaptation processes in *Escherichia coli*: The RpoS paradigm. *Mol. Microbiol.* **48**, 855–861 (2003).
- Reuter, J. S. & Mathews, D. H. RNAstructure: software for RNA secondary structure prediction and analysis. *BMC Bioinformatics* **11**, 129 (2010).
- Reynolds, T. S., Courtney, C. M., Erickson, K. E., *et al.* ROS Mediated Selection for Increased NADPH Availability in *Escherichia coli*. *Submitted*
- Rodgers, M. a. J. & Snowden, P. T. Lifetime of O₂ (1deltag) in Liquid Water as Determined by Time-resolved Infrared Luminescence Measurements. *J. Am. Chem. Soc.* **104**, 5541–5543 (1982).

- Rosner, J. L. & Martin, R. G. Reduction of cellular stress by TolC-dependent efflux pumps in *Escherichia coli* indicated by BaeSR and CpxARP activation of spy in efflux mutants. *J. Bacteriol.* **195**, 1042–1050 (2013).
- Rouquette, C., Harmon, J. B. & Shafer, W. M. Induction of the mtrCDE-encoded efflux pump system of *Neisseria gonorrhoeae* requires MtrA, an AraC-like protein. *Mol. Microbiol.* **33**, 651–658 (1999).
- Rowe, W., Baker, K. S., Verner-jeffreys, D., *et al.* Search Engine for Antimicrobial Resistance: A Cloud Compatible Pipeline and Web Interface for Rapidly Detecting Antimicrobial Resistance Genes Directly from Sequence Data. *PLoS One* **10**, e0133492 (2015).
- Rukavishnikov, A., Gee, K. R., Johnson, I. & Corry, S. Fluorogenic cephalosporin substrates for β -lactamase TEM-1. *Anal. Biochem.* **419**, 9–16 (2011).
- Rupnik, M., Wilcox, M. H. & Gerding, D. N. *Clostridium difficile* infection: new developments in epidemiology and pathogenesis. *Nat. Rev. Microbiol.* **7**, 526–36 (2009).
- Salgado, H., Santos-Zavaleta, A., Gama-Castro, S., *et al.* The comprehensive updated regulatory network of *Escherichia coli* K-12. *BMC Bioinformatics* **7**, 5 (2006).
- Sánchez-Romero, M. A. & Casadesús, J. Contribution of phenotypic heterogeneity to adaptive antibiotic resistance. *Proc. Natl. Acad. Sci. U. S. A.* **111**, 355–60 (2014).
- Sayed, N., Jousselin, A. & Felden, B. A cis-antisense RNA acts in trans in *Staphylococcus aureus* to control translation of a human cytolytic peptide. *Nat. Struct. Mol. Biol.* **19**, 105–12 (2012).
- Schlüter, J.-P., Reinkensmeier, J., Daschkey, S., *et al.* A genome-wide survey of sRNAs in the symbiotic nitrogen-fixing alpha-proteobacterium *Sinorhizobium meliloti*. *BMC Genomics* **11**, 245 (2010).
- Schmidt, M. Xenobiology: A new form of life as the ultimate biosafety tool. *BioEssays* **32**, 322–331 (2010).
- Scott, J. A., Homcy, C. J., Khaw, B.-A. & Rabito, C. A. Quantitation of Intracellular Oxidation in a Renal Epithelial Cell Line. *Free Radic. Biol. Med.* **4**, 79–83 (1988).
- Seemann, T. Prokka: rapid prokaryotic genome annotation. *Bioinformatics* **30**, 2068–2069 (2014).
- Sesto, N., Wurtzel, O., Archambaud, C., Sorek, R. & Cossart, P. The excludon: a new concept in bacterial antisense RNA-mediated gene regulation. *Nat. Rev. Microbiol.* **11**, 75–82 (2013).
- Sharma, C. M., Hoffmann, S., Darfeuille, F., *et al.* The primary transcriptome of the major human pathogen *Helicobacter pylori*. *Nature* **464**, 250–5 (2010).

- Shearwin, K. E., Callen, B. P. & Egan, J. B. Transcriptional interference-a crash course. *Trends Genet.* **21**, 339–45 (2005).
- Shimizu, K. Regulation Systems of Bacteria such as Escherichia coli in Response to Nutrient Limitation and Environmental Stresses. *Metabolites* **4**, 1–35 (2013).
- Shishkin, A. a, Giannoukos, G., Kucukural, A., *et al.* Simultaneous generation of many RNA-seq libraries in a single reaction. *Nat. Methods* **12**, 323–325 (2015).
- Shlaes, D. M. New β-lactam-β-lactamase inhibitor combinations in clinical development. *Ann. N. Y. Acad. Sci.* **1277**, 105–114 (2013).
- Shu, C.-C., Chatterjee, A., Dunny, G., Hu, W.-S. & Ramkrishna, D. Bistability versus Bimodal Distributions in Gene Regulatory Processes from Population Balance. *Plos Comput. Biol.* **7**, (2011).
- Simon, D. F., Domingos, R. F., Hauser, C., *et al.* Transcriptome Sequencing (RNA-seq) Analysis of the Effects of Metal Nanoparticle Exposure on the Transcriptome of Chlamydomonas reinhardtii. *Appl. Environ. Microbiol.* **79**, 4774–4785 (2013).
- Singh, V., Beltran, I. J. C., Ribot, J. C. & Nagpal, P. Photocatalysis deconstructed: Design of a new selective catalyst for artificial photosynthesis. *Nano Lett.* **14**, 597–603 (2014).
- Sneppen, K., Dodd, I. B., Shearwin, K. E., *et al.* A mathematical model for transcriptional interference by RNA polymerase traffic in Escherichia coli. *J. Mol. Biol.* **346**, 399–409 (2005).
- Sommer, M. O. a & Dantas, G. Antibiotics and the resistant microbiome. *Curr. Opin. Microbiol.* **14**, 556–563 (2011).
- Sommer, M. O., Dantas, G. & Church, G. M. Functional characterization of the antibiotic resistance reservoir in the human microflora. *Science* **325**, 1128–1131 (2009).
- Soofi, M. A. & Seleem, M. N. Targeting essential genes in *Salmonella enterica* serovar typhimurium with antisense peptide nucleic acid. *Antimicrob. Agents Chemother.* **56**, 6407–6409 (2012).
- Sorek, R. & Cossart, P. Prokaryotic transcriptomics: a new view on regulation, physiology and pathogenicity. *Nat. Rev. Genet.* **11**, 9–16 (2010).
- Sorek, R., Kunin, V. & Hugenholtz, P. CRISPR-a widespread system that provides acquired resistance against phages in bacteria and archaea. *Nat. Rev. Microbiol.* **6**, 181–6 (2008).
- Stazic, D., Lindell, D. & Steglich, C. Antisense RNA protects mRNA from RNase E degradation by RNA-RNA duplex formation during phage infection. *Nucleic Acids Res.* **39**, 4890–9 (2011).

- Stiernagle, T. in *Wormbook*, ed Maintenance of *C. elegans*. (2005). doi:Available at: doi/10.1895/wormbook.1.7.1, <http://www.wormbook.org>.
- Stork, M., Di Lorenzo, M., Welch, T. J. & Crosa, J. H. Transcription termination within the iron transport-biosynthesis operon of *Vibrio anguillarum* requires an antisense RNA. *J. Bacteriol.* **189**, 3479–88 (2007).
- Stork, M., Grijpstra, J., Bos, M. P., et al. Zinc Piracy as a Mechanism of *Neisseria meningitidis* for Evasion of Nutritional Immunity. *PLoS Pathog.* **9**, (2013).
- Storz, G., Tartaglia, L. a., Farr, S. B. & Ames, B. N. Bacterial defenses against oxidative stress. *Trends Genet.* **6**, 363–368 (1990).
- Stougaard, P., Molin, S. & Nordstrom, K. RNAs involved in copy-number control and incompatibility of. *Proc. Natl. Acad. Sci. U. S. A.* **78**, 6008–6012 (1981).
- Sun, Q. C., Mundoor, H., Ribot, J. C., et al. Plasmon-enhanced energy transfer for improved upconversion of infrared radiation in doped-lanthanide nanocrystals. *Nano Lett.* **14**, 101–106 (2014).
- Sun, Q.C., Ding, Y., Goodman, S. M., H. Funke, H. & Nagpal, P. Copper plasmonics and catalysis: role of electron–phonon interactions in dephasing localized surface plasmons. *Nanoscale* **6**, 12450–12457 (2014).
- Sunde, M. & Norström, M. The genetic background for streptomycin resistance in *Escherichia coli* influences the distribution of MICs. *J. Antimicrob. Chemother.* **56**, 87–90 (2005).
- Tacconelli, E. & Magrini, N. *Global priority list of antibiotic-resistant bacteria to guide research, discovery, and development of new antibiotics*. (2017).
- Tängdén, T. Combination antibiotic therapy for multidrug-resistant Gram-negative bacteria. *Ups. J. Med. Sci.* **97**³⁴, 149–153 (2014).
- Tängdén, T., Hickman, R. a., Forsberg, P., et al. Evaluation of double- and triple-antibiotic combinations for VIM- and NDM-producing *klebsiella pneumoniae* by in vitro time-kill experiments. *Antimicrob. Agents Chemother.* **58**, 1757–1762 (2014).
- Thannickal, V. J. & Fanburg, B. L. Reactive oxygen species in cell signaling. *Am. J. Physiol. Lung Cell. Mol. Physiol.* **279**, L1005–L1028 (2000).
- The European Committee on Antimicrobial Susceptibility Testing. Breakpoint tables for interpretation of MICs and zone diameters. *Version 5.0* (2015).
- Thisted, T. & Gerdes, K. Mechanism of Post-segregational Killing of Plasmid R1 by the hok / sok System Sok Antisense RNA Regulates hok Gene Expression Indirectly Through the Overlapping mok Gene. *J. Mol. Biol.* 41–54 (1997).

- Thomas, P. D., Campbell, M. J., Kejariwal, A., Mi, H. & Karlak, B. PANTHER: A Library of Protein Families and Subfamilies Indexed by Function. *Genome Res.* **13**, 2129–2141 (2003).
- Thomason, M. K. & Storz, G. Bacterial antisense RNAs: how many are there, and what are they doing? *Annu. Rev. Genet.* **44**, 167–88 (2010).
- Thorvaldsdóttir, H., Robinson, J. T. & Mesirov, J. P. Integrative Genomics Viewer (IGV): high-performance genomics data visualization and exploration. *Brief. Bioinform.* **14**, 178–92 (2013).
- Tikhomirov, G., Hoogland, S., Lee, P. E., *et al.* DNA-based programming of quantum dot valency, self-assembly and luminescence. *Nat. Nanotechnol.* **6**, 485–90 (2011).
- Tjaden, B. De novo assembly of bacterial transcriptomes from RNA-seq data. *Genome Biol.* **16**, 1 (2015).
- Toledo-Arana, A., Dussurget, O., Nikitas, G., *et al.* The Listeria transcriptional landscape from saprophytism to virulence. *Nature* **459**, 950–956 (2009).
- Tomizawa, J.-I. & Itoh, T. Plasmid ColE1 incompatibility determined by interactionn of RNA I with primer transcript. *Proc. Natl. Acad. Sci. United States Am.* **78**, 6096–6100 (1981).
- Toussaint, K. a & Gallagher, J. C. β -Lactam/ β -Lactamase Inhibitor Combinations: From Then to Now. *Ann. Pharmacother.* **49**, 86–98 (2015).
- Triglia, T., Menting, J.G., Wilson, C. & Cowman, A.F. Mutations in dihydropteroate synthase are responsible for sulfone and sulfonamide resistance in Plasmodium falciparum. *Proc. Natl. Acad. Sci. U. S. A.* **94**, 13944–13949 (1997).
- Troxell, B. & Hassan, H. M. Transcriptional regulation by Ferric Uptake Regulator (Fur) in pathogenic bacteria. *Front. Cell. Infect. Microbiol.* **3**, 59 (2013).
- United States Center for Disease Control. *Antibiotic Resistance Threats*. (2013).
- Valko, M., Izakovic, M., Mazur, M., Rhodes, C. J. & Telser, J. Role of oxygen radicals in DNA damage and cancer incidence. *Mol. Cell. Biochem.* **266**, 37–56 (2004).
- Valko, M., Leibfritz, D., Moncol, J., *et al.* Free radicals and antioxidants in normal physiological functions and human disease. *Int. J. Biochem. Cell Biol.* **39**, 44–84 (2007).
- Van der Heijden, J., Bosman, E. S., Reynolds, L. A. & Finlay, B. B. Direct measurement of oxidative and nitrosative stress dynamics in Salmonella inside macrophages. *Proc. Natl. Acad. Sci. U. S. A.* **112**, 560–5 (2015).

- Vatansever, F., de Melo, W. C. M. A., Avci, P., *et al.* Antimicrobial strategies centered around reactive oxygen species - bactericidal antibiotics, photodynamic therapy, and beyond. *FEMS Microbiol. Rev.* **37**, 955–989 (2013).
- Vazquez-Torres, A., Jones-Carson, J., Bäumler, A., *et al.* Extraintestinal dissemination of *Salmonella* by CD18-expressing phagocytes. *Nature* **401**, 804–808 (1999).
- Wagner, J., Gruz, P., Kim, S. R., *et al.* The dinB gene encodes a novel *E. coli* DNA polymerase, DNA pol IV, involved in mutagenesis. *Mol. Cell* **4**, 281–286 (1999).
- Walker, G. C. Mutagenesis and inducible responses to deoxyribonucleic acid damage in *Escherichia coli*. *Microbiol. Rev.* **48**, 60–93 (1984).
- Walsh, C. Molecular mechanisms that confer antibacterial drug resistance. *Nature* **406**, 775–781 (2000).
- Wan, Y., Kertesz, M., Spitale, R. C., Segal, E. & Chang, H. Y. Understanding the transcriptome through RNA structure. *Nat. Rev. Genet.* **12**, 641–55 (2011).
- Wang, J., Lu, Z., Wientjes, M. G. & Au, J. L.-S. Delivery of siRNA therapeutics: barriers and carriers. *AAPS J.* **12**, 492–503 (2010).
- Wang, J., Nielsen, P. E., Jiang, M., *et al.* Mismatch-sensitive hybridization detection by peptide nucleic acids immobilized on a quartz crystal microbalance. *Anal. Chem.* **69**, 5200–5202 (1997).
- Wang, X.-J., Gaasterland, T. & Chua, N.-H. Genome-wide prediction and identification of cis-natural antisense transcripts in *Arabidopsis thaliana*. *Genome Biol.* **6**, R30 (2005).
- Ward, D. F. & Murray, N. E. Convergent Transcription in Bacteriophage lambda: Interference with Gene Expression. *J. Mol.* **133**, 249–266 (1979).
- Waters, L. S. & Storz, G. Regulatory RNAs in bacteria. *Cell* **136**, 615–28 (2009).
- Weber, H., Polen, T., Heuveling, J., *et al.* Genome-Wide Analysis of the General Stress Response Network in *Escherichia coli*: S -Dependent Genes, Promoters, and Sigma Factor Selectivity. *J. Bacteriol.* **187**, 1591–1603 (2005).
- Wilson, R. C. & Doudna, J. a. Molecular mechanisms of RNA interference. *Annu. Rev. Biophys.* **42**, 217–39 (2013).
- World Health Organization. *Global Tuberculosis Report*. (2012).
- Wu, J. & Weiss, B. Two-stage induction of the soxRS (superoxide response) regulon of *Escherichia coli*. *J. Bacteriol.* **174**, 3915–3920 (1992).
- Wu, Y., Vulić, M., Keren, I. & Lewis, K. Role of oxidative stress in persister tolerance. *Antimicrob. Agents Chemother.* **56**, 4922–6 (2012).

- Wurtzel, O., Yoder-Himes, D. R., Han, K., *et al.* The single-nucleotide resolution transcriptome of *Pseudomonas aeruginosa* grown in body temperature. *PLoS Pathog.* **8**, e1002945 (2012).
- Yamada, K., Lim, J., Dale, J. M., *et al.* Empirical analysis of transcriptional activity in the *Arabidopsis* genome. *Science* **302**, 842–6 (2003).
- Yamaguchi, Y., Park, J.-H. & Inouye, M. Toxin-antitoxin systems in bacteria and archaea. *Annu. Rev. Genet.* **45**, 61–79 (2011).
- Yeaman, M. R. & Yount, N. Y. Mechanisms of Antimicrobial Peptide Action and Resistance. *Pharmacol. Rev.* **55**, 27–55 (2003).
- Yeh, P., Tschumi, A. I. & Kishony, R. Functional classification of drugs by properties of their pairwise interactions. *Nat. Genet.* **38**, 489–494 (2006).
- Yelin, R., Dahary, D., Sorek, R., *et al.* Widespread occurrence of antisense transcription in the human genome. *Nat. Biotechnol.* **21**, 379–86 (2003).
- Yin, N., Ma, W., Pei, J., *et al.* Synergistic and antagonistic drug combinations depend on network topology. *PLoS One* **9**, (2014).
- Yu, B. P. Cellular defenses against damage from reactive oxygen species. *Physiol. Rev.* **74**, 139–162 (1994).
- Yu, W. W., Qu, L., Guo, W. & Peng, X. Experimental Determination of the Extinction Coefficient of CdTe, CdSe, and CdS Nanocrystals. *Chem. Mater.* **125**, 2854–2860 (2003).
- Zerbino, D. R. & Birney, E. Velvet: algorithms for de novo short read assembly using de Bruijn graphs. *Genome Res.* **18**, 821–829 (2008).
- Zhang, Y., Liu, X. S., Liu, Q.-R. & Wei, L. Genome-wide in silico identification and analysis of cis natural antisense transcripts (cis-NATs) in ten species. *Nucleic Acids Res.* **34**, 3465–75 (2006).
- Zheng, M., Wang, X., Templeton, L. J., *et al.* DNA Microarray-Mediated Transcriptional Profiling of the *Escherichia coli* Response to Hydrogen Peroxide. *J. Bacteriol.* **183**, 4562–4570 (2001).
- Zhou, K., Zhou, L., Lim, Q. 'En, *et al.* Novel reference genes for quantifying transcriptional responses of *Escherichia coli* to protein overexpression by quantitative PCR. *BMC Mol. Biol.* **12**, 18–26 (2011).
- Zhu, Z.-J., Yeh, Y.-C., Tang, R., *et al.* Stability of quantum dots in live cells. *Nat. Chem.* **3**, 963–968 (2011).

Zou, J., Ji, P., Zhao, Y.-L., *et al.* Neighbor communities in drug combination networks characterize synergistic effect. *Mol. Biosyst.* **8**, 3185 (2012).